

ABSTRACT

SOLTANI, IMAN. Using Layer-by-Layer Coating and Nanocomposite Technologies to Improve the Barrier Properties of Polymeric Materials. (Under the direction of Richard J. Spontak and Russell E. Gorga.)

Means for improving barrier properties of polymers against gases, particularly for promoting their applications as packaging materials, are divided into surface coating and embedding nanoparticles in the bulk of the polymeric membranes. In this research, we mainly investigated improvement in barrier properties of polymers against oxygen and carbon dioxide, through layer-by-layer (LBL) coating and bulk nanocomposite methods.

Initially, we studied the morphology of layer-by-layer assemblies comprising alternating layers of polyelectrolyte (PE) and natural montmorillonite (MMT) platelets, where polyethyleneterephthalate ionomer was used as our proposed alternative PE, to be compared with already examined polyethyleneimine. For both investigated PEs, while microscopic images showed the formation of tortuous networks of galleries between subsequent layers of oriented clay platelets parallel to the substrate surface, x-ray diffractometry (XRD) traces pointed to the intercalation of PE layers between clay platelets.

As a confirmation of forming tortuous networks between oriented and high aspect ratio clay platelets to increase the path length of diffusing gas species dramatically, LBL-coated polystyrene-based membranes demonstrated pronounced decreases in permeability of oxygen and carbon dioxide (e.g. about the scale of 500 times decrease in permeability, with only five cycles of bilayer deposition). Before LBL deposition, the surface of the hydrophobic polymeric substrate was pretreated with oxygen plasma to improve its interaction with the coating.

In the next study, previously LBL-coated samples were melt pressed in a cyclic manner to embed and to crush the coating inside the polystyrene-based matrix, aiming the exfoliated

polymer-clay nanocomposites. The morphological investigations by transmission electron microscopy (TEM) revealed the tortuous internal structure of crushed LBL assemblies' portions, mainly comprising swollen intercalated stacks of clay, as well as flocculated exfoliated tactoids of a few clay platelets, down to about 2nm thickness. Moreover, XRD traces confirmed this increase in intercalation and exfoliation of clay platelets.

Following ahead, dynamic mechanical thermal analysis (DMA) revealed significant increases in the storage and loss moduli values for our PNCs over those of pristine polystyrene-based matrix, hypothesizing the occurrence of substantial interactions between clay and the polymeric matrix, induced by intervening effect of PE interlayers. Also, permeation experiments showed noticeable improvement in gas barrier properties of processed PNCs. Considering the low content of clay particles and their limited level of global dispersions throughout the matrix, it may theorize the significant efficiency of high aspect ratio and tortuous LBL assemblies portions, oriented (induced by cycling pressing into thin films) perpendicular to the permeants' path routes. Thus, it might act almost as scavenging hubs against transport of diffusing gases.

Finally, using PVAc, as the matrix, with this novel two-step approach of preparing PNCs, showed relatively higher clay content, when prepared with similar coating conditions. Also, DMA and permeation experiments pointed to significant improvements in mechanical and gas barrier properties of the PNCs, prepared by only 25 times melt pressing steps. Additionally, XRD traces postulated occurrence of noticeable irregularities in the interdistance of clay platelets. So, it is conjectured that semi-hydrophilic PVAc matrix promotes stronger interactions with clay particles, compared with those of polystyrene-based PNCs. However, moderate global dispersion of clay throughout the matrix points to the insufficient efficiency

of repetitive melt pressing procedure to apply intensive enough stresses on samples, in order to overcome internal cohesion in LBL assemblies, which established initial intercalation and exfoliation in the otherwise aggregately clustered natural clay platelets. In addition, it is postulated that possibly occurring slight thermal degradations induce adverse results on the dispersion level and aforementioned properties of PNCs, processed over extended times.

© Copyright 2016 by Iman Soltani

All Rights Reserved

Using Layer-by-Layer Coating and Nanocomposite Technologies to Improve the Barrier
Properties of Polymeric Materials

by
Iman Soltani

A dissertation submitted to the Graduate Faculty of
North Carolina State University
in partial fulfillment of the
requirements for the Degree of
Doctor of Philosophy

Fiber and Polymer Science

Raleigh, North Carolina

2016

APPROVED BY:

Richard J. Spontak
Committee Co-Chair

Russell E. Gorga
Committee Co-Chair

Jan Genzer

Richard Kotek

DEDICATION

To my dearest mom's memory, Ms. Sheyda Khamei, the real inspiration throughout my life, from whom I learned the meanings of selflessness, unconditional love, endless passion for learning, hardworking manner, and thoughtfulness; to whom I owe whole my life.

To my lovely, selfless, kind, and patient wife, Ms. Anahita Kamyab, who has always helped me and has stood beside me by all means, particularly throughout my Ph.D. years, without whose support, I could not have gained this achievement.

BIOGRAPHY

Iman Soltani was born in 1977, in Tehran, the capital of Iran, in a highly educated and open-minded family, with a noble background. He is a descendant of Fazel Naraghi, the famous Persian philosopher, mathematician, and poet of 19th century, and Mohammad Hosein Natanzi, a prominent philosopher and poet. Also, Iman's great grandfather, Yahya Kashani, was a prominent scholar, liberal politician, philanthropist, and one of the pioneers of Persian modern journalism, who is sometimes referred to as the father of Persian modern journalism.

Yahya Kashani devoted his life to promoting democracy in Iran, by raising peoples' level of social knowledge and making them aware of their civil rights and responsibilities. In addition, he spent most of his wealth to diminish poverty in Tehran, particularly during the disastrous famine occurred through the WWI, and from his prominent picture, Iman has been inspired enormously throughout his life. Iman also has a royal background, as a descendant of Prince Dowlatshah, brave and capable son of Fath Ali Shah, the second Qajar King of Persia (19th Century), although nowadays these titles may not be very á la mode.

After finishing his high school studies in Mathematics and Physics, Iman gained admission and undergraduate scholarship to study Polymer Engineering in Amirkabir University of Technology (Tehran Polytechnic), the oldest and most prestigious technological university in Iran, in 1996. In fact, through years of high school he had studied so hard, and finally after earning his diploma in mathematics and physics, by achieving an outstanding grade in the nationwide entrance exam for undergraduate studies, he was awarded scholarship and admissions for studying in many top universities of the country, between which he had chosen

for Amirkabir University of Technology, where, in addition to his favorite discipline, polymer engineering, he had been awarded admissions in generally popular disciplines like mechanical engineering, industrial engineering, and chemical engineering as well.

In Polymer Engineering faculty of Polytechnic, which is the best of its type in the country, he learned many theoretical and practical lessons about polymers, plastics, rubbers, and composites, their structure, properties, and their processing. His undergraduate thesis was titled polymerization of acrylic acid.

Gaining his BS degree, in 2001, he joined Iran Polymer and Petrochemical Institute, considered as the most equipped polymer research center in the Middle East, to pursue his graduate studies in Polymer Engineering. There, he took advanced level theoretical courses and hands-on labs in domains of polymers and composites microstructure, properties, and their processing, beyond the level he had already enjoyed during his undergraduate studies. His MS thesis was entitled "Rheology of Nylon 6,6, EPDM and Short Glass Fiber Hybrid Composites", through which he gained more experiences about polymer processing and blending, their microstructure and physical and mechanical properties. The goal of the project was to prepare toughened hybrid composites, through grafting EPDM on Nylon6,6 and adding short glass fibers, via reactive extrusion.

He was hired as a Polymer Engineer and Scientist, by Iran Khodro Co, the main partner of Renault and Peugeot car manufacturing companies in the Middle East, with manufacturing volume of about one million vehicles per annum. Iman worked for nine years in the New Product Development Center of the company, where he enjoyed both crossed-discipline and

crossed-culture collaborations with many engineers and scientists in different fields of research, design, manufacturing, and testing, from various countries, mainly France, UK, Germany, Italy, and South Korea.

There, through applying his academic background knowledge in current industrial projects, he gained a more comprehensive view of the world of polymers, particularly their wide applications, designing and processing in automotive industries. In addition, to working as an expert for plastic parts design and processing, he continued his research on polymers and composites blending and processing, from which he published a few scientific research articles. Iman also worked on processes involved in online paint-shop of the factory, including sealers and different coatings.

After nine years of working in IKCo, Iman decided to return to academia and began his works towards a Ph.D. degree in polymer science at North Carolina State University in 2011, under the supervision of Professor Richard Spontak, from whom he learned even more about polymers, as well as approaches for conducting research projects and academic writing. Iman's Ph.D. research mainly concentrated on improving barrier properties of polymer-based membranes against different gases through coating and nanocomposite approaches.

Having had more than dozens of his relatives as prominent figures (intellectuals) in UNESCO, including, his granduncle, Dr. Anvar Khamei and Dr. Ehsan Naraghi (Officier de la Légion d'Honneur), Iman has had a deep concern about history and culture for most of his life. This might be the reason that besides having pursued three majors in polymer engineering and science fields, he holds a broad knowledge about history, geography, architecture,

intellectual cinema, music, psychology, journalism, literature, and languages. Therefore, it would not be surprising if he ends up as a journalist, a UNESCO fellow, or so, along with his career in the world of polymers and plastics.

ACKNOWLEDGMENTS

First and foremost, I would like to express my sincere gratitude to Prof. Richard Spontak, who opened my eyes to the most efficient approaches to academic research conduction and writing, and supported me by all means throughout my Ph.D. research. In fact, it was my good fortune to be supervised by one of the main figures in polymer science at North Carolina State University. Then, I would like to appreciate the support and help of Prof. Russell Gorga, as my co-advisor.

I would like to thank my committee members, Prof. Richard Kotek and Prof. Jan Genzer for their guidance and insightful comments on my work, and helping me for preparing this dissertation. Also, I am grateful to Mr. Carlos Gutierrez and URRC for their financial support to this project.

My truehearted gratitude is for my kind and patient wife, Ms. Anahita Kamyab, who has helped and supported me selflessly, during my Ph.D. years and beforehand, without whom passing through various difficulties I faced was not possible. Dearest Anahita, I am the luckiest man on earth for having you.

My dearest Mom, words cannot begin to describe my eternal appreciation and gratitude for all you have done for me. I am deeply and strongly grateful to you and everything you did for me. Although I have never been able to keep up with, I have always been inspired by your larger-than-life personality, your absolute selflessness and devotion, your extreme kindness, your broad knowledge in various domains, your hardworking manner, your charismatic appeal,

and your everlasting sweet speeches. Whenever I hear in news, from your peers and friends like Shirin Ebaadi (Noble Peace Prize Laureate), Mehrangiz Kaar, and Zahra Rahnavard, I remember how, different from them, you sacrificed your career, brilliant talents, and social and academic goals to devote yourself to the lives of me and my brother. I owe you for every prominent piece of work I have done and every noteworthy aim I have achieved. I miss you deeply, and I enlighten my life with your memory.

I am cordially grateful to my kind, sweet, and knowledgeable grandmother, Ms. Rafat Pezeshki, from whom my passion for learning diverse topics in various fields of knowledge, from history, geography, literature, and different languages to chemistry and physics was initiated. My dearest Grandma, your memory is always with me.

Mr. Kit Yeong is the most helpful gentleman I have seen in the college of engineering, who is always sincerely ready to use his proficient hands-on skills to help you with technical problems you may face. I am really thankful to him for his help, including making a temperature controller for our permeation cell equipment.

I appreciate help and support of all graduate and undergraduate students and friends in Macromolecular Materials & Morphology Group of Prof. Spontak, in particular Anand Patel and Kenny Mineart, who went further for helping me, and I wish them ultimate success in their careers.

Finally, I would like to thank all people in Chemical Engineering and Material Science & Engineering departments, also in College of Textiles, who helped me by any means.

TABLE OF CONTENTS

LIST OF TABLES.....	xv
LIST OF FIGURES.....	xvi
CHAPTER 1 Investigating Improvement in Gas Barrier Properties of Polymer-Based Membranes through Different Coating and Nanocomposite Approaches.....	1
Abstract.....	1
1.1. Introduction.....	1
1.2. Different Coating Methods for Improving Barrier Properties.....	5
1.2.1. Single-Layer Coating.....	5
1.2.2. Multilayer Coating.....	15
1.3. Polymer Nanocomposites (PNCs).....	24
1.3.1. Background of PNCs.....	24
1.3.2. Three Types of Polymer-Clay Composites.....	26
1.3.3. Montmorillonite (MMT).....	28
1.3.4. Preparation Methods of Polymer-Clay Nanocomposites.....	29
1.3.5. Morphology of PNC, a Measure of Exfoliation.....	33
1.4. Transport via Membranes.....	34
1.4.1. Permeability and its Measurement by Pressure-Decay Tools.....	34
1.4.2. Sorption and Solubility.....	36
1.4.3. Diffusivity and its Measurement by Fick's Law through a Sorption Test....	36
1.4.4. Theories of Barrier Properties in PNCs.....	38
1.4.5. Comparison between Different Models Predictions for MMT.....	45
1.5. Barrier Improvement Results in Literature and Concerned Discussions.....	46
1.5.1. Sputtering.....	46
1.5.2. Evaporation.....	47
1.5.3. PECVD.....	47
1.5.4. PVD vs. CVD.....	49
1.5.5. Effect of Defects.....	50
1.5.7. LBL Assemblies.....	53

1.5.8. Polymer Nanocomposites (PNCs)	56
1.6. Conclusions	60
1.7. Dissertation Overview	62
1.8. Appendix	64
1.8.1. A Comparison between Oxygen Barrier Properties of Different Coatings and PNC Approaches	64
Tables	65
Figures	69
References	91
Nomenclature	105
CHAPTER 2 Nanotechnological Strategies Yielding High-Barrier Plastic Food Packaging	106
Abstract	106
2.1. Introduction	107
2.2. Existing Demands and Challenges	109
2.3. Coating Methods for Improved Barrier Properties	111
2.3.1. Single-Layer Coatings	111
2.3.2. Multilayer Coatings	115
2.4. Polymer Nanocomposites for Improved Barrier Properties	121
2.4.1. Methods to Prepare PCNs	125
2.4.2. Methods to Characterize PCNs	126
2.5. Molecular Transport in Polymers and Nanocomposites	127
2.5.1. Single-Gas Permeability in Dense Polymers	128
2.5.2. Barrier Properties of Polymer Nanocomposites	129
2.6. Case Studies of Enhanced Barrier Performance	133
2.6.1. Single-Layer PVD/CVD Coatings	133
2.6.2. Single-Layer ALD Coatings	138
2.6.3. Multilayer LBL Coatings	139
2.6.4. Polymer-Clay Nanocomposites	140
2.7. Conclusions and Outlook	142
2.8. Acknowledgments	144
Tables	145

Figures.....	146
References.....	160
CHAPTER 3 Investigating Morphology of Layer-by-Layer Coated Polystyrene-Based Membranes, Using Clay with Alternative Interlayers of Polyethyleneimine or Polyethyleneterephthalate Ionomer	171
Abstract.....	171
3.1. Introduction.....	172
3.2. Experimental	174
3.2.1. Materials	174
3.2.2. Thin Film Preparation.....	175
3.2.3. Plasma Treatment.....	175
3.2.4. Layer-by-Layer (LBL) Coating of Thin Films.....	175
3.2.5. Transmission Electron Microscopy (TEM).....	176
3.2.6. Scanning Electron Microscopy (SEM).....	177
3.2.7. X-Ray Diffractometry (XRD)	177
3.2.8. Gas Permeation	177
3.3. Results and Discussion.....	178
3.3.1. Proposed Mechanism of Formation and Morphology of Nanobrick LBL Assemblies.....	178
3.3.2. TEM Results for PEI-MMT LBL Assemblies.....	179
3.3.3. SEM Results for PEI-MMT LBL Assemblies	180
3.3.4. TEM Results for PETi-MMT LBL Assemblies	181
3.3.5. Quantifying Intercalation of Polymeric Interlayers between Clay Platelets in LBL Assemblies through X-Ray Diffractometry (XRD).....	182
3.3.6. Transport Properties in LBL Assemblies.....	186
3.4. Proposed Mechanism of Deposition for PETi-Containing LBL Assemblies	187
3.5. Conclusions.....	188
Tables	191
Figures.....	192
References.....	203
CHAPTER 4 Effect of Polyelectrolyte on the Barrier Properties of Layer-by-Layer Nanoclay Coatings	207
Abstract.....	207

4.1. Introduction	208
4.2. Experimental	210
4.2.1. Materials	210
4.2.2. Specimen Preparation	211
4.2.3. Specimen Characterization	211
4.3. Results and Discussion	212
4.3.2. Effect of Plasma Treatment	214
4.3.3. Effect of Suspension Concentration	215
4.3.4. Effect of Bilayer Number	217
4.3.5. Effect Permeation Temperature	218
4.4. Conclusions	220
Figures	223
References	232
CHAPTER 5 Morphology of Polymer Nanocomposites Derived From Layer-by-Layer Coated Polystyrene-Based Membranes	236
Abstract	236
5.1. Introduction	237
5.2. Experimental	240
5.2.1. Materials	240
5.2.2. Thin Film Preparation	241
5.2.3. Plasma Treatment	241
5.2.4. Layer-by-Layer (LBL) Coating of Thin Films	242
5.2.5. Cyclic Melt Pressing	243
5.2.6. Thermogravimetry (TGA)	243
5.2.7. Polarized Optical Microscopy (POM)	243
5.2.8. Transmission Electron Microscopy (TEM)	243
5.2.9. X-Ray Diffractometry (XRD)	244
5.3. Results and Discussion	244
5.3.1. Polarized Optical Microscopy	244
5.3.2. Transmission Electron Microscopy	246
5.3.3. X-Ray Diffractometry	249
5.4. Conclusions	251

Tables	253
Figures.....	254
References	262
CHAPTER 6 Transport, Mechanical, and Thermal Properties of Polymer Nanocomposites Derived from Layer-by-Layer Coated Polystyrene-Based Membranes	266
Abstract	266
6.1. Introduction	267
6.2. Experimental	270
6.2.1. Materials	270
6.2.2. Thin Film Preparation	271
6.2.3. Plasma Treatment	271
6.2.4. Layer-by-Layer (LBL) Coating of Thin Films	271
6.2.5. Cyclic Melt Pressing	272
6.2.6. Thermogravimetry (TGA)	272
6.2.7. Differential Scanning Calorimetry (DSC)	273
6.2.8. Dynamic Mechanical Analysis (DMA)	273
6.2.9. Gas Permeation	273
6.3. Results and Discussion	274
6.3.1. Examining Thermal Stability of Ingredients	275
6.3.2. Clay Content Estimation in PNCs	277
6.3.3. Physical Properties of Interlayers	279
6.3.4. Dynamic Mechanical Investigations	279
6.3.5. Permeation Properties	283
6.4. Conclusion	288
Tables	290
Figures	293
6.5. Supplementary Information	304
6.5.1. Effect of Initial MMT Content in DIW on PNC's Thermal Stability	304
6.5.2. Thermogravimetry under Nitrogen Purge	304
6.5.3. DSC for PNCs Containing PEI Interlayers	304
References	309

CHAPTER 7 Morphology, Gas Transport, and Dynamic Mechanical Properties of Polymer Nanocomposites Derived From Layer-by-Layer Coated Polyvinylacetate Membranes	313
Abstract.....	313
7.1. Introduction.....	315
7.2. Experimental	317
7.2.1. Materials	317
7.2.2. Thin Film Preparation.....	318
7.2.3. Plasma Treatment.....	318
7.2.4. Layer-by-Layer (LBL) Coating of Thin Films.....	319
7.2.5. Cyclic Melt Pressing	319
7.2.6. Polarized Optical Microscopy (POM).....	320
7.2.7. Transmission Electron Microscopy (TEM).....	320
7.2.8. X-Ray Diffractometry (XRD)	320
7.2.9. Dynamic Mechanical Analysis (DMA).....	321
7.3. Results and Discussion.....	322
7.3.1. Polarized Optical Microscopy.....	322
7.3.2. Transmission Electron Microscopy.....	324
7.3.3. X-Ray Diffractometry.....	328
7.3.4. Dynamic Mechanical Investigations.....	329
7.3.5. Permeation Properties	331
7.4. Conclusion	332
Tables.....	335
Figures.....	337
References.....	346
CHAPTER 8 Conclusions and Future Steps	350
8.1. Conclusions.....	350
8.2. Future Steps.....	353
Figures.....	357

LIST OF TABLES

Table 1.1. Explanation of abbreviations in Figure 1.1.....	65
Table 1.2. Sputtering condition for fabricating barrier AlO _x Ny film	65
Table 1.3. OTR of pure and coated PET and PP at 30°C and 0%RH.....	66
Table 1.4. (a) Decrease in the oxygen permeability (at 0%RH and 23°C) of epoxy resin through synthesizing PNC with 3.5 vol. % OMMT. (b) Dependence of the OTR (at 0%RH and 23°C) on loading level of clay.....	67
Table 1.5. Comparison between barrier properties of different coating systems and PNCs.	68
Table 2.1. Comparison between the barrier properties of different polymer-based materials.....	145
Table 3.1. Interplanar spacings of 001 crystallographic planes in clay and location of their corresponding diffraction angle peaks for neat Na ⁺ MMT and its 30BL assemblies with PEI, for corresponding contents of PEI and MMT in DIW.....	191
Table 3.2. Interplanar spacings of 001 crystallographic planes in clay and location of their corresponding diffraction angle peaks for neat Na ⁺ MMT and its 30BL assemblies with PETi, for corresponding contents of PETi and MMT in DIW..	191
Table 5.1. Estimation of the clay content in PNCs containing PEI interlayers through both image analysis and TGA residue at 600°C (Inorganic residues of PNC samples after being heated under airflow up to 600°C).....	253
Table 5.2. Estimation of the clay content in PNCs containing PETi interlayers through image analysis.....	253
Table 6.1. Estimation of the clay content in PNCs containing PEI interlayers through both image analysis and TGA residue at 600°C.....	290
Table 6.2. Estimation of the clay content in PNCs containing PETi interlayers through image analysis.....	290
Table 6.3. Permeability results for O ₂ , through cyclically melt pressed PNCs, based on LBL-coated PS* membranes at the standard atmospheric conditions.....	291
Table 6.4. Permeability results for CO ₂ , through cyclically melt pressed PNCs, based on LBL-coated PS* membranes at the standard atmospheric conditions.....	292
Table 7.1. Estimation of the clay content in PNCs through image analysis.....	333
Table 7.2. Permeability results for O ₂ through cyclically melt pressed PNCs, based on LBL-coated PVAc membranes at the standard atmospheric conditions.....	335
Table 7.3. Permeability results for CO ₂ through cyclically melt pressed PNCs, based on LBL-coated PVAc membranes at the standard atmospheric conditions.....	336

LIST OF FIGURES

- Figure 1.1.** (a) Barrier requirements for packaging some food products polymeric at 23°C. (b) A comparison of oxygen transmission rate of some typical polymeric films with thickness 100 μm at 23°C. Adapted with permission. (c) The initial loss of CO_2 from Cola PET bottle. (d) Longtime CO_2 flux through PET bottle wall during shelf life. Both graphs data are measured at 24°C and gas pressure of 3bar. Reproduced with permission69
- Figure 1.2.** (a) Schematic figure of a continuous e-beam evaporation chamber. Adapted with permission. (b) Schematic illustration of a single- and double-frequency reactor of PECVD. Adapted with permission70
- Figure 1.3.** Schematic drawing of sequential order in an ALD process of TMA and water. Adapted with permission70
- Figure 1.4.** Schematic diagram of cross-section of a multilayer film, where (a) and (c) depict layers of silica with 100 μm thickness; (b) and (d) are layers of colloidal boehmite fibrils; and (e) represents the glass substrate. Adapted with permission71
- Figure 1.5.** Schematic representation of assemblies of alternating polycation and polyanions. (a) Linear polyanion and polycations. (b) Linear polyion and oppositely charged protein. (c) Linear polyion and clay platelets. Adapted with permission72
- Figure 1.6.** (a) Schematic of layer-by-layer deposition of polyethyleneimine and clay solution and suspension, respectively. Adapted with permission. (b) Cross-sectional TEM image of an assembly of 30-bilayer of PEI/MMT deposited on PS substrate. Adapted with permission.....73
- Figure 1.7.** (a) The thickness of LBL assemblies versus the number of deposited bilayer coatings of PEI (solution pH=10) and MMT. Adapted with permission. (b) The thickness of QL assembly plotted versus the number of QL depositing cycles. Adapted with permission74
- Figure 1.8.** Schematic process of LBL deposition of two redox polymers (polycation) and an exfoliated anionic zirconium phosphate sheets on a silica particle with high surface area. Reproduced with permission. Adapted with permission.....75
- Figure 1.9.** Geometries of common particles used for polymer reinforcement and their respective surface area to volume ratios. Adapted with permission.....75
- Figure 1.10.** (a) Schematic illustration of different types of composites (labeled) made from layered silicates and polymers. (b) TEM image of a nanocomposite of dispersed clay (black) in PP matrix (gray), where A, B, and C respectively show parallel intercalated stacks of clay, disordered intercalated clay tactoids, and exfoliated platelets of clay. A schematic representation of an intercalated clay stack (A), where parallel platelets are separated with PP chains. Reprinted with permission.....76
- Figure 1.11.** Basic structures of 2:1 clay minerals. Adapted with permission77

Figure 1.12. The schematic illustration of organically-modified silicates. Adapted with permission	77
Figure 1.13. TGA graph, showing atmospheric degradation behavior of natural MMT (Na ⁺ MMT) and its organically-modified samples with different alkyl ammoniums: methyl, tallow, bis-2-hydroxyethyl quaternary ammonium (C30B) ; dimethyl, dehydrogenated tallow quaternary ammonium (C15A); dimethyl, benzyl, hydrogenated tallow quaternary ammonium (C10A). The region assigned with dotted lines is the processing window for PNC of PET and clay, at which only Na ⁺ MMT shows appropriate thermal stability	78
Figure 1.14. Schematic illustration of the composite synthesis. Adapted with permission	78
Figure 1.15. (a) Constant-volume variable-pressure permeation test setup. Adapted with permission. (b) An example of CO ₂ permeation through a polymer membrane. Adapted with permission.....	79
Figure 1.16. Models for a fluid diffusing path through (a) plate-shaped and (b) cube-shaped clay-filled polymers. Adapted with permission	79
Figure 1.17. (a) Schematic model for random like ribbons. Adapted with permission. (b) Schematic periodically ordered and ribbon-like clay platelets. Adapted with permission	80
Figure 1.18. A schematic model for hexagonal flakes as a replacement for the original ribbon-like model. Idealistically, the flakes are assumed with complete periodic distribution. Adapted with permission	80
Figure 1.19. Predictions of decreasing the relative permeability of PNCs with an increase in clay weight fraction, according to the Cussler model, in a constant aspect ratio of 100, for different clay shapes and distribution order.....	81
Figure 1.20. (a) A sketch of a Mont Carlo simulated computer model for 25 parallel identical disk shape platelets with aspect ratio 50 and without any overlapping and in 2 vol% of clay. (b) A view of finite element meshes generated for the model by a commercial microprocessor. Adapted with permission. (c). Relative permeability of the Mont Carlo simulated model mentioned, where each point shows a numerical solution for a particular model for a certain aspect ratio (α) and volume fraction (ϕ) of clay. Also, the curve shows the least square fit of the model. Adapted with permission	82
Figure 1.21. Schematic layout of a PNC with (a) completely aligned clay platelets perpendicular to permeant molecule path and (b) partially misaligned platelets. (c) A TEM image of a real epoxy PNC with misaligned morphology. Adapted with permission	82
Figure 1.22. (a) Schematic presentation of typical states possible, regarding the orientation of clay platelets and corresponding order parameter values. Adapted with permission. (b) Comparison between predictions for relative permeability of corresponding PNCs containing 5wt% MMT.....	83
Figure 1.23. Comparison between relative permeability predictions by different models, Nielsen, Cussler, and Gusev-Lusti for PNCs containing 5wt% MMT.....	84

- Figure 1.24.** Predictions for relative permeability of filled PNC to the unfilled matrix for two different hypothetical aspect ratios of clay, (a) 100 and (b) 1000.....85
- Figure 1.25.** OTR versus coating thickness of (a) SiO₂ and (b) SiN deposited through different plasma modes of (Δ) RF, (*) MW, (■) MW/RF, on 13 μm PET. Adapted with permission85
- Figure 1.26.** (a) The OTR values versus temperature for three different SiO_x-coated PET produced under different conditions and neat PET, which are discriminated on the basis of their OTR (in. cm³/(m².day.atm)) at 30°C: 0.18 (Δ), 1.6 (○), 16 (■), and 80 (PET, ▲). Arrhenius behavior is observed as the OTR values are fitted to the exponential solid lines. Adapted with permission. (b) In another system of SiO_x-coated PC, increasing barrier properties of the coated films resulted in the increased activation energy of permeation, with Arrhenius behavior. It implies occurring a change in permeation mechanism. Adapted with permission86
- Figure 1.27.** Schematic representation of suggested O₂ diffusion through SiO_x-coated PC. (a) Due to either very low thickness of the coating or its large pores, compared with the size of the oxygen molecule, the coating does not behave efficiently in impeding gas transport. (b) With either decrease in the size of pores down to lower than size of O₂ molecules or increasing their tortuosity, due to the increased coating's thickness, it behaves as a good barrier against gas molecules passing through. Adapted with permission. (c) OTR versus defect density for different coatings (○) SiN, (Δ) SiO₂, (◆) Al when the coating thickness is above its critical value (dc). Adapted with permission.....87
- Figure 1.28.** OTR of PET coated with LBL assembly of PEI (0.1wt% in solution) and MMT (0.2wt% in suspension) versus number of bilayers. Adapted with permission88
- Figure 1.29.** Schematic comparison between (a) tortuosity in dilute regimes ($\alpha\phi < 1$) modeled properly by Nielsen equation. (b) Tortuosity in semidilute regime $\alpha\phi > 1$ more suitably with Cussler Equation. Adapted with permission88
- Figure 1.30.** Lower experimental relative permeability (P_f/P_u) compared with predictions by Cussler model. Adapted with permission89
- Figure 1.31.** TEM micrographs of PNCs containing oxide paraffin compatibilizer with different components: (a) HDPE/20wt% low-viscosity paraffin/5wt% MMT, (b) LDPE-g-MA/20wt% low-viscosity paraffin/5wt% MMT, (c) LDPE-g-MA/20wt% high-viscosity paraffin/5wt% MMT. Reprinted with permission...89
- Figure 1.32.** (a) Relative permeability of three different gases, O₂, N₂, and CO₂, in LDPE nanocomposites versus weight fraction of MMT. The points are experimental data, and curves illustrate Nielsen predictions for presumed clay aspect ratio of 120. Adapted with permission. (b) Comparison between the experimental relative permeability of HNBR/FHT-EODA nanocomposites and corresponding predicted values by Nielsen and Bharadwaj models versus volume fraction of filler. Adapted with permission90

Figure 2.1.	The 2014 mass quantities (on a CO ₂ equivalent basis) of various polymeric materials employed in various food packaging functions in the U.S (adapted from Franklin Associates with permission).....	146
Figure 2.2.	(a) Oxygen barrier requirements for various food packaging at 23°C and (b) typical OTR values of commercially relevant polymer films measuring 100 μm thick at 23 °C as functions of the WVTR (adapted from Hanika et al. 2003 with permission from Wiley). Included here are ethylene vinyl alcohol (EVOH) with two different degrees of substitution, poly(vinylidene chloride) (PVDC), poly(ethylene naphthalate) (PEN), poly(ethylene terephthalate) (PET), nylon-6 (PA-6), unplasticized poly(vinyl chloride) (uPVC), plasticized poly(vinyl chloride) (pPVC), poly(lactic acid) (PLA), polycarbonate (PC), and polypropylene (PP). (c) The initial loss of CO ₂ from a PET bottle containing a carbonated soft drink measured at 24 °C and a gas pressure of 3 bar (adapted with permission from the Composite Agency).....	147
Figure 2.3.	A series of two- and three-dimensional AFM height images (top and bottom rows, respectively) acquired from SiO _x coatings varying in OTR (labeled) on PET substrates at 30°C (adapted from Erlat et al. 1999 with permission from the American Chemical Society).....	148
Figure 2.4.	(a) The sequence of events corresponding to ALD conducted over a single cycle using TMA as the reactive precursor to generate an Al ₂ O ₃ coating. (b) Thickness as a function of deposition cycle number for Al ₂ O ₃ coatings on PVA fibers and silicon wafers (labeled). The lines are linear regressions to the data. The inset is a TEM image of the coating (about 14 nm thick) on a PVA fiber (adapted from Peng et al. 2007 with permission from the American Chemical Society).....	149
Figure 2.5.	(a) The sequence of events corresponding to LBL deposition conducted with alternating immersions of the substrate in an aqueous poly(ethylene imine) (PEI) polycation solution and an aqueous MMT suspension. (b) Schematic illustration of the bilayers formed by LBL deposition onto a polymeric substrate. (c) Cross-sectional TEM image confirming the existence of numerous layers of clay platelets on the surface of a PS substrate (all adapted from Priolo et al. 2010a with permission from the American Chemical Society).....	150
Figure 2.6.	LBL coating thickness presented as a function of the number of (a) bilayers and (b) quadlayers for depositions employing either PEI alone or alternating immersions in PEI and poly(acrylic acid). The lines correspond to linear (a) and exponential (b) regressions of the data from Priolo et al. 2010a and 2010b, respectively.....	151
Figure 2.7.	(a) Schematic illustration showing the results of incorporating layered silicates into polymeric matrices to yield either phase-separated microcomposites or different types of nanocomposites (labeled), depending on the level of dispersion achieved (adapted from Galimberti 2012). (b) TEM image of a nanocomposite composed of dispersed clay platelets in a PP matrix. Here, A, B and C identify intercalated stacks, disordered intercalated tactoids and exfoliated platelets, respectively. A schematic representation of an intercalated	

- clay stack wherein parallel platelets are separated by PP chains (reproduced from Manias 2001 with permission from the Materials Research Society)..... 152
- Figure 2.8.** (a) Schematic diagram illustrating the diffusion pathway for a penetrant species through platelet-shaped nanoscale fillers embedded in a polymer matrix (adapted from Galimberti 2012). (b) Predictions of the relative permeability of PCNs as a function of plate concentration according to the Cussler model (Eq. 8) in which $\alpha = 100$ and μ is assigned discrete values (labeled) according to the spatial arrangements and platelet descriptions discussed in the text..... 153
- Figure 2.9.** (a) Graphical representations of three different orientations (labeled with the corresponding order parameter, S) that clay platelets can adopt in a PCN (adapted from Bharadwaj 2001 with permission from the American Chemical Society). (b) Predictions for the relative permeability of PCNs containing 5vol% clay as a function of the platelet aspect ratio for the three values of S (labeled) that are schematically depicted in (a)..... 154
- Figure 2.10.** (a) Arrhenius-type temperature dependence of the OTR of four SiO_x coatings (labeled) deposited by PECVD on PET substrates (reproduced from Erlat et al. 1999 with permission from the American Chemical Society). The regressed lines correspond to Eq. 11, and the resulting slopes yield the thermal activation energy, which is provided as a function of OTR for SiO_x coatings deposited on PC substrates in (b). The solid line serves as a guide for the eye, whereas the dashed line approximates the position of the abrupt change in slope (adapted from Erlat et al. 2000 with permission from the Materials Research Society)..... 155
- Figure 2.11.** A pair of TEM images collected from SiO_x coatings deposited by PECVD on PET substrates and varying in OTR (in cm³/m²-day-atm): (a) 0.52 and (b) 16. The enlargements of the boxed regions reveal the contiguity of the coatings, with interparticle pore defects clearly visible (adapted from Erlat et al. 1999 with permission from the American Chemical Society)..... 156
- Figure 2.12.** Schematic diagrams of molecular transport through (a) thin and (b) thick single-layer coatings illustrating the effect of defect size and shape (adapted from Erlat et al. 2000 with permission from the Materials Research Society). In (c), OTR values are provided as a function of defect density for three different single-layer coatings (labeled) measured above their critical thicknesses by da Silva Sobrinho et al. (2000). The solid lines are power-law regressions to the data and are provided as guides for the eye..... 157
- Figure 2.13.** Experimental relative permeability values of LBL multilayer coatings as a function of clay concentration, as well as corresponding predictions from the Cussler model (adapted from Priolo et al. 2011 with permission from the American Chemical Society)..... 158
- Figure 2.14.** (a) Relative permeabilities of O₂ and CO₂ (labeled) in LDPE PCNs as a function of MMT concentration. The solid line corresponds to predictions from the Nielsen model in which $\alpha = 120$ (adapted from Shah et al. 2006 with permission from Elsevier). (b) Relative permeability of O₂ in PCNs prepared from hydrogenated acrylonitrile butadiene rubber with predictions from the

original Nielsen model (solid line with $\alpha = 50$) and the Bharadwaj modification (dashed line with $\alpha = 50$ and $S = 0.92$) illustrating the marginal improvement achieved by adding the order parameter (adapted from Gatos & Karger-Kocsis 2007 with permission from Elsevier).....159

- Figure 3.1.** (a) Neat MMT (stack), where exchangeable Na^+ cations keep MMT platelets close to each other (0.2nm) in agglomerated stacks. (b) Exfoliated MMT in DIW, where only a few MMT platelets are in parallel order close to each other (almost stack) and water molecules diffuse in the space between platelets, negatively charged on the surface, and increases the size of d (basal planar spacing). (c) Deposition of negatively charged MMT layers, in DIW media, on the substrate film, already coated by positively-charged PE. (d,e) Intercalation of positively-charged PE chains in between negatively charged MMT platelets in a layer. (f) LBL deposited assemblies, with increased tortuosity in their nanobrick wall structure, and schematic of the tortuous path made in LBL assemblies against permeant molecules.....192
- Figure 3.2.** Cross-sectional image of 30-bilayer assemblies made from PEI solution (0.5wt%) and MMT suspension (1wt%), respectively, in different magnification scales, of (a)10,000X, (b)40,000X.(c) structural representation of branched PEI.....193
- Figure 3.3.** Cross-sectional image of 30-bilayer assemblies made from PEI solution and MMT suspension of (a) 0.5wt% and 5wt%, (b) 0.1wt% and 3wt%, (c) 10wt% and 3wt%, respectively.....194
- Figure 3.4.** Cross-sectional images of 20-bilayer assemblies made from PEI solution (0.5wt%) and MMT suspension (1wt%), respectively, in two different magnification scales of (a) 20,000X and (b) 50,000X. The gray sides on the right are PS substrate.....195
- Figure 3.5.** Cross-sectional image of 20-bilayer assemblies made from PEI solution and MMT suspension of (a) 0.5wt% and 3wt% (b) 0.1wt% and 1wt%, respectively. The left dark side is PS substrate.....196
- Figure 3.6.** (a), (b) Cross-sectional images of 30-bilayer assemblies made from PETi solution (0.5wt%) and MMT suspension (1wt%), respectively, at two different magnification scales. (c) The chemical representation of PETi.....197
- Figure 3.7.** Cross-sectional images of 30-bilayer assemblies made from PETi solution and MMT suspension of (a) 0.5wt% and 3wt%, (b) 0.5wt% and 5wt%, and (c) 10wt% and 1wt%, respectively.....198
- Figure 3.8.** XRD patterns for neat Na^+ MMT and 30-BL films made from varying MMT content in suspension of 0.1, 1, and 3 wt%, for constant (a) 0.1wt% , (b) 1wt%, and (c) 0.5wt% PEI solution in DIW.....199
- Figure 3.9.** XRD patterns for neat Na^+ MMT and 30-BL films made from varying MMT content in suspension of 0.1 and 1wt% for constant (a) 0.5wt% and (b) 10wt% PETi(S) solution in DIW.....200
- Figure 3.10.** A comparison of oxygen permeability and BIF values, for 5 times deposition of two type of BL coatings, containing interlayers of PEI and PETi (S) (both

0.5wt% in DIW), when the clay concentration varies from 0.1wt% to 5wt% in its suspensions. Lines are guides for eyes201

Figure 3.11. (a) Deposition of MMT layers, with positive charges on their edges, on a substrate film, already coated by negatively charged PE. (b) The intercalation of mobile chain segment of PE between clay galleries. (c,e) Laminar layout and (d,f) tilted layout of deposited clay platelets, in low and high concentrations of MMT in its suspensions, respectively.....202

Figure 4.1. Illustration of a layer-by-layer (LBL) coating applied as a gas barrier to the surface of a polymer substrate. Alternating cyclic deposition of a polyelectrolyte and nanoclay platelets generates a "nanobrick" morphology that greatly increases the tortuous pathway for diffusing molecules. The LBL coating depicted here possesses 5 polyelectrolyte/nanoclay bilayers (BLs).....223

Figure 4.2. Schematic of chemical structures of the two polyelectrolytes employed as adhesives in this study: polyethyleneimine (PEI) and poly(ethylene-terephthalate) ionomer (PETi).....224

Figure 4.3. Gas Cross-sectional transmission electron microscopy (TEM) image of an LBL coating deposited on PS and embedded in epoxy (to facilitate preparation). The coating was prepared with 30 BLs from a 0.5 wt% PEI aqueous solution and a 1.0 wt% MMT aqueous suspension.....225

Figure 4.4. Schematic depiction of the mechanism by which MMT nanoclay deposits onto PEI. Platelets with a negative face charge complex with the polycation and arrange themselves in a nearly surface-parallel orientation. The PEI molecules diffuse into the platelet galleries and promote intercalation.....226

Figure 4.5. Permeability Dependence of O₂ and CO₂ permeabilities (labeled) through a glassy SB film at 20°C on surface O₂ plasma treatment before and after the addition of an LBL coating consisting of 5 BLs prepared from 0.5 wt% PEI and 1.0 wt% MMT in DIW. The error bars denote the standard error in the data.....227

Figure 4.6. Permeabilities of O₂ (○) and CO₂ (Δ) through LBL-coated SB substrates at 20°C presented as a function of MMT concentration in aqueous suspension for 5 BL coatings fabricated from 0.5 wt% PEI (a) or PETi (b) in DIW. The lines serve to connect the data, and the error bars denote the standard error in the data.....228

Figure 4.7. Schematic depiction of the mechanism by which MMT nanoclay deposits onto PETi. Platelets with a positive edge charge complex with the polyanion and arrange themselves in a nearly surface-normal orientation. The PETi molecules diffuse into the edges of the platelet galleries and promote limited intercalation. At low MMT suspension concentrations, the platelets subsequently adopt a more surface-parallel orientation upon drying. At high concentrations, however, deposited platelets are crowded and retain a less-effective columnar morphology.....229

Figure 4.8. Permeabilities of O₂ (○) and CO₂ (Δ) through LBL-coated SB substrates at 20°C presented as a function of BL number for coatings produced from 1.0 wt%

	MMT and 0.5 wt% PEI (a) or PETi (b) in DIW. The lines serve to connect the data, and the error bars denote the standard error in the data.....	230
Figure 4.9.	Permeabilities of (a) O ₂ and (b) CO ₂ through LBL-coated SB substrates presented as a function of reciprocal temperature for 5 BL coatings fabricated from 3.0 wt% MMT and 0.5 wt% PEI (a) or PETi (b) in DIW. The lines represent regressions of Eq. 3 to the data, confirming that permeation through uncoated (□) and LBL-coated (PEI, ● ; PETi, ○) SB substrates exhibits Arrhenius behavior. Values of EP extracted from the slopes of the lines are provided in the text.....	231
Figure 5.1.	(a) Cross-section of a TEM image of a polymeric membrane coated with LBL assemblies of PEI and MMT. (b) Schematic of a polymer layer coated with LBL assemblies, the polymer nanocomposite (PNC) resulted after cyclic hot pressing and gas permeation route in them. (c) Chemical formulae of two alternative polyelectrolyte interlayers, PEI and PETi.....	254
Figure 5.2.	Optical microscope images of PNCs of PS* matrix, with PEI and MMT LBL assemblies, for (a) 10 times deposition of BL coating, after 25 cycles of melt pressing, and for 100 cycles pressing when the samples were coated with (b) 10, (c) 5, and (d) 15 times of BL depositions.....	255
Figure 5.3.	Optical microscope images of PNC of PS* matrix, with PETi and MMT LBL assemblies, for (a) 10 times deposition of BL coating, after 25 cycles of melt pressing, and for 100 cycles pressing when the samples were coated with (b) 10, (c) 5, and (d) 15 times of BL depositions.....	256
Figure 5.4.	Schematic Figures of LBL assemblies' portions in PNC and their typical morphologies: (a) face-face coagulated intercalation of expanded stacks, (b) face-edge and (c) edge-edge flocculated and exfoliated platelets or tactoids of a few platelets, beside their TEM images. (d) Schematic of overall dispersion and distribution of crunched LBL assemblies inside the polymeric matrix.....	257
Figure 5.5.	TEM micrographs of 100 cycles pressed PNCs containing PEI interlayers in their LBL assemblies portions comprising (a) 5, (b), (c), (d) 10, and (e) 15, -BL coatings.....	258
Figure 5.6.	TEM micrographs of PNCs containing PETi interlayers in their LBL assemblies portions comprising (a) 10BL coatings, pressed for 25cycles, and (b), (c) 100 cycles; (d) 5BL coatings, (e) 15BL coatings, both pressed for 100 cycles.....	259
Figure 5.7.	XRD patterns for neat MMT, its LBL assemblies coating with PEI, and melt processed PNC with (a) different numbers of pressing cycles of 25 and 100 and (b) different numbers of deposited BL's coatings of 5, 10, and 15.....	260
Figure 5.8.	XRD patterns for neat MMT, its LBL assemblies coating with PETi, and melt processed PNC with (a) different numbers of pressing cycles of 25 and 100 and (b) different numbers of deposited BLs coatings of 5, 10, and 15.....	261
Figure 6.1.	(a) Cross-section of a TEM image of a polymeric membrane coated with LBL assemblies of PEI and MMT. (b) Schematic of a polymer film coated with LBL assemblies, the polymer nanocomposite (PNC) resulted after cyclic hot pressing, and gas permeation route in them. (c) Detailed schematic of LBL	

	portions in PNC. (d) Chemical formulae of two alternative polyelectrolyte interlayers, PEI and PETi.....	293
Figure 6.2.	LBL portions in PNCs, processed through 100 cycle of melt pressing at 200°C, for LBL coatings deposited from 1wt% suspension of MMT and 0.5wt% solution in deionized water of alternative polyelectrolyte layers (a) PEI and (b) PETi.....	294
Figure 6.3.	TGA thermograms showing degradation behavior under air flow for: (a) Na ⁺ MMT, PS*, PEI, and PETi. (b) Na ⁺ MMT in comparison with three conventional organically-modified clays with alkyl ammonium (C30B is Na ⁺ MMT modified with methyl, tallow, bis-2-hydroxyethyl quaternary ammonium; C15A is Na ⁺ MMT modified with dimethyl, dehydrogenated tallow quaternary ammonium; C10A is Na ⁺ MMT modified with dimethyl, benzyl, hydrogenated tallow quaternary ammonium.). (c) Isothermal heating at 200°C of PEI, PETi, and PNC made from 10 bilayer deposition of PEI (0.5wt% in DIW) and MMT (1wt% in DIW) on PS* films, followed by melt pressing for 25 times at 150°C.....	295
Figure 6.4.	TGA thermograms showing degradation behavior under air flow for: (a) PNCs prepared from 10BL deposition of PEI (0.5wt% in DIW) and MMT (1wt% in DIW) on PS* films, followed by melt pressing for 25 and 100 cycles at 200°C. (b) PNCs prepared from 5, 10, 15BL deposition of PEI (0.5wt% in DIW) and MMT (1wt% in DIW) on PS* films, followed by melt pressing for 100 cycles at 200°C.....	296
Figure 6.5.	DSC plots depicting thermal properties glass transition and degradation temperatures (T _g , T _d) of two different interlayers studied PEI, PETi.....	297
Figure 6.6.	(a) Storage and (b) Loss modulus as a function of temperature for PS* and its PNCs made from 10BL deposition of PEI(0.5wt% in DIW) and MMT(1wt% in DIW), followed by 25 and 100 melt pressing cycles at 200°C.....	298
Figure 6.7.	(a) Storage and (b) Loss modulus as a function of temperature for PS* and its PNCs made from 5, 10, 15BL deposition of PEI(0.5wt% in DIW) and MMT(1wt% in DIW), followed by 100 melt pressing cycles at 200°C.....	299
Figure 6.8.	(a) Storage and (b) Loss modulus as a function of temperature for PS* and its PNCs made from the 10BL deposition of PETi(0.5wt% in DIW) and MMT (1wt% in DIW), followed by 25 and 100 melt pressing cycles at 200°C.....	300
Figure 6.9.	(a) Storage and (b) Loss modulus as a function of temperature for PS* and its PNCs made from 5, 10, 15BL deposition of PETi(0.5wt% in DIW) and MMT(1wt% in DIW), followed by 100 melt pressing cycles at 200°C.....	301
Figure 6.10.	Permeation values of oxygen and carbon dioxide at 20°C, in PS* and PNCs, comprising PEI and PETi interlayers, as a function of (a) number of melt pressing cycles, and (b) number of BL coating applied initially on PS* substrate.....	302
Figure 6.11.	Oxygen permeation as a function of MMT volume content, for our novel PNCs compared with theoretical modified Nielsen Model (Bharadwaj 2001) and literature results for PS-based PNCs, Na ⁺ MMT PNC, VDAC PNC,	

	C18DMB PNC (Nazarenko et al. 2007), and biaxially stretched PS-based PNCs (Huang et al. 2015). Lines between data points are guides for eyes.....	303
Figure 7.1.	(a) Cross-section of a TEM image of a polymeric membrane coated with LBL assemblies. (b) Schematic of a polymer layer coated with LBL assemblies, the polymer nanocomposite (PNC) resulted after cyclic hot pressing, with gas permeation route in them. (c) A detailed schematic of LBL portions in PNC. (d) Chemical formulae of PETi as macromolecular glue. (e) The chemical formula of PVAc used as the polymeric matrix.....	337
Figure 7.2.	Optical microscope images of PNC of PVAc with PETi and MMT LBL assemblies, for (a) 10 times deposition of BL coating, after 25 cycles of melt pressing, and for 100 cycles pressing when the samples were coated with (b) 10, (c) 5, and (d) 15 times of BL depositions.....	338
Figure 7.3.	TEM micrographs of 100 cycles pressed PNCs containing PEI interlayers in their LBL assemblies' portions comprising 10-BL coatings.....	339
Figure 7.4.	TEM micrographs of 25 cycles pressed PNCs containing PEI interlayers in their LBL assemblies' portions comprising 10-BL coatings.....	340
Figure 7.5.	TEM micrographs of 100 cycles pressed PNCs containing PETi interlayers in their LBL assemblies' portions comprising (a) 5, (b) and (c) 15-BL coatings...	341
Figure 7.6.	XRD patterns for neat MMT, its LBL assemblies coating with PETi, and melt processed PNC with (a) different numbers of pressing cycles of 25 and 100 and (b) different numbers of deposited BL coatings of 5, 10, and 15.....	342
Figure 7.7.	(a) Storage and (b) Loss Modulus as a function of temperature for PVAc and its PNCs made from 5, 10, 15BL deposition of PETi(0.5wt% in DIW) and MMT(1wt% in DIW), followed by 100 melt pressing cycles at 150°C.....	343
Figure 7.8.	(a) Storage and (b) Loss Modulus as a function of temperature for PVAc and its PNCs made from the 10BL deposition of PETi(0.5wt% in DIW) and MMT (1wt% in DIW), followed by 25 and 100 melt pressing cycles at 150°C.....	344
Figure 7.9.	Permeation values of oxygen and carbon dioxide at 20°C, in PVAc and PNCs, as a function of (a) the number of melt pressing cycles, and (b) the number of BL coating applied initially on PVAc substrate.....	345
Figure 8.1.	POM images of our innovative PNCs prepared after 25 melt pressing cycle at 260°C on PET films (thickness=100µm), already coated with 10BL deposition in PETi solution (0.5wt%) and MMT suspension (1wt%) in DIW.....	357
Figure 8.2.	TEM images of our novel PNCs prepared after 25 melt pressing cycle at 260°C on PET films (thickness=100µm), already coated with 10BL deposition in PETi solution (0.5wt%) and MMT suspension (1wt%) in DIW.....	358

CHAPTER 1

Investigating Improvement in Gas Barrier Properties of Polymer-Based Membranes through Different Coating and Nanocomposite Approaches

Abstract

Improving barrier properties of polymeric membranes has been a necessity, since their advent as alternatives for traditional packaging materials. This article tries to present a review of different coating and nanocomposite approaches to improve barrier properties of polymeric membranes against gases, mainly oxygen, while investigating their microscopic structures and making a comparison between them, along with explaining some barrier theories on polymer bulk modification approaches. In view of that, the article is commenced with investigating single coatings with metals and oxide metals, through techniques as sputtering, evaporation, chemical vapor deposition, and atomic layer deposition. Then, multilayer coatings, mainly layer-by-layer deposition and their advantages over single coatings are discussed. Afterward, different methods of preparing polymer nanocomposites, as the main bulk approach for improving barrier properties of polymeric membranes, and resulting microstructures are described, while different models for predicting the mechanism of barrier improvement in such nanocomposite membranes are discussed.

1.1. Introduction

Polymeric materials due to their lower weight and price (source materials and production) are gradually replacing traditional materials like metals and ceramics in everyday applications. Packaging application, especially for food products, is considered an important domain of

these usages. However, polymeric substitutes are inferior to those older opponents, in some features, including barrier properties. Thus, improving the barrier characteristics of polymeric membranes against gases and fluids, in order to improve the shelf life of the enwrapped products, has been an important goal for scientists and industrialists. One of the main approaches to improve such performance has been covering polymeric membranes with barrier coatings. Barrier coatings need to be quite thin to maintain enough flexibility against cracking [1–7]. Still, in many of applications, they need to result in almost one to two orders of magnitude improvement in barrier properties of polymeric substrate films, to keep up with requirements in concerned packaging applications [6,8]. Thus, assuming that such films would maintain thicknesses in the order of a few tens of nanometers (from about 10nm for atomic layer deposition (ALD) up to a few hundred nm for layer-by-layer (LBL) assemblies) as coatings, on a polymeric film substrate with the thickness of couples of hundred micrometers; they should roughly possess barrier properties about 4 to 5 order of magnitudes better than their polymeric substrates [1,8–15]. History of using the thin coating to improve barrier properties of polymeric membranes turns back to 1970s when vacuum metallization was used to evaporate a thin opaque layer of aluminum on polyester [8]. In fact, developing physical evaporation methods for coating in vacuum were considered as the most significant trend in barrier improvements of polymeric films for a few decades [6,8,9,16–21]. However, single coatings are prone to defects, which had adverse effects on their otherwise impermeable characteristics. Thus, other approaches, involving multilayers of coating emerged as alternatives, amongst which layer-by-layer deposition, due to its ease of processing, lower expenses, and environmentally friendly nature, considered as a real good substitute for single

barrier coatings [1,3,13–15,22–36]. Another new method, atomic layer deposition resulted in almost defect-free coatings with the highest ever barrier results in the thickness of only a few nanometers. They also showed superiority in the coating of 3-dimensional objects to other single coating methods [11,37–44]. Far from all of these coating methods, bulk modification approaches, such as polymer nanocomposites, despite their lower potential for barrier improvement, due to their very high flexibility, being free from typical problems of inorganic coatings like cracking and peeling, and also their ease of processing especially in large industrial scales, have always been sought by technologists and researchers as a serious alternative approach for barrier improvement in food packaging applications, on the basis of increasing the tortuosity of the polymeric matrix [36,45–64]. Accordingly, this review, despite reviewing various existing approaches, would mainly focus on LBL coating and polymer nanocomposites (PNCs), particularly polymer-clay nanocomposites (PCN), as approaches to improve barrier properties of polymeric membranes used in the packaging industry, and tries to provide a discursive comparison for their resulting barrier properties.

Packaging materials require high barrier properties, to protect the packaged contents against gases like oxygen [8]. According to the presented schematic photo, in order to satisfy the barrier properties needed for most of the food products, polymeric films, which due to their chemical inert nature are proper for contact with foods [4], for the typical thickness of 100 μ m should demonstrate oxygen transmission rate (OTR) of about 0.1 to 30 cm³/(m².day.bar) (presuming STP conditions). It can be seen that most of typical polymeric films, except for ethylene vinyl alcohol copolymer (EVOH) and liquid crystal polymers (LCP), show

permeation rates higher than $10 \text{ cm}^3/(\text{m}^2.\text{day}.\text{bar})$. Thus, despite being close to minimum needed requirements, further improvement in their barrier properties can result in extended shelf life of those products (Figures 1.1a and 1.1b, Table 1.1) [6,39]. Particularly, in the case of carbohydrate beverages, keeping carbon dioxide inside the bottle requires high barrier properties against this gas. In fact, PET bottles that are used nowadays as a substitution for traditional glass, despite benefits like holding less weight and costs, do not show competitive barrier properties. Thus, the shelf life of PET bottled beverages is noticeably shorter than glass bottled ones [50,65]. In fact, experimental measurements show that after only 4 hours first CO_2 molecules start to permeate through the polymeric membrane and finally by 2 years 90% of the gas exit the bottle (Figures 1.1c and 1.1d) [65]. Such escaping trend has resulted in the shelf life of almost 3-4 months for a PET bottled carbonated soft drink [66]. In addition, virgin PET replacement with recycled PET, which due to environmentally friendly policies has had an increasing trend, has exacerbated existing permeation problem [56,67]. So, to increase this time, for instance, about two times, and simultaneously decreasing the thickness of the film by about 30%, to keep up with the downward weight trend of PET bottles. Roughly estimating, in constant solubility, the diffusivity of packaging material against CO_2 , according to the following equation should increase at least more than four times, along with retaining enough mechanical strength against possibly occurring crashes and other stresses during their service time [68]

$$D = \frac{M_t^2 \cdot \pi \cdot l^2}{4 \cdot M_\infty^2 \cdot t} \quad (1)$$

where D , M_t , M_∞ , l , and t are diffusivity, absorbed mass by time t , absorbed mass in equilibrium, barrier thickness, and time t passed from the beginning of permeation (This

equation will be discussed later.) [69,70]. Therefore, to improve oxygen barrier properties of transparent plastic films in food packaging industries, many different coatings and nanocomposite approaches and technologies have been developed [1]. However, the problem is that the barrier properties are not as easily and precisely measurable as other physical and mechanical properties. In addition, interpretation of barrier properties is difficult because they are related to the complicated relation between the permeant molecule and polymer membrane structure. It becomes even more difficult in coated polymers and polymer nanocomposites, as other parameters like interphase properties and interaction of individual components should be considered too. Because of these difficulties and complication, progress on investigating barrier properties of existing approaches has been much less than progress on developing and commercializing those approaches themselves [8,71,72].

1.2. Different Coating Methods for Improving Barrier Properties

One of the main methods to improve barrier properties of various polymeric membranes against gas is covering with thin ultra-barrier coatings. These coating approaches, on the basis of the number of layers deposited on the polymeric substrate in coating approaches, can be categorized into two major groups of single-layer and multilayers.

1.2.1. Single-Layer Coating

Single-layer coating for plastics, based on the material type, are separated into metal coatings that are opaque, and oxides of metals and ceramics that are, differently, transparent to optical light. Metals as the coating for plastic substrates have been used since early 1970's in food packaging. For instance, aluminized polyethylene terephthalate (PET) and polypropylene

(PP) have been widely used in snack food and beverage packaging. Other important applications of metalized plastics include packaging of pharmaceuticals and sensitive electronic components. Such vacuum-metalized plastics are mainly made through evaporation and deposition of a, 10-100 nm thick, single aluminum (Al) film on a moving polymeric substrate through a roll-to-roll configuration inside a large vacuum chamber [73]. Thus, they resulted in improvement in barrier properties of polymeric substrates. For instance, OTR of a 13 μm PET by applying a thin (20nm) Al coating at 25°C, decreases from about 100 $\text{cm}^3(\text{STP})/(\text{m}^2.\text{day}.\text{atm})$ to 1 [8,74].

The key towards developing a good adhesion between Al coating and polymeric substrates is in forming covalent bonds between them (Al-O-C) while hydrogen bonding part is negligible. Examples are thermal evaporation of Mg, Si, and Cu [75,76] on PET that form covalent complexes of M-O-C, mainly with the carboxylic group of PET. In some of them like Al, these covalent bonds form automatically, but in some others like Cu, pretreatment of PET surface with plasma is required to increase the number of polar groups and surface energy of the polymer substrate [21]. The problem with these metalized films is that they are opaque, and their recycling is not easy [73]. In addition to the aesthetic value of a transparent coating for food packaging, many of those plastics used in food packaging are transparent to microwave and are considered microwaveable e.g. LDPE, HDPE, and PP. Therefore, they need a transparent barrier coating to remain microwaveable [77]. The answer to that objection was using oxide metals. Transparent but barrier nature of metal oxides and nitrides like SiO_x , AlO_x , Si_3N_4 , TiO_x in packaging makes the food product viewable and microwaveable. In addition, such transparent packagings, due to easier recycling, pose less environmental problems.

However, problems with metal oxides and nitrides are that they are dielectric and with extremely high melting points, so their high rate vacuum deposition is so difficult, whereas, polymeric substrates require deposition process to be performed at temperatures below 100°C [73,78]. The other advantage of transparent oxide metal coatings, compared with metals, is that they provide higher barrier properties. For instance, transparent silicon oxide (SiO_x), due to the tight interstitial spacing of its crystal lattices and holding a proper thermal stability over a wide temperature range, provides excellent barrier properties, like oxygen diffusivity in the range of 10^{-5} to 10^{-9} cm^2/s . In fact, due to the very high barrier properties of metal oxides, gases like oxygen can only permeate through the defects existing in the coating. Accordingly, barrier properties of these barrier films strongly depend on the density of defects (their number and size) occurred during fabrication of metal oxide coating, and these are dependent on intrinsic properties of the metal oxide, related to its chemical composition [18,21]. Transparent coating with metal oxide and nitride, applied through methods of evaporation (thermal or electron beam), sputtering, chemical vapor deposition (CVD) decrease the oxygen permeation of polymeric substrates by about 2 orders of magnitude [5,6,8,10–12,16–19,21,79].

1.2.1.1. Evaporation

Evaporation is a physical vapor deposition (PVD) coating method that is divided into thermal and electron beam-assisted methods. The name evaporation involves equity of the material in source and resulting deposited film. The evaporation method is performed on the scale of molecular flow dimension; in other words, the distance between source and substrate is less than the mean free path of gas molecule species. As a result of thermal heating or

electron beam (e-beam) bombardment of the source material, its molecules get enough energy to leave the source and after traveling through the evacuated chamber deposit and condense on the target surface [19]. Thermal or ordinary evaporation method has been done successfully for many different systems [4]. However, when materials with higher melting points like metal oxide are used as the coating, the evaporation technique is assisted by e-beam e.g. e-beam evaporation of silica (SiO_2) when a slight partial pressure of oxygen exists [4,8]. Figure 1.2a shows a schematic drawing of a continuous e-beam evaporation chamber. It can be seen that the transparent polymeric film substrate in the form of a roll is continuously fed to the chamber, to form a uniform barrier coating on it. The film can be any commercial polymer, oriented or not oriented with the thickness range of 3-400 micron, and can be pretreated by corona discharge, plasma, flame and other treatment techniques. All the system is positioned in a chamber, evacuated to 1.316×10^{-7} - 1.316×10^{-9} atm by a vacuum pump. All the film has been wound on the feed roller, 1, and is unrolled continuously to feed a cooling roller, 4, via a dancer roller, 2, and an expander roller, 3. While rolling on the cooling roller, the magnesium oxide vapor contacts film and condenses on its surface, forming a thin film. On the other side, the sintered, high-density source material (e.g. magnesium oxide) is placed in the source evaporation vessel (Crucible), 5, and by applying e-beam, is heated and evaporated towards cooling roller, 4, to deposit on the film there. Then coated film is rolled on a roller [20].

1.2.1.2. Sputtering

In the sputtering coating, which is especially proper for materials with high melting points like metal oxides and nitrides [6], the source material is bombarded by a plasma discharge.

Thus, source molecules or atoms are sputtered as vapor from the surface and hit the substrate surface that are either deposited on it or reflected from it [80]. Due to existing many controlling parameters in sputtering method, like plasma gas pressure and plasma pressure, compared with evaporation; the film properties can be manipulated appropriately in this method [16]. Furthermore, in sputtering, a uniform film can be deposited on a larger area, and a wider choice of source materials can be used with this technique. In addition, sputtering only needs a low vacuum that is easy to reach. Besides, its coating makes a better adhesion to the substrate, and it is easily possible for even high melting point materials. Also, due to being water-cooled no hot point occurs in sputtering that is proper for polymers with low thermal resistance [18,81].

1.2.1.3. Chemical Vapor Deposition (CVD)

In chemical vapor deposition, in the vapor phase, molecules containing metal move from the source to the substrate. However, coating procedure through CVD includes steps different from PVD. First, gaseous source transports to the substrate through convection. Then, source material diffuses in the region close to the substrate. Afterward, the material is absorbed on the substrate surface. Finally, it reacts with the surface, and some gaseous products are released and desorbed from the surface. In fact, CVD has been mostly used for depositing amorphous Si obtained from the silane (SiH_4) source while SiO_2 from silane and in the presence of O_2 . Thermal and plasma-enhanced CVD (PECVD) are two types of CVD, between which thermal one, due to depositing metals or oxide metals, at very high temperatures can degrade polymers [8]. In PECVD, plasma is used to activate the precursor at lower temperatures. In fact, the activation energy needed for the reaction between the gaseous source materials absorbed on

the substrate surface and the substrate is provided by a plasma source. PECVD is done through either of microwave (MW) excited plasma or radio frequency (RF) plasma or both of them together [5,10,12,79]. As a matter of fact, MW excited plasma, provides better fragmentation of the gas phase and a higher degree of ionization, thus, it offers a higher deposition rate than RF plasma. Differently, RF plasma, involves plasma excitation at lower frequencies, and controls the energy and the flux of the ions bombarding the cathode better. Thus, for a polymeric substrate that due to their low glassy transition temperature (T_g) cannot stand increasing their temperature more than a few tens of degrees above ambient temperature, this feature of RF plasma is actually beneficial. Another variation is dual-frequency (RF and MW simultaneously), which uses combined advantages of both plasma frequencies. Therefore, it offers high deposition rates and separately controlled hitting by energetic ions. Typically, PECVD components according to the following schematic figure include microwave generator, synchronous motor driven feed and uptake rolls, water-cooled RF bias electrodes, and rotary vacuum pump (Figure 1.2b) [79].

1.2.1.4. Atomic Layer Deposition (ALD)

Atomic layer deposition for the first time was invented by Suntola (1977) with the name Atomic layer epitaxy (ALE) for depositing zinc sulfide (ZnS) coating on corning glass at 320°C. However, for the first time in 2003 ALD was applied for polymers to deposit Al_2O_3 (as a nucleating base layer) and then titanium nitride (TiN) on a polymeric compound, SiLK (an organic compound produced by Dow Chemical Company and with a dielectric constant of $k=2.65$) [37,82].

In vacuum condition, two subsequent evaporated single elements at sufficiently high temperatures react alternately with the surface and deposit on it in atomic layers. First, the A gaseous precursor reacts with the surface species and changes the surface chemistry, through depositing an atomic element. Then, the B gaseous precursor reacts with new surface species to deposit the second atomic element and to make the surface chemical species similar to original one, which is proper for reaction with A precursor. Such bilayer deposition cycle can be repeated until achieving to the required thickness of the coating [11,40,41,82].

In effect, ALD has been mostly investigated for depositing Al_2O_3 coatings [11,39–41]. Amongst different chemical precursors trimethylaluminum (TMA) and water have been used more for polymers, due to their deposition process that can occur at lower temperatures, typically 120°C (temperature range of $100\text{--}175^\circ\text{C}$) [11,39]. In fact, other common precursors of Al_2O_3 , like TMA with ozone and aluminum trichloride (AlCl_3) with water have high deposition temperatures (above 350°C), which can be destructive for most polymers [83].

1.2.1.5. Self-Limiting Feature of ALD

ALD has a self-limiting feature that results in extremely thin and uniform films. In fact, initially one type of gaseous precursors, react with active sites available on the substrate surface and deposits on it (dose mode). Then the excessive gaseous precursors are removed from the system by purging with an inert gas (purge mode) and second gaseous precursor enters the chamber. Such separation of two precursors with inert gas avoids any chance of the reaction between them in the gaseous phase; that otherwise would form the layer with a gradient of two precursors concentrations, decreasing coating uniformity, like in CVD. Also, in the deposition

step of each type of gaseous precursors, as they are under their decomposition temperature, they only react with active sites on the substrate, instead of with already chemically absorbed precursors of their own types. Then, once all active sites of the substrate reacted, the surface saturates and coating thickness remains constant that shows the self-limiting feature of ALD (Figure 1.3) [42,43,83].

1.2.1.6. Comparing ALD with PVD and CVD

Since, ALD is deposited through reaction (like CVD), not through physical hitting the substrate with source materials and the subsequent condensation, it does not have the sight line limitation. So it can be coated on 3-D substrates (like CVD) [83,84]. On the other hand, although ALD has similarities with binary reaction CVD, where the coating product is the result of the reaction between two reactants, in this process, those reactants are deposited and reacted individually and subsequently, divided by alternating purging of the substrate with an inert gas. So, ALD can be considered a cyclic procedure instead [42]. As a result of separating its precursors by an inert gas, they do not react with each other in the gaseous phase. This results in the coating with higher uniformity than CVD coatings [43,83,84].

1.2.1.7. Typical ALD Examples

The ALD of almost defect-free Al_2O_3 coatings (with precursors TMA ($\text{Al}(\text{CH}_3)_3$) and water) can be done at temperatures as low as 30°C (It is typically done in 120°C , and with changing this temperature, as mentioned above, some deviation in growth rate is resulted.), which is proper for thermally sensitive nature of many polymers [39]. ALD is usually done in a hot-wall flow reactor chamber (equipped with a loading port) containing nitrogen flow of 100

standard cubic cm per minute (sccm), at a pressure of 1.316×10^{-3} atm, with exposure of polymeric substrates taped to Si wafers to trimethylaluminum (TMA) and water. Typically, for an ALD coating cycle like this at 120°C, a prerinsed polymeric substrate is exposed to TMA (0.1s), nitrogen gas purge at 100sccm (30s), water (0.15s), and again nitrogen (30s), respectively. Thus, the growth rate for Al₂O₃ is about 1.2-1.3 Å/cycle [11,39].

1.2.1.8. Nucleation and Growth Mechanism in ALD

In the case of the prevalence of active sites on the polymeric substrate, like hydroxide groups for the system of TMA and water, TMA reacts with it as mentioned above. Otherwise, for many polymers, such as PE, in the lack of such active sites on their surface, TMA, initially diffuses into the region near to the polymer surface. Then, after purging with inert gas, during subsequent dosing, water reacts with TMA, forming hydroxide aluminum (AlOH*) species, which can react with the TMA in the next dosing step. Accordingly, other cycles are done, as mentioned previously. Thus, the clusters gradually grow and aggregate to form a continuous Al₂O₃ film on the polymeric substrate, that prevents subsequent reactant molecules from diffusion into the polymer close to surface area, instead, they deposit and grow linearly on the already deposited ALD film. Finally, after a few tens of ALD cycles (e.g. 40 cycles) a thin layer of Al₂O₃ forms on the polymer substrate [38,85].

1.2.1.9. ALD Challenges

As mentioned before, most polymers have glassy transition and threshold of degradation temperature at about 100°C, so their ALD should be done below 100°C to avoid any problems [38]. Therefore, due to the requirement for higher temperatures by many basic ALD systems,

their applications on polymeric substrates were not possible [42]. Thus, from one side it was tried to use ALD systems with lower processing temperatures, like TMA and water with typical processing window of 100-175°C for Al₂O₃ ALD (It also was done successfully for PP, PS at 85°C [38,43]), or Tungsten (W) ALD, with processing range of 30-325°C, from which lower temperatures are used for polymers [11,40,41]. Moreover, from the other side, polymers with higher thermal stability, like polyimide (PI) or polyethylene naphthalate (PEN), are mainly used for ALD [11,41]. Also, for ALD coating, polymeric substrates need to have proper chemical functional groups, like –OH or NH₂, to react with gaseous precursors and initiate ALD. In fact, organometal precursors, such as TMA, need to react with a metal hydroxyl group MOH* in the first ALD cycle to start nucleation. Then, such precursor reacts with water or NH₃ in the next step to form oxide or nitride of the metal, respectively [42]. Nevertheless, as mentioned above, their nucleation and growth is possible in polymers without such active sites. All in all, ALD has been successfully experienced on many polymers including PI, PEN, PET, PS, PP, PMMA, and PE [11,38–41]. Films with higher porosities and free volumes, like PP, PMMA, and PE are supposed to have higher TMA sorption. In contrast, PVC and then PS with least porosity and free volume show the least TMA sorption. In the case of PS, although permeation of TMA into the near surface region is less than for PE, PP, and PMMA, after TMA exposure the surface retains the TMA and does not lose it. However, PMMA and PP do lose a major fraction of TMA, following its exposure. For PMMA, this lack of retention is mainly due to the polar nature of its carbonyl groups that results in a low solubility for nonpolar TMA. In contrast, PE and benzene, which are so hydrophobic and nonpolar would dissolve TMA properly [38].

1.2.2. Multilayer Coating

Due to existing defects in single-layer coatings deposited by methods such as PVD and CVD, they provide less barrier improvement, for their substrates, than the value expected from the bulk of those metal oxides (e.g. SiO_x and AlO_x). This problem raised the motivation for investigating the alternating deposition of multilayers of organics and inorganics, as an alternative method for enhancing barrier properties of polymeric membranes [6,73].

1.2.2.1. Polymer Multilayer/Oxide Metal/Polymer Multilayer Coating

In this multilayer coating method, the polymer substrate is coated with an assembly of a few alternating polymer and ceramic layers, through methods like polymer multilayer (PML), sputtering and evaporation. For instance, initially monomers are vacuum flash-evaporated and condensed on the substrate. Then, this liquid layer is solidified through being cured by ultraviolet (UV) or e-beam; such process is called PML. Subsequently, a metal oxide layer is deposited on polymeric layer, through sputtering or evaporation approaches, followed by another polymeric coating deposition through PML technic. In fact, the first polymeric coating increases the smoothness of substrate to decrease the risk of pinhole formation in further deposited oxide layer. Also, the external polymeric layer covers the oxide layer, protecting it against stresses applied during subsequent handlings. However, despite decreasing the number and size of the defects formed in this sandwich structure, it cannot eliminate the risk of previously mentioned defect formations. In addition, polymeric coating deposition, used in these sandwich structures, is itself a complicated technic that involves subsequent vacuum evaporation and curing of monomers into solid polymeric layers. Some of the examples of

these barrier structures have been developed to be used as packaging for electrical appliances such as organic light emitting diodes (OLED) and photovoltaic cells [1–3,25].

1.2.2.2. Layer-by-Layer (LBL) Deposition

Layer-by-layer (LBL) deposition, which is a technology for making multifunctional thin films, is done by alternate immersion of a polar (or charged) substrate in oppositely charged aqueous solutions. Compared with the above-mentioned sandwich structure, LBL has more layers with lower thicknesses. Depending on the components' molecular weight [67], their chemistry [1,13,36], ionic strength [14], and pH [14], the structure of LBL assembly and its properties would vary. For instance, the thickness of each two different layers, called bilayer (BL), can vary in the range of a few nm to a few hundreds of nm [1].

A very simple and practical example of LBL approach is making multilayer thin films by putting different components in one-dimensional order. The main concept of making such nanostructured films is through forming monolayers on a water surface and then depositing on a solid substrate that is called Langmuir-Blodgett (LB) technique. In fact, Blodgett and Langmuir, for the first time, made assemblies of various stearates, containing thousands of nanoscale (24 Å) thin films [86]. Then, Kuhn used this technique for the first time for the organic components in 1971 [87]. However, the main problem with LB technique is in the frequent rearrangement of deposited layers due to lack of firm spatial constraints and the limited choice of molecular components that are suitable for this technique [88]. Later, stable LBL assemblies were initiated by Iler who constructed multilayer thin films through alternating deposition of colloidal particles, such as silica and alumina [22], which were

positively and negatively charged, respectively (Figure 1.4). Afterward, Decher actually developed the field of LBL deposition in the 1990s [88–92]. Indeed, he and his coworkers invented layer-by-layer (LBL) deposition technique by electrostatic interactions that can use a very wide range of different components. They started with alternating deposition of anionic and cationic bipolar amphiphiles [90] and then developed it by using only polyelectrolytes [89]. Then, gradually other components like functional polymers, biological nanoparticles, and inorganic nanoparticles were practiced. Although initially LBL coatings were used only for planar substrates, further developments made deposition on small nonplanar surfaces possible. For instance, Keller et al. deposited multilayers of two polycations (redox polymers) and anionic inorganic exfoliated sheets of zirconium phosphate on high surface area silica [23].

1.2.2.3. Variation of Existing Driving Forces in LBL

Although nowadays electrostatic interaction is widely considered as the main driving force for making LBL assemblies, other practical approaches include: hydrogen bridging [28,29,31,34,35], covalent bonds [28], hydrophobic interactions [26,30], coordination interactions [31], and complementary post-chemical reactions [31]. Any actual interaction between different constructing components can result in a multilayer film. In fact, a simple test before deposition, showing the possibility of multilayer formation between some components, in case they are soluble in the same media, is seeing if flocculation occurs when they are mixed in the same media with each other. Nevertheless, forming multilayer can still be possible even if they do not aggregate together [88]. As mentioned above, LBL assembly is mainly made

through electrostatic interactions between its oppositely charged (species) alternating components [91].

In order to assemble a multilayer thin film through electrostatic force, the components should be soluble in water and so make electrostatically charged species in water [31]. Generally, LBL assembly on the basis of the electrostatic interaction between polyanions and polycations is divided into three main methods: In the first or primary method both alternating polyions are linear molecules that stack on each other. In other words, they are oppositely charged polymers that make a polyelectrolyte multilayer (PEM) [89]. The second type of electrostatically-driven LBL assembly employs charged particles, such as globular proteins, which are deposited alternately on linear polyions [30,35]. Finally, in the last method mentioned charged particles are replaced with charged plates, like delaminated montmorillonite (MMT) (Figure 1.5) [1,13,14,24,30,36]. This latter group turned up to demonstrate great barrier properties. In fact, from this particular method, using clays like MMT and polyelectrolytes like polyethyleneimine and polyacrylamide, membranes with extremely high barrier properties were made that with deposition of a few tens of them on polymeric substrates, like PET, oxygen transmission rates (OTR) values lower than detection limit of sensitive permeation detectors like MOCON OX-TRAN $<0.005 \text{ cm}^3/(\text{m}^2.\text{day.atm})$ were achieved [13–15,33].

1.2.2.4. Different LBL Deposition Techniques

The first method for making LBL assembly from oppositely charged polyelectrolytes in 1992 was through dipping, and still it is the main method of fabricating such multilayer films

[1,13,15,36]. However, alternative approaches such as deposition by spraying, initiated by Schlenoff [93], and spin-coating aided deposition [35] are investigated as well, where both have two main benefits of using less solution for coating a larger substrate and higher speed of coating. Nevertheless, controversy exists in the literature on what really is the best method, which in fact, is mainly dependent on the special type of desired application [94].

Dipping method is on the basis of alternating immersion of the substrate in aqueous polycation and polyanion solutions. Accordingly, the substrate needs to have some excess surficial charge, like glass or silicon substrate, to interact with polyelectrolyte layers, or be pretreated with methods like plasma or corona treatments. The other approach for improving the interaction between the substrate and the thin layers is through using glue-type interlayers such as polyelectrolyte of branched polyethyleneimine (PEI) [1,13–15]. For hydrophobic polymer substrates using both surface treatment technic like plasma treatment and glue-type interlayers give even better results [36]. One major problem with dipping method is its time-consuming nature, as in each immersion cycle, a few minutes time is needed for completion of adsorption. Also, dipping has an unfortunate potential for cross contamination between different solutions. Thus it requires proper subsequent rinsing steps. On the other hand, one main benefit of dipping compared with spraying and spin-coating is the less material waste [94], although by recycling the sprayed step its waste can be decreased as well [93]. For instance, in a typical LBL procedure through dipping (Figure 1.6a), after immersing the substrate in the polyelectrolyte solution for a predetermined time and then rinsing with deionized water (DIW) and drying with filtrated air, the substrate is immersed in the clay suspension in DIW followed by rinsing in DIW and drying with filtered air. The subsequent

steps are repeated similarly to reach to a desired number of bilayers. In addition, in some studies, the dipping procedure has been performed automatically with a home-built robotic system [1,13–15,36].

In the second deposition method for dipping that was introduced by Schlenoff, solutions are sprayed to the substrate, typically twice in each step with short intervals. The main advantage of this method is in decreasing exposure time by a factor of 100 compared with dipping, due to a higher throughput of LBL fabrication, which is more significant for large areas. The structure and many properties of made multilayers are almost similar to the one made by dipping, when the deposition time is kept constant [27,93]. In fact, sprayed multilayers are stratified correctly, and usually show less interfacial and surface roughness and thinner assemblies, compared with dipped ones [27].

The other LBL approach is spin-assisted (SA) LBL Coating. This approach was initially used as a drying step for dipping deposition, where, due to the applied shear rate, swelling of the next layer. Hence the roughness of the assembly decreases to improve its surface quality. In addition, this technic results in increased speed of LBL deposition. The spinning substrate was used for the first time to deposit PEM of PEI and poly[1-[4-(3-carboxy-4-hydroxyphenyl-azo)benzenesulfonamido]-1,2-ethanediyl, sodium salt] (PAZO), by Chiarelli [95–97]. Also, due to relatively strong nature of LBL assemblies formed, in this method evenly charged layers can be used as well [95].

1.2.2.5. Different LBL Growth Regimes

Based on the speed of thickness increase for the assembly, with the number of layers increase, LBL growth rates are categorized in three groups of linear, superlinear, and supralinear. This categorization does not necessarily mean that other types of growth are not possible. In fact, the reason for this limitation of growth types is the restriction of the types of polyelectrolytes already investigated. Nevertheless, in the case of using completely different polyelectrolytes, other types of growth, like two successive linear growths are possible [28]. Linear growth usually occurs in low ionic strength and at low temperatures [28], as the linear growth of PEM of poly[styrene-4-sulfonate] (PSS) and poly[allylamine hydrochloride] (PAH), after passing the first 15 layers [94], and linear growth for PEI, MMT LBL films (Figure 1.7a) [13–15]. Superlinear growth often occurs in high ionic strength and at high temperature, and it is mainly exponential, due to the possibility of one of the components (polyelectrolytes) to diffuse freely through the whole film [28]. For instance, in quadlayers (QLs) of PEI, polyacrylic acid (PAA), PEI, MMT, different from LBL assemblies of PEI and MMT that showed linear thickness growth by layer increase, the rate of growth is exponential, reaching quickly to the thickness of 174nm only after 6 QL deposition. This high growth rate is probably due to interdiffusion of PE's layers, during deposition, (Figure 1.7b) [33].

1.2.2.6. Key benefits of LBL Deposition

Compared with other traditional thin films, LBL is easier to be produced, as it is processed under ambient conditions. In addition, as the media for the solution is usually water, the risk of environmental problems, which are usually posed by chemical solutions, is cleared [36].

Accordingly, LBL deposition is a very low-cost and environmentally friendly technique, capable of using many different components from small organic and inorganic molecules to various polymers and colloids, in order to reach to nanoscale assemblies, with the high level of complexity in the structure, to offer desired properties. From the nanoscale particles and tubes to huge macroscale substrate, nearly every substrate that its surface is accessible by solvent can be used for LBL deposition [88]. The other important feature of LBL assemblies is that after depositing more than a few layers, they show nearly identical properties independent from the substrate surface properties. Hence, it is possible to analyze their structure and physicochemical properties by depositing them on some even surfaces, like silicon wafers, for investigations, such as thickness measurement and atomic force microscopy (AFM), instead of coating on their main substrates like textiles or polymeric sheets [1,13,15,24,30].

In traditional compounding approaches, due to the small entropic driving force of polymer chains for making homogeneous mixing, reaching to homogeneity in the incorporation of small molecules in polymers only in small fractions is possible, and consistent blending of polymers, even in low fractions, seems challenging [98,99]. Differently in LBL, strong electrostatic attraction between charged groups of alternating polymeric layers forms stable multivalent ionic complexes and makes their molecular level blending possible. Furthermore, precise controlling of the relative composition that is not feasible for traditional blends becomes easy in LBL multilayers, through pH and ionic strength manipulations [29].

1.2.2.7. Existing Challenges and Developments in LBL Deposition

Theoretically, LBL deposition is possible on any surface with repetitive deposition of the solution and rinsing with water procedures; differently, it is not always the case in practice. In fact, although LBL deposition on the macroscopic object is a straightforward operation with an easy procedure; in order to coat micro and nanoscale objects, it is required that the depositing material would be flexible enough that can make adequate bonding with the surface of the substrate, despite existing geometrical constraints. Thus, to coat micro and nanoscale objects, they need to make contact with oppositely charged solution of macromolecules to provide a proper condition for occurring flocculated bridges. This innovation was initially demonstrated by Keller and Mallouk 1995, through onion-shaped LBL deposition of redox-active component on SiO₂ particles (Figure 1.8) [23].

1.2.2.8. Morphology of LBL Assemblies

The high level of orientation and exfoliation seen in transmission electron microscopy (TEM) images and tightly packing observed in AFM is the unique feature of the LBL structures, due to their self-assembling and self-terminating growth mechanisms. In fact, owing to the strong electrostatic attraction of positively-charged PEI, negatively charged clay platelets are absorbed mainly oriented with their largest dimension parallel to the surface of the film. Thus, a highly laminar, oriented and tightly packed structure of highly exfoliated clay platelets layers is constructed to result in both very high barrier and optical properties, which are not achievable with any other method of direct mixing of polymers and clays (Figure 1.6b) [33,36].

1.3. Polymer Nanocomposites (PNCs)

Aforementioned, coating methods, despite improving the barrier properties of polymers, hold certain drawbacks for many industrial applications: They are vulnerable to occurring defects by stresses applied during service life [2,4–6,8,12,18,21,73,79,100]. In addition, there always exists the possibility of their peeling from the substrate. Furthermore, coated substrates cannot be processed by conventional processing techniques such as extrusion and injection molding. These are the problems that can be removed through the isotropic bulk modification approach of polymer nanocomposites [36,51,52,56,61,62,68,101–103]. Moreover, many of the recycled polymers, like recycled PET, which due to environmental reasons have had increasing industrial applications in the recent decades, undergo several chain scissions during recycling, which decreases their melt strength and worsens their processability through many of industrial processing approaches like blow molding or flat-die extrusion. Thus, the inclusion of interactive and well-dispersed clay particles can increase melt viscosity of polymers and improve their processability [58,59,64,103–109]. Therefore, PNCs are considered as an important approach to improve barrier properties of polymeric materials, along with a few other of its physical-mechanical properties, in different packaging applications [36,45–60,62,64].

1.3.1. Background of PNCs

By decreasing the size of composites dispersed phase particles down to nanometer range, a drastic increase in interfacial contact, much more than commercial composites, is resulted [62,110]. By the way of example, if the smallest dimensions of the dispersed phase, particulate,

fibrous (like single and multiwalled carbon nanotubes; SWCNTs, MWCNTs, respectively), or layered decrease from micron-scale to the nanoscale, the surface-to-volume ratio would increase by 3 orders of magnitude (Figure 1.9), resulting in dramatic change in interfacial properties of their composite [61,111,112]. For instance, barrier properties of nanocomposites of clay and polymers, due to the very high aspect ratio of nanoscale layered silicate fillers, increase significantly, through the evident increase in permeant path distance [62,111]. The other main difference between nano and microcomposites is the lower required concentration of the dispersed phase in the former one. In fact, higher efficiency of nanoparticles provides the opportunity for gaining modified properties like higher barrier properties, higher flame resistance, and higher mechanical properties in low levels of loading, which is the key towards less weight, compared with conventional microcomposites [112]. In addition, due to tiny size of nanoparticles, transparency of the base polymer is maintained, that along with holding a low density and high barrier properties mentioned above makes PNCs appropriate choices in the packaging industry, particularly for food products [62,72,110]. In fact, from about 1 billion dollars market of PNCs in 2012, about 32% was used in packaging applications. Amongst PNCs polymer layered silicate nanocomposites (PSLNs), or in other words polymer-clay nanocomposites (PCNs), comprising about 50% of PNC market [113], initially introduced in 1987 by Okada from Toyota research lab, due to availability of clay and its nontoxicity, are one of the most popular ones [62,64]. In fact, PCNs, according to a definition, are the hybrid mixture of organic polymers and inorganic silicate layers, in which the layered silicate fillers are dispersed in a way that at least in one dimension are less than 100nm [64,110,114]. One of the main reasons for great attention on PCNs is the superior features of layered clays. The

platelets of clay in the exfoliated condition hold a thickness of a few nanometers, which due to planar dimensions of about 150nm, result in a very high aspect ratio for them. Silicate layers are considered nontoxic with the classification of “generally regarded as safe” (GRAS), by FDA (Food and Drug Administration), and can be used in many applications like food packaging. They have a high modulus of 180GPa, and due to the refractive index close to polymers make transparent PNCs. So, these PCNs with good optical properties can be used as clear packaging in food and pharmaceutical industries. Furthermore, due to the high aspect ratio of clay platelets, fabricated PCNs have a real potential to make a tortuous network and improve barrier properties, consequently, even superior to other PNCs, made with spherical particles or carbon nanotubes. In addition to all these advantages, they are naturally made by mother nature and widely available [61,62,64]. On account of these superiorities, this article focuses on different features of PCNs amongst all PNCs.

1.3.2. Three Types of Polymer-Clay Composites

Generally, composites of polymer matrix and layered silicate clay filler based on the degree of mixing between two phases are categorized into three groups (Figure 1.10a) [63,111]. If the attractive force between clay platelets would be too strong or shear of mixing would not be high enough, polymer chains cannot diffuse between interlayer spaces of clay platelets. Hence, the level of mixing would be low, in a way that unaltered layered silicate aggregates make a separate phase in the polymeric matrix. Therefore, regarding the size of the layered silicates, these composites are considered as conventional macro or microcomposites. The microcomposites lack significant improvement in properties with a slight content of clay,

different from nanoscale composites. In the higher level of mixing between two phases, polymer chains diffuse between platelets of silicate and increase their basal planar spacing, without disorienting their parallel alignment. These are called intercalated polymer-clay nanocomposites, where their crystallographic regularity is repeated within distances of a few nanometers, independent of the clay content. Finally, if the polymer chains intercalate between clay platelets and thoroughly overcome their electrostatic interactions, they completely delaminate into near-monolayer platelets far from each other, with a nanoscale range of thickness and without any initially aligned arrangement, and form exfoliated PCNs, where the average distance between clay platelets depends on their content. This latter type of PCNs, due to holding superior properties, had been much more attracted by scientists [45,63,101,105,110,111].

In reality, both exfoliated and intercalated morphologies exist together in a nanocomposite, and assessment as either exfoliated or intercalated is on the basis of the qualitatively higher value of each of those microstructures. For instance, the figure below depicts the existence of both (A) intercalated parallel clay platelets being separated by 2-3nm of PP and (C) exfoliated disordered platelets, each containing up to about 3 nano-sheets of clay, separated by more than 10 nm of PP matrix. In fact, for an organically-modified MMT (OMMT) exfoliated nanocomposite with PP, in the presence of PP-g-MA as the compatibilizer, the mean thickness and diameter of OMMT were obtained about 3nm and 200nm, respectively. In addition, a third intermediate state (B) exists, in which the polymer intercalation between clay platelets has increased in a way to divide them further from each other and in a disordered way, but still it cannot be considered as a complete exfoliation (Figure 1.10b) [36,115,116].

1.3.3. Montmorillonite (MMT)

Inorganic silicates used for PNCs are usually layered aluminosilicates (montmorillonite, mica, vermiculite,...), amongst which montmorillonite (MMT), due to having a good surface area, as a result of its high aspect ratio, high cation exchange capacity, and proper surface reactivity is one the most popular clays for use with polymers [101,110,111]. Aluminosilicates are schematically composed of layers of metal oxide octahedral sandwiched between two silica tetrahedral layers. The metal in the middle layer is usually aluminum (Al), so, these clays are called aluminosilicates. Now, as a result of isomorphic substitutions, replacing silicon ions (Si^{4+}) in tetrahedral and Al^{3+} in octahedral with e.g. Al^{3+} , and magnesium ion (Mg^{2+}), respectively, in this uncharged layered aluminosilicates that are called pyrophyllite, negative charges are induced on the surface of their sheets that are in counterbalance with positively-charged alkali and alkali earth cations, mainly sodium (Na), located between layers. These latter ones are called montmorillonite, which their layers are stuck together firmly by mentioned attraction between counterions [64,111]. As each layer has a thickness of about 1nm, and the lateral dimension of them is from 30nm up to a few microns, the average aspect ratios up to 1000 are theoretically accepted. However, due to breakage of MMT platelets during mixing procedure, its effective aspect ratio is something between 30 and 300 [111,117]. The strong electrostatic force between adjacent platelets, with such high aspect ratios that have a distance of only about 0.3nm, makes reaching to the high level of exfoliation of nanoscale platelets so difficult, and demands high shear environments (Figure 1.11) [64,111,118].

1.3.3.1. Organic Modification of MMT

In order to be more compatible with hydrophobic polymers, such highly hydrophilic clay surfaces with high surface energies need to be organically modified to increase their hydrophobicity. Accordingly, after swelling the MMT in water and somewhat delaminating its platelets, the inorganic surface cations are replaced by organic cations such as alkylammonium, to make MMT layers more hydrophobic, and decrease their surface energy. Thus, it makes them compatible with polymers. In this manner, long-chained alkyl ammonium, through increasing the interlayer distance in MMT increases its exfoliation as well [64,101,118]. Accordingly, in the figure below from left to right with increasing the length of alkyl chains, clay interlayer spacing increases (Figure 1.12) [118]. Although, traditionally, quaternary ammonium ion is used for organic modification of clay platelets and promoting exfoliation, resulting in barrier properties improvement, they are not approved as GRAS, by FDA [64]. Moreover, due to the low thermal stability of such organo-modified clays, and the high processing temperature of many engineering polymers like PET, problem of thermal degradation occurs for the PCNs that rules out their usage in food packaging and other clean applications (Figure 1.13) [67,119–121].

1.3.4. Preparation Methods of Polymer-Clay Nanocomposites

On the basis of the practiced starting materials and processes, the methods for synthesizing PCNs through polymer intercalation can be classified into three groups of solution mixing, in-situ polymerization, and melt compounding methods.

1.3.4.1. Solution Mixing Method

In this technique, the media is a solvent, in which the clay layers and polymer chains are swellable and soluble, respectively. Initially, the clay layers are swollen in a media like water or toluene. Then the polymer is solved in the solvent and replaces the clay interlayer solvent. Thus, upon removal of solvent, intercalated structure of polymer-clay nanocomposite remains. In fact, solvent works as the reaction medium and decreases the viscosity of the polymer to intercalate easier amongst already swollen clay particles [64,101,111,115,122–125].

1.3.4.2. In-Situ Polymerization Method

In this approach, first liquid or solved monomers conform a medium, in which silicate layers can be swelled and intercalated. Then, polymerization produces polymers within intercalated clay platelets [101,111,115,117,126–129]. In this method that initially was used for nylon and MMT [111], the problem with intercalating large polymer macromolecules between clay layers does not exist [115]. For instance, polymerization of ϵ -caprolactone, diffused between clay platelets, with heating Cr^{3+} -exchanged fluorohectorite to 100C, resulted in an intercalated PNC (Figure 1.14) [130]. Also, another example was polymerization of methyl methacrylate (MMA) and styrene (St) with each of initiators benzoyl peroxide (BPO) and azobis(isobutyronitrile) (AIBN), diffused in between organically-modified MMT (Cloisite2A), a dimethyl dehydrogenated tallow ammonium MMT, clay platelets [54].

1.3.4.3. Melt Compounding Method

Initially, a polymer is mixed with the organically-modified clay, with higher interlayer spacing than natural MMT, and then the mixture is annealed above the polymer's softening

point. Major advantages of this method are, its compatibility with the industrial procedures such as extrusion, especially in a twin-screw extruder (TSE) and injection molding, its environmentally friendly nature, in the absence of an organic solution, and also a wider range of polymers that can be used [36,67,121,131–135]. By the way of example, melt intercalation of PS and Cloisite 2A in co-rotating TSE (L/D=40, d=27mm), with the screw speed of 90rpm and barrel temperature of 200°C, can be mentioned [54]. Although organic surface modification of clay by ammonium-based chemicals results in materials with low thermal stabilities that begin to degrade at about 200°C, the temperature needed for melting of many polymers [67,121,132,133,135,136], and despite typically lower dispersion resulted from melt blending, compared with solution method [62,137]; this method of direct intercalation and exfoliation of clay platelets with polymers, due to the advantages mentioned above, as the only method with a real potential to be used in large industrial scale [62,113] has recently become more popular, and is considered as the standard way of fabricating PCNs.

1.3.4.4. Combinative Methods

In reality, the categorization mentioned above is not strict, and above methods can be combined to provide better results. For instance, in the case of nylon6, which due to holding polar groups makes a better interaction with clay, water can assist synthesis of intercalated and exfoliated PCNs, through melt mixing of the polymer and natural Na⁺MMT, that otherwise in the absence of water, would require organically modification of MMT [138]. Differently, for nonpolar PP, extrusion of PP-MA, being aided by water, with untreated Na⁺MMT does not result in a significant intercalation. Nevertheless, using organically-modified MMT instead,

results in intercalated and exfoliated PNCs, depended on applied shear in co-rotating TSE. In fact, it is believed that water improves the exfoliation through increasing the distance between clay platelets and dispersing them, and promoting interaction between polymer and clay through hydrolyzing MA, which then its carboxylic group does esterification reaction with the hydroxyl group of OMMT [139]. Ammala et al. also reached to exfoliated PCNs for different natural and organically-modified clays from a combinative method. In fact, they mixed the clays in water and, using a PET ionomer as a dispersant, stabilized clay exfoliation. Then they mechanically mixed the aqueous exfoliated clay suspension with PET, while the water was driven off by the heat of the process [140]. In another approach, first a high clay content (about 20wt%) PNC composite (masterbatch) was made by a shear device, preferably TSE. The masterbatch itself could be made through in-situ polymerization of styrene monomer, diffused between OMMT platelets. In the next step, by adding more resin with the same shear machine, the concentration of clay decreased [126]. Also, PP-g-MA with OMMT (15%) through melt mixing in a twin-screw extruder in the presence of water made a masterbatch, which then was diluted with pure PP. This two-step procedure made PNCs with better exfoliation compared with one- step similar extrusion of PP-g-MA and OMMT [98,139]. In another attempt by Shah et al., first the high clay content masterbatch was made through melt mixing of OMMT with nylon6, with high molecular weight (Mw), which has a better potential for making exfoliated PCN than its type with lower Mw. Then, in the second step, the dilution was done by melt mixing of the masterbatch with lower Mw of nylon6, which compared with the alternative, with higher Mw, provides a lower melt viscosity and so better processability through commercial equipment, like injection molding [53]. In our study, LBL coating of a styrenic

polymer, polyvinyl acetate (PVAc), and polyethylene terephthalate (PET), by alternating layers of polyethylene terephthalate ionomer and Na⁺MMT was followed by repetitive melt pressing of coated samples to crush the clay platelets into the polymeric matrices. Where, the resulted PNCs showed swollen intercalated and flocculated morphologies with noticeably increased gas barrier and mechanical properties [36].

1.3.5. Morphology of PNC, a Measure of Exfoliation

One of the most important features of PNCs is the quality of dispersion and exfoliation of nanoparticles in the polymeric matrix that has a significant role in determining physical, mechanical, and more important for this research, barrier properties of PNCs. Thus, investigating their morphology through microscopic techniques is very important.

1.3.5.1. Microscopic Investigations

Development of nanocomposites has been done in parallel with developing microscopic techniques; for the reason that, understanding their nanoscale structure and their morphology have been possible only through developing high-resolution microscopic techniques like scanning electron microscopy (SEM), transmission electron microscopy (TEM), and atomic force microscopy (AFM) [112]. Due to the higher resolution of the prepared images, TEM is the main microscopic technique used to investigate the dispersion and exfoliation of nanoparticle inside the matrix [112]. As it usually has a higher resolution than SEM (typically 0.2nm, compared with 2nm) and shows inside the bulk, instead of the topography of the surface [36,106]. Also compared with x-ray diffractometry (XRD) that only measures the interplanar spacing in ordered, intercalated or immiscible systems, TEM can qualitatively assess any type

of possible morphologies of PNCs, including disordered, intercalated and exfoliated, ones [61,141]. In the TEM image of PCNs, clay platelets are observed as dark lines in the lighter polymeric matrix (Figure 1.10b) [59,64,116].

1.3.5.2. Influence of the Polarity of the Polymer on Exfoliation

Typically, polymers that have polar groups make better interactions with hydrophilic clay and have a better potential for exfoliation. PA6, from which the first intercalated PNC was made by Toyota research labs [49,53,114] and PET [36,140] are good examples for this claim. In contrast, polymers that are nonpolar like aliphatic polymers, due to making weaker interactions with clay, have a lower potential for exfoliation, e.g. PP-g-MA [58]. Thus, many of them even in presence of organic modification of clay and or using compatibilizers like maleic anhydride (MA), particularly when melt mixing method is chosen, only make intercalated PNCs, like PS-co-MA [108]. Nevertheless, cases of exfoliation for PNCs of aliphatic polymers have been reported, too (e.g. PE-g-MA) [108].

1.4. Transport via Membranes

1.4.1. Permeability and its Measurement by Pressure-Decay Tools

Permeation of a fluid through a homogeneous media is a three-step process, including adsorption of the fluid into the first side of the media, its diffusion through the media, and finally desorption from the opposite side of the media, with the lower partial pressure of the fluid [6,8]. Permeability or permeation coefficient (P), as the main variable for evaluating permeability of a media against a gas or fluid, according to definition is:

$$P = \frac{(\text{amount of gas under a stated condition}).(\text{membrane thickness})}{(\text{membrane area}).(\text{time}).(\text{driving pressure})} \quad (2)$$

and one typical unit for permeation coefficient, Barrer, is [142]:

$$\frac{10^{-10}(\text{cm}^3 \text{ at STP}).\text{cm}}{\text{cm}^2.\text{s}.\text{cm Hg}} = 1 \text{ Barrer} \quad (3)$$

where STP is standard temperature (0°C) and pressure (1.013bar) condition [6].

After fabricating a polymeric film, which can be through solution casting and subsequent vacuum drying, permeability is obtained by measuring the pressure drop after passing gas through a polymeric film, by apparatus like permeation cell [36,143]. So, the gas permeability is measured by the constant-volume, variable-pressure unit, shown in the schematic Figure 1.15a. Therefore, using the membrane, the permeation cell is divided into upstream and downstream sides. The downstream side volume is determined, and the pressure in downstream is measured by a pressure transducer [143–144].

After the evacuation of the entire system, the upstream side of the cell is charged by a gas within constant pressure. Thus, due to permeation of the gas through the membrane, downstream pressure increases. Although, initially downside pressure increases nonlinearly with time ($\frac{dP}{dt}$), by reaching the concentration profile into steady-state condition, downstream pressure shows linear increase with time (Figure 1.15b). Hence, the permeability can be calculated from this equation:

$$P = \frac{VL}{ART\Delta P} \frac{dP}{dt} \quad (4)$$

where V , L , A , R , ΔP , are the downstream volume, membrane thickness, membrane exposure area, universal gas constant, the difference between constant upstream and initial downstream pressures [143,144].

1.4.2. Sorption and Solubility

Measuring the quantity of fluid adsorbed in a media or particularly polymer membrane is a major method to obtain barrier properties. In order to obtain sorption and solubility, the weighing method is the most usual method, due to being both direct and simple. Amongst a few existing gravimetric tools for measuring sorption, magnetic suspension balance (MSB), due to isolating balance from the sample chamber, can measure the sorption at very high fluid pressures temperatures [69,70,146–150].

1.4.3. Diffusivity and its Measurement by Fick's Law through a Sorption Test

Diffusivity of gas in a polymeric sample, which is a measure of the speed of diffusion, is the squared distance that fluid passes through the sample divided by time unit and is usually obtained by Fick's Law. Before reaching to the equilibrium sorption, a non-steady condition exists, where the concentration of the gas in the sample increases towards its equilibrium value at steady-state condition. Fick's 2nd law models the kinetic of sorption during this unsteady condition [151].

$$\frac{dC}{dt} = - \left(\frac{d\phi_x}{dx} + \frac{d\phi_y}{dy} + \frac{d\phi_z}{dz} \right);$$

$$\phi_i = -D_i \left(\frac{dC}{dz} \right) \quad (5)$$

Now for one-dimensional flux (only ϕ_x) and in constant D , independent of C , or Fickian diffusion we have [69,70,146,147,151,152].

$$\frac{dC}{dt} = D \left(\frac{d^2C}{dx^2} \right) \quad (6)$$

In such film, the boundary conditions can be defined as:

B.C.:

$$C = C_0 \quad \text{for } 0 < x < l, t = 0,$$

$$\partial C / \partial x = 0 \quad \text{for } x = l, t = 0,$$

$$C = C_1 \quad \text{for } x = 0, t = 0$$

where C_0 is the initial gas concentration inside the film, C_1 is the initial gas concentration on the film surface, l is the film thickness, $x=0$ is the surface of the sample exposed to the gas, and $x=l$ is the sealed surface of the sample. So, the above-mentioned simplified differential equation can be solved by Laplace transform or by separation of variables [142,152]

$$\frac{C_t - C_0}{C_1 - C_0} = 1 - \frac{4}{\pi} \sum_{n=0}^{\infty} \frac{(-1)^n}{2n+1} \exp\left(\frac{-D(2n+1)^2 \pi^2 t}{4l^2}\right) \cos\left(\frac{(2n+1)\pi x}{2l}\right) \quad (7)$$

where C_t is the gas concentration at time t .

Then, by integrating over film thickness l , we have [142,146,147]

$$\frac{M_t - M_0}{M_{\infty} - M_0} = 1 - \frac{8}{\pi^2} \sum_{n=0}^{\infty} \frac{1}{(2n+1)^2} \exp\left[\frac{-(2n+1)^2 \pi^2 D t}{4l^2}\right] \quad (8)$$

M_t denotes the total amount of diffusing substance that has entered the sheet at time t , and M_{∞} the corresponding quantity after infinite time, and M_0 gas absorbed in the film at $t=0$.

Then, assuming no gas existed in film in the beginning $M_t=0$ [142,152]

$$\frac{M_t}{M_\infty} = 1 - \frac{8}{\pi^2} \sum_{n=0}^{\infty} \frac{1}{(2n+1)^2} \exp\left[-\frac{(2n+1)^2 \pi^2 D t}{4l^2}\right] \quad (9)$$

For small times, this solution is simplified to

$$\frac{M_t}{M_\infty} = 2 \left(\frac{D t}{l^2}\right)^{\frac{1}{2}} \left(\frac{1}{\pi^2} + 2 \sum_{n=0}^{\infty} (-1)^n \operatorname{ierfc} \frac{n l}{(D t)^{\frac{1}{2}}}\right) \quad (10)$$

Both M_t and M_∞ can be measured with sorption balance as mentioned before in solubility

section. This equation for $\frac{\Delta M_t}{\Delta M_\infty} < 0.5$, which occurs in early time of sorption, can be

approximated as [69,70]

$$\frac{M_t}{M_\infty} = \frac{2}{\pi} \left(\frac{D t}{l^2}\right)^{\frac{1}{2}} \quad (11)$$

Then, by plotting the $\frac{M_t}{M_\infty}$ vs. $t^{1/2}$, initial slope = $\frac{2}{l} \left(\frac{D}{\pi}\right)^{\frac{1}{2}}$ is measured [69,70].

$$D = \frac{\pi l^2 (\text{Initial Slope})^2}{4} \quad (12)$$

For Fickian diffusion assumption, the slope of $\frac{M_t}{M_\infty}$ vs. $t^{1/2}$ remains constant until $\frac{M_t}{M_\infty} = 0.5$, then it decreases towards zero in equilibrium [153].

1.4.4. Theories of Barrier Properties in PNCs

When impermeable particles exist inside the permeable polymeric matrix, the diffusing molecule should turn around those particles. So, assuming many of these impermeable particles, a tortuous path is formed inside the membrane that affects its barrier properties. Several scientists tried to model such behavior, through different methods and by considering different assumptions.

1.4.4.1. Maxwell's Model

In 1873, Maxwell derived a relationship to describe dielectric properties of a suspension of spheres that later was developed to predict permeability in a similar membrane containing impermeable spheres [144].

$$P_c = P_m \left(\frac{1 - \phi_f}{1 + \left(\frac{\phi_f}{2}\right)} \right) \quad (13)$$

where ϕ_f , P_c , and P_m are fillers volume fraction, composite permeability, and pure matrix permeability, respectively [144]. But, the Maxwell did not consider large aspect ratios that occur in PCN [154,155].

1.4.4.2. Nielsen's 2-Dimensional Model

Although the first model used for a tortuous path was made by Maxwell, Nielson for the first time developed a model for describing the barrier properties of polymers filled with high aspect ratio of platelets [154,155]. Accordingly, existing impermeable filler particles poses a long tortuous path for the diffusant to pass through. So, considering the term tortuosity factor, τ , as ratio of length of the diffusion path through the film to the film thickness, also assuming that volume fraction of polymer (ϕ_p) equals the fractional area of polymer in each cross-section of matrix; the relative permeability of filled polymer, P_f , to unfilled one, P_u , can be approximated from the equation [154]

$$\frac{P_f}{P_u} = \frac{\phi_p}{\tau} \quad (14)$$

In fact, this relation had been previously used by Klute et al. for estimating permeability of small molecules like water inside semicrystalline polymers [156]. Nevertheless, one problem

with this equation is that the reduction in permeant concentration as it passes around filler particle is ignored that makes the determined permeability higher than its real value. Nielsen assumed filler particles as rectangular or circular impermeable plates, uniformly and completely dispersed (gaining full exfoliation) and oriented parallel to the film surface to model permeation behavior of the composite. Also, he assumed minimal interaction between clay and polymer [64]. Such assumptions give the maximum path for the diffusant, or in other words, maximum possible tortuosity factor, τ , which can be approximated by this equation.

$$\tau = 1 + \left(\frac{L}{2W}\right) \phi_f \quad (15)$$

at which L , W , and ϕ_f are filler particle length, width (thickness), and volume fraction, respectively. Hence, combining two above equations, the equation for permeability would be

$$\frac{P_f}{P_u} = \frac{\phi_p}{1 + \left(\frac{L}{2W}\right) \phi_f} \quad (16)$$

and assuming aspect ratio as α :

$$\alpha = \frac{L}{2W} \quad (17)$$

thus [154]:

$$\frac{P_f}{P_u} = \frac{\phi_p}{1 + \alpha \phi_f} \quad (18)$$

Also, assuming $\phi_f \ll 1$, $\alpha \phi_f < 1$, the equation is more simplified to [157]

$$\frac{P_f}{P_u} = \frac{1}{1 + \alpha \phi_f} \quad (19)$$

It can be seen from the equation that effect of fillers in reducing permeation would be significant when the aspect ratio of the particle is high (Figure 1.16a). Also, it can be seen that if the platelets are considered only cubic ($L=W$), from the general relation of tortuosity and

Equation (14), Maxwell equation above is resulted. It demonstrates the correctness of general approximation made for τ (Figure 1.16b) [154]. In addition, assuming that the sorption is only done on amorphous polymer part Klute et al. concluded that the solubility coefficient of a semicrystalline polymer is solubility coefficient of amorphous component multiplied by amorphous fraction ratio. Similarly, it can be developed for amorphous polymer filled with impermeable particles.

$$\frac{S_f}{S_u} = \phi_p \quad (20)$$

Thus, assuming that the gas transport properties in polymer obey Fick and Henry rules [156]

$$P=D.S \quad (21)$$

So, modified Nielsen (by Fredrickson) is [155]

$$\frac{D_{||}}{D_u} = \frac{1}{1+\alpha\phi_f} \quad (22)$$

where $D_f = D_l$ and D_u are the diffusivities of PNC parallel to the sample surface and unfilled matrix, respectively. Also as the Nielsen model fit better for dilute regimes, where $\alpha\phi_f \ll 0$.

The equation can be approximated as [155]

$$\frac{D_f}{D_u} \approx 1 - \alpha\phi_f \quad (23)$$

1.4.4.3. Cussler's 3-Dimensional Model

In Nielsen model, the platelets are assumed with equal size and aspect ratio that are uniformly distributed in the polymeric matrix, which is not the case in reality. Thus, Cussler added a geometric factor, dependent on the geometric shape, size, shape irregularities, and level of positional disorder of clay platelets, to enter the effect of randomness in clay plate shapes and distribution in the equation. In fact, they assumed fully aligned and randomly

distributed, impermeable platelets with different aspect ratio (Figure 1.17a) [158]. Thus, they ended up with equation

$$\frac{J}{J_N} = 1 + \mu\alpha^2 \left(\frac{\phi_f^2}{1-\phi_f} \right) \quad (24)$$

for flux through a unit cell of area $2dW$, and with N barrier slits, J_N , respectively [158].

Similarly, this equation can be developed for permeability [1,14]

$$\frac{P_u}{P_f} = 1 + \mu\alpha^2 \left(\frac{\phi_f^2}{1-\phi_f} \right) \quad (25)$$

and considering the low content of the clay the equation can be simplified to

$$\frac{P_f}{P_u} = \frac{1}{1+\mu\alpha^2\phi_f^2} \quad (26)$$

This equation fits better to experimental data for the semidilute regime where $\phi_f \ll 1$ but $\alpha\phi_f > 1$ [157]. Similarly, for diffusivity, the modified Cussler Eq. is

$$\frac{D_{||}}{D_0} = \frac{1}{1+\mu\alpha\phi_f^2} \quad (27)$$

where μ is the geometric factor [155]. These following equations work properly for semidilute regimes where $\phi_f \ll 1$ and $\alpha\phi_f \gg 1$, but still for the dilute regime, where $\phi_f \ll 1$ and $\alpha\phi_f < 1$, they are simplified to Nielsen equations [14,155,157]. Geometric factor, which is dependent on the geometric shape, size, shape irregularities, and level of positional disorder of clay platelets, is not completely understood, but based on experimental results different values are estimated for it. In the case of periodic and ribbon-like flakes, which have lengths much higher than width, the value of μ is estimated as 1 (Figure 1.17b) [1,157].

On the other hand, for ribbon-like plates in random distribution (the equal probability of alignment and misalignment), the geometric factor is estimated as $\frac{1}{2}$, between complete

periodic distribution ($\mu=1$) and complete misalignment ($\mu=0$) [159]. Also, assuming the flakes as periodic hexagons, μ is estimated as $\frac{4}{9}$ (Figure 1.18) [15,157], and in the case of random hexagons, the estimated value is $\frac{2}{27}$. In addition, Fredrickson for randomly distributed disk-like platelets estimated the geometric factor as [155]

$$\mu = \frac{\pi^2}{16\ln^2\alpha} \quad (28)$$

Therefore, in reality that clay particle are between random ribbons and hexagons (or disks), the geometric factor should vary in range $\frac{2}{27}$ (or $\frac{\pi^2}{16\ln^2\alpha}$) to $\frac{1}{2}$ [159,160]. Also, it was understood that polydispersity of size of platelets does not pose a significant influence on geometrical factor obtained for identical ones [157]. Accordingly, comparing the relative permeability graphs for different geometric factors, it can be seen that with increasing the value of geometric factor, the efficiency of clays in decreasing the permeability of the fluid through the composite increases (Figure 1.19).

1.4.4.4. Gusev-Lusti Model

They simulated a 3D computer model of 25 aligned and randomly distributed identical round shape clay platelets, without any overlapping, inside an isotropic matrix, with Mont Carlo simulation, while the volume fraction of platelets and their aspect ratio varied in the range 0.01-0.05 and 1-400, respectively (Figure 1.20a) [161]. In view of that, direct finite element (FE) calculations for permeability was done, to predict permeation decrease with clay inclusion. In conclusion, a master curve depicting reduction of the total permeability, influenced by both clay geometric factor and molecular level transformation in the matrix was

generated (Figure 1.20b). The individual points in the figure above are numerical solutions for P (in the varying range of 0.01-0.05 for volume fraction, f , and 1-400 for aspect ratio, a). Furthermore, through a least square fit for such points the following equation is resulted.

$$\frac{P_f}{P_u} = \exp \left[- \left(\frac{x}{x_0} \right)^\beta \right] \quad (29)$$

at which x_0 and β are, 3.47 and 0.71, respectively, and $x = \alpha \cdot \phi$. To sum up, through finite element method (FEM) calculations, Gusev-Lusti 2001 models have shown that for a permeant that diffuses perpendicularly to the direction of aligned platelets, the rate of transmission decreases exponentially as a function of the product of aspect ratio and volume fraction of clay particles [161]. However, some practical problems occur with all models explained above: First, they assume complete alignment of the filler platelets, whereas in reality dependent on the intensity of shear along compounding flow direction; they have complete misalignment or partial alignment (Figure 1.21). Moreover, they assume complete exfoliation of clay platelets in nanoscale that is not the case in real experience [72].

1.4.4.5. Bharadwaj's Model (Modified Nielsen)

As mentioned above, one reason for the deviation between experimental relative permeability and Nielsen model roots back in its assumption that all clay platelets are oriented horizontally, which is usually not the case. Therefore, Bharadwaj 2001 modified the Nielsen model by adding an order parameter to address such deviation.

$$\frac{P_f}{P_u} = \frac{\phi_p}{1 + \left(\frac{L}{2W} \right) \phi_f \left(\frac{2}{3} \right) \left(S + \frac{1}{2} \right)} \quad (30)$$

In fact, as the complete orientation of clay platelets in PNC, parallel to the surface, seems impossible, in the modified equation, Bharadwaj added an order parameter $S=1/2(3\cos^2 \theta-1)$. Where θ is the angle between vectors P (perpendicular to the clay surface) and n (normal to the PNC sample). When all the clay particles are horizontally oriented ($\theta=0^\circ$), the S gets the value 1 and equation equals Nielsen's, and in the case of the pure polymer the value of $S = -\frac{1}{2}$ is assumed. That is like all stacks oriented vertically or $\theta=90^\circ$. In addition, with decreasing the clay platelets alignment, efficiency of clay particles in decreasing the permeability of the fluid in PNC decreases (Figure 1.22) [162,163].

1.4.5. Comparison between Different Models Predictions for MMT

For a typical PNC, containing 5wt% MMT clay, with average aspect ratio of 100[111,114,164] and density of 2.35 g/cm³ [165], the resulted relative permeability predicted by models of Nielsen[154], Cussler[158], assuming MMT as periodically distributed hexagonal with $\mu=\frac{4}{9}$ [1,14], and Gusev-Lusti [161], are 0.31, 0.33, and 0.49, respectively. In other words, barrier improvement factor predicted by those models are 3.2, 3.0, and 2.0, respectively (Figure 1.23). According to these models, in the case of existing a good interaction between the polymer matrix and clay or its attached compatibilizers (e.g. alkyl ammonium, PEI, PET ionomer), and strong enough shear stress is applied, resulting in high level of clay exfoliation in PNC; about 2-3 times decrease in permeability is achievable. Also, comparing predictions of different models for PNC of MMT, the existing differences are somewhat because those models are either tuned to fit the experimental results or are derived by certain approximations [161].

Relating only Nielsen and Cussler results, it can be concluded that, although in dilute regime reduction in permeability is proportional to $\phi\alpha$, which was the case in Nielsen model, in semidilute one; in less dilute regimes the rate of reduction in permeability shows a higher sensitivity to the loading and aspect ratio of clay, and it is proportional to $\phi\alpha^2$ [155,157]. Accordingly, with increasing the aspect ratio (Figure 1.23) and MMT content (Figure 1.24), Cussler model shows a sharper decrease in permeability than Nielsen. Overall, amongst the three models, Gusev-Lusti seems the most comprehensive one, as in both dilute and semidilute regimes predicts permeability values close to Nielsen and Cussler, respectively. In addition, according to different permeation models mentioned, PNCs show diminishing points of return for clay content, above which their barrier properties do not continue to improve significantly. Also, these models show that with increasing the aspect ratio of clay particles from 100 (MMT) to 1000, the diminishing point of return decreases from about 9wt% to almost 2-3wt% [64].

1.5. Barrier Improvement Results in Literature and Concerned Discussions

1.5.1. Sputtering

A good example of reactive sputtering was deposition of AlO_xN_y (aluminum oxy nitride) on PET by medium frequency (40kHz) alternative current (AC) magnetron sputtering with a commercial Al source (target). In fact, N_2 was used as the main reactive gas and argon (Ar) as its background (Table 2) [18]. Thus, as a result of the low density of defect in the barrier film, the intrinsic property of AlO_xN_y , OTR of $1\text{cm}^3/(\text{m}^2\cdot\text{day}\cdot\text{atm})$ at 0%RH, 30°C was achieved [18].

1.5.2. Evaporation

Nonpolar polymers like PP, due to lack of polar group on their surface, show less adhesion with inorganic coating compared with polar polymers like PET. Thus plasma treatment is needed to provide such polar groups on their surface, e.g. evaporation of Al on biaxially oriented PP (BOPP). Otherwise, due to lack of interaction, the inorganic coating cannot increase the substrate barrier properties significantly [6,19]. A good comparative example is e-beam evaporation of aluminum oxide on PET and PP. In fact, in the equal coating thickness of 10nm, while in the case of PET more than 20 times decrease in permeability of oxygen was resulted, for the PP no significant change was observed. This difference is referred to the interaction made between carbonyl group of PET and aluminum oxide that promotes the nucleation and growth of the inorganic film on the substrate, which is not the case for PP substrate (Table 3) [19].

1.5.3. PECVD

PECVD of silicon dioxide (SiO_2) and silicon nitride (SiN) from gaseous sources of hexamethyl disiloxane (HMDSO) with O_2 , and SiH_4 with NH_3 , respectively, on a 13 micron biaxially oriented PET, in Ar gas, was done, resulted in coatings with the thickness range $8\text{nm} < d < 200\text{nm}$. Thus, OTR of $0.5 \text{ cm}^3/(\text{m}^2.\text{day})$ was reached, when the coating thickness exceeded critical value of $d_c=15\text{nm}$ for SiO_2 and 8nm for SiN (Figure 1.25). It means that resulting coatings similarly improved barrier resistance of the coated film by about 1000 times for O_2 . However, examined SiN showed less critical thickness (d_c) than commercially used SiO_2 [79]. Also, tetramethoxysilane (TMOS)/ O_2 mixture was used as the monomer (precursor),

for synthesizing and depositing SiO_x coating on PET through RF-PECVD, and demonstrated its suitability. In fact, they reached to OTR of 0.1 cm³/(m².day.atm) for the coated PET and permeability coefficient of 1.4E-17 cm³.cm/(cm².s.cm Hg) for the merely SiO_x coating, in their best conditions[10]. Furthermore, in other study two different organosilane monomers, hexamethyldisiloxane (HMDSO) and trimethylsilane monomers were used, but the resulted barrier properties for the SiO_x-coated PET was not significantly different from that of other PECVD coatings [12]. In another study PECVD of SiO_x on PET was done, by using hexamethyldisiloxane (HMDSO) and trimethylsilane monomers. Thus, it was concluded that using two different organosilane monomers does not change the barrier properties of the coating [12].

1.5.3.1. Relation between Permeability and Temperature in PECVD Coated Films

Ideally, permeation rate of non-interacting gases (e.g. O₂, N₂, and almost CO₂) through a silicon oxide glass or polymeric membrane below its glass transition, obeys the Arrhenius equation (with increasing Temperature, OTR exponentially increases.)

$$\Pi = \Pi_0 \exp(-\Delta G^\ddagger / RT) \quad (31)$$

where ΔG^\ddagger , R, T, and Π_0 are thermal activation energy, universal gas constant, absolute temperature, and permeation rate at 0°K, respectively [5,12,100]. Now, if the Arrhenius equation fits the permeation data for the SiO_x-coated PET as well, it can be used to investigate permeation mechanism in those coated films (Figure 1.26a). Accordingly, by fitting the Arrhenius equation for the permeation data of the coated films, the activation energy for permeation, ΔG^\ddagger , can be obtained. In addition, it is known that ΔG^\ddagger value is

sensitive to the mechanism of permeation; therefore, its change in constant temperature indicates that the permeation mechanism has changed [12]. For instance, decrease in the size of the coating defects in a SiO_x coating on PC, (e.g. RF-PECVD of SiO_x on PC), down to the scale of permeant molecule size, forces the molecules to diffuse into it, only along the axis of their smallest projected area, which poses an increase to the ΔG^\ddagger . It shows that coating changes the permeation mechanism (Figure 1.26b) [5,100]. On the other hand, when such significant change does not occur in ΔG^* value for coated films, (e.g. magnetron PECVD of SiO_x , or dual-frequency MW/RF-PECVD of SiO_2 and SiN , on PET), compared with neat PET, it can be noticed that the permeation mechanism has not changed. In other words, diffusion through the PET substrate is the only temperature-dependent permeation occurred. It can be rationalized as a result of enough large size of defect in the coating, despite increasing barrier properties (about 180 times decrease in permeability) (Figure 1.26a) [5,12].

1.5.4. PVD vs. CVD

For depositing a coating with a homogeneous thickness on substrates that are not 2D planar, like PET bottles, CVD is more appropriate. This is due to line-of-sight nature of PVD, where with increasing surface roughness efficiency of coating decreases. In fact, source material before reaction with the substrate has enough time to experience several collisions with the surface, in contrast with PVD, in which gaseous source is condensed on the substrate instantly after contact [5,6,17]. Furthermore, comparing deposition of different oxides along with nitride of silicon (Table 5 at the end of this article), shows that SiO_x coatings deposited by PVD

provide significantly less barrier resistance against oxygen than different experiences mentioned with CVD [4,79]. A possible reason for this result can be columnar morphology of the silicon oxide film (less density) deposited by evaporation PVD compared with featureless structure (higher density) of silicon oxide resulted from RF and MW/RF-PECVD. The second reason for inferior results of PVD is the lack of forming the organic-inorganic interphase layer that is formed in CVD technique. Such a few tens of nanometers wide region, with a composition that gradually transits from inorganic coating to organic polymeric substrate, is formed in PECVD during the first few seconds of plasma exposure, as a result of releasing volatile organic species from polymer surface in interaction with plasma. As a result of mixing of such volatile organic species and gaseous precursors, the organic-inorganic interphase forms. Such interphase with improving adhesion between the polymer film and its coating can result in superior barrier properties of PECVD compared with PVD [79].

1.5.5. Effect of Defects

As aluminum and the oxide of silicon and aluminum have good barrier properties against water and oxygen, they are usually considered as traditional materials used to make barrier films. However, due to existing defects and nano-pores, when such superbarrier materials are coated in a single layer on polymeric substrates, with different methods of sputtering, evaporation (PVD), or PECVD, the resulting assembly shows only two or three orders of magnitude higher barrier properties compared with neat polymers [2,8,39]. In fact, by analyzing the defects and their relation to barrier properties of the coated films, it was noticed that the mechanism for permeation, instead of classic mechanism of solubility/ diffusion is

through flux (mass transport) via defects in thin barrier coating. This is the reason that the permeation of O_2 usually only decreases about two orders of magnitude [79]. The silica (SiO_2) coating through PECVD has more mechanical flexibility, in comparison with PVD, which can cause fewer defects, thus, maintains higher barrier properties; nevertheless, due to the low crack resistance of brittle SiO_x layers, still it is prone to cracking.[4] The following figure shows that how OTR of Al, SiO_x , and SiN_x increases with increasing the density of defects including pinholes, subnanometer pores,... in the film [2,5,18]. Such defects can be resulted from different stresses. First intrinsic stress, due to non-equilibrium nature of both PVD and CVD techniques, results in quenched disorder state of the final metal oxide coating. Thus, it forms nanodefects. In addition, there are thermal stress generated through final cooling, due to different coefficient of thermal expansions between the polymer substrate and oxide coating [21]. Although the procedures involved in nucleation and growth of glassy film are the main reasons for small defects, usually large defect are related to damages occurred while handling the film or cleanliness problems that impede proper deposition of the film (Figures 1.27a and 1.27b) [18]. Therefore, the density of the defects occurred during film fabrication, and their size, both dependent on the intrinsic properties of the metal oxide and its chemical composition, determine the barrier properties of the single-layer metal oxide (Figure 1.27c) [18].

Also, due to intrinsic stress difference between metal or metal oxide coating layer and the polymeric substrate, the thickness of the coating cannot go further than about 100nm, otherwise increased cracking pose an adverse effect on barrier properties of the coating. Therefore, one

optimized thickness is defined for each coating, where barrier properties are maximum [6,7]. For instance, due to decreasing flexibility and occurring more cracks in SiO_x coating, above 40 nm thickness, barrier improvement effect decreases with increase in its thickness [7].

1.5.6. ALD

The ALD coating of Al₂O₃ on flexible substrates of polyimide (Kapton) (T_g~300°C) and polyethylene naphthalate (PEN) (T_g=125°C) at temperature range of 100-175°C (Typically at 120°C) for films with thickness above 5nm (single sided) resulted in OTR values below minimum detectable data with MOCON OX-TRAN 2/21 instrument (<5x10⁻³ cm³/m².day) [39].

1.5.6.1. Superiority to PECVD

In one of the best barrier results for PECVD, a 50 nm SiN-coated PET with 50 μm thickness led to OTR values lower than the detection limit (<5x10⁻³ cm³/m².day) while only a single 10 nm Al₂O₃ layer coating on the same substrate was needed to achieve to OTR lower than that detection limit. It also shows that MOCON is not sensitive enough to evaluate this barrier system, and Carcia et al. continued with water vapor transmission rate (WVTR) investigations, which result in more detectable values [11].

1.5.6.2. Substrate Temperature Control

Controlling the temperature of the substrate in the ideal range for proper precursor chemical deposition is critical. In fact, if the temperature is lower than optimum level, it can increase the growth rate, due to condensation of precursors on it; or otherwise decrease it, as a result of improper removing of the previous excess precursor, when the second precursor enters the

chamber. On the other hand, a very high temperature can either have decreasing effect on the coating growth through re-evaporation of already deposited precursors, or pose increasing effect on it, as very high temperatures may cause decomposition of precursors in their gaseous state, before depositing on the substrate surface [41,43].

1.5.6.3. Influence of ALD Processing Temperature

As mentioned before, by varying the ALD processing temperature, critical coating thickness (threshold thickness) and so barrier properties change. For instance, Carcia [41], by increasing the processing temperature from 50 to 100°C observed a decrease in critical coating thickness, from 9.6nm to 7.5nm, and improve in barrier properties against water vapor, for coated PET substrates. Showing that, by increasing the ALD processing temperature, fewer ALD cycles are needed to reach to a coating with ultra-barrier properties, lower than Ca test detection limit of 5×10^{-5} g/m.day.

1.5.7. LBL Assemblies

LBL deposition of alternating layers of polymer, PE, and clay is aimed as a good potential to reach to a uniform, layer-by-layer structure of nanoscale thin alternating layers of polymer and highly exfoliated and oriented impermeable clay platelets, to gain very high barrier properties. In fact, the idea is to make a nanobrick wall that permeating gas molecules pass through very long, tortuous, but less resistant, polymer layers that are located alternately between oriented layers of impermeable clay platelets layer, instead of openings between clay platelets perpendicularly to the film surface. So, it is important that polymer layers, as the spacing between clay layers, have the appropriate thickness for traveling gas molecules

through [14,62]. Such long diffusion paths can withdraw very high residence time, resulting in extremely high barrier properties for the LBL assemblies, when the number of layers increases to more than a few ones. In reality, when the exfoliated clay platelets, especially the ones like MMT that have high aspect ratio, are positioned with their largest dimension perpendicular to the permeant molecule of gas, they increase the diffusion path. Hence they decrease permeability [1,13–15,62]. In fact, Jang et al. for the first time achieved to very significant increase in barrier properties for LBL assembly of (0.25wt% in solution) polyacrylamide and (0.2wt% in suspension) Na⁺MMT, where the 571nm thick, 30-BL assemblies after deposition on a PET substrate (with thickness 179μm) resulted in an OTR <0.005 cm³/(m².day.atm), at 23°C, 0%RH, which is the minimum measurable value with the existing equipment. Such dramatic decrease in transmission of oxygen through the film was interpreted as a result of nanobrick structure of LBL formed from completely exfoliated clay platelets. They also for 20-BL reached to OTR value of 0.217 cm³/(m².day.atm), similar with SiO_x-coated PET [1,12]. It should be mentioned that although the multilayers' thickness usually increases linearly with increasing the number of layers, barrier resistance increases superlinearly (e.g. exponentially). It proposes that this LBL assembly, in a high number of layers, can be a good alternative to SiO₂ in food and even electronic packaging applications. For instance, for LBL made from solutions of 0.1wt% PEI and 0.2wt%MMT in DIW, after deposition of 70-BL films on a 179 μm PET film, an OTR lower than detectable limit for conventional tools (OX-TRAN 2/21) (<0.005 cm³/(m².day.atm)) and permeability of < 0.90x10⁻⁶ cm³/(m².day.atm) are reached (Figure 1.28). So, by a decoupling of the permeability of LBL from total permeability,

permeability of LBL would be $<0.002 \times 10^{-6} \text{ cm}^3/(\text{m}^2 \cdot \text{day} \cdot \text{atm})$ that is the lowest ever reported oxygen permeability for a polymer composite [9,14].

Yang et al. in other progressing step, reached to undetectable OTR ($<0.005 \text{ cm}^3/(\text{m}^2 \cdot \text{day} \cdot \text{atm})$) (23°C, 0%RH) for a 179 PET film coated with assembly of 30 (0.1wt%)PEI/(1wt%)MMT bilayer films, even for as short as 10 second immersion time in PEI solution (5min in MMT solution), which implies achieving to a defect-free structure only in such short time of immersion. This is also a key towards commercializing LBL assembling process for transparent packaging for food and beverage and flexible packagings for electrical devices. Even 10-second immersion in both solutions decreases OTR of PET from 8.48 down to 0.168 that is close to OTR of SiO_x -coated 25 μm PET film, through PECVD [12,13]. It demonstrates a high clay concentration (above 89%) and a perfect alignment of clay platelets parallel to the surface [13,14,158]. In fact, the reason for less improvement in barrier properties with lower immersion time in MMT suspensions can be more loosely packing of MMT platelets in layers.

1.5.7.1. Modeling Transport Properties in LBL Assemblies

LBL assembly is itself a particular type of PNC, only with higher packing density and higher alignment of clay layers, owing to its specific type of deposition and existing strong electrostatic forces between alternating layers. Thus, researchers tried to model their barrier properties with tortuous path models. In other words, assuming that impermeable particles inside a permeable matrix provide a tortuous path for the permeant molecule, they needed a tortuosity model for permeation to estimate the permeability of the LBL composite [14,160].

As mentioned before, Nielsen initially developed a model for permeability of gases through permeable matrices filled with a low concentration of impermeable particles, to estimate the permeability of the resulting composite [154]. However, the problem with Nielsen model is that it fits with experimental barrier properties only in a dilute regime ($\alpha\phi < 1$) [155]. Thus, in the high contents of clay, which is the case in LBL assembly, Nielsen can only model accurately the permeability of the commercial composites, where due to lack of exfoliation, tortuosity is not very high ($\alpha\phi < 1$). Hence, for LBL assembly that contains a high percentage of clay (about 80wt%) and makes much higher tortuosity ($\alpha\phi \gg 1$), Nielsen could not predict permeability of the composite properly [1,155]. Therefore, Cussler model, which is more fitted for a semidilute regime, was used to do so, due to predicting a sharper decrease in permeability of the composite than what Nielsen model predicts, with increased clay content. Hence, it is in closer agreement with experimental results (Figure 1.29) [1,158]. Nevertheless, due to existing some differences between the LBL assembly and Cussler model, including much higher distribution order and vary high loading level of tightly packed clay platelets in LBL, resulting in a tortuosity degree far higher than assumed by Cussler model, also due to existing some possible linkages between amine moieties of PEI and oxygen that affects the permeability, the barrier properties predicted by Cussler model were much lower than real experimental results (Figure 1.30) [14,15].

1.5.8. Polymer Nanocomposites (PNCs)

In Toyota Technological Institute, Ray et al. prepared intercalated of biodegradable poly(lactic acid) PLA and MMT, organically modified with alkyl ammonium. In fact, after

melt mixing in a twin-screw extruder and in 4wt% loading of OMMT they reached to barrier improvement factor of 1.13, compared with neat PLA [51]. In the other study, solution intercalated PNC of epoxy resin with MMT, organically modified with some short alkyl chains Benzyltributyl(2-hydroxyethyl) ammonium chloride (Bz1OH), Benzylbis(2-hydroxyethyl) butyl ammonium chloride (Bz2OH), and Benzyltriethanol ammonium chloride (Bz3OH), barrier properties showed significant improvements, compared with the pure epoxy matrix (Table 4a). It can be rationalized as a result of interaction between matrix and OH group of those alkyl ammonium groups, attached on the MMT surface. Thus, due to forming firm interactions between matrix and OMMT platelets, exfoliated PNCs with superior barrier properties are prepared that increase tortuosity of the matrix, resulting in a decrease in permeability. Also, in Table 4b it is shown that with the increase in clay content in such PNCs permeability decreases, as a confirmation for their exfoliation [102].

In contrast, for PNC made with MMT modified with long chain alkyl ammoniums, BzC16, BzC18OH, 2C18 (the number in the name is a measure of the number of carbons in alkyl chain), observing no significant change in barrier properties, compared with neat polymeric matrix, is connected to phase separation between polymeric matrix and alkyl chain on MMT and no tethering to those clay platelets. It was perhaps due to the covering of the OH group (of ammonium) with long chain alkyl that prevents its reaction with the matrix. So, the increased planar spacing posed by organic modification of clay can only cause intercalation in these nanocomposites, and despite higher intercalation compared with short alkyl chains, barrier improvement is inferior to them. The existence of such intercalated structure was confirmed

by microscopic investigations. Because, in the case of no exfoliation, intercalated tactoids did not hold a high aspect ratio. Thus, in the typical low loading of PNC, most of the matrix remained free of clay platelets, resulting in no significant improvement in barrier properties of the polymer nanocomposite. Accordingly, even increasing the clay content did not show significant improvement in their barrier properties (BzC16) (Table 4(b)) [102]. In fact, these arguments were already confirmed by Ray et al. observation, where they did not observe significant improvement in the barrier properties of their intercalated PNCs, made from organic modification of MMT with long chain alkyl ammonium [51].

In another study, carbon dioxide barrier properties through preparing PNC of two different matrices, metallocene polyethylene (high-density polyethylene (HDPE) made by metallocene catalyst) and maleic anhydride grafted low density polyethylene (LDPE-g-MA), with organically-modified MMT (using short alkyl chain dimethyl tallow benzyl ammonium and through melt mixing in co-rotating TSE at 180) were studied. In addition, as compatibilizers to improve the exfoliation of clay in the matrix through increasing its interaction with the polymeric matrix, they used maleic anhydride grafted high-density polyethylene and two types of low-viscosity and high-viscosity oxidized paraffin. Microscopic investigations of processed samples showed a complex morphology of exfoliated platelets, intercalated tactoids and microscale agglomerations of clay (Figure 1.31) [52]. Overall, systems holding oxidized paraffin showed better barrier improvements, where in the best results, in PNCs based on HDPE and LDPE-g-MA, decreases of CO₂ permeability from 6.29 to 3.74 barrer, and 5.37 to 3.41 barrer, with 20wt% low-viscosity oxidized paraffin (PEoLV20), in 5wt% loading were

reached, respectively. Also, oxygen permeation test showed the similar order of results with slightly lower barrier improvements. All in all, one problem with PNCs, particularly the one prepared by melt intercalation, is the significant decrease in dispersion level with increasing clay loading, which usually results in reaching to a turning point in barrier properties at clay content of about 5wt% [62,137].

1.5.8.1. Comparison between Experimental and Model-Calculated Barrier Properties

One factor that can cause a good agreement between the calculated permeability and experimental data is the way that the assumptions taken for the model are correspondent with reality. Typically, the reasons for the deviation between permeability calculated and experimental results are two inaccurate assumptions. One is assuming complete exfoliation for PNC, and then it is assuming complete horizontal orientation of clay platelets [64].

Complete exfoliation assumption is one of the main reasons of observing deviation of experimental results from presented models. For instance, in Shah's experience of barrier properties for melt processed LDPE and OMMT (Cloisite 6A) nanocomposite against gases, it is assumed that the clay platelets are completely exfoliated, and with high aspect ratio of 120 (width/thickness). This assumption is close to reality in 1wt% clay loading, resulting in a good agreement with experimental data and predicted permeability by the Nielsen's tortuosity model. However, when it comes to higher loadings, like 3wt%, due to not occurring a complete exfoliation, a deviation occurs between predicted and experimental data (Figure 1.32a) [55]. The reason is that in 1wt% clay, the exfoliation is high. Thus, the real aspect ratio is retained about 120, which is for individual platelets, but in higher clay contents clay particles adhere to

each other forming tactoids with lower aspect ratio. Thus, for the aspect ratio of 120, barrier properties do not improve as the Nielsen model predicted.

Complete horizontal orientation assumption of clay is the second reason for the deviation between experimental relative permeability and Nielsen model. But it is usually not the case in reality [102]. So, as already mentioned, Bharadwaj modified the Nielsen model by adding an order parameter to decrease such deviation. Accordingly, by using this modified Nielsen model a better agreement was concluded for the HNBR NC of Gatos and Karger-Koscis (Figure 1.32b) [162,163].

In the experience of Gatos and Karger-Koscis, assuming order factor, $S=0.9$, makes the best fit with experimental data, implying that not all the platelet stacks are oriented horizontally. Nevertheless, $S=0.9$, which is more close to 1 than 0, shows almost a good horizontal orientation. This relative alignment is considered as one of the reasons why Nielsen model itself, made a good prediction for this PNC. Still, with increasing the clay content above 6vol%, a slight deviation occurs that shows sticking of clay particles and more decrease in exfoliation in higher loading levels [163].

1.6. Conclusions

Considering single-layer coatings and between PVD and CVD, the former one due to its line-of-sight nature has less efficiency for coating 3-D objects. In addition, PVD coatings generally hold significantly less barrier resistance against gases such as oxygen. Inferior barrier properties of PVD coatings mainly accounts for their relatively higher defected structures, due to lower density and less mechanical flexibility. The other reason can be the lack of an

interphase layer in PVD coating compared with PECVD ones. Nevertheless, even CVD coatings that are mainly silicon oxide are prone to cracking, primarily due to the stresses induced in the system and low spontaneous flexibility of silicate layers. Also, attempts to increase the thickness in order to increase the density of such coatings and to decrease their defects are not reliable. Since, intrinsic stress of the coating is different from that of the substrate, and with increasing its thickness above an optimum level its cracks more that consequently decreases its barrier properties. One answer to these problems were nearly defect-free ALD layers, which only in thicknesses as low as 5nm resulted in OTR values lower than detectable limits of conventional permeation measurement apparatus. The reason for such defect-free aluminum oxide coating through this competent technique can be connected to special step-by-step deposition procedure for precursors, which are separated by an inert purging gas. Alternatively, using multilayers, mainly flexible LBL assemblies, through increasing tortuosity, happened to result in great barrier improvement for polymeric substrates. As a matter of fact, through depositing a few tens of clay and polymer bilayers on thin PET membranes a nanobrick wall of clay platelets and polymer mortar is built. It is the result of strong electrostatic attractions between oppositely charged layers that form a packed assembly of highly oriented layers of clay platelets, alternating with polymer layers. These flexible and transparent LBL assemblies, which are deposited without any demand for evacuation or high temperatures that previous single-layer technologies needed, demonstrate OTR levels lower than $0.005 \text{ cm}^3/(\text{m}^2 \cdot \text{day} \cdot \text{atm})$.

Also, in case of PNC synthesis, whenever due to proper interaction between clay or its compatibilizers, like short alkyls of ammonium, a good level of exfoliation is concluded, the barrier properties can reach to about 3 times improvement in loadings about 5wt%. Otherwise, in case of intercalated morphology no significant improvement is achieved. Accuracy in the prediction of barrier properties of these PNC with theoretical models like Nielsen is depended on how correct are the assumptions such as complete exfoliation and perfect horizontal orientation presumed by those models.

Despite lower barrier improvement resulted in PNC approach compared with different coating approaches, it shows higher mechanical stability as it rules out the risk of occurring defects in coatings and their possible peeling from the surface. Also, it results in a material with isotropic mechanical properties capable of being processed through conventional polymer processing techniques like extrusion and blow molding that otherwise is not possible for coated substrates.

1.7. Dissertation Overview

This dissertation is comprised of 8 chapters, based on studying various coating and nanocomposite approaches for improving barrier properties of polymer-based membranes. The aforementioned Chapter 1 mainly was a comprehensive literature review on these approaches. Then Chapter 2, which is in-press as a book chapter, in a tailor-made way, reviews different nanotechnology strategies, which yield high-barrier plastic food packaging.

Thereafter, experimental part of our research begins, where chapters 3 and 4 discuss layer-by-layer coated polystyrene-based membranes. In fact, after investigating the morphology of

LBL coatings formed from alternating layers of MMT with either of two different polyelectrolytes, polyethyleneimine and polyethyleneterephthalate ionomer, through microscopic and x-ray diffractometric techniques in Chapter 3, Chapter 4 mainly investigates barrier improvement resulted by those LBL coatings.

Then, through cyclic melt pressing of LBL-coated polystyrene-based membranes, it is tried to crush the LBL assemblies inside the polymer bulk to exploit the intercalation and exfoliation already provided in them, for promoting exfoliated nanocomposites, aiming improvement in their barrier properties. In fact, Chapters 5 and 6 of this dissertation after investigating processing and morphologies of pressed polymer nanocomposites, based on polystyrene, discuss their physical, thermal, dynamic mechanical, and transport properties, respectively. In fact through those chapters different characterization techniques of microscopy, x-ray diffractometry, dynamic mechanical analysis, differential scanning calorimetry, and thermogravimetry are investigated on the processed PNCs. In addition, transport properties of oxygen and carbon dioxide in processed polymer nanocomposites are measured. Afterwards, in Chapter 7, this two-step processing technique of polymer nanocomposites, through layer-by-layer coating and cyclic melt pressing, is applied on polyvinylacetate to scrutinize the effect of increased functional groups in polymeric matrix on the interaction it makes with layer-by-layer coating, where resulted morphologies and mechanical and barrier properties of the resulted polymer nanocomposites are investigated.

Finally, Chapter 8 briefs the conclusions resulted from this research study, and suggests further steps including possible approaches and materials that can potentially reach to higher improvements in barrier properties of polymer-based membranes against gases.

1.8. Appendix

1.8.1. A Comparison between Oxygen Barrier Properties of Different Coatings and PNC Approaches

In the following Table, it is tried to provide a summarized comparison of barrier properties determined for some different coating systems and polymer nanocomposites discussed before, which are displayed in the same order as in the article. All things considered, it can be noticed that the best barrier improvement results are obtained for ALD, and LBL coatings, followed by PECVD and PVD (evaporation and sputtering) coatings. At the end, least barrier improvement has been obtained for PNCs. However, they are superior to those coating systems based on their higher flexibility of processing and design, plus their exclusive mechanical stability (Table 5).

Tables

Table 1.1. Explanation of abbreviations in Figure 1.1 [6].

Abbreviation	Explanation	Abbreviation	Explanation
PE-LD	low-density polyethylene	COC	cycloolefin copolymer
PE-HD	high-density polyethylene	PLA	polylactic
PS	polystyrene	PUR	polyurethane
PP	polypropylene	PET	polyethylene terephthalate
PVC-P	plasticized polyvinyl chloride	PA6	polyamide6
PVC-U	hard polyvinyl chloride	PEN	polyethylene naphthalate
BOPP	biaxially oriented polypropylene	Ormocer	lacquer/adhesive system
PC	polycarbonate	PVDC	polyvinylidene chloride

Table 1.2. Sputtering condition for fabricating barrier AlOxNy film [18].

Parameter	Condition
Power	850 watts
Argon flow rate	0-40 sccm
Nitrogen flow rate	80-100 sccm
Sputtering pressure	0.26-0.5 Pa
Deposition rate	0.3-0.4 nm/s

Table 1.3. OTR of pure and coated PET and PP at 30°C and 0%RH [19].

Substrate	Oxide Thickness (nm)	OTR (nmol/m².s)	(OTR)₀/(OTR)
PET	0.0	91	1.0
PET	1.0	83	1.1
PET	2.5	12	7.6
PET	5.0	4.9	18.6
PET	10.0	3.7	24.2
PET	17.0	2.4	37.9
PP	0.0	1250	1.0
PP	1.0	1230	1.0
PP	10.0	463	2.7

Table 1.4. (a) Decrease in the oxygen permeability (at 0%RH and 23°C) of epoxy resin through synthesizing PNC with 3.5 vol. % OMMT. (b) Dependence of the OTR (at 0%RH and 23°C) on loading level of clay [102].

(a) Composite	Permeability coefficient cm³.μm/(m².day.mmHg)	(b) Composite	Permeability coefficient cm³.μm/(m².day.mmHg)
neat epoxy	2.0	neat epoxy	2.0
Na ⁺ MMT	1.6	Bz1OH(1vol%)	1.4
Bz1OH	0.77	Bz1OH(2vol%)	0.91
Bz2OH	0.78	Bz1OH(3.5vol%)	0.77
Bz3OH	1.0	Bz1OH(5vol%)	0.55
BzC18OH	2.2	BzC16(1vol%)	1.9
BzC16	1.6	BzC16(2vol%)	1.7
2C18	3.7	BzC16(3.5vol%)	1.6

Table 1.5. Comparison between barrier properties of different coating systems and PNCs.

Technique ^{a)}	Substrate	Coating	Ps ^{b)}	Pt ^{b)}	BIF ^{c)}	T (°C)	Ref.
Sputtering	PET	80nm AlO _x N _y	1.8x10 ⁻³	5.0x10 ⁻⁵	36	23	[18]
Evaporation	PET ^{d)}	17nm Al ₂ O ₃	2.1x10 ⁻³	5.6x10 ⁻⁵	38	30	[9]
PECVD	PET	100nm SiO _x	1.7x10 ⁻⁵	3.8x10 ⁻⁶	440	30	[10]
PECVD	PET	20-200 nm SiO _x	2.0x10 ⁻³	4.5x10 ⁻⁶	444	30	[12]
ALD	PET	10nm Al ₂ O ₃	-	<2.510 ⁻⁷	-	23	[11]
Al ₂ O ₃	PET	1.25 μm	6.0x10 ⁻²	<3.1x10 ⁻⁵	>1935	—	[3]
LBL(30) ^{e)}	PET	571 nm	1.5x10 ⁻³	<9x10 ⁻⁷	>1700	23	[1]
LBL(30) ^{e)}	PET	118nm	1.5x10 ⁻³	<9x10 ⁻⁷	>1700	23	[13]
LBL(70) ^{e)}	PET	231nm	1.5x10 ⁻³	<9x10 ⁻⁷	>1700	23	[14]
LBL(24) ^{e)}	PET	120nm	1.5x10 ⁻³	<9x10 ⁻⁷	>1700	23	[15]
PNC	Epoxy	5vol%	1.5x10 ⁻³	4.2x10 ⁻⁴	3.6	23	[102]
PNC	PLA	4wt%	2.0x10 ⁻²	1.8x10 ⁻²	1.13	20	[51]
PNC	HDPE	5wt%	4.1x10 ⁻¹	2.46x10 ⁻¹	1.68	20	[52]

^{a)} Except for Jacquelot et al. data [52], which is for CO₂, all other data are given for O₂.

^{b)} The mentioned permeability data for polymeric substrate (Ps) and the coated system or nanocomposite (Pt) in the table is in cm³.m/(m².day.atm).

^{c)} Barrier Improvement Factor (BIF) = $\frac{\text{permeation rate of neat polymer film}}{\text{permeation rate of coated polymer or PNC}}$, which is a sign of the effectiveness of the barrier system.

^{d)} The PET substrate contains silica particles.

^{e)} In the case of LBL deposition, the number in parentheses identifies the number of bilayers.

Figures

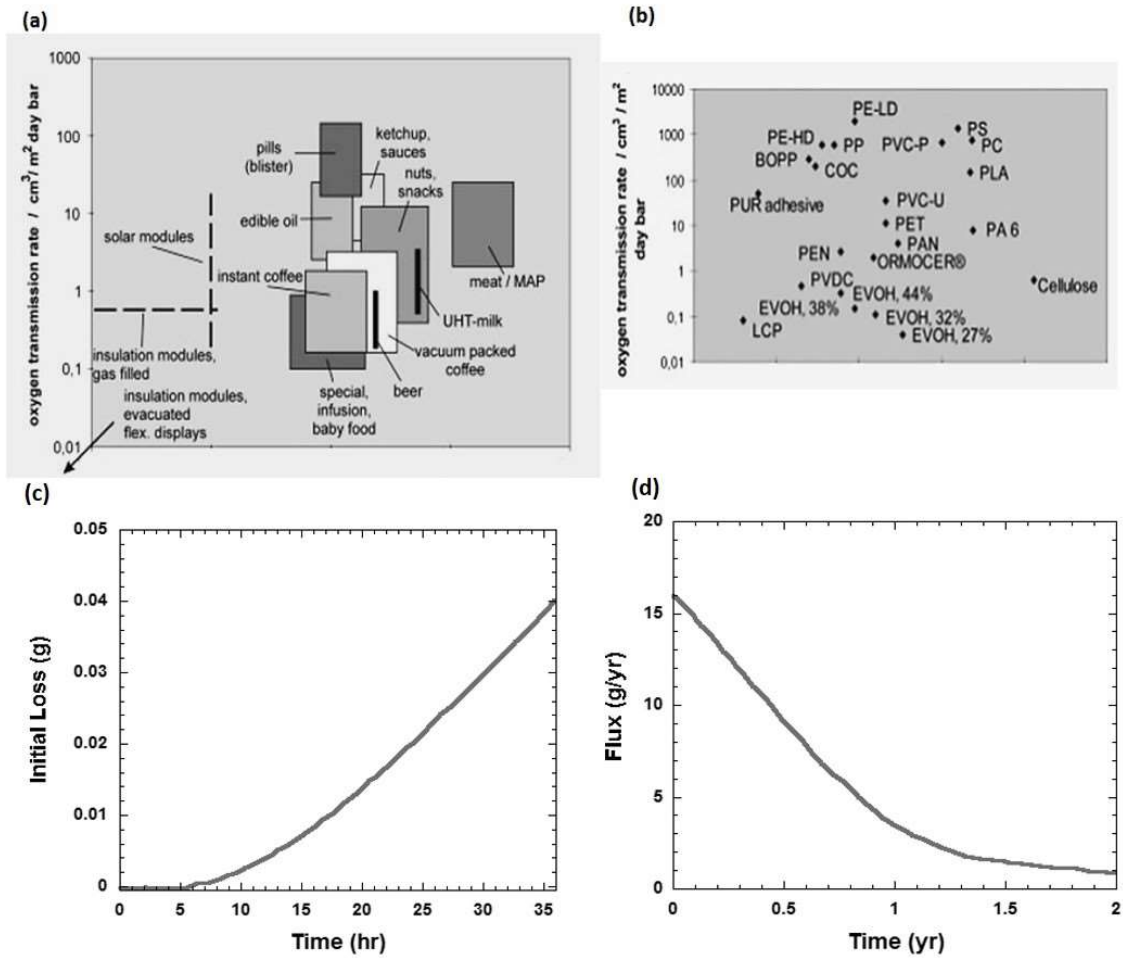


Figure 1.1. (a) Barrier requirements for packaging some food products polymeric at 23°C. (b) A comparison of oxygen transmission rate of some typical polymeric films with thickness 100 μm at 23°C. Adapted with permission [6]. (c) The initial loss of CO_2 from Cola PET bottle. (d) Longtime CO_2 flux through PET bottle wall during shelf life. Both graphs data are measured at 24°C and gas pressure of 3bar. Reproduced with permission [65].

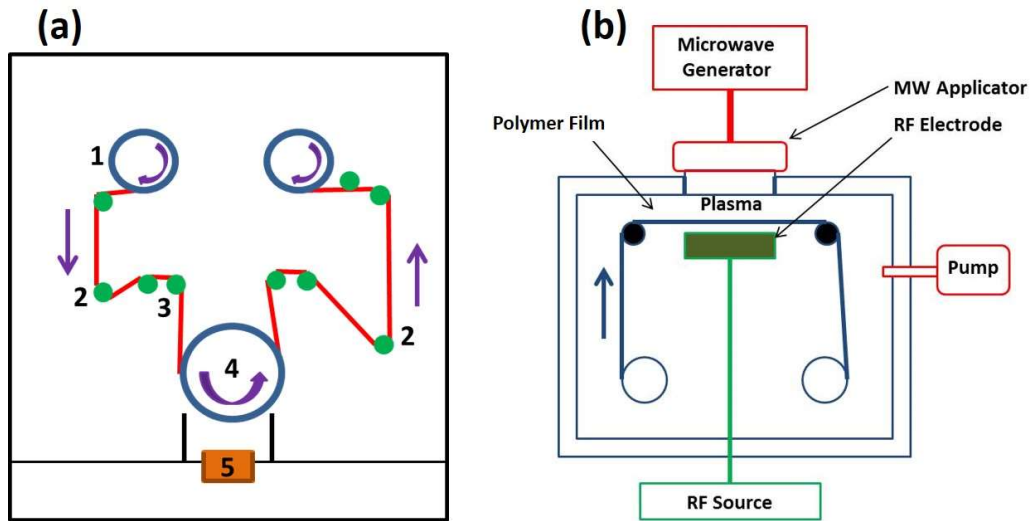


Figure 1.2. (a) Schematic figure of a continuous e-beam evaporation chamber. Adapted with permission [20]. (b) Schematic illustration of a single- and double-frequency reactor of PECVD. Adapted with permission [79].

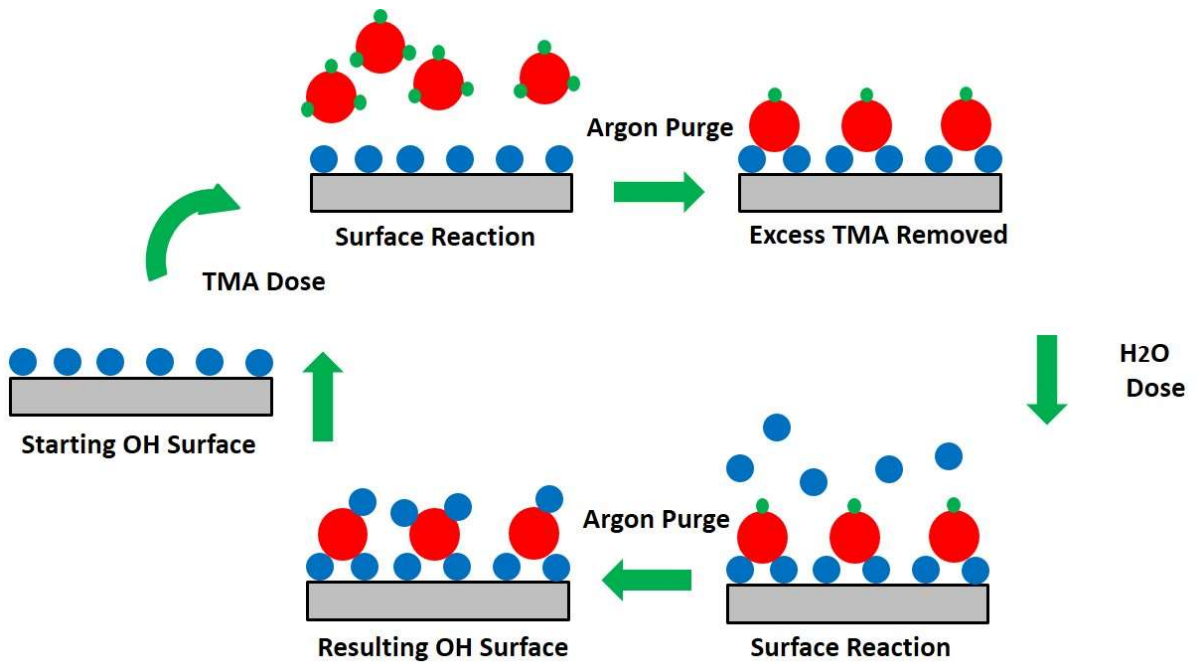


Figure 1.3. Schematic drawing of sequential order in an ALD process of TMA and water. Adapted with permission [83].

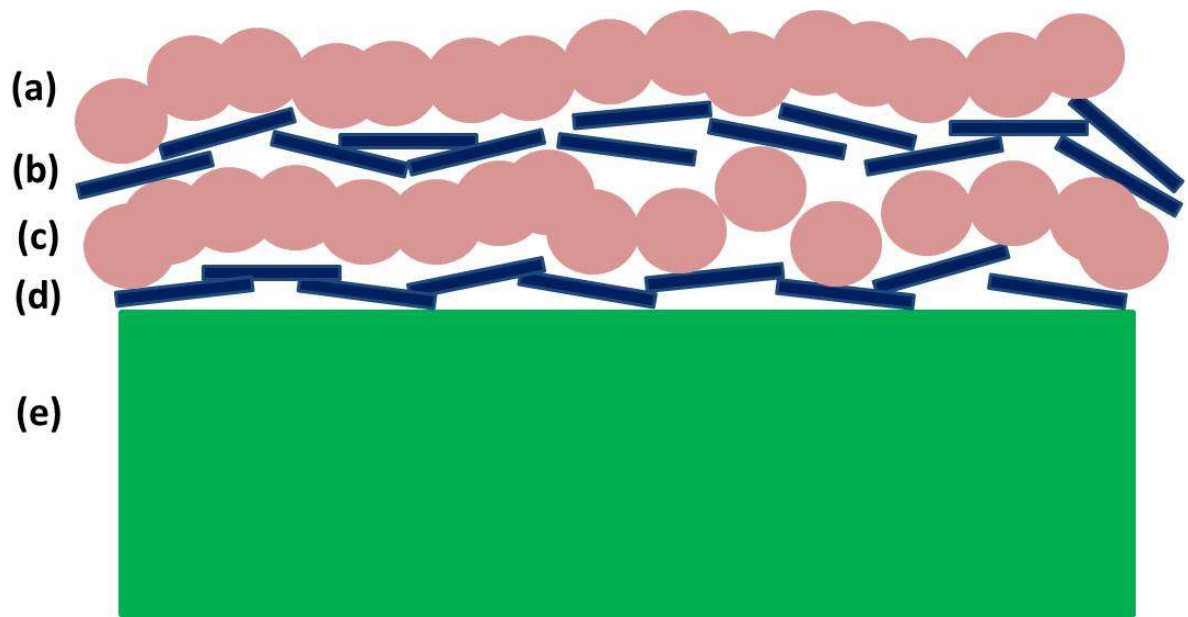


Figure 1.4. Schematic diagram of cross-section of a multilayer film, where (a) and (c) depict layers of silica with 100 μm thickness; (b) and (d) are layers of colloidal boehmite fibrils; and (e) represents the glass substrate. Adapted with permission [22].

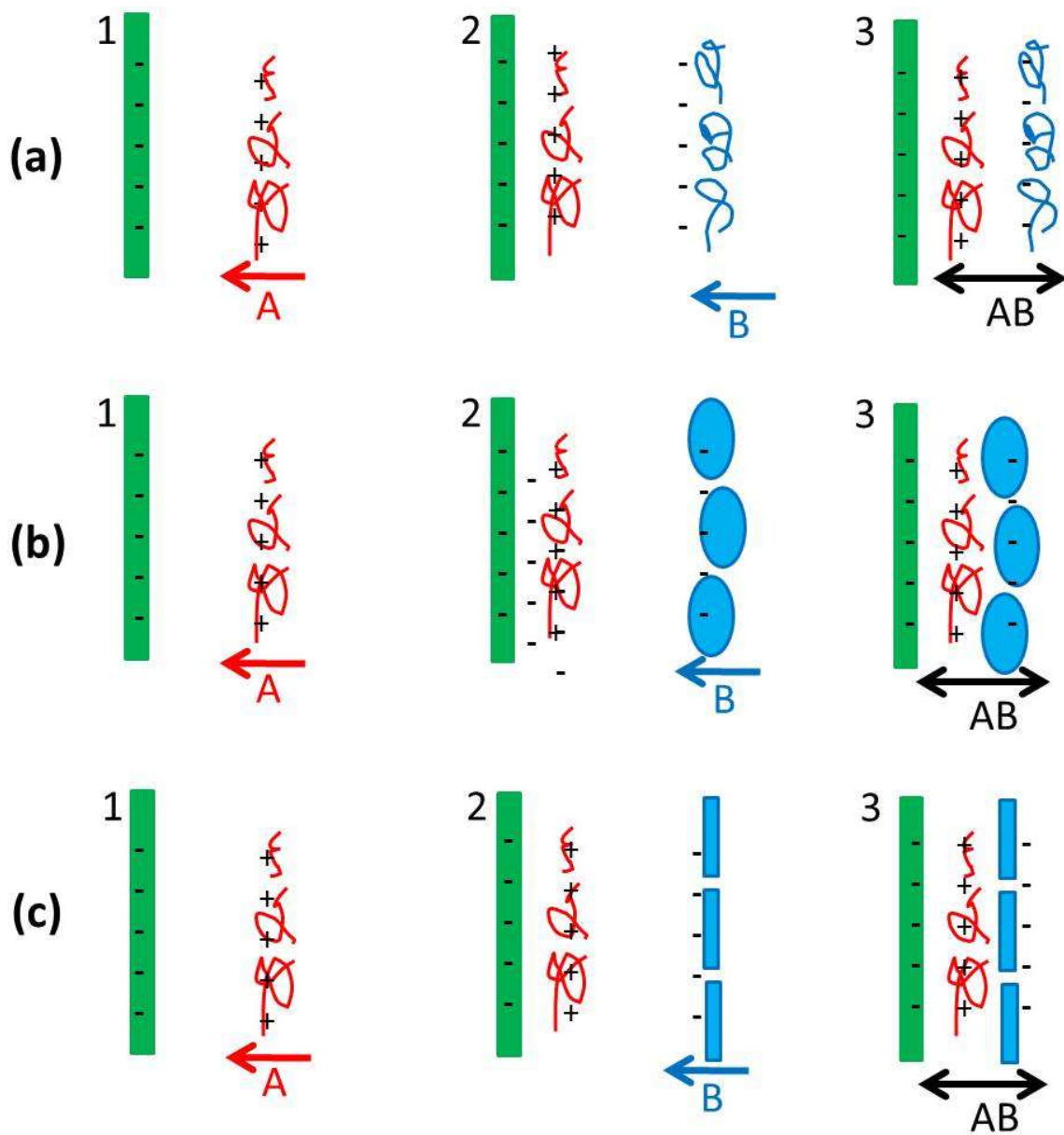


Figure 1.5. Schematic representation of assemblies of alternating polycation and polyanions. (a) Linear polyanion and polycations. (b) Linear polyanion and oppositely charged protein. (c) Linear polyanion and clay platelets. Adapted with permission [24].

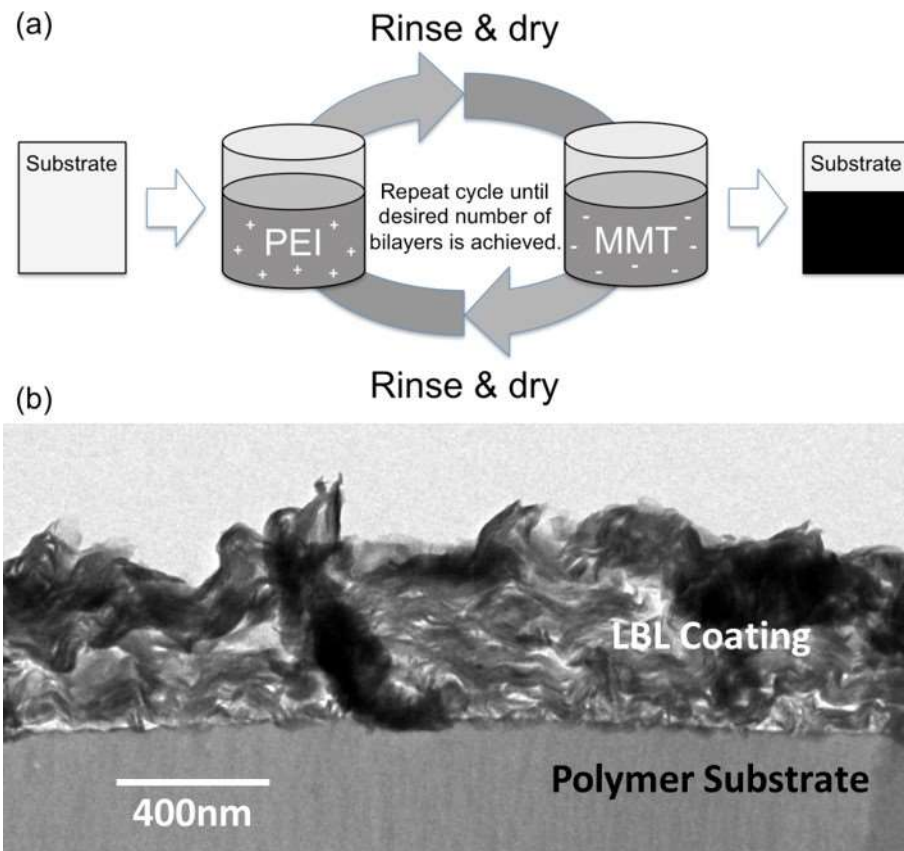


Figure 1.6. (a) Schematic of layer-by-layer deposition of polyethyleneimine and clay solution and suspension, respectively. Adapted with permission [14]. (b) Cross-sectional TEM image of an assembly of 30-bilayer of PEI/MMT deposited on PS substrate. Adapted with permission [36].

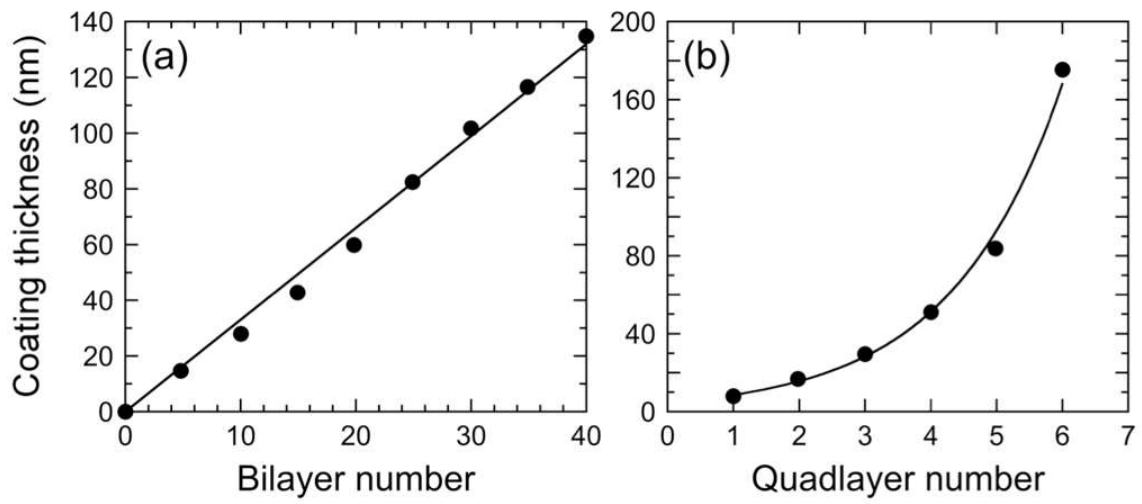


Figure 1.7. (a) The thickness of LBL assemblies versus the number of deposited bilayer coatings of PEI (solution pH=10) and MMT. Adapted with permission [14]. (b) The thickness of QL assembly plotted versus the number of QL depositing cycles. Adapted with permission [33].

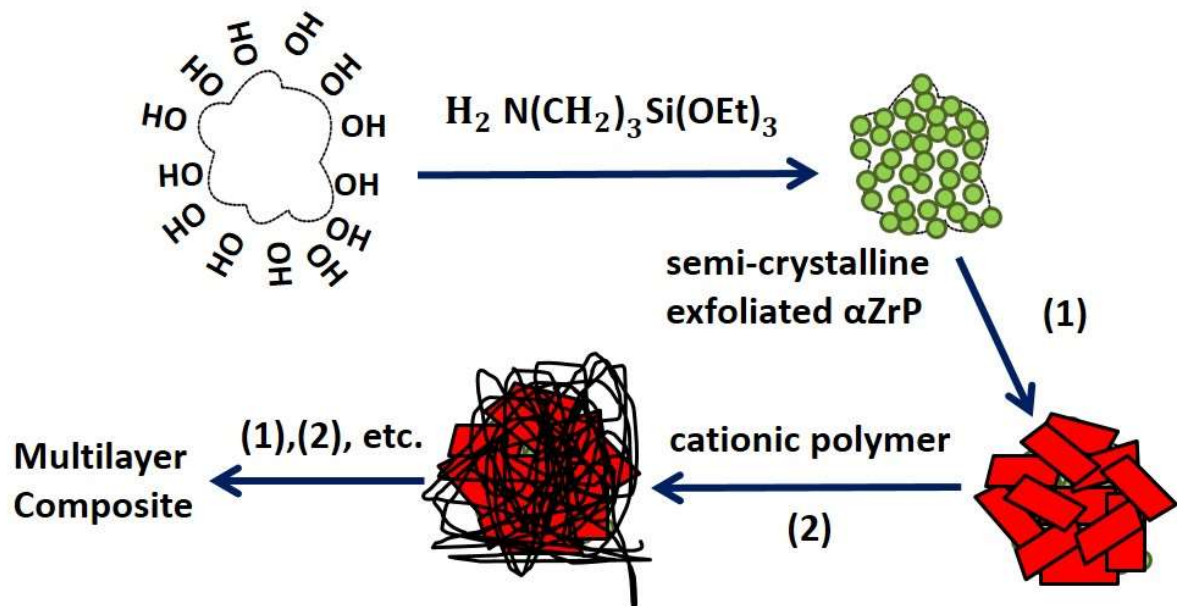


Figure 1.8. Schematic process of LBL deposition of two redox polymers (polycation) and an exfoliated anionic zirconium phosphate sheets on a silica particle with high surface area. Reproduced with permission. Adapted with permission [23].

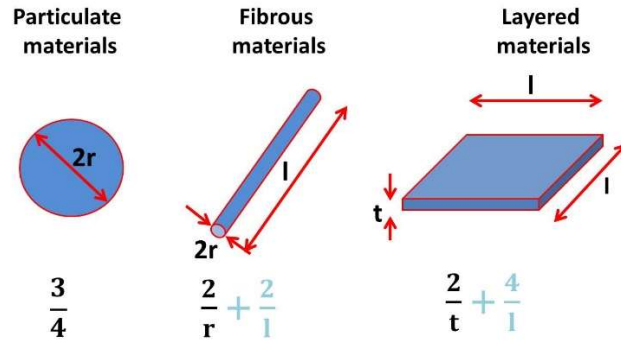


Figure 1.9. Geometries of common particles used for polymer reinforcement and their respective surface area to volume ratios. Adapted with permission [111].

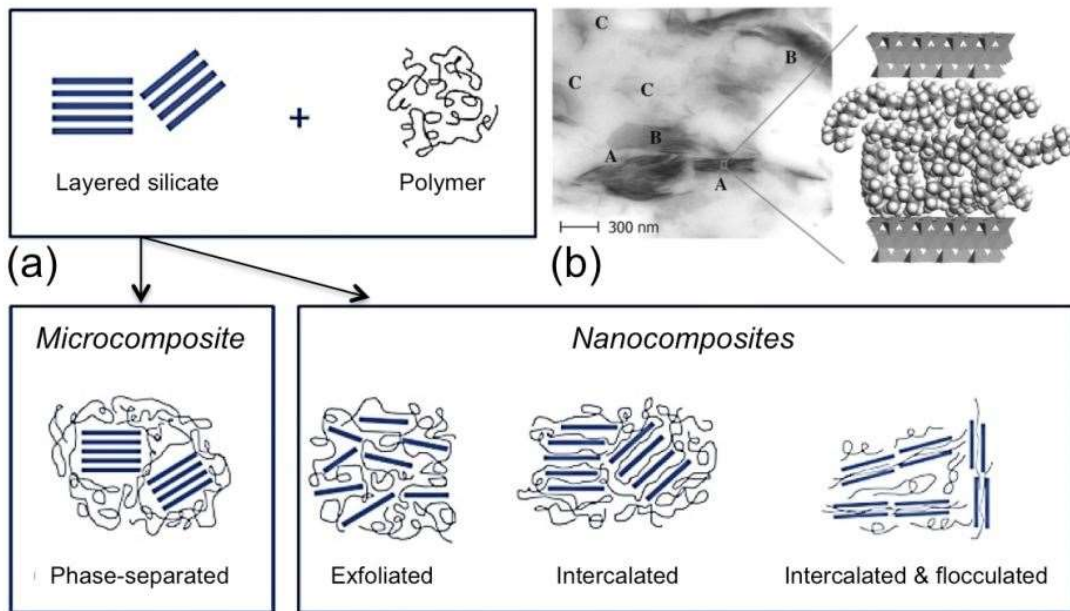


Figure 1.10. (a) Schematic illustration of different types of composites (labeled) made from layered silicates and polymers [63]. (b) TEM image of a nanocomposite of dispersed clay (black) in PP matrix (gray), where A, B, and C respectively show parallel intercalated stacks of clay, disordered intercalated clay tactoids, and exfoliated platelets of clay. A schematic representation of an intercalated clay stack (A), where parallel platelets are separated with PP chains. Reprinted with permission [116].

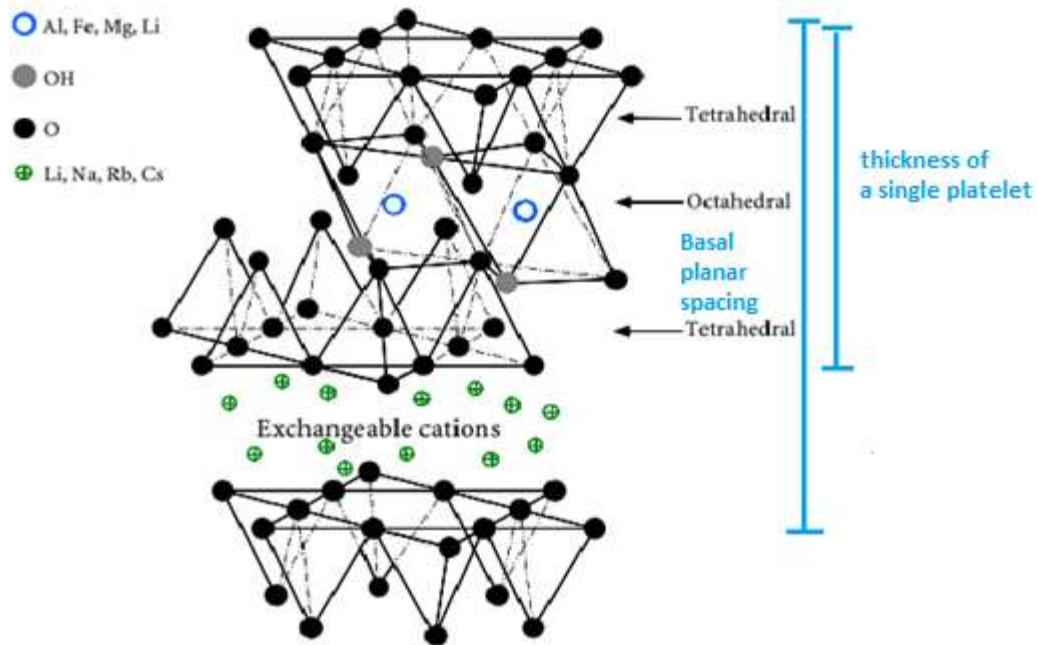


Figure 1.11. Basic structures of 2:1 clay minerals. Adapted with permission [118].

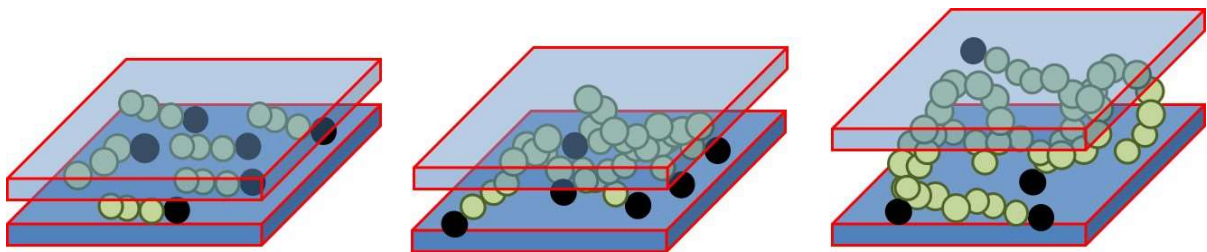


Figure 1.12. The schematic illustration of organically-modified silicates. Adapted with permission [118].

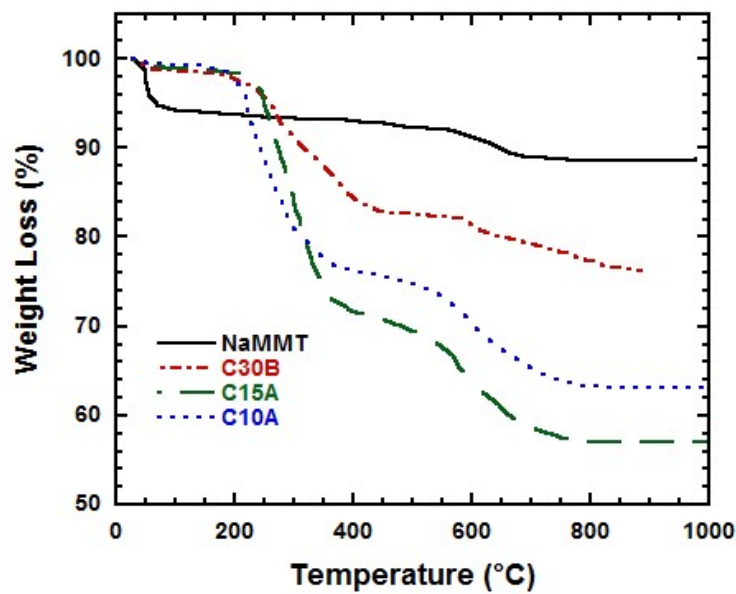


Figure 1.13. TGA graph, showing atmospheric degradation behavior of natural MMT (Na+MMT) and its organically-modified samples with different alkyl ammoniums: methyl, tallow, bis-2-hydroxyethyl quaternary ammonium (C30B); dimethyl, dehydrogenated tallow quaternary ammonium (C15A); dimethyl, benzyl, hydrogenated tallow quaternary ammonium (C10A). The region assigned with dotted lines is the processing window for PNC of PET and clay, at which only Na+MMT shows appropriate thermal stability [67].

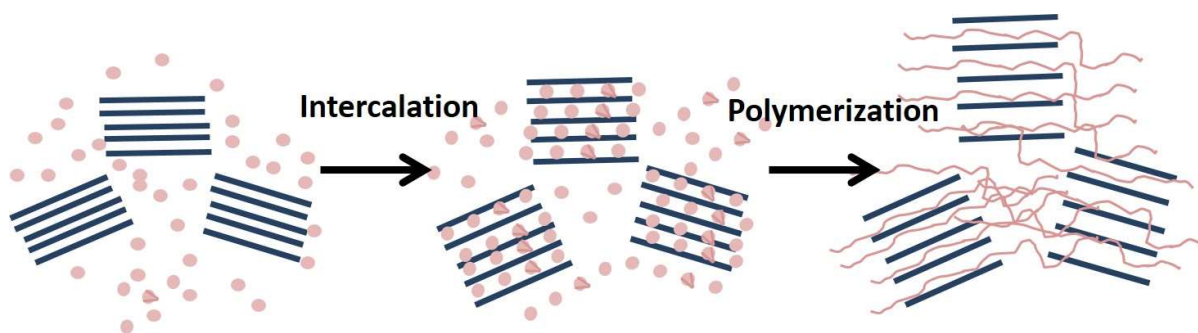


Figure 1.14. Schematic illustration of the composite synthesis. Adapted with permission [130].

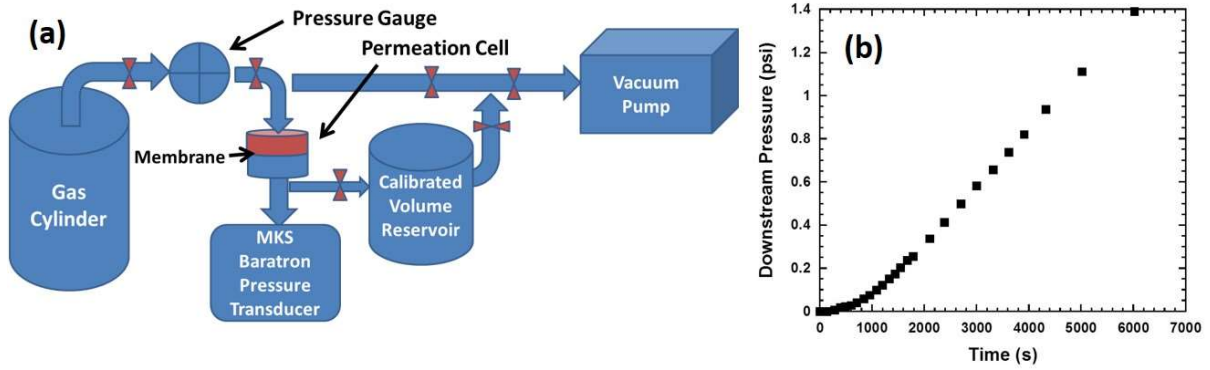


Figure 1.15. (a) Constant-volume variable-pressure permeation test setup. Adapted with permission [143]. (b) An example of CO₂ permeation through a polymer membrane. Adapted with permission [143].

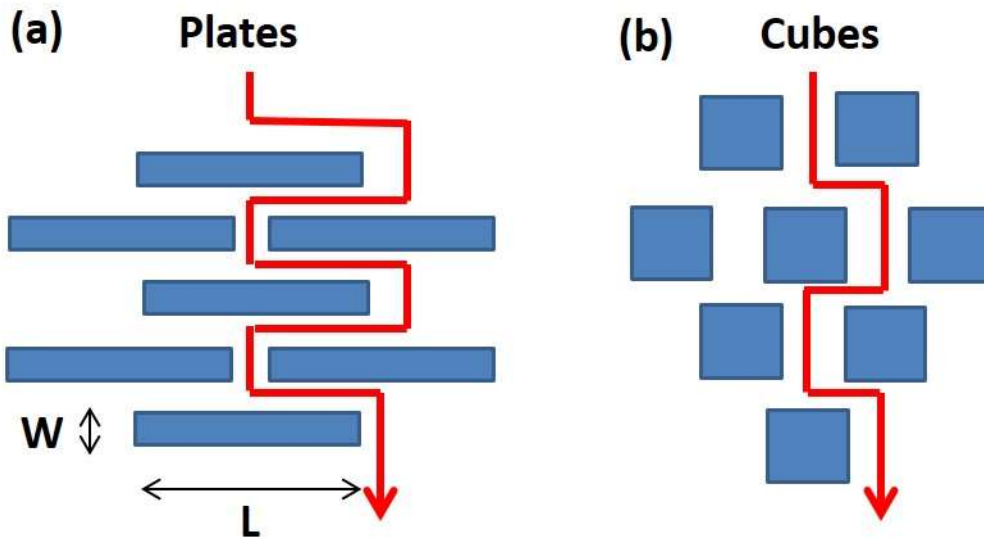


Figure 1.16. Models for a fluid diffusing path through (a) plate-shaped and (b) cube-shaped clay-filled polymers. Adapted with permission [154].

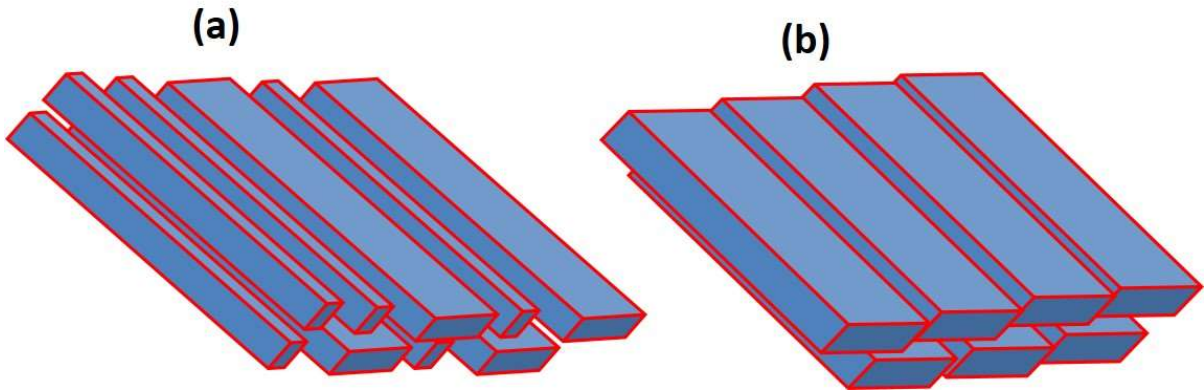


Figure 1.17. (a) Schematic model for random like ribbons. Adapted with permission [158]. (b) Schematic periodically ordered and ribbon-like clay platelets. Adapted with permission [159].

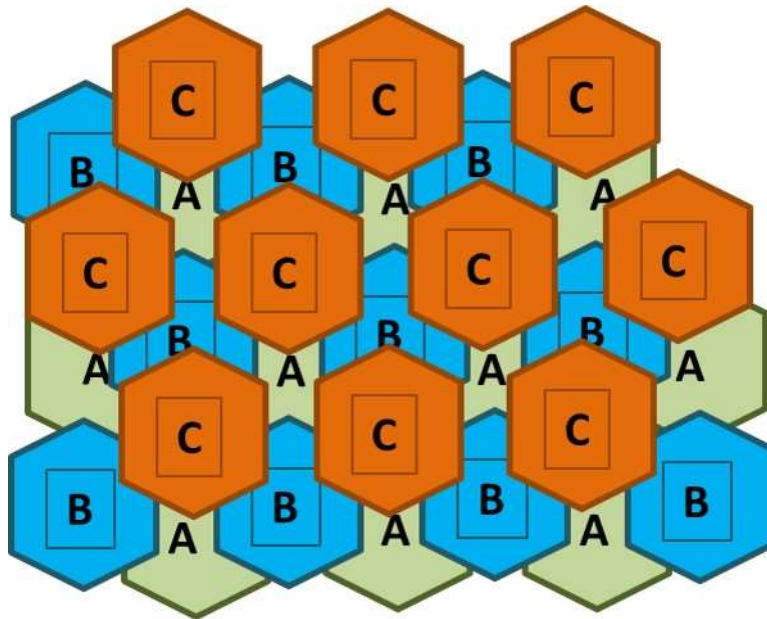


Figure 1.18. A schematic model for hexagonal flakes as a replacement for the original ribbon-like model. Ideally, the flakes are assumed with complete periodic distribution. Adapted with permission [159].

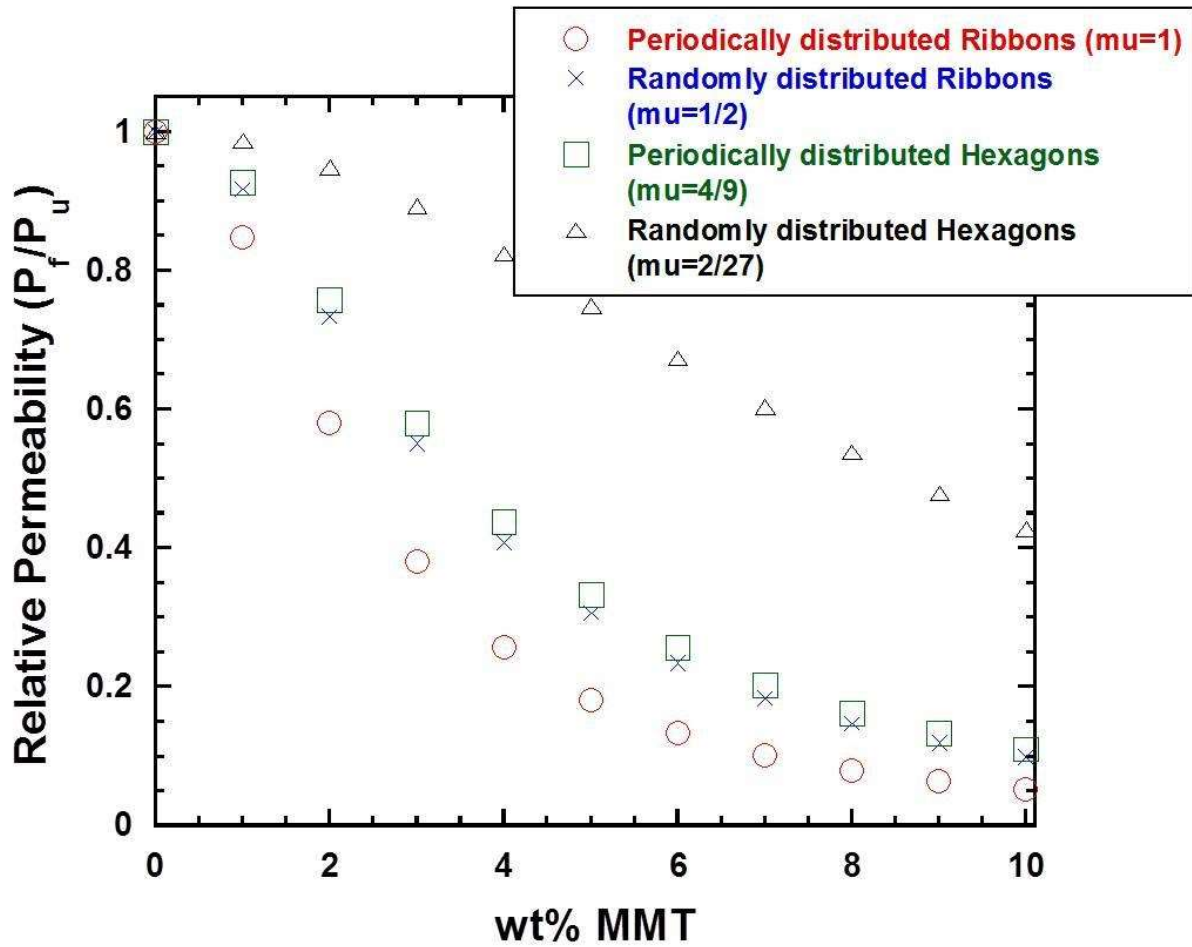


Figure 1.19. Predictions of decreasing the relative permeability of PNCs with an increase in clay weight fraction, according to the Cussler model, in a constant aspect ratio of 100, for different clay shapes and distribution order.

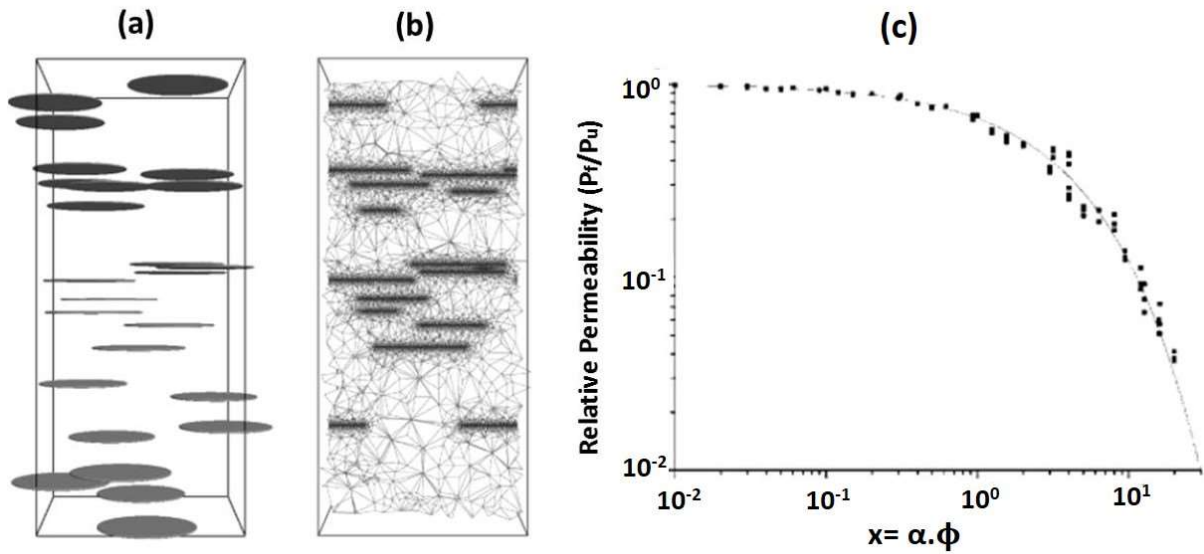


Figure 1.20. (a) A sketch of a Mont Carlo simulated computer model for 25 parallel identical disk shape platelets with aspect ratio 50 and without any overlapping and in 2 vol% of clay. (b) A view of finite element meshes generated for the model by a commercial microprocessor. Adapted with permission [161]. (c). Relative permeability of the Mont Carlo simulated model mentioned, where each point shows a numerical solution for a particular model for a certain aspect ratio (α) and volume fraction (ϕ) of clay. Also, the curve shows the least square fit of the model. Adapted with permission [161].

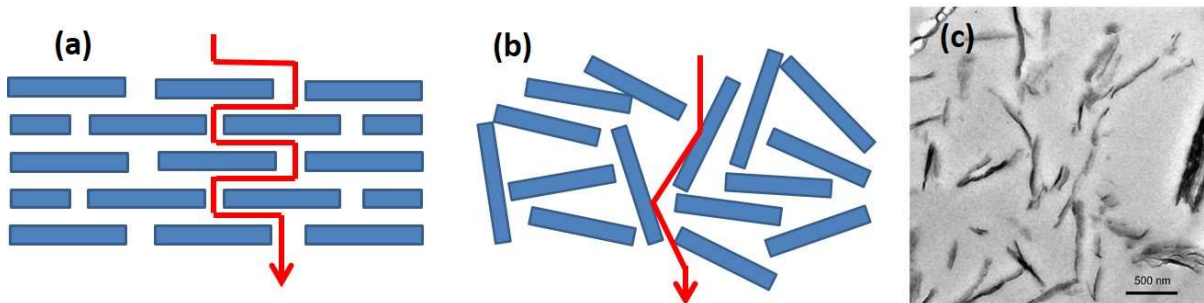


Figure 1.21. Schematic layout of a PNC with (a) completely aligned clay platelets perpendicular to permeant molecule path and (b) partially misaligned platelets. (c) A TEM image of a real epoxy PNC with misaligned morphology. Adapted with permission [72].

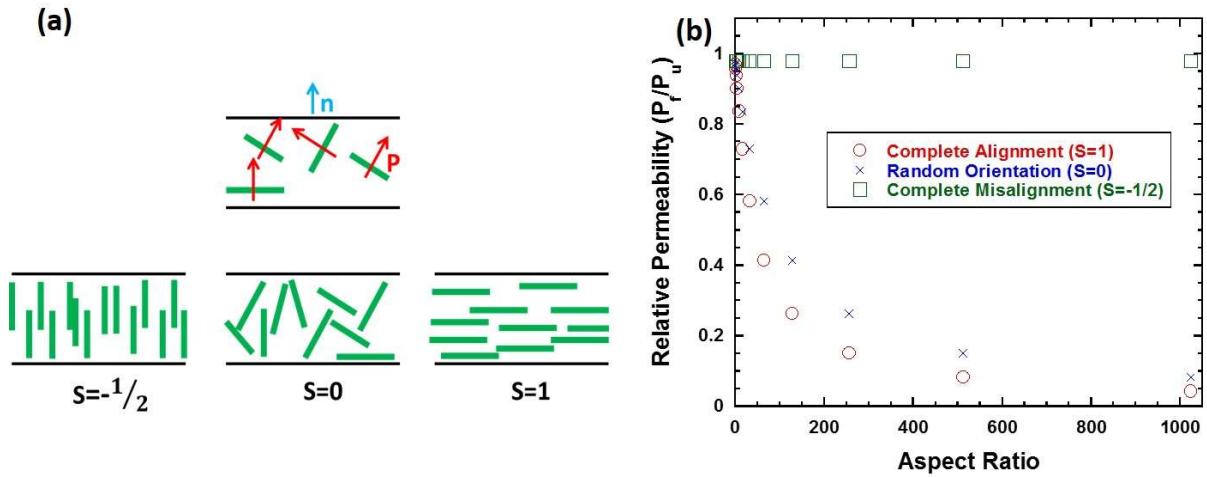


Figure 1.22. (a) Schematic presentation of typical states possible, regarding the orientation of clay platelets and corresponding order parameter values. Adapted with permission [162]. (b) Comparison between predictions for relative permeability of corresponding PNCs containing 5wt% MMT.

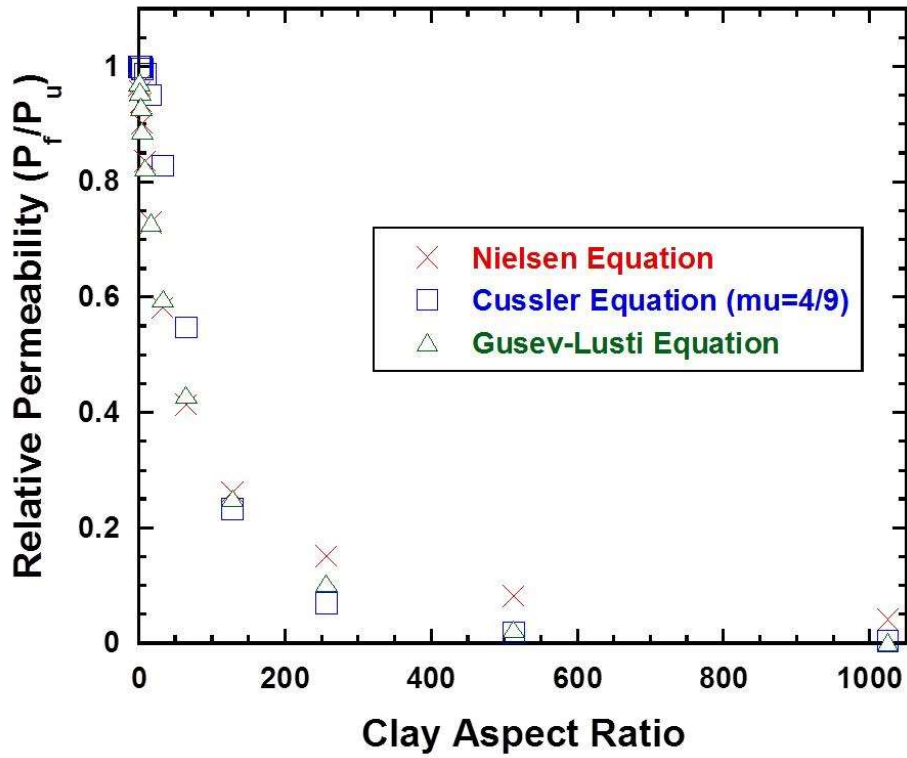


Figure 1.23. Comparison between relative permeability predictions by different models, Nielsen, Cussler, and Gusev-Lusti for PNCs containing 5wt% MMT.

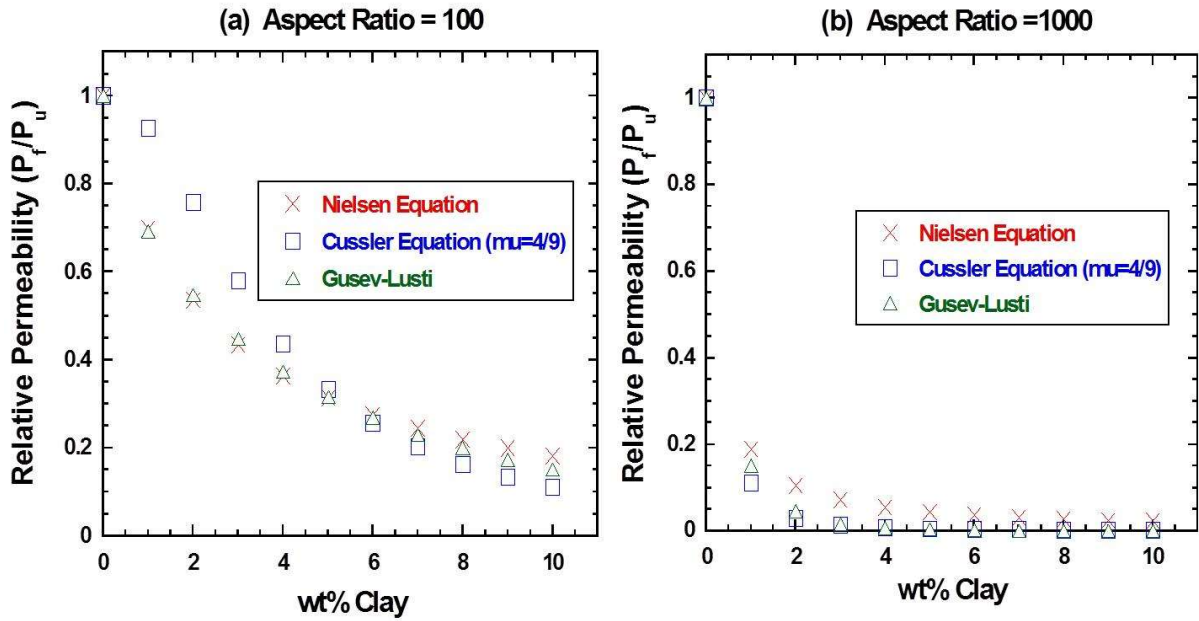


Figure 1.24. Predictions for relative permeability of filled PNC to the unfilled matrix for two different hypothetical aspect ratios of clay, (a) 100 and (b) 1000.

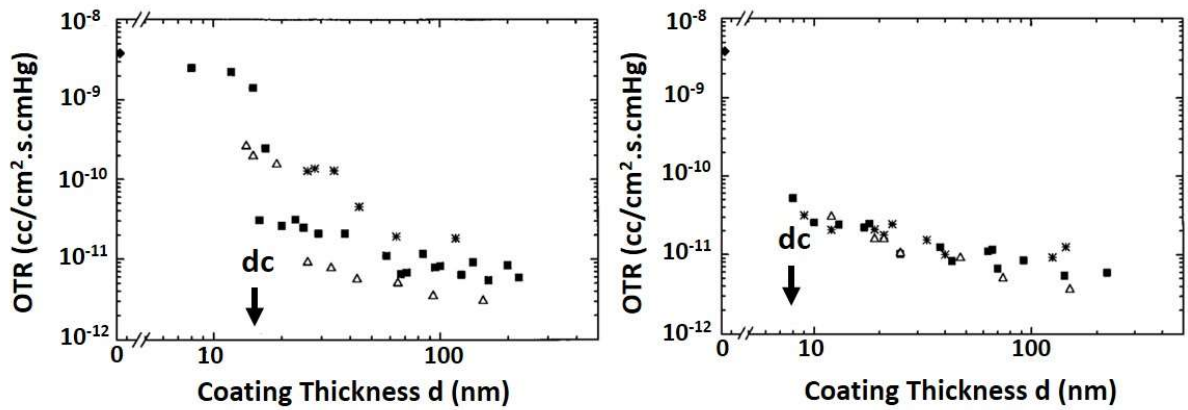


Figure 1.25. OTR versus coating thickness of (a) SiO₂ and (b) SiN deposited through different plasma modes of (Δ) RF, ($*$) MW, (\blacksquare) MW/RF, on 13 μm PET. Adapted with permission [79].

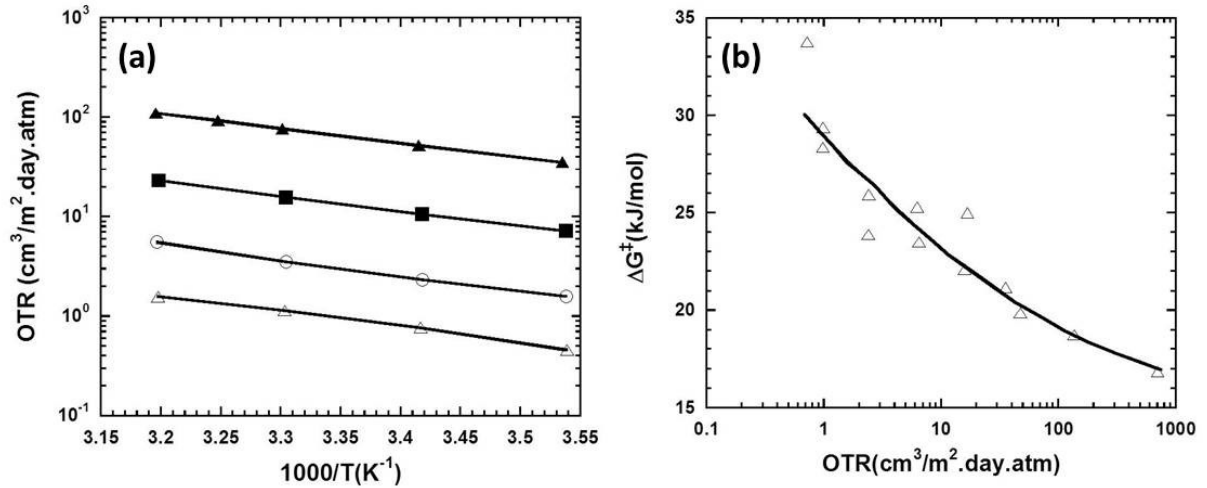


Figure 1.26. (a) The OTR values versus temperature for three different SiOx-coated PET produced under different conditions and neat PET, which are discriminated on the basis of their OTR (in. $\text{cm}^3/(\text{m}^2 \cdot \text{day} \cdot \text{atm})$) at 30°C : 0.18 (Δ), 1.6 (\circ), 16 (\blacksquare), and 80 (PET, \blacktriangle). Arrhenius behavior is observed as the OTR values are fitted to the exponential solid lines. Adapted with permission [12]. (b) In another system of SiOx-coated PC, increasing barrier properties of the coated films resulted in the increased activation energy of permeation, with Arrhenius behavior. It implies occurring a change in permeation mechanism. Adapted with permission [100].

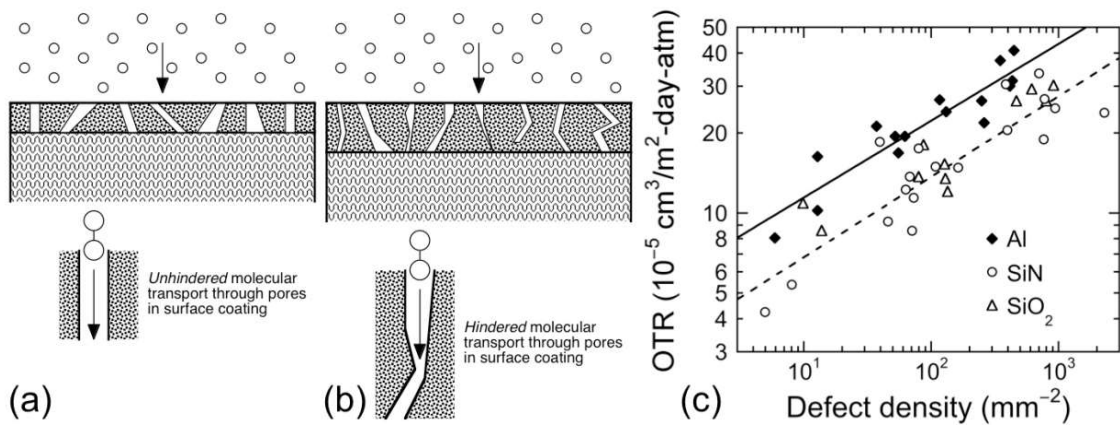


Figure 1.27. Schematic representation of suggested O₂ diffusion through SiO_x-coated PC. (a) Due to either very low thickness of the coating or its large pores, compared with the size of the oxygen molecule, the coating does not behave efficiently in impeding gas transport. (b) With either decrease in the size of pores down to lower than size of O₂ molecules or increasing their tortuosity, due to the increased coating's thickness, it behaves as a good barrier against gas molecules passing through. Adapted with permission [100]. (c) OTR versus defect density for different coatings (○) SiN, (△) SiO₂, (◆) Al when the coating thickness is above its critical value (dc). Adapted with permission [5].

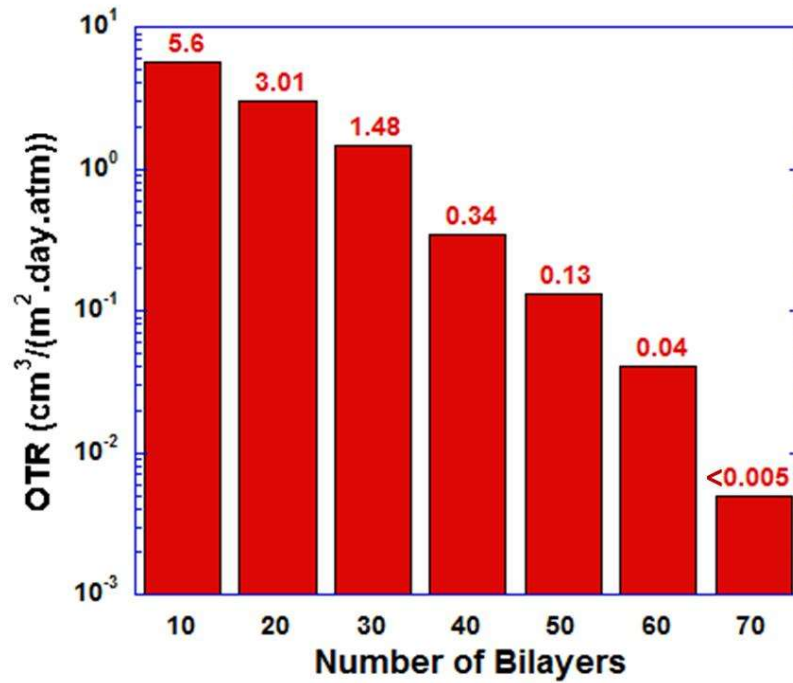


Figure 1.28. OTR of PET coated with LBL assembly of PEI (0.1wt% in solution) and MMT (0.2wt% in suspension) versus number of bilayers. Adapted with permission [14].

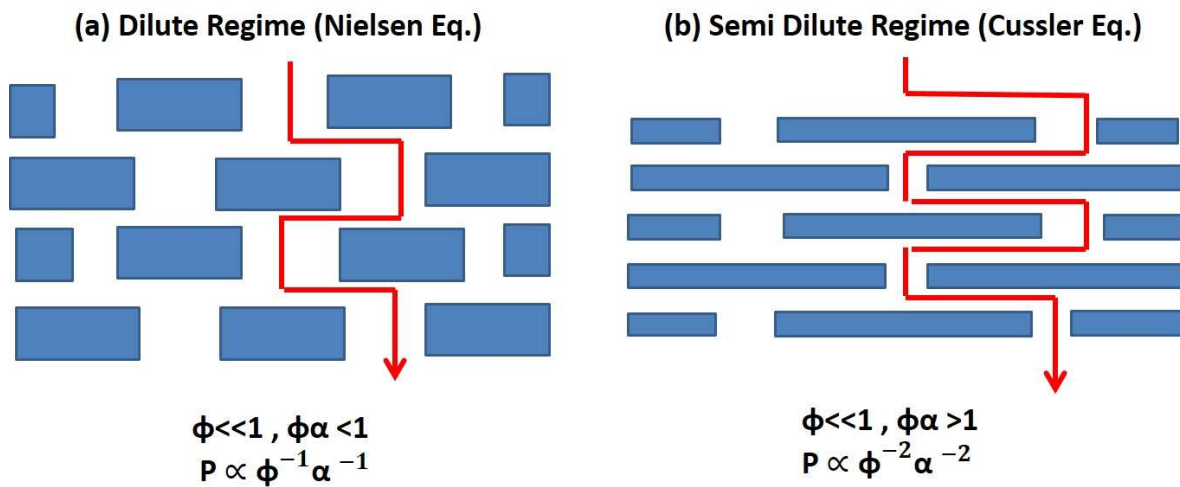


Figure 1.29. Schematic comparison between (a) tortuosity in dilute regimes ($\alpha\phi < 1$) modeled properly by Nielsen equation. (b) Tortuosity in semidilute regime $\alpha\phi > 1$ more suitably with Cussler Equation. Adapted with permission [1].

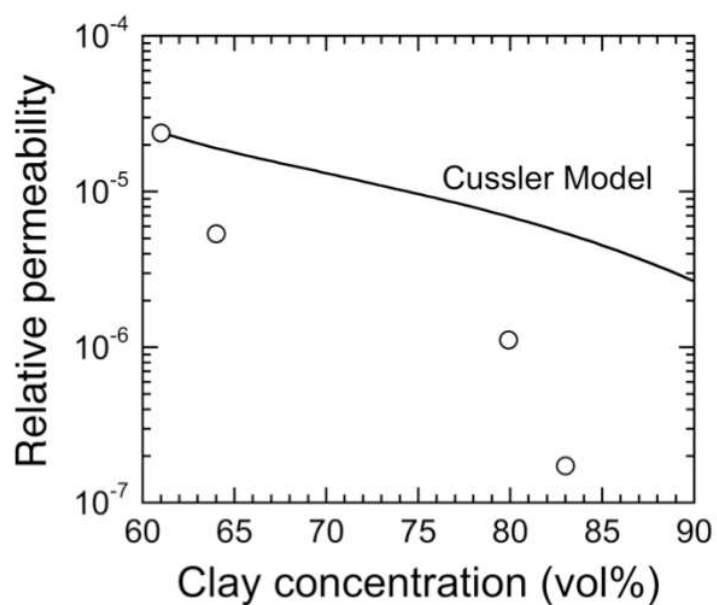


Figure 1.30. Lower experimental relative permeability (P_f/P_u) compared with predictions by Cussler model. Adapted with permission [15].

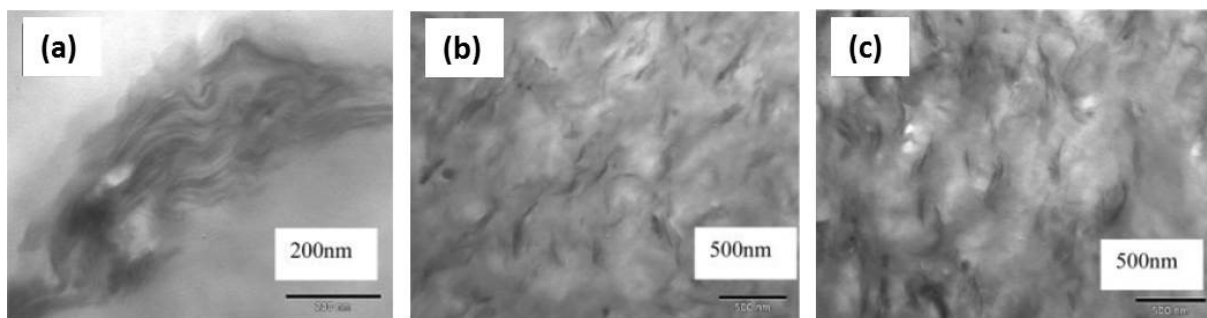


Figure 1.31. TEM micrographs of PNCs containing oxide paraffin compatibilizer with different components: (a) HDPE/20wt% low-viscosity paraffin/5wt% MMT, (b) LDPE-g-MA/20wt% low-viscosity paraffin/5wt% MMT, (c) LDPE-g-MA/20wt% high-viscosity paraffin/5wt% MMT. Reprinted with permission [52].

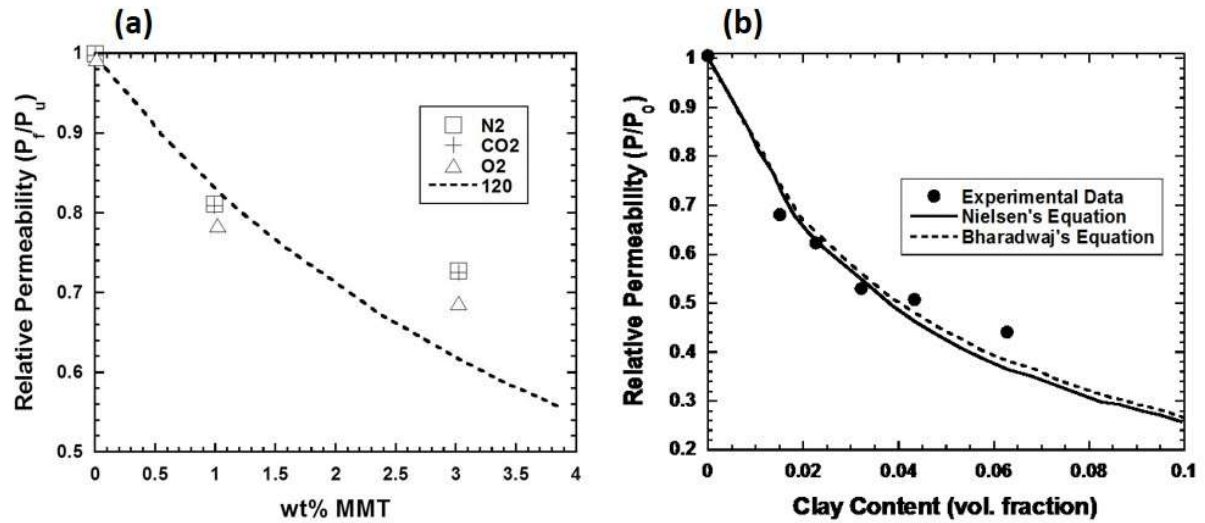


Figure 1.32. (a) Relative permeability of three different gases, O₂, N₂, and CO₂, in LDPE nanocomposites versus weight fraction of MMT. The points are experimental data, and curves illustrate Nielsen predictions for presumed clay aspect ratio of 120. Adapted with permission [55]. (b) Comparison between the experimental relative permeability of HNBR/FHT-EODA nanocomposites and corresponding predicted values by Nielsen and Bharadwaj models versus volume fraction of filler. Adapted with permission [163].

References

- [1] W.-S. Jang, I. Rawson, J.C. Grunlan, Layer-by-layer assembly of thin film oxygen barrier, *Thin Solid Films*. 516 (2008) 4819–4825.
- [2] J. Lewis, Material challenge for flexible organic devices, *Mater. Today*. 9 (2006) 38–45.
- [3] J.D. Affinito, M.E. Gross, C.A. Coronado, G.L. Graff, E.N. Greenwell, P.M. Martin, A new method for fabricating transparent barrier layers, *Thin Solid Films*. 290-291 (1996) 63–67.
- [4] G. Czeremuszkina, M. Latrèche, M.R. Wertheimer, a. S. da Silva Sobrinho, M. Latreche, M.R. Wertheimer, et al., Ultrathin silicon-compound barrier coatings for polymeric packaging materials: An industrial perspective, *Plasmas Polym.* 6 (2001) 107–120.
- [5] A.S. da Silva Sobrinho, G. Czeremuszkina, M. Latreche, M.R. Wertheimer, Defect-permeation correlation for ultrathin transparent barrier coatings on polymers, *J. Vac. Sci. Technol. A Vacuum, Surfaces, Film*. 18 (2000) 149–157.
- [6] M. Hanika, H.C. Langowski, U. Moosheimer, W. Peukert, Inorganic layers on polymeric films—Influence of defects and morphology on barrier properties, *Chem. Eng. Technol.* 26 (2003) 605–614.
- [7] J. Jiang, M. Benter, R. Taboryski, K. Bechgaard, Oxygen barrier coating deposited by novel plasma-enhanced chemical vapor deposition, *J. Appl. Polym. Sci.* 115 (2010) 2767–2772.
- [8] H. Chatham, Oxygen diffusion barrier properties of transparent oxide coatings on polymeric substrates, *Surf. Coatings Technol.* 78 (1996) 1–9.
- [9] A.P. Roberts, B.M. Henry, A.P. Sutton, C.R.M. Grovenor, G.A.D. Briggs, T. Miyamoto, et al., Gas permeation in silicon-oxide/polymer (SiO_x/PET) barrier films: role of the oxide lattice, nano-defects and macro-defects, *J. Memb. Sci.* 208 (2002) 75–88.
- [10] N. Inagaki, S. Tasaka, H. Hiramatsu, Preparation of oxygen gas barrier poly (ethylene terephthalate) films by deposition of silicon oxide films plasma-polymerized from a mixture of tetramethoxysilane and oxygen, *J. Appl. Polym. Sci.* 71 (1999) 2091–2100.
- [11] P.F. Carcia, R.S. McLean, M.D. Groner, A.A. Dameron, S.M. George, Gas diffusion ultrabarriers on polymer substrates using Al₂O₃ atomic layer deposition and SiN plasma-enhanced chemical vapor deposition, *J. Appl. Phys.* 106 (2009) 23533.

- [12] A.G. Erlat, R.J. Spontak, R.P. Clarke, T.C. Robinson, P.D. Haaland, Y. Tropsha, et al., SiO_x gas barrier coatings on polymer substrates: morphology and gas transport considerations, *J. Phys. Chem. B.* 103 (1999) 6047–6055.
- [13] Y.-H. Yang, F.A. Malek, J.C. Grunlan, Influence of deposition time on layer-by-layer growth of clay-based thin films, *Ind. Eng. Chem. Res.* 49 (2010) 8501–8509.
- [14] M.A. Priolo, D. Gamboa, J.C. Grunlan, Transparent clay– polymer nano brick wall assemblies with tailorable oxygen barrier, *ACS Appl. Mater. Interfaces.* 2 (2010) 312–320.
- [15] M.A. Priolo, K.M. Holder, D. Gamboa, J.C. Grunlan, Influence of clay concentration on the gas barrier of clay–polymer nanobrick wall thin film assemblies, *Langmuir.* 27 (2011) 12106–12114.
- [16] R. Cuffe, G. Baud, M. Benmalek, J.P. Besse, J.R. Butruille, H.M. Dunlop, et al., Characterization and adhesion study of thin alumina coatings sputtered on PET, *Thin Solid Films.* 270 (1995) 230–236.
- [17] H. Low, Y. Xu, Moisture barrier of Al_xO_y coating on poly(ethylene terephthalate), poly(ethylene naphthalate) and poly(carbonate) substrates, *Appl. Surf. Sci.* 250 (2005) 135–145.
- [18] A.G. Erlat, B.M. Henry, J.J. Ingram, D.B. Mountain, A. McGuigan, R.P. Howson, et al., Characterisation of aluminium oxynitride gas barrier films, *Thin Solid Films.* 388 (2001) 78–86.
- [19] C. Deng, H.E. Assender, F. Dinelli, O. V Kolosov, G.A.D. Briggs, T. Miyamoto, et al., Nucleation and growth of gas barrier aluminium oxide on surfaces of poly (ethylene terephthalate) and polypropylene: effects of the polymer surface properties, *J. Polym. Sci. Part B Polym. Phys.* 38 (2000) 3151–3162.
- [20] N. Imai, M. Sekiguchi, M. Kano, T. Krug, G. Steiniger, A. Meier, Evaporation method of forming transparent barrier film, U.S. Patent #5,378,506, issued January 3, 1995.
- [21] Y. Leterrier, Durability of nanosized oxygen-barrier coatings on polymers, *Prog. Mater. Sci.* 48 (2003) 1–55.
- [22] R.K. Iler, Multilayers of colloidal particles, *J. Colloid Interface Sci.* 21 (1966) 569–594.
- [23] S.W. Keller, S.A. Johnson, E.S. Brigham, E.H. Yonemoto, T.E. Mallouk, Photoinduced charge separation in multilayer thin films grown by sequential adsorption of

- polyelectrolytes, *J. Am. Chem. Soc.* 117 (1995) 12879–12880.
- [24] Y. Lvov, K. Ariga, I. Ichinose, T. Kunitake, Molecular film assembly via layer-by-layer adsorption of oppositely charged macromolecules (linear polymer, protein and clay) and concanavalin A and glycogen, *Thin Solid Films*. 284 (1996) 797–801.
- [25] J.D. Affinito, S. Eufinger, M.E. Gross, G.L. Graff, P.M. Martin, PML/oxide/PML barrier layer performance differences arising from use of UV or electron beam polymerization of the PML layers, *Thin Solid Films*. 308 (1997) 19–25.
- [26] N.A. Kotov, Layer-by-layer self-assembly: The contribution of hydrophobic interactions, *Nanostructured Mater.* 12 (1999) 789–796.
- [27] O. Félix, Z. Zheng, F. Cousin, G. Decher, Are sprayed LBL-films stratified? A first assessment of the nanostructure of spray-assembled multilayers by neutron reflectometry, *Comptes Rendus Chim.* 12 (2009) 225–234.
- [28] N. Cini, T. Tulun, G. Decher, V. Ball, Step-by-step assembly of self-patterning polyelectrolyte films violating (almost) all rules of layer-by-layer deposition, *J. Am. Chem. Soc.* 132 (2010) 8264–8265.
- [29] P.T. Hammond, Form and function in multilayer assembly: New applications at the nanoscale, *Adv. Mater.* 16 (2004) 1271–1293.
- [30] P. He, N. Hu, J.F. Rusling, Driving forces for layer-by-layer self-assembly of films of SiO₂ nanoparticles and heme proteins, *Langmuir*. 20 (2004) 722–729.
- [31] X. Zhang, H. Chen, H. Zhang, Layer-by-layer assembly: from conventional to unconventional methods, *Chem. Commun.* (2007) 1395–1405.
- [32] W.-S. Jang, J.C. Grunlan, Robotic dipping system for layer-by-layer assembly of multifunctional thin films, *Rev. Sci. Instrum.* 76 (2005) 103904.
- [33] M.A. Priolo, D. Gamboa, K.M. Holder, J.C. Grunlan, Super gas barrier of transparent polymer–clay multilayer ultrathin films, *Nano Lett.* 10 (2010) 4970–4974.
- [34] O. Shchepelina, I. Drachuk, M.K. Gupta, J. Lin, V. V Tsukruk, Silk on Silk Layer by Layer Microcapsules, *Adv. Mater.* 23 (2011) 4655–4660.
- [35] V.H. Orozco, V. Kozlovskaya, E. Kharlampieva, B.L. López, V. V Tsukruk, Biodegradable self-reporting nanocomposite films of poly (lactic acid) nanoparticles engineered by layer-by-layer assembly, *Polymer*. 51 (2010) 4127–4139.

- [36] I. Soltani, Using Layer-by-Layer Coating and Nanocomposite Technologies to Improve the Barrier Properties of Polymeric Materials, Ph.D. Dissertation, North Carolina State University, 2016.
- [37] J.W. Elam, C.A. Wilson, M. Schuisky, Z.A. Sechrist, S.M. George, Improved nucleation of TiN atomic layer deposition films on SiLK low-k polymer dielectric using an Al₂O₃ atomic layer deposition adhesion layer, *J. Vac. Sci. Technol. B Microelectron. Nanom. Struct.* 21 (2003) 1099–1107.
- [38] C.A. Wilson, R.K. Grubbs, S.M. George, Nucleation and growth during Al₂O₃ atomic layer deposition on polymers, *Chem. Mater.* 17 (2005) 5625–5634.
- [39] M.D. Groner, S.M. George, R.S. McLean, P.F. Carcia, Gas diffusion barriers on polymers using Al₂O₃ atomic layer deposition, *Appl. Phys. Lett.* 88 (2006) 51903–51907.
- [40] C.A. Wilson, J.A. McCormick, A.S. Cavanagh, D.N. Goldstein, A.W. Weimer, S.M. George, Tungsten atomic layer deposition on polymers, *Thin Solid Films.* 516 (2008) 6175–6185.
- [41] P.F. Carcia, R.S. McLean, M.H. Reilly, Permeation measurements and modeling of highly defective Al₂O₃ thin films grown by atomic layer deposition on polymers, *Appl. Phys. Lett.* 97 (2010) 221901–221903.
- [42] S.M. George, Atomic layer deposition: an overview, *Chem. Rev.* 110 (2010) 111–131.
- [43] J.C. Spagnola, B. Gong, S.A. Arvidson, J.S. Jur, S.A. Khan, G.N. Parsons, Surface and sub-surface reactions during low temperature aluminium oxide atomic layer deposition on fiber-forming polymers, *J. Mater. Chem.* 20 (2010) 4213–4222.
- [44] E. Langereis, M. Creatore, S.B.S. Heil, M.C.M. Van de Sanden, W.M.M. Kessels, Plasma-assisted atomic layer deposition of Al₂O₃ moisture permeation barriers on polymers, *Appl. Phys. Lett.* 89 (2006) 81915.
- [45] M. Alexandre, P. Dubois, Polymer-layered silicate nanocomposites: preparation, properties and uses of a new class of materials, *Mater. Sci. Eng. R Reports.* 28 (2000) 1–63.
- [46] S.S. Ray, Rheology of polymer/layered silicate nanocomposites, *J. Ind. Eng. Chem.* 12 (2006) 811.
- [47] M. Bousmina, Study of intercalation and exfoliation processes in polymer nanocomposites, *Macromolecules.* 39 (2006) 4259–4263.

- [48] M. Tokihisa, K. Yakemoto, T. Sakai, L.A. Utracki, M. Sepehr, J. Li, et al., Extensional flow mixer for polymer nanocomposites, *Polym. Eng. Sci.* 46 (2006) 1040–1050.
- [49] L.A. Utracki, M. Sepehr, J. Li, Melt compounding of polymeric nanocomposites, *Int. Polym. Process.* 21 (2006) 3–16.
- [50] S. Ray, S.Y. Quek, A. Eastal, X.D. Chen, The potential use of polymer-clay nanocomposites in food packaging, *Int. J. Food Eng.* 2 (2006).
- [51] S.S. Ray, K. Yamada, M. Okamoto, K. Ueda, S. Sinha Ray, K. Yamada, et al., Polylactide-layered silicate nanocomposite: a novel biodegradable material, *Nano Lett.* 2 (2002) 1093–1096.
- [52] E. Jacquilot, E. Espuche, J.F. Gérard, J. Duchet, P. Mazabraud, Morphology and gas barrier properties of polyethylene-based nanocomposites, *J. Polym. Sci. Part B Polym. Phys.* 44 (2006) 431–440.
- [53] R.K. Shah, D.R. Paul, Nylon 6 nanocomposites prepared by a melt mixing masterbatch process, *Polymer.* 45 (2004) 2991–3000.
- [54] Zeng C, Lee LJ. Poly (methyl methacrylate) and polystyrene/clay nanocomposites prepared by in-situ polymerization. *Macromolecules* 2001;34:4098–103.
- [55] R.K. Shah, R.K. Krishnaswamy, S. Takahashi, D.R. Paul, Blown films of nanocomposites prepared from low density polyethylene and a sodium ionomer of poly (ethylene-co-methacrylic acid). *Polymer.* 47 (2006) 6187–6201.
- [56] S. Hamzehlou, A.A. Katbab, Bottle-to-bottle recycling of PET via nanostructure formation by melt intercalation in twin screw compounder: Improved thermal, barrier, and microbiological properties, *J. Appl. Polym. Sci.* 106 (2007) 1375–1382.
- [57] W. Lertwimolnun, B. Vergnes, Influence of compatibilizer and processing conditions on the dispersion of nanoclay in a polypropylene matrix, *Polymer.* 46 (2005) 3462–3471.
- [58] J. Li, C. Zhou, G. Wang, D. Zhao, Study on rheological behavior of polypropylene/clay nanocomposites, *J. Appl. Polym. Sci.* 89 (2003) 3609–3617.
- [59] Y. Zhong, Z. Zhu, S.-Q. Wang, Synthesis and Rheological Properties of Polystyrene/Layered Silicate Nanocomposite, *Polymer.* 46 (2005) 3006–3013.
- [60] E. Moncada, R. Quijada, J. Retuert, Comparative effect of metallocene and Ziegler-

- Natta polypropylene on the exfoliation of montmorillonite and hectorite clays to obtain nanocomposites, *J. Appl. Polym. Sci.* 103 (2007) 698–706.
- [61] D.R. Paul, L.M. Robeson, Polymer nanotechnology: Nanocomposites, *Polymer*. 49 (2008) 3187–3204.
- [62] S.S. Ray, Recent Trends and Future Outlooks in the Field of Clay-Containing Polymer Nanocomposites, *Macromol. Chem. Phys.* 215 (2014) 1162–1179.
- [63] M. Galimberti, Rubber Clay Nanocomposites. In: Boczkowska A, editor. *Advanced Elastomers – Technology, Properties and Applications*. Rijeka, Croatia: InTech; 2012, Available from <http://www.intechopen.com/books/advanced-elastomers-technology-properties-and-applications/rubber-clay-nanocomposites>
- [64] G.W. Beall, C.E. Powell, *Fundamentals of Polymer-Clay Nanocomposites*, 1st ed., Cambridge University Press, Cambridge, UK, 2011.
- [65] Composite Agency. Carbon Dioxide Diffusion Loss from PET Bottle. <http://www.composite-agency.com/archive/Carbon-Dioxide-Diffusion-PET.pdf> (accessed October 1, 2013).
- [66] R. Boyer, J. McKinney, Food Storage Guidelines for Consumers, Virginia Coop. Ext. 2013 (2013) 1–12.
- [67] A.E. Özçam, Surface Modification and Characterization of Polymeric Materials for Targeted Functionality, Ph.D. Dissertation, North Carolina State University, 2011.
- [68] University of South Carolina Research Foundation. Polymer Nanocomposite Technology Brief 2003. [http://ip.research.sc.edu/PDF/Polymer Nanocomposite Technology Brief v1.pdf](http://ip.research.sc.edu/PDF/Polymer%20Nanocomposite%20Technology%20Brief%20v1.pdf) (accessed November 1, 2013).
- [69] E. Aionicesei, M. Škerget, Ž. Knez, Measurement of CO₂ solubility and diffusivity in poly (L-lactide) and poly (D,L-lactide- co-glycolide) by magnetic suspension balance, *J. Supercrit. Fluids*. 47 (2008) 296–301.
- [70] E. Markočič, M. Škerget, Ž. Knez, Solubility and diffusivity of CO₂ in poly (l-lactide)–hydroxyapatite and poly (D, L-lactide-co-glycolide)–hydroxyapatite composite biomaterials, *J. Supercrit. Fluids*. 55 (2011) 1046–1051.
- [71] A. Sorrentino, G. Gorrasi, M. Tortora, V. Vittoria, Barrier properties of polymer/clay nanocomposites, in: Y.W. Mai, Z.Z. Yu (Eds.), *Polym. Nanocomposites*, Woodhead Publishing, 2006: pp. 273–296.

- [72] V. Mittal, Barrier Resistance Generation in Polymer Nanocomposites, in: V. Mittal (Ed.), *Optim. Polym. Nanocomposite Prop.*, 1st ed., Wiley-VCH, Weinheim, Germany, 2010: pp. 173–194.
- [73] G.L. Graff, P.E. Burrows, R.E. Williford, R.F. Praino, Barrier layer technology for flexible displays, in: G. Crawford (Ed.), *Flex. Flat Panel Displays*, John Wiley & Sons, Hoboken, NJ, 2005: pp. 57–77.
- [74] E.H. Jamieson, A. H. Windle, Structure and oxygen-barrier properties of metallized polymer film, *J. Mater. Sci.* 18 (1983) 64–80.
- [75] J.F. Silvain, A. Veyrat, J.J. Ehrhardt, Effect of the temperature on the adhesion and the morphology of thin metal films evaporated on polyethylene terephthalate, *Thin Solid Films.* 221 (1992) 114–119.
- [76] F. Milde, K. Goedicke, M. Fahland, Adhesion behavior of PVD coatings on ECR plasma and ion beam treated polymer films, *Thin Solid Films.* 279 (1996) 169–173.
- [77] K.L. Yam, C.C. Lai, Microwaveable Frozen Food or Meals, in: Y.H. Hui (Ed.), *Handb. Food Sci. Technol. Eng.*, vol. 3, CRC press, Boca Raton, FL., 2006: p. 113.
- [78] P. Gonzalez, E. Garcia, J. Pou, D. Fernandez, J. Serra, B. Leon, et al., Silicon oxide thin films grown by Xe₂ excimer lamp chemical vapour deposition: the role of the substrate temperature and the window-substrate distance, *Thin Solid Films.* 241 (1994) 348–351.
- [79] A.S. da Silva Sobrinho, M. Latreche, G. Czeremuskin, J.E. Klemberg-Sapieha, M.R. Wertheimer, Transparent Barrier coatings on polyethylene terephthalate by single-and dual-frequency plasma-enhanced chemical vapor deposition, *J. Vac. Sci. Technol. A Vacuum, Surfaces, Film.* 16 (1998) 3190–3198.
- [80] D.L. Smith, *Thin-film deposition: principles and practice*, 1st ed., McGraw-Hill, New York, 1995.
- [81] N.B. Matsko, Advances in Microscopic Characterization of Polymer Nanocomposites, in: V. Mittal (Ed.), *Adv. Polym. Nanocomposite Technol.*, 1st ed., Nova Science Publishers, New York, 2010: pp. 407–429.
- [82] T. Suntola, J. Autson, Method for producing compound thin films, U.S. Patent, 4058430, 1977.
- [83] J.C. Spagnola, Atomic layer deposition on fiber forming polymers and nonwoven fiber structures, PhD Dissertation, North Carolina State University, 2010.

- [84] Q. Peng, X.-Y. Sun, J.C. Spagnola, G.K. Hyde, R.J. Spontak, G.N. Parsons, Atomic layer deposition on electrospun polymer fibers as a direct route to Al₂O₃ microtubes with precise wall thickness control, *Nano Lett.* 7 (2007) 719–722.
- [85] J.D. Ferguson, A.W. Weimer, S.M. George, Atomic layer deposition of Al₂O₃ films on polyethylene particles, *Chem. Mater.* 16 (2004) 5602–5609.
- [86] K.B. Blodgett, I. Langmuir, Built-up films of barium stearate and their optical properties, *Phys. Rev.* 51 (1937) 964.
- [87] H. Kuhn, D. Möbius, Systems of Monomolecular Layers Assembling and Physicochemical Behavior, *Angew. Chemie Int. Ed. English.* 10 (1971) 620–637.
- [88] G. Decher, Layer-by-Layer Assembly, in: G. Decher, J.B. Schlenoff (Eds.), *Multilayer Thin Film.*, Willey-VCH, Weinheim, Germany, 2012: pp. 1–22.
- [89] G. Decher, J.D. Hong, J. Schmitt, Buildup of ultrathin multilayer films by a self-assembly process: III. Consecutively alternating adsorption of anionic and cationic polyelectrolytes on charged surfaces, *Thin Solid Films.* 210 (1992) 831–835.
- [90] G. Decher, J.-D. Hong, Buildup of ultrathin multilayer films by a self-assembly process: II. Consecutive adsorption of anionic and cationic bipolar amphiphiles and polyelectrolytes on charged surfaces, in: *Berichte Der Bunsengesellschaft Für Phys. Chemie*, Wiley Online Library, 1991: pp. 1430–1434.
- [91] G. Decher, Fuzzy nanoassemblies: toward layered polymeric multicomposites, *Science* (80-.). 277 (1997) 1232–1237.
- [92] G. Decher, J.-D. Hong, Buildup of ultrathin multilayer films by a self-assembly process, I. consecutive adsorption of anionic and cationic bipolar amphiphiles on charged surfaces, in: *Makromol. Chemie. Macromol. Symp.*, Hüthig & Wepf Verlag, 1991: pp. 321–327.
- [93] J.B. Schlenoff, S.T. Dubas, T. Farhat, Sprayed polyelectrolyte multilayers, *Langmuir.* 16 (2000) 9968–9969.
- [94] R. von Klitzing, R. Kohler, C. Chenigny, Neutron Reflectometry at Polyelectrolyte Multilayers, in: G. Decher, J.B. Schlenoff (Eds.), *Multilayer Thin Film.*, Willey-VCH, Weinheim, Germany, 2012: pp. 219–268.
- [95] P.A. Chiarelli, M.S. Johal, D.J. Holmes, J.L. Casson, J.M. Robinson, H.-L. Wang, Polyelectrolyte spin-assembly, *Langmuir.* 18 (2002) 168–173.

- [96] P.A. Chiarelli, M.S. Johal, J.L. Casson, J.B. Roberts, J.M. Robinson, H. Wang, Controlled fabrication of polyelectrolyte multilayer thin films using spin-assembly, *Adv. Mater.* 13 (2001) 1167–1171.
- [97] C. Jiang, S. Markutsya, V. V Tsukruk, Compliant, robust, and truly nanoscale free standing multilayer films fabricated using spin assisted layer by layer assembly, *Adv. Mater.* 16 (2004) 157–161.
- [98] I. Soltani, M.E. Zeynali, A.A. Yousefi, Toughening of glass fiber reinforced Nylon 66 with EPDM-MAH: Dynamic mechanical, rheological, and morphological investigations, *E-Polymers*. (2012) 1–14.
- [99] M.E. Zeynali, a. a. Yousefi, I. Soltani, Effects of Malienated Ethylene Propylene Diene Monomer (EPDM) Rubber on Dynamic-Mechanical and Rheological Properties of Polyamide 66 (PA 66) Composites, *Polym. Plast. Technol. Eng.* 48 (2008) 42–47.
- [100] A.G. Erlat, B.-C. Wang, R.J. Spontak, Y. Tropsha, K.D. Mar, D.B. Montgomery, et al., Morphology and gas barrier properties of thin SiO_x coatings on polycarbonate: Correlations with plasma-enhanced chemical vapor deposition conditions, *J. Mater. Res. Pittsburgh.* 15 (2000) 704–717.
- [101] S.S. Ray, M. Okamoto, Polymer/layered silicate nanocomposites: a review from preparation to processing, *Prog. Polym. Sci.* 28 (2003) 1539–1641.
- [102] M. A. Osman, V. Mittal, M. Morbidelli, U.W. Suter, Epoxy-layered silicate nanocomposites and their gas permeation properties, *Macromolecules*. 37 (2004) 7250–7257.
- [103] M. Song, J. Jin, Rheological behavior of polymer nanocomposites, in: V. Mittal (Ed.), *Optim. Polym. Nanocomposite Prop.*, 1st ed., Wiley-VCH, Weinheim, Germany, 2010: pp. 93–122.
- [104] M. Kráčalík, M. Studenovský, J. Mikešová, A. Sikora, R. Thomann, C. Friedrich, et al., Recycled PET organoclay nanocomposites with enhanced processing properties and thermal stability, *J. Appl. Polym. Sci.* 106 (2007) 2092–2100.
- [105] R. Krishnamoorti, K. Yurekli, Rheology of polymer layered silicate nanocomposites, *Curr. Opin. Colloid Interface Sci.* 6 (2001) 464–470.
- [106] S.N. Bhattacharya, M.R. Kamal, R.K. Gupta, *Polymeric nanocomposites: theory and practice*, Carl Hanser Publishers, Munich, 2008.
- [107] L. Shen, Y. Lin, Q. Du, W. Zhong, Y. Yang, Preparation and rheology of polyamide-

- 6/attapulgite nanocomposites and studies on their percolated structure, *Polymer*. 46 (2005) 5758–5766.
- [108] Y.T. Lim, O.O. Park, Phase morphology and rheological behavior of polymer/layered silicate nanocomposites, *Rheol. Acta*. 40 (2001) 220–229.
- [109] T.H. Kim, S.T. Lim, C.H. Lee, H.J. Choi, M.S. Jhon, Preparation and rheological characterization of intercalated polystyrene/organophilic montmorillonite nanocomposite, *J. Appl. Polym. Sci.* 87 (2003) 2106–2112.
- [110] V. Mittal, Polymer nanocomposites: synthesis, microstructure, and properties, in: V. Mittal (Ed.), *Optim. Polym. Nanocomposite Prop.*, 1st ed., Wiley-VCH, Weinheim, Germany, 2010: pp. 1–20.
- [111] F. Hussain, M. Hojjati, M. Okamoto, R.E. Gorga, Review article: polymer-matrix nanocomposites, processing, manufacturing, and application: an overview, *J. Compos. Mater.* 40 (2006) 1511–1575.
- [112] L.C. Sawyer, D.T. Grubb, G.F. Meyers, *Polymer microscopy*, 3rd ed., Springer, New York, NY, USA, 2007.
- [113] S.S. Ray, *Clay-containing polymer nanocomposites: from fundamentals to real applications*, First, Elsevier, Amsterdam, 2013.
- [114] M. Kawasumi, The discovery of polymer clay hybrids, *J. Polym. Sci. Part A Polym. Chem.* 42 (2004) 819–824.
- [115] M. Fujiyama, Morphology development in polyolefin nanocomposites, in: V. Mittal (Ed.), *Optim. Polym. Nanocomposite Prop.*, 1st ed., Wiley-VCH, Weinheim, Germany, 2010: pp. 67–92.
- [116] E. Manias, A direct-blending approach for polypropylene/clay nanocomposites enhances properties, *Mater. Res. Soc. Bull.* 26 (2001) 862–863.
- [117] S. Nazarenko, P. Meneghetti, P. Julmon, B.G. Olson, S. Qutubuddin, Gas barrier of polystyrene montmorillonite clay nanocomposites: Effect of mineral layer aggregation, *J. Polym. Sci. Part B Polym. Phys.* 45 (2007) 1733–1753.
- [118] E.P. Giannelis, R. Krishnamoorti, E. Manias, Polymer-Silicate Nanocomposites: Model Systems for Confined Polymers and Polymer Brushes, in: S. Granick (Ed.), *Polym. Confin. Environ.*, Springer, Berlin Heidelberg, 1999: pp. 107–147.
- [119] C.D. Gutierrez, A.E. Ozcam, R.J. Spontak, J. Genzer, Surface Functionalization of

Polyester. U.S. Patent 0,199,692 A1, issued August 28, 2013.

- [120] M. Kráčalík, M. Studenovský, J. Mikešová, A. Sikora, R. Thomann, C. Friedrich, et al., Recycled PET Nanocomposites Improved by Silanization of Organoclays, *J. Appl. Polym. Sci.* 106 (2007) 926–937.
- [121] D.J. Frankowski, M.D. Capracotta, J.D. Martin, S. a. Khan, R.J. Spontak, Stability of organically modified montmorillonites and their polystyrene nanocomposites after prolonged thermal treatment, *Chem. Mater.* 19 (2007) 2757–2767.
- [122] A. Ranade, N.A. D'Souza, B. Gnade, Exfoliated and intercalated polyamide-imide nanocomposites with montmorillonite, *Polymer.* 43 (2002) 3759–3766.
- [123] A. Bansal, H. Yang, C. Li, K. Cho, B.C. Benicewicz, S.K. Kumar, et al., Quantitative equivalence between polymer nanocomposites and thin polymer films., *Nat. Mater.* 4 (2005) 693–698.
- [124] J. Zhao, A.B. Morgan, J.D. Harris, Rheological characterization of polystyrene–clay nanocomposites to compare the degree of exfoliation and dispersion, *Polymer.* 46 (2005) 8641–8660.
- [125] A. Giannakas, C.G. Spanos, N. Kourkoumelis, T. Vaimakis, a. Ladavos, Preparation, characterization and water barrier properties of PS/organo-montmorillonite nanocomposites, *Eur. Polym. J.* 44 (2008) 3915–3921
- [126] U. Yilmazer, G. Ozden, Polystyrene–organoclay nanocomposites prepared by melt intercalation, in situ, and masterbatch methods, *Polym. Compos.* 27 (2006) 249–255.
- [127] K.J. Lin, C.H. Lee, K.F. Lin, Extraordinary mechanical behavior of exfoliated montmorillonite/polymer nanocomposite films cast from soap-free emulsion polymerized latices, *J. Polym. Sci. Part B Polym. Phys.* 48 (2010) 1064–1069.
- [128] P. Uthirakumar, M.K. Song, C. Nah, Y.S. Lee, Preparation and characterization of exfoliated polystyrene/clay nanocomposites using a cationic radical initiator-MMT hybrid, *Eur. Polym. J.* 41 (2005) 211–217.
- [129] P. Uthirakumar, Y.B. Hahn, K.S. Nahm, Y.S. Lee, Exfoliated high-impact polystyrene/MMT nanocomposites prepared using anchored cationic radical initiator-MMT hybrid, *Eur. Polym. J.* 41 (2005) 1582–1588.
- [130] P.B. Messersmith, E.P. Giannelis, Polymer-layered silicate nanocomposites: in situ intercalative polymerization of. epsilon.-caprolactone in layered silicates, *Chem. Mater.* 5 (1993) 1064–1066.

- [131] J. Golebiewski, A. Galeski, Thermal stability of nanoclay polypropylene composites by simultaneous DSC and TGA, *Compos. Sci. Technol.* 67 (2007) 3442–3447.
- [132] M. Sepehr, L. a. Utracki, X. Zheng, C. a. Wilkie, Polystyrenes with macro-intercalated organoclay. Part II. Rheology and mechanical performance, *Polymer*. 46 (2005) 11569–11581
- [133] M. Sepehr, L. a. Utracki, X. Zheng, C. a. Wilkie, Polystyrenes with macro-intercalated organoclay. Part I. Compounding and characterization, *Polymer*. 46 (2005) 11557–11568.
- [134] F. Bertini, M. Canetti, G. Audisio, G. Costa, L. Falqui, Characterization and thermal degradation of polypropylene-montmorillonite nanocomposites, *Polym. Degrad. Stab.* 91 (2006) 600–605.
- [135] D.J. Frankowski, S. a. Khan, R.J. Spontak, Chain-scission-induced intercalation as a facile route to polymer nanocomposites, *Adv. Mater.* 19 (2007) 1286–1290.
- [136] K. P. Pramoda, T. Liu, Z. Liu, C. He, H.-J.J. Sue, Thermal degradation behavior of polyamide 6/clay nanocomposites, *Polym. Degrad. Stab.* 81 (2003) 47–56.
- [137] M. Ziadeh, B. Fischer, J. Schmid, V. Altstädt, J. Brey, On the importance of specific interface area in clay nanocomposites of PMMA filled with synthetic nano-mica, *Polymer*. 55 (2014) 3770–3781.
- [138] V. Molajavadi, H. Garmabi, Water assisted exfoliation of PA6/clay nanocomposites using a twin screw extruder: Effect of water contact time, *J. Appl. Polym. Sci.* 119 (2011) 736–743.
- [139] D.J. Rousseaux, N. Sallem-Idrissi, A.-C. Baudouin, J. Devaux, P. Godard, J. Marchand-Brynaert, et al., Water-assisted extrusion of polypropylene/clay nanocomposites: A comprehensive study, *Polymer*. 52 (2011) 443–451.
- [140] A. Ammala, C. Bell, K. Dean, Poly (ethylene terephthalate) clay nanocomposites: improved dispersion based on an aqueous ionomer, *Compos. Sci. Technol.* 68 (2008) 1328–1337.
- [141] A.B. Morgan, J.W. Gilman, Characterization of polymer layered silicate (clay) nanocomposites by transmission electron microscopy and x-ray diffraction: A comparative study, *J. Appl. Polym. Sci.* 87 (2003) 1329–1338.
- [142] J. Comyn, Introduction to Polymer Permeability and the Mathematics of Diffusion, in:

- J. Comyn (Ed.), *Polym. Permeability*, 1st ed., Elsevier, London and New York, 1985: pp. 1–10.
- [143] X. Hu, J. Tang, A. Blasig, Y. Shen, M. Radosz, T.C. Merkel, et al., CO₂ permeability, diffusivity and solubility in polyethylene glycol-grafted polyionic membranes and their CO₂ selectivity relative to methane and nitrogen, *J. Memb. Sci.* 281 (2006) 130–138.
- [144] N.P. Patel, A.C. Miller, R.J. Spontak, Highly CO₂-Permeable and Selective Polymer Nanocomposite Membranes, *Adv. Mater.* 15 (2003) 729–733.
- [145] M. Perez-Blanco, J.R. Hammons, R.P. Danner, Measurement of the solubility and diffusivity of blowing agents in polystyrene, *J. Appl. Polym. Sci.* 116 (2010) 2359–2365.
- [146] Y. Sato, T. Takikawa, S. Takishima, H. Masuoka, Solubilities and diffusion coefficients of carbon dioxide in poly (vinyl acetate) and polystyrene, *J. Supercrit. Fluids.* 19 (2001) 187–198.
- [147] Y. Sato, T. Takikawa, A. Sorakubo, S. Takishima, H. Masuoka, M. Imaizumi, Solubility and diffusion coefficient of carbon dioxide in biodegradable polymers, *Ind. Eng. Chem. Res.* 39 (2000) 4813–4819.
- [148] B.I. Chaudhary, A.I. Johns, Solubilities of nitrogen, isobutane and carbon dioxide in polyethylene, *J. Cell. Plast.* 34 (1998) 312–328.
- [149] A. Blasig, J. Tang, X. Hu, Y. Shen, M. Radosz, Magnetic suspension balance study of carbon dioxide solubility in ammonium-based polymerized ionic liquids: Poly (p-vinylbenzyltrimethyl ammonium tetrafluoroborate) and poly ([2-(methacryloyloxy) ethyl] trimethyl ammonium tetrafluoroborate), *Fluid Phase Equilib.* 256 (2007) 75–80.
- [150] A. Blasig, J. Tang, X. Hu, Y. Shen, M. Radosz, Carbon dioxide solubility in polymerized ionic liquids containing ammonium and imidazolium cations from magnetic suspension balance: P [VBTMA][BF₄] and P [VBMI][BF₄], *Ind. Eng. Chem. Res.* 46 (2007) 5542–5547.
- [151] J. Crank, G.S. Park, *Methods of Measurement*, in: G.S. Park, J. Crank (Eds.), *Diffus. Polym.*, Academic Press, London and New York, 1968: pp. 1–37.
- [152] J. Crank, *The Mathematics of Diffusion*, Oxford University Press, Oxford, 1975.
- [153] G.S. Park, *The Glassy State and Slow Process Anomalies*, in: J. Crank, G.S. Park (Eds.), *Diffus. Polym.*, Academic Press, London and New York, 1968: pp. 141–162.

- [154] L.E. Nielsen, Models for the permeability of filled polymer systems, *J. Macromol. Sci.* 1 (1967) 929–942.
- [155] G.H. Fredrickson, J. Bicerano, Barrier properties of oriented disk composites, *J. Chem. Phys.* 110 (1999) 2181–2188.
- [156] C.H. Klute, Diffusion of small molecules in semicrystalline polymers: water in polyethylene, *J. Appl. Polym. Sci.* 1 (1959) 340–350.
- [157] J.P. DeRocher, B.T. Gettelfinger, J. Wang, E.E. Nuxoll, E.L. Cussler, Barrier membranes with different sizes of aligned flakes, *J. Memb. Sci.* 254 (2005) 21–30.
- [158] Cussler EL, Hughes SE, Ward III WJ, Aris R. Barrier membranes. *J Memb Sci* 1988;38:161–74.
- [159] G.D. Moggridge, N.K. Lape, C. Yang, E.L. Cussler, Barrier films using flakes and reactive additives, *Prog. Org. Coatings.* 46 (2003) 231–240.
- [160] W.-S. Jang, Layer-by-layer assembly of clay-filled polymer nanocomposite thin films, Texas A&M University, 2008.
- [161] A.A. Gusev, H.R. Lusti, Rational design of nanocomposites for barrier applications, *Adv. Mater.* 13 (2001) 1641.
- [162] R.K. Bharadwaj, Modeling the barrier properties of polymer-layered silicate nanocomposites, *Macromolecules.* 34 (2001) 9189–9192.
- [163] K.G. Gatos, J. Karger-Kocsis, Effect of the aspect ratio of silicate platelets on the mechanical and barrier properties of hydrogenated acrylonitrile butadiene rubber (HNBR)/layered silicate nanocomposites, *Eur. Polym. J.* 43 (2007) 1097–1104.
- [164] H.J. Ploehn, C. Liu, Quantitative analysis of montmorillonite platelet size by atomic force microscopy, *Ind. Eng. Chem. Res.* 45 (2006) 7025–7034.
- [165] Mineralogy Database. General Montmorillonite Information, 2013. <http://webmineral.com/data/Montmorillonite.shtml>.

Nomenclature

Abbreviations

AC
AFM
ALD
ALE
CVD
FE
FEM
GRAS
LB
LBL
LCP
MA
MSB
OLED
OTR
PCN
PEM
PSLN
PVD
RF
SEM
TEM
TiN
TSE
UV
WVTR
XRD

Definitions

Alternative current
Atomic force microscopy
Atomic Layer Deposition
Atomic layer epitaxy
Chemical vapor deposition
Finite element
Finite element method
Generally regarded as safe
Langmuir-Blodgett
Layer-by-Layer
Liquid crystal polymers
Maleic anhydride
Magnetic suspension balance
Organic light emitting diodes
Oxygen transmission rate
Polymer-clay nanocomposites
Polyelectrolyte multilayer
Polymer layered silicate nanocomposites
Physical vapor deposition
Radio frequency
Scanning electron microscopy
Transmission electron microscopy
Titanium nitride
Twin-screw extruder
Ultra violet
Water vapor transmission rate
X-ray diffractometry

CHAPTER 2

Nanotechnological Strategies Yielding High-Barrier Plastic Food Packaging

Iman Soltani¹ and Richard J. Spontak^{2,3}

¹Fiber and Polymer Science Program

Departments of ²Chemical & Biomolecular Engineering and ³Materials Science & Engineering
North Carolina State University, Raleigh, NC 27695, USA

(in press Chapter at Nanotechnology in Food Industry)

Abstract

Polymers and their hybrid nanocomposites serve as inexpensive, lightweight and processable alternatives to more traditional materials, such as metals and ceramics, employed for barrier purposes in food packaging. In light of the impact of solid waste on environmental integrity, these systems must be designed to minimize material use and yet impede molecular transport into or out of packaged food/beverage products. To achieve these objectives, a variety of different physico-chemical approaches have been developed on the basis of either deposited/assembled coatings or incorporated nanoscale objects. In this chapter, we explore the motivation for and application of these strategies as routes by which to enhance barrier properties. Established sputtering and chemical vapor deposition technologies involving metal/silica-like coatings will be compared with current approaches relying on atomic layer deposition and layer-by-layer techniques to generate conformal coatings. Nanocomposites designed to not only hinder molecular transport but also improve physical/thermal properties will be systematically examined to identify key design rules. The objective of the present work

is to describe the coating and nanocomposite approaches developed to enhance barrier performance in food packaging, as well as introduce developing trends and future needs.

Key words: food packaging, polymer crosslinking, nanocomposites, impermeable coatings, barrier properties

Contact: Professor Dr. Richard J. Spontak (+1-919-417-3554 or Rich_Spontak@ncsu.edu)

2.1. Introduction

In light of their lower weight and price (due to source materials and production) and their inert nature and robust mechanical properties, polymeric materials continue to replace traditional materials such as metals and ceramics in food packaging applications. A recent study by Franklin Associates (2014) indicates that the food industry earns about 38% of the market share for flexible plastic packaging used in the U.S. last year. Within this category, the top three subcategories requiring flexible plastic packaging include meat products (16%), baked goods (13%) and snack foods (11%). In addition, the top three U.S. market share categories for rigid beverage containers include carbonated soft drinks (31%), water (23%), and beer (14%). A complementary breakdown on the basis of mass is provided in Figure 2.1. In addition to the considerations listed above, use of plastics in food packaging can significantly reduce material and energy expenditures, as well as greenhouse pollution, relative to alternative packaging materials. For example, plastics employed in the production of beverage containers account for annual energy savings of about 1.2×10^{11} MJ and decreased CO₂ emissions by 9.7×10^6 metric tons [1,2]. Although they exhibit distinct advantages compared to their inorganic counterparts in food packaging, polymeric substitutes generally

remain inferior in terms of their barrier performance. Thus, identification of economically viable strategies by which to improve the barrier properties of polymers to extend the transportation and shelf lives of food products has become an important fundamental and technological objective. One of the primary approaches commercially developed for this purpose depends on the post-processing application of impermeable metal or ceramic coatings, which must be sufficiently thin to remain flexible and avoid cracking. This tactic nonetheless is in need of further improvement to satisfy ongoing requirements in food packaging applications [3–11]

The development of thin inorganic coatings designed to improve the barrier properties of polymeric films can be traced back to the 1970s when vacuum metallization was utilized to evaporate a thin opaque layer of aluminum on polyester [12]. In fact, coatings based on physical evaporation methods applied under vacuum were considered as the most effective means by which to enhance the barrier performance of polymeric films for several subsequent decades [13–19]. A practical drawback to single-layer thin coatings was the existence of discrete defects, which expectedly had an adverse effect on their otherwise impermeable characteristics. Solutions to this nontrivial shortcoming prompted the development of multilayer coatings, such as those afforded by layer-by-layer (LBL) procedures [11,20–35], and almost defect-free atomic layer deposition (ALD) coatings [9,36–44]. Inorganic modification of bulk polymers promoted the introduction of polymer nanocomposites (PNCs) as attractive alternatives to coating processes. Such hybrid materials were effectively free from the typical problems that plagued inorganic coatings (*e.g.*, cracking and delamination), and the incorporation of nanoscale objects into a polymer matrix concurrently augmented other

physical, often mechanical, properties. Lastly, the processing required to generate PNCs at large, industrial scales was facile and less expensive relative to high-vacuum coating processes, and it provided a largely unexplored route by which to tune barrier properties via tortuosity considerations at nanoscale dimensions [45–60]. In the following sections, we address fundamental aspects of various polymer coating and nanocomposite strategies designed for improved barrier performance, and discuss their efficacy in the food packaging industry.

2.2. Existing Demands and Challenges

Food and medical packaging materials must be designed with high barrier properties against reactive gases such as oxygen to increase the transportation and shelf life of the packaged contents. According to the results of Hanika et al. (2003) presented in Figure 2.2a, the oxygen transmission rate (OTR) required for most food products should lie between about 0.1 and 30 cm³/m²-day-bar (assuming STP conditions), depending on the oxygen sensitivity of the food type. Baby food and beer are much more susceptible to oxidation than, for instance, ketchup and nuts. Two principal factors govern the OTR: polymer thickness and polymer chemistry, the latter of which dictates the diffusivity (D) and solubility (S) [and, hence, permeability ($P = D \times S$)] of penetrant molecules through a dense polymer matrix. Polymer chemistry must also be considered on the basis of safety since some polymers may contain residual monomer (*e.g.*, bisphenol A, BPA) that can leach into and contaminate food products upon contact [61]. Reported OTR values for polymer films measuring 100 μm thick [6,38] are also displayed as a function of water vapor transmission rate (WVTR) in Figure 2.2b and reveal that most commercially relevant polymers, with notable exception of liquid crystalline

polymers (not shown) and some ethylene vinyl alcohol (EVOH) copolymers, exhibit an OTR greater than $0.1 \text{ cm}^3/\text{m}^2\text{-day-bar}$, which makes most of these polymers generally suitable for food packaging applications.

In the specific case of carbonated beverages packaged in melt-blown bottles and maintained at elevated pressures of $\approx 3 \text{ bar}$ (Composite Agency)[62], however, retention of carbon dioxide requires high barrier properties against an acid gas that is known to act as a plasticizer for many thermoplastic polymers [63]. Although polyethylene terephthalate (PET) is widely employed as a substitute for traditional glass bottles, its inferior barrier properties promote a significantly shorter shelf life [56]. In fact, the experimental results provided in Figure 2.2c indicate that pressurized carbon dioxide permeates through conventional PET soft drink bottles after only a few seconds, resulting in a mass loss of $\approx 20 \text{ mg}$ after only 24 h. After a single year, the mass of CO_2 remaining decreases by 75%. This barrier performance is responsible for a PET-bottled carbonated soft drink typically having a shelf life of 3-4 months [64]. Recent considerations that have exacerbated this shelf-life problem include the use of thinner walls to reduce bottle weight and the infusion of recycled PET to reduce solid landfill [59,65–68]. Therefore, for this and related reasons, the need for effective barrier properties in the food packaging industry has prompted numerous polymer coating and nanocomposite technologies [30]. Due to complications arising from, for instance, specific interactions between penetrant molecules and the matrix polymer or the presence of nano/microscale interfaces, however, improving barrier properties has proven to be scientifically challenging. Advances in barrier properties achieved on the basis of new or existing material strategies have

been less than the progress devoted to developing and commercializing the approaches themselves [12,69,70].

2.3. Coating Methods for Improved Barrier Properties

One of the primary classifications of methods intended to improve the barrier properties of polymer substrates involves the deposition of a thin high-barrier inorganic coating. Such coatings can be further categorized on the basis of the number of layers as either single-layered or multilayered. In the following sections, we discuss both coating categories.

2.3.1. Single-Layer Coatings

Single-layer barrier coatings for plastics are conveniently divided into metal and oxide/nitride coatings on the basis of their optical transparency. Opaque metal coatings have been commercialized since the early 1970s and are responsible for the aluminized PET and polypropylene (PP) packaging commonly encountered in snack food and beverage packaging. These vacuum-metalized plastics, in particular, are produced at an industrial scale through evaporation and deposition of a 10-100 nm thick Al film on a moving polymeric substrate maintained in a roll-to-roll configuration inside a large vacuum chamber [71]. The OTR of a PET film measuring 13 μm thick and coated with a thin (20 nm) Al coating decreases by about 2 orders of magnitude from about 100 to 1 $\text{cm}^3/\text{m}^2\text{-day-bar}$ [72]. Satisfactory performance of such laminates inherently depends on good adhesion between the coating and polymer substrate through the formation of chemical bonds during deposition [73,74]. Two obvious shortcomings of metalized coatings are that they are optically opaque and recycling can be problematic [71]. Conversely, transparent oxide and nitride coatings derived from SiO_x , AlO_x ,

TiO_x, and Si₃N₄ are frequently used in polymer packaging to facilitate product viewing and microwaving. Polymers modified with such coatings are easier to recycle, thereby reducing environmental concerns. The primary advantage of transparent oxide/nitride coatings relative to metal coatings is that they provide higher barrier properties wherein gas permeation is restricted to existing defects. Thus, the properties of these barrier coatings strongly depend on the density of defects that develop during fabrication due to factors such as deposition conditions and coating thickness [17,18]. The series of atomic force microscopy (AFM) images presented in Figure 2.3 [16] demonstrates how the coating uniformity changes with thickness due to the transverse propagation of defects. Since metal oxides and nitrides are dielectric and possess high melting points, high-throughput vacuum deposition can become technologically challenging, especially when performed on polymer substrates that must be maintained at temperatures below 100 °C to avoid softening, distortion or undesirable expansion [71,75].

Generally speaking, transparent oxide and nitride coatings are deposited on polymer substrates through the use of three commercial processes: evaporation (thermal or electron beam), sputtering and chemical vapor deposition [6,9,13,19,76]. Evaporation is a physical vapor deposition (PVD) coating process that is divided into thermal and electron beam-assisted methods. It is performed on the scale of molecular flow, in which case the distance between the source undergoing evaporation and the substrate is less than the mean free path of the source species in the gas state. As a result of thermal heating, molecules become sufficiently energized to leave the source and, after traveling through the evacuated deposition chamber, condense on the substrate surface [15]. While strictly thermal evaporation has been conducted with many different coatings, the evaporative deposition of high-melting metal oxides often

requires assistance from a focused electron beam [5,12,14]. In sputtering, the source material is bombarded by a plasma discharge, and source molecules are deposited as a vapor [6]. Due to greater parameter tunability available in sputtering relative to evaporation, the properties of sputtered coatings can be more precisely manipulated [13]. Moreover, sputtering requires a lower vacuum for deposition and provides a uniform film on a larger area with a wider choice of source materials than evaporation, and sputtered coatings tend to possess better adhesion to polymer substrates. Chemical vapor deposition (CVD) operates on the principle that vapor-phase metal-containing molecules migrate from the source to the substrate in a manner that differs from PVD. Source gas molecules undergo convective diffusion close to the substrate surface, where they absorb and react to release gaseous products that desorb from the surface. Unlike evaporation and sputtering, CVD does not rely on line of sight and thus yields a conformal coating. In the case of polymer substrates, plasma-enhanced CVD (PECVD) involves the use of microwave- or radio frequency-activated plasma to activate the source material at low temperatures [3,4,16]. Plasmas excited by microwave radiation yield greater ionization and thus higher deposition rates than radio frequency plasmas, whereas radio frequency plasmas are excited at lower frequencies and permit more precise control over the ion energy and flux. This feature is particularly beneficial for polymer substrates that possess a relatively low glass transition temperature and cannot be subjected to very much heat [76].

The last and most recently developed single-layer coating process included here is atomic layer deposition (ALD), which was introduced by Suntola & Autson (1977)[77] under the name of atomic layer epitaxy to describe the deposition of ZnS on glass at 320 °C. In 2003,

ALD was applied for the first time to deposit Al_2O_3 on a polymer substrate as nucleating base layer [36]. In the same fashion as CVD, ALD is deposited through a chemical reaction, not physical bombardment, and provides conformal coverage, which makes it particularly valuable for coating complex 3D shapes [40,78]. During ALD performed under vacuum, two species are alternatively introduced to react with a surface of interest and each deposit a single atomic layer. As schematically depicted in Figure 2.4a for the deposition of Al_2O_3 onto a hydrophilic polymer substrate, trimethylaluminum (TMA) is used to react with surface hydroxyl groups to form a hydrophobic layer (dose mode). Excess (unreacted) TMA is removed by purging with an inert gas (purge mode) and water vapor is introduced into the chamber to react with the newly formed layer and make the surface hydrophilic again. In this fashion, the surface is prepared for subsequent reaction with TMA. This highly controlled deposition cycle can be repeated until a coating of desired thickness is achieved with atomic precision, as evidenced by the thickness measurements displayed in Figure 2.4b [40]. Separation of the reactive species by an inert gas purge prevents the possibility of gas-phase reactions, which increases coating uniformity relative to CVD [43,44]. Thus far, ALD has been extensively investigated as a means by which to deposit Al_2O_3 coatings at relatively low temperatures (typically $\approx 120^\circ\text{C}$) on a wide variety of thermoplastic polymers including PET, PP, polyethylene (PE), polyimide (PI), polystyrene (PS), poly(vinyl alcohol) (PVA), and poly(methyl methacrylate) (PMMA) [9,37,38,40–42].

2.3.2. Multilayer Coatings

Despite the improved barrier properties attained with polymer substrates coated with single metal and metal oxide layers, a drawback to single layer coatings deposited by methods such as PVD and CVD that is responsible for inconsistent results is the formation of defects. Such defects, usually associated with inefficient particle packing, can become increasingly problematic, especially as the coating thickness is increased and associated stresses develop. This issue, coupled with commercial costs related to high-throughput processing, is largely responsible for motivating complementary studies of alternative deposition strategies, such as multilayers composed of organic and inorganic species, for enhancing the barrier properties of polymeric substrates [6,71]. The polymer/metal oxide/polymer design, for instance, refers to a hybrid coating composed of alternating polymer and ceramic layers and deposited through methods such as polymer multilayer (PML), sputtering and evaporation. In the PML process, monomers are first flash-evaporated under vacuum and permitted to condense on the target substrate. This liquid layer is then solidified (cured) through exposure to UV radiation or a focused electron beam. A metal oxide layer is subsequently deposited on the newly formed polymeric coating via sputtering or evaporation, and this cycle is repeated to generate a multilayer architecture. An important benefit of this approach is that the first polymeric coating increases the smoothness of the target substrate, thereby reducing the risk of pinhole defects as additional layers are deposited. Moreover, the topmost polymeric coating completely covers the final metal oxide layer, protecting it against stresses that arise during handling. Although the number and size of the defects that develop as this organic/inorganic multilayer is fabricated are less numerous and problematic than those encountered in single-layer processes,

this approach cannot altogether eliminate the possibility of defect formation. In addition, the polymeric coating process is somewhat complicated from a commercial standpoint, requiring both the vacuum evaporation and curing of monomers in highly controllable fashion [22,24,30].

Layer-by-layer (LBL) deposition, a relatively new technology intended for fabricating multilayer thin films, is performed through alternating immersion of a polar substrate in an oppositely charged aqueous solution or suspension. Relative to the multilayer framework discussed above, the LBL strategy results in a larger number of thinner layers. The nanostructure and properties of LBL assemblies depend sensitively on the molecular weight of the components employed [67], their chemistry [33], ionic strength and pH [11]. A typical LBL assembly consists of a multilayer with alternating layers of a charged organic binder and a natural (*i.e.*, not organically modified) clay nanoparticles, and the thickness can range from a few nanometers to several hundreds of nanometers [30]. This process is relatively straightforward and effectively relies on constructing the multilayer from the ground-up, resulting in a one-dimensional sandwich arrangement. One strategy by which to control the deposition of nanoscale organic layers on a solid substrate relies on the Langmuir-Blodgett (LB) technique for the formation of a monolayer on the surface of water, followed by attachment of the monolayer to the substrate. This methodology, which reproducibly yielded stearate coatings measuring less than 3 nm thick [79], has become ubiquitous in the study of thin organic layers [80]. According to Decher (2012) [81], drawbacks associated with the LB technique in multilayer fabrication are two-fold: (1) frequent rearrangement of deposited layers

due to insufficiently firm spatial constraints and (2) limited choice of molecular species that are suitable for this technique. These disadvantages can be overcome in the design of LBL assemblies through the use of oppositely charged species, as demonstrated by Iler (1966) [23], who generated stable LBL multilayers by alternating the deposition of positively-charged silica and negatively charged alumina colloidal particles. The use of electrostatic interactions to produce charged multilayers of organic compounds has been largely pioneered by Decher [81–85], who started with the alternating deposition of anionic and cationic amphiphiles and later introduced simple polyelectrolytes. Other charged species such as functional polymers, biological nanoparticles and inorganic nanoparticles have been gradually incorporated into the LBL methodology. Although LBL coatings were initially applied to planar substrates, further developments have established that multilayer deposition on small nonplanar surfaces is also possible. For example, multilayers of polycations and anionic exfoliated zirconium phosphate have been successfully deposited on high-surface-area silica [20].

While electrostatic interaction between oppositely charged species is widely accepted as the main driving force in the preparation of LBL assemblies, other mechanisms that can be used for this purpose include hydrogen bridging [26,32,35], covalent bonds [31], hydrophobic interactions [25,27], coordination interactions [29], and complementary post-chemical reactions [81]. In the case of multilayer coatings generated via electrostatic interactions, LBL deposition is further divided into three primary methods. According to the first approach, linear polyions constitute the alternating species that stack on top of each other, thereby forming a polyelectrolyte multilayer composed of oppositely charged polymers [84]. The second type of

electrostatically-driven LBL assembly is based on the use of charged particles, such as globular proteins, successively deposited on linear polyions [27,32]. In the last category, charged particles are replaced with charged platelets exemplified by exfoliated natural clays such as montmorillonite (MMT) deposited from suspension [21,27,30,33]. This latter approach, schematically depicted in Figure 2.5a, has been found to yield coated polymer substrates exhibiting remarkable barrier properties. In fact, use of natural nanoclays such as MMT in conjunction with polyelectrolytes (*e.g.*, polyethylene imine and polyacrylamide) has yielded coated PET substrates possessing extremely high barrier properties after deposition of relatively few layers. Independent studies [11,33,86] report OTR values lower than the detection limit of oxygen permeation sensors capable of measuring $0.005 \text{ cm}^3/(\text{m}^2\text{-day-bar})$.

Methods developed to deposit alternating layers in LBL assemblies have evolved over the years, but dipping, first introduced for producing multilayers from oppositely charged polyelectrolytes in 1992, still remains the most widely used deposition method. Several complementary deposition strategies that have likewise been explored rely on spraying [87] and spin-coating [88–91]. Multilayer preparation by dipping requires alternating immersion of the polymer substrate in aqueous oppositely charged solutions or suspensions. It immediately follows that the surface to be coated must possess an excess charge that is either naturally occurring or introduced (by plasma or corona treatment) to bind with the organic layers. Previous studies [11,30,33,86] have established that this interaction is significantly improved through the use of adhesive polyelectrolyte interlayers composed of branched polyethyleneimine (PEI). In a typical LBL process conducted by dipping (Figure 2.5a),

immersion of the substrate in a PEI solution of predetermined concentration for a predetermined period of time is followed by rinsing with deionized water (DIW) and drying with filtered air. The cycle continues with immersion of the PEI-coated substrate in an aqueous clay suspension, which is also followed by rinsing in DIW and drying with filtered air. These steps are repeated until a desired number of bilayers, depicted in Figure 2.5b, is deposited. To achieve more uniform multilayers and consistent properties, several studies have demonstrated that the dipping process can be fully automated [11,33,86,92].

The impressive orientation and exfoliation of nanoclay particles observed in transmission electron microscopy (TEM) micrographs of LBL assemblies (*cf.* Figure 2.5c) are unique features of these multilayer coatings. Due to the strong electrostatic attraction of positively-charged PEI, the negatively charged nanoclay platelets absorb with their largest dimension parallel to the PEI-coated surface, resulting in a highly laminar, oriented and packed arrangement of exfoliated nanoclay platelet layers that promote unique barrier and optical properties that are not achievable by any other method of combining polymers and nanoclay [34]. The rate at which the LBL assembly is constructed layer-by-layer is classified as either linear or superlinear. On one hand, linear growth usually occurs in solutions with low ionic strength at low temperature, such as the growth of bilayers composed of PEI and MMT presented in Figure 2.6a [31,33,86,91]. Superlinear growth, on the other hand, occurs in solutions with high ionic strength and at high temperature, and is characterized by an exponential increase due to free diffusion of the polyelectrolyte through the entire multilayer. In quadlayers composed of PEI, poly(acrylic acid) (PAA), PEI, and MMT, the rate by which

the thickness increases appears closer to exponential in Figure 2.6b, attaining a thickness of 174 nm after only 6 deposition steps, due to interdiffusion of the polyelectrolyte layers during deposition [34]. In marked contrast, 40 bilayers in Figure 2.6a produces a multilayer thickness of < 140 nm.

Compared to other coating technologies developed to enhance the barrier properties of polymer substrates, LBL is generally more facile, as it is conducted under ambient conditions in the presence of aqueous solutions/suspensions [30]. Thus, LBL deposition is considered to be a low-cost and environmentally friendly process method that is capable of depositing a wide spectrum of different species, ranging from small organic molecules and inorganic nanoparticles to polymers and colloids, on polymer substrates to fabricate precise nano/microscale assemblies possessing desired properties. From nanoscale particles and platelets to macroscale substrates, nearly every substrate with a solvent-accessible surface can be subjected to LBL deposition [81]. Conversely, in traditional compounding, the negligibly small entropy of mixing associated with long polymer chains and generally endothermic interactions thwart homogenous mixing even at low additive concentrations. Because of the strong electrostatic attraction between oppositely charged species in the LBL approach, cyclic deposition of layers, coupled with the formation of ionic complexes (an exothermic process), help to make nanoscale mixtures possible, and the composition of the multilayer assembly can be controlled through tunable variations in solution/suspension factors such as pH and ionic strength [20,26].

2.4. Polymer Nanocomposites for Improved Barrier Properties

Despite their ability to improve the barrier properties of thermoplastic substrates, the various coating technologies mentioned above inherently possess nontrivial shortcomings for many commercial packaging applications, especially those encountered in the food industry. First and foremost, surface coatings are vulnerable to the development of defects promoted by stresses introduced during handling over the course of their service life. [4–7,12,16,18,71,76,93] In addition, the possibility always exists that a deposited surface coating delaminates and completely peels from the substrate due to insufficient adhesion. Another important technological consideration that warrants mention at this juncture is that coated plastic substrates cannot be processed by conventional processing routes such as extrusion and injection molding. One strategy to overcome all of these drawbacks involves the production of polymer nanocomposites in which the bulk, rather than surface, properties are modified through the physical or chemical incorporation of impermeable nanoparticles [47,57,59,94–96]. While nanoparticles conveniently serve as obstacles to molecular diffusion, they can serve other important purposes. For instance, as the global need for polymer recycling continues to escalate due to growing environmental concerns, the intrinsic barrier performance and overall processability of recycled thermoplastics such as PET becomes increasingly compromised as a consequence of repeated chain scission, which tends to reduce molecular weight and the melt strength required for processes such as blow molding and flat-die extrusion. Inclusion of highly dispersed clay nanoparticles can increase the melt viscosity of recycled polymers and, thus, improve their processability. [48,51,97–104]. Therefore, polymer nanocomposites are rightfully considered a technologically attractive approach by which to enhance the barrier

properties, as well as other physical properties, of polymeric materials in a wide variety of packaging applications.

By decreasing the size of typical micrometer-sized particles down to the nanometer range, the surface-to-volume ratio can be dramatically increased by orders of magnitude, thereby promoting a corresponding increase in interfacial contact with the polymer matrix [105]. As the degree of contact between the particles and polymer is increased, important material properties (*e.g.*, barrier, flame resistance and mechanical) require a systematically lower particle loading level, which constitutes a critical consideration in terms of weight reduction and the energy required to transport packaged goods [106]. Amongst different types of polymer nanocomposites that have been successfully developed, polymer-clay nanocomposites (PCNs) containing layered silicates, initially introduced in 1985 [107] to improve the mechanical properties of polymeric materials, remain one of the most popular [104]. For such organic/inorganic hybrid materials to be considered nanocomposites, the silicate layers must be dispersed throughout the polymer matrix in such fashion that at least one dimension of the layers is less than 100 nm [105,108]. Since the individual platelets comprising a layered silicate typically measure a few nanometers thick and, depending on the type of clay, greater than 100 nm across, the result upon exfoliation (discussed further below) is a polymer nanocomposite with nanoscale sheets possessing a relatively high aspect ratio. For this reason, PCNs can be implemented to create a highly tortuous pathway for molecular diffusion and, by doing so, generate barrier properties that are vastly superior to many other polymer nanocomposites. Moreover, layered silicates are considered nontoxic by the U.S. Food and Drug Administration (FDA) and hold a "generally recognized as safe" (GRAS) classification. Another material

property that merits consideration especially in food packaging is optical transparency, since consumers frequently desire to inspect the contents prior to purchase or consumption. Since the platelets of layered silicates are very thin and the refractive indices of clay nanoparticles and typical thermoplastics are not very dissimilar, the resulting PCNs generally retain their transparency[69]. Taken together, these advantages unequivocally make PCNs an ideal class of candidates for food packaging.

Hybrid materials composed of a polymer matrix and a layered silicate nanofiller are categorized into three groups on the basis of their degree of mixing, as depicted in Figure 2.7a [45,109]. If the attractive force between adjacent clay platelets is sufficiently strong or the degree of shear mixing is low, long polymer chains are unable to diffuse into the interlayer spaces (galleries) between the platelets. In this case, the level of mixing is low, and layered silicate stacks that remain intact form a distinctly separate phase in the polymeric matrix. Such hybrid composites, classified as conventional microcomposites due to their large size scale and relatively low interfacial area, lack the significant property improvement afforded by nanocomposites. When the polymer chains diffuse between adjacent clay platelets in layered silicates and increase their basal spacing without disrupting their parallel alignment, the resulting PCNs are considered to be intercalated, in which crystallographic regularity is preserved over distances of a few nanometers. Finally, if the polymer chains overcome the electrostatic interactions of the clay platelets and completely disrupt platelet stacking, individual platelets are forced to disperse randomly throughout the polymer matrix to yield exfoliated PCNs wherein the average distance between platelets is composition-dependent. Due to the level of dispersion achieved and the interfacial area generated, exfoliated PCNs

hold the most promise for remarkable property improvement and are therefore of greatest technological interest [45,95,97,110]. Realistically, exfoliated and intercalated morphologies frequently coexist in PCNs, and classification reflects the more prevalent level of dispersion. For example, as observed in Figure 2.7b [111], a PCN composed of PP contains intercalated clay platelets separated by 2-3 nm and exfoliated platelets containing up to ~3 clay platelets separated by more than 10 nm in the PP matrix. In this case, polymer intercalation induces limited platelet disordering that falls far short of complete exfoliation, resulting in the existence of an intermediate state [112].

Layered silicates used to produce PNCs are commonly aluminosilicates that include such minerals as MMT, mica and vermiculite. Of these, MMT is one of the most popular aluminosilicates due to its high aspect ratio and, hence, surface area, high cation exchange capacity, and surface reactivity. This latter attribute is particularly important for the fabrication of PCNs from most commercial polymers, which are intrinsically hydrophobic. To achieve satisfactory levels of intercalation or exfoliation in such polymer matrices, the hydrophilic MMT platelet surfaces are organically modified to increase their hydrophobicity and polymer compatibility. This conversion requires replacement of the surface cations of water-swollen MMT platelets with organic cations (such as alkyl ammonium) that serve to decrease the surface energy and increase the interlayer distance [95,104,113]. Although quaternary ammonium ions are traditionally employed to modify MMT and promote exfoliation for improved barrier performance, the resulting PCNs are not approved as GRAS by the FDA [104]. This disadvantage, coupled with (i) the low thermal stability of such organically-modified clays [114] and (ii) the high processing temperatures required for many engineering

polymers such as PET, hinders the widespread utilization of so-called "organoclays" in food packaging and other clean applications [67,101].

2.4.1. Methods to Prepare PCNs

On the basis of the starting materials and processes to be used, the methods developed to produce PCNs can be broadly divided into three approaches: solution mixing, *in-situ* polymerization and melt compounding. In the first, a solvent is introduced for two concurrent purposes: to swell/disperse the clay platelets and dissolve the polymer chains. In an idealized scenario, the polymer chains located between swollen platelets remain in place upon solvent removal, thereby yielding an intercalated or exfoliated PCN insofar as the platelets do not undergo sedimentation. This problem can be largely prevented by ultrasonication, coupled with the increase in solution viscosity that accompanies solvent drying [95,104,109,112]. For *in-situ* polymerization, the layered silicates of interest are directly incorporated into liquid or dissolved monomers. Polymerization of the monomers produces a continuous polymeric matrix containing intercalated or exfoliated clay platelets. In this method (which was initially used to prepare PCNs consisting of nylon and MMT), the problem associated with coercing large macromolecules to diffuse between clay platelets to induce intercalation simply does not exist [46,95,109,112,115,116]. Both of these liquid-based approaches can result in uniformly dispersed PCNs wherein the silicates are either intercalated or exfoliated (preferred) because the processes start with highly swollen platelets. In melt compounding, however, a premade, high-molecular-weight polymer is typically mixed with an MMT-based organoclay that possesses a higher interlayer spacing than natural MMT. Mixing proceeds in the presence of

high shear during extrusion at elevated temperatures in the melt state of the polymer. As mentioned earlier, the temperatures must be sufficiently low to preclude degradation of the organic surfactants attached to the clay platelets [114]. Significant advantages of this method are (i) its compatibility with high-throughput production processes such as injection and blow molding, (ii) its environmental friendliness because organic solvents are avoided, and (iii) its applicability for a wide range of commercially relevant commodity and engineering polymers. Although caution must be exercised to minimize damage to the organoclay, this method of intercalating and exfoliating clay platelets in polymers has become an expedient method of fabricating PCNs with excellent barrier properties for packaging [46,98,99,117,118].

2.4.2. Methods to Characterize PCNs

One of the most important features of PCNs relates to the level of dispersion of layered silicates in the polymer matrix, since it plays an important role in determining the resultant mechanical and barrier properties. Thus, the morphological characterization of PCNs by microscopy techniques is critical. Because of this intimate structure-property design relationship, the development of nanocomposites parallels the development of high-resolution microscopy techniques, such as AFM, TEM and scanning electron microscopy (SEM). Due to its inherently high spatial resolution and ability to reveal the internal nanostructure of (cryo)sectioned or spin/dip-coated specimens that are electron-transparent, TEM remains the primary microscopy technique utilized to examine the level of nanoparticle dispersion and, in particular, the degree of exfoliation of layered silicates embedded within a polymer matrix. To complement the real-space images acquired from TEM, x-ray diffractometry (XRD) provides a reciprocal-space measurement of intercalation. While XRD is capable of quantitating the interplanar spacing of

layered silicates in ordered (intercalated or immiscible) systems and inferentially identifying exfoliation (due to the absence of a scattering peak from the layered silicate), TEM can qualitatively assess any type of PCN morphology and affords a more definitive exfoliation classification. In conventional phase-contrast TEM images of PCNs, clay platelets appear as dark, often linear features residing in a lighter polymer matrix due to the higher electron density of (and greater scattering from) the platelets, as evidenced by the TEM image presented in Figure 2.7b [51,96,119]. Typically, polymers that possess polar groups are more prone to interact with hydrophilic clay platelets and promote exfoliation. An excellent example of a polymer that permits a high level of platelet dispersion is nylon-6 [49,55], which comprised the matrix in the first reported PCN. In marked contrast, nonpolar polymers such as PS and PP undergo weaker molecular interactions with natural clay and are much less likely to induce exfoliation [48]. In fact, even when organically-modified clay or compatibilizers such as maleic anhydride are incorporated to promote dispersion during melt mixing, nonpolar polymer matrices frequently generate intercalated, rather than exfoliated, PCNs.

2.5. Molecular Transport in Polymers and Nanocomposites

Permeation of a penetrant species through a homogeneous medium proceeds via a three-step process that commences with adsorption of the species onto one side of the medium and is followed by diffusion of the species through the medium before desorption of the species at the opposite side of the medium. The driving force for this process is unbalanced chemical potentials for the penetrant species on the opposing sides of the permeable medium. In the limit of ideal gas mixtures, the chemical potentials can be expressed in terms of partial pressures of the penetrant species so that permeation is attributable to a pressure difference and occurs in

the direction from high to low pressure. The permeability or permeation coefficient (P) serves as the principal metric for systematically evaluating the ability of a gas (or liquid) to undergo molecular transport through a membrane and is given by

$$P = \frac{(\text{amount of gas under a stated condition})(\text{membrane thickness})}{(\text{membrane area})(\text{time})(\text{pressure difference})} \quad (1)$$

Although CGS and SI units can be written for the permeability, a named unit that remains in common use for this purpose is the Barrer, which is defined as [120]

$$1 \text{ Barrer} = \frac{10^{-10}(\text{cm}^3 \text{ STP})\cdot\text{cm}}{\text{cm}^2\cdot\text{s}\cdot\text{cm Hg}} \quad (2)$$

where STP corresponds to the *standard temperature and pressure* conditions of 25 °C and 1.013 bar, respectively [6].

2.5.1. Single-Gas Permeability in Dense Polymers

Although single-component gas permeabilities can be measured through the direct use of compound-specific sensors (typically used in oxygen and water transport studies), reported values are routinely determined from the pressure change that accompanies the molecular transport of a gas through a polymer membrane in an apparatus generically referred to as a constant-volume variable-pressure permeation cell. The cell is divided into upstream and downstream sides relative to the membrane to be analyzed. The downstream (receiving) volume is known and the associated gas pressure is measured as a function of time (t). The upstream side of cell is charged with a gas maintained at constant pressure (p). Due to permeation of the gas through the membrane, the downstream pressure expectedly increases. Although the downstream pressure initially increases nonlinearly with time, a linear p(t)

response eventually develops when the permeation reaches steady-state conditions. In this experimental arrangement, the permeability can be calculated from

$$P = \frac{VL}{ART\Delta p} \frac{dp}{dt} \quad (3)$$

where V is the downstream volume, L is the membrane thickness, A represents the exposed membrane area, R is the universal gas constant, T denotes absolute temperature, Δp corresponds to the difference between the constant upstream and initial downstream pressures, and dp/dt is the linear change in pressure with respect to time at steady-state conditions [121,122].

2.5.2. Barrier Properties of Polymer Nanocomposites

When impermeable particles are present in a permeable polymeric matrix, diffusing species are forced to change their trajectory so that they can proceed around such particles. If these impermeable particles are numerous, a tortuous path that affects the barrier properties of the organic/inorganic hybrid material develops inside the membrane. Attempts to model the permeability through such heterogeneous materials have yielded different results on the basis of the assumptions employed. A classic example is the mathematical relationship derived by Maxwell (1873) to describe the dielectric properties of a composite consisting of spherical objects suspended in a continuous dielectric medium. Surprisingly, the functional form of this relationship can be used to obtain accurate predictions for the permeability of a single gas through a dense polymer membrane containing a dispersion of impermeable spheres, insofar

as the spheres measure on macroscale, not nanoscale, dimensions [123]. Expressed in terms of permeabilities, this relationship takes the form of

$$P_c = P_m \left(\frac{1 - \phi_f}{1 + \phi_f / 2} \right) \quad (4)$$

where P_c and P_m identify the composite and matrix permeabilities, respectively, and ϕ_f is the volume fraction of spherical objects hereafter referred to as the "filler" [121,124]. To account for the high aspect ratio encountered with clay platelets, a molecular tortuosity factor (τ), defined as the path length of molecular diffusion to the membrane thickness, has been introduced by Nielson (1967). In the context of this formalism, P_c can be conveniently written as [125–127]

$$P_c = P_m \left(\frac{1 - \phi_f}{\tau} \right) \quad (5)$$

Comparing Eqs. 4 and 5 immediately reveals that $\tau = 1 + \phi_f / 2$ in the limit as the filler aspect ratio approaches unity. A shortcoming of Eq. 5, however, is that the change in permeant concentration as it passes around a filler particle is neglected, thereby making the predicted permeability higher than its experimentally measured value. A maximum in τ is achieved if (i) the impermeable filler is envisaged as either rectangular or circular platelets that are uniformly and completely dispersed and oriented parallel to the membrane surface and (ii) minimal interactions exist between the platelets and polymer matrix [126]. Also, he assumed minimal interaction between clay and polymer. In light of these assumptions, τ can be approximated by

$$\tau = 1 + \left(\frac{L}{2W} \right) \phi_f \quad (6)$$

where L and W represent the characteristic length and thickness of the platelets, respectively, that are schematically depicted in Figure 8a. Substituting Eq. 6 into Eq. 5 yields

$$P_c = P_m \left(\frac{1 - \phi_f}{1 + \alpha \phi_f / 2} \right) \quad (7)$$

where $\alpha (= L/W)$ is defined as the aspect ratio. In the case of a spherical particle, $L = W$ and $\alpha = 1$ so that Eq. 7 simplifies to Eq. 4. Moreover, in the limit as $\phi_f \rightarrow 0$ for $\alpha \approx 1$, $P_c \rightarrow P_m$ as intuitively expected. Within this same limit, however, the product $\alpha \phi_f$ in the denominator of Eq. 7 becomes non-negligible if $\alpha \gg 1$ [128]. It therefore follows that, at very low concentrations, impermeable platelets are effective at reducing gas permeation when they are highly anisotropic and the aspect ratio is very large [126].

Within the framework of the Nielsen model, the uniformly distributed platelets are presumed to possess equal size and aspect ratio, as well as spatial arrangement, which are obvious oversimplifications of real PCNs. To account for variations in size, shape and positional order, Cussler et al. [129] have considered several different scenarios and, for the case of randomly spaced thin platelets, introduced a second geometric factor (μ) in their expression for P_c , *viz.*,

$$P_c = P_m \left(\frac{1 - \phi_f}{1 - \phi_f + \mu \alpha^2 \phi_f^2} \right) \quad (8)$$

In the limit of low concentrations ($\phi_f \rightarrow 0$) of highly anisotropic filler particles (with $\alpha \gg 1$), Eq. 8 reduces to

$$P_c = P_m \left(\frac{1}{1 + \mu \alpha^2 \phi_f^2} \right) \quad (9)$$

Predictions from this equation are in favorable agreement with experimental data in the semidilute regime where $\phi_f \ll 1$ for the case of $\alpha \phi_f > 1$. While the geometric factor μ accounts for a combination of several different factors (although the interplay of these factors is not presently understood), experimental results provide sensible estimates. In the case of randomly distributed clay platelets whose shape lies between ribbons and hexagons (or disks), μ is anticipated to vary from 2/27 to 1/2 [128,130,131]. If these are periodically distributed, corresponding values of μ are 1 (ribbons) and 4/9 (hexagons). According to the predictions obtained from Eq. 9 and displayed in Figure 8b, the relative permeability (P_c/P_m) decreases, and the barrier performance improves, with increasing clay content and the value of μ at constant α .

One reason for deviation between experimental results and the Nielsen model can be traced back to its assumption that all platelets within the polymer matrix are perfectly aligned horizontal to the membrane surface, which is not the case. A modified Nielsen model has also been proposed [132,133] in which an order parameter, $S = (3\cos^2 \theta - 1)/2$, is incorporated to account for variations in platelet orientation (*cf.* Figure 2.9a):

$$P_c = P_m \left(\frac{1 - \phi_f}{1 + (2/3)(\alpha/2)(S + 1/2)\phi_f} \right) \quad (10)$$

In the event that all the clay platelets are horizontally oriented parallel to the PCN surface, $\theta = 0^\circ$ and $S = 1$, which allows Eq. 10 to simplify to Eq. 7. Conversely, if the platelets are oriented normal to the membrane surface (and the diffusive pathway through the polymer matrix is unobstructed), then $\theta = 90^\circ$, $S = -1/2$ and the parenthetical factor in Eq. 10 reduces to $1 - \phi_f$. In this scenario as $\phi_f \rightarrow 0$, $P_c \rightarrow P_m$. The predicted relative permeabilities included in Figure 9b for PCNs with 5 vol% clay filler demonstrate how platelet orientation influences barrier performance for the three physically relevant values of S : 1 (horizontal orientation), 0 (random orientation) and $-1/2$ (vertical orientation). As anticipated from Eq. 10, predictions corresponding to the random orientation converge with those from the horizontal orientation at large α .

2.6. Case Studies of Enhanced Barrier Performance

In this section, we examine the results of several studies that have either elucidated beneficial design rules or shown commercial promise for developing polymeric materials with improved barrier performance. While such materials might have originally focused on applications other than food packaging, the technological innovations responsible for the materials can, in most cases, be directly translated to the food packaging industry.

2.6.1. Single-Layer PVD/CVD Coatings

As mentioned earlier, several contemporary production strategies are available for depositing single inorganic coatings on polymer surfaces to enhance barrier performance. One of these is reactive sputtering, and an excellent example of this approach is the deposition of AlO_xN_y (aluminum oxynitride) on PET at medium frequency (40 kHz) in an AC magnetron with a

commercial Al source and N₂ as the primary reactive gas. Due to the low density of defects in the resultant barrier coating (which is an intrinsic property of AlO_xN_y), OTR values as low as $\approx 1 \text{ cm}^3/(\text{m}^2\text{-day-atm})$ at 30 °C and 0% relative humidity (RH) have been reported [93]. Relative to polar polymers such as PET, however, nonpolar polymers such as PP tend to adhere poorly to inorganic coatings and, as a consequence, achieve less effective barrier improvement. The study conducted by Deng et al. [15] directly compares aluminum oxide coatings measuring 10 nm thick and evaporated on PET and PP substrates. Their results unequivocally establish that the permeability of oxygen decreases by more than 20x through surface-coated PET but displays no significant change through surface-coated PP. This difference is attributed to the presence of the PET carbonyl groups, which promote nucleation and growth of the inorganic coating on the PET surface. Without the existence of such specific interactions (as in the case of PP), a more defective and hence permeable coating develops.

Similarly impressive results have been documented for the PECVD of SiO₂ and SiN on a biaxially oriented PET substrate from hexamethyldisiloxane (HMDSO) in the presence of O₂ and SiH₄ in the presence of NH₃, respectively. Over a range of coatings varying from 8 to 200 nm in thickness, a minimum OTR of $0.5 \text{ cm}^3/(\text{m}^2\text{-day})$, which corresponds to a barrier improvement of 1000x, can be achieved when the coating thickness exceeds a critical value of 15 nm for SiO₂ and 8 nm for SiN [76]. By substituting a tetramethoxysilane (TMOS)/O₂ mixture as the gaseous precursor for radio-frequency- (RF-) PECVD on PET, Inagaki et al. [3] have measured an OTR of $0.1 \text{ cm}^3/(\text{m}^2\text{-day-atm})$ under their best experimental conditions. An independent study employing two different organosilane monomers, HMDSO and trimethylsilane, for the PECVD of SiO_x coatings on PET reveal no significant differences in

coating characteristics or barrier efficacy [16]. Since permeation depends on molecular diffusion and solubility (both of which are thermally-activated processes), the permeation of non-interacting gases that are important in the food packaging industry (*e.g.*, O₂) through dense polymer membranes is expected to obey an Arrhenius expression of the form

$$P = P_0 \exp\left(\frac{-\Delta G^\ddagger}{RT}\right) \quad (11)$$

where P_0 is the permeation at infinite temperature (a pre-exponential factor) and ΔG^\ddagger denotes the thermal activation energy. This behavior is evident from the experimental data included in Figure 10a. Interestingly, Arrhenius behavior is likewise apparent for SiO_x-coated PET over the same temperature range [4,16,17]. Since ΔG^\ddagger provides a measure of the energy barrier that must be overcome for permeation to occur, it embodies several factors, ranging from free-volume considerations in dense polymers to defects in inorganic coatings, which together influence permeation. Changes in the magnitude of ΔG^\ddagger under isothermal conditions therefore provide indirect evidence of variations in the permeation mechanism. In Figure 10b, the reduction in OTR — to below 0.8 cm³/(m²-day-atm) — induced by varying the coating thickness of SiO_x deposited by RF-PECVD on PC is accompanied by a substantial increase in ΔG^\ddagger , indicating that the pores in the coating that permit molecular diffusion are approaching the cross-sectional size of the diffusing O₂ molecules. In contrast, systematic changes in ΔG^\ddagger are not observed in SiO_x-, SiO₂- or SiN-coated PET, which suggests that molecular transport through the PET matrix, and not the coating, is rate-limiting most likely due to sufficiently large pores that exist as defects in the coatings.

Other important considerations regarding the deposition of single-layer coatings that have not yet been addressed include the shape and surface roughness of the polymer substrate. For uniformly thick coatings on non-planar substrates (*e.g.*, beverage bottles), CVD is more effective than PVD. The line-of-sight feature of deposition process, by which PVD operates, becomes increasingly problematic as the surface becomes more curved and/or rougher. Studies endeavoring to elucidate the molecular mechanisms of the two deposition processes have demonstrated that a gaseous species deposited by CVD is able to undergo several collisions with the substrate before reacting (thereby achieving better conformal coverage), whereas the species deposited by PVD immediately condenses on the surface after initial contact [4,6,19]. Comparison of the barrier improvement factor ($BIF = 1 / \text{relative permeability}$) measured for Al-based PVD coatings and SiO_x-based CVD coatings in Table 1 confirms that the latter materials provide better barrier performance against O₂ (by over an order of magnitude in terms of their BIF values) due to their inherently conformal coverage. Another reason why PVD is believed to produce inferior surface coatings is the inadequate formation of an organic/inorganic interphase layer, which develops during CVD. Over this interphase layer measuring a few tens of nanometers thick, the composition gradually transitions from inorganic coating to organic polymer. In PECVD processes, this layer forms during the first few seconds of exposure to the plasma as volatile organic compounds are released from the polymer surface and interact with the plasma and its associated gases. The presence of this interphase greatly improves adhesion between the deposited coating and polymer substrate, thereby yielding superior barrier properties relative to PVD coatings [5,76].

Since aluminum metal and oxides of silicon and aluminum are known to have excellent barrier properties against water and oxygen, they are good candidates for barrier coatings. When such superbarrier materials are coated as single layers on polymeric substrates, however, the resulting material exhibits only two to three orders of magnitude improvement in barrier properties compared to the neat polymers [7,12,31]. The reason for such meager performance enhancement is the existence of nanoscale defects and pores that develop during deposition (*cf.* Figure 2.11). By analyzing the defects and corresponding barrier properties of coated polymers, da Silva Sobrinho et al. [76] have concluded that the mechanism of permeation changes from classic solution/diffusion in polymers to porous media transport in thin barrier coatings. Silicon-derived coatings deposited by PECVD possess more mechanical flexibility compared to those prepared by PVD, and such mechanical robustness is at least partly responsible for fewer defects and longer retention of enhanced barrier properties, even though such coatings suffer from low crack resistance and are prone to crack failure [5]. Small, nanoscale defects in thin barrier coatings tend to form as a consequence of two types of stress encountered during nucleation and growth in PVD and CVD processes. The first is the intrinsic stress that develops due to the non-equilibrium nature of the deposition processes and the disordered state of the coating, while the second includes thermal stresses that arise because of differences in thermal contraction between the coating and substrate upon cooling. The extent to which these defects compromise barrier improvement is dependent on coating thickness, as illustrated in Figures 2.12a and 2.12b for barrier coatings differing in thickness. To avoid cracking induced by differences in intrinsic stresses between the coating and polymer, coating thicknesses should not exceed *ca.* 100 nm. For a variety of coatings, an optimum thickness that

provides maximum barrier performance has been reported. In the specific case of SiO_x coatings, those greater than 40 nm thick have been found to display evidence of cracks that diminish their barrier improvement [6,8]. Large defects are frequently introduced into barrier coatings by poor handling or substrate/equipment cleanliness [93]. With the importance of large defects notwithstanding, the density of nanoscale defects incurred during coating fabrication is dependent on the intrinsic properties of the coating and the deposition conditions. According to the results presented on dual-logarithmic coordinates in Figure 2.12c, the barrier performance, expressed in terms of the OTR, scales directly with the defect density [4].

2.6.2. Single-Layer ALD Coatings

Recent advances in ALD as a commercially competitive process by which to enhance the barrier properties of polymer substrates have been very promising. Groner et al. [38] report that Al₂O₃ coatings measuring 5 nm thick and deposited by ALD on PI with a glass transition temperature (T_g) of 300 °C and poly(ethylene naphthalate) (PEN) with $T_g = 125$ °C yield OTR values below the minimum detectable limit of the MOCON OX-TRAN 2/21 instrument (with a detection limit of $< 5 \times 10^{-3}$ cm³/m²-day). For comparison with barrier coatings achieved by PECVD, we hasten to point out that a SiN coating measuring 50 nm thick and an Al₂O₃ coating measuring 10 nm thick have also resulted in non-detectable OTR values on the same instrument, which indicates that the barrier performance of some coatings must be characterized by other means [9]. In ALD, control over the temperature of the substrate is critically important to ensure suitable precursor chemical deposition. If, on one hand, the temperature is lower than an optimum level, the growth rate either increases due to surface condensation of gas precursors or decreases due to incomplete removal of unreacted precursor

during the purge step. If the temperature is excessive, on the other hand, the growth rate can be reduced because of re-evaporation of deposited species or increased as a consequence of thermal decomposition of gaseous precursors prior to deposition [42,44]. If thermal control is adequate and the ALD growth rate is precisely regulated, this relatively new deposition process is poised to elucidate the multitude of factors governing the evolution of barrier properties provided by thin inorganic coatings on polymer substrates.

2.6.3. Multilayer LBL Coatings

In similar fashion as ALD, the LBL deposition process is now sufficiently developed to achieve a uniform, coating assembly composed of alternating nanoscale layers of polymer and highly exfoliated and oriented impermeable clay platelets. This type of transparent sandwich structure is capable of promoting very high barrier performance. The idea underpinning LBL coatings is essentially to construct, through repetitive dipping action, a nanoscale brick wall that requires permeating gas molecules to pass through long, tortuous polymer layers that are separated by oriented layers of impermeable clay platelets. The polymer layers must therefore be suitably thick to increase the residence time of penetrant molecules and, in doing so, provide excellent barrier performance with just a few layers. In this case, exfoliated clay platelets with a high aspect ratio must be positioned with their large dimension parallel to the substrate surface to increase the diffusion path length, and concurrently decrease the permeability, of permeating species [33,86]. While this strategy relies on the same increase in tortuosity sought in the design of PCNs, existing models fail to predict the very low relative permeability of LBL assemblies, as evidenced by the results provided in Figure 2.13 [86,128]. Using this conceptual approach, Jang et al. [30] have generated a high-barrier LBL assembly composed of

polyacrylamide (0.25 wt%) and Na⁺MMT (0.20 wt%) and measuring 571 nm thick with 30 bilayers on a PET substrate. They report OTR values below 0.005 cm³/(m²-day-atm) at 23 °C and 0% RH. Interestingly, with only 20 bilayers, they measure an OTR value of 0.217 cm³/(m²-day-atm), which is comparable to the barrier performance of SiO_x-coated PET [16,30]. It should be recognized here that, although the multilayer thickness usually increases linearly with an increasing number of layers, the barrier performance increases superlinearly (*e.g.*, exponentially), indicating that LBL assemblies with a large number of layers can serve as a viable alternative to metal oxide coatings in food and electronic packaging applications. In this spirit, a record-setting LBL assembly with 70 bilayers fabricated from PEI (0.1 wt%) and MMT (0.2 wt%) on PET yields an oxygen permeability of < 0.2 x 10⁻⁸ cm³/(m²-day-atm), which is the lowest ever reported for a polymer composite [11,134]. An important consideration in the production of LBL assemblies is the immersion time within the polymer solution and clay suspension. Even with 10 s in a 0.1 wt% PEI solution and 5 min in a 1 wt% MMT suspension, an assembly with 30 bilayers has been observed to exhibit an undetectable OTR. Short immersion times and complete automation are crucial for the commercialization of LBL processing in the food and beverage packaging industries [11,33].

2.6.4. Polymer-Clay Nanocomposites

Early studies of intercalated PCNs prepared by twin-screw extrusion from biodegradable poly(lactic acid) (PLA) and 4 wt% organically-modified MMT exhibit a BIF of only 1.13 relative to neat PLA [47]. By using MMT modified with benzyldibutyl(2-hydroxyethyl) ammonium chloride, benzylbis(2-hydroxyethyl) butyl ammonium chloride and benzyltriethanol ammonium chloride, however, Osman et al. [96] have demonstrated that the

barrier properties of PCNs containing epoxy are significantly improved compared to pure epoxy due to greater chemical interactions and the likelihood of exfoliation. Higher BIF levels have been reported for PCNs composed of a thermoplastic: 1.45 through the melt extrusion of nylon-6 with 1.6 wt% MMT [135], 1.48 through the *in-situ* polymerization of styrene in the presence of 5 wt% organically-modified MMT [136], and 1.71 through the melt extrusion of PP with about 6 wt% organically-modified MMT and maleic anhydride [137]. While these BIF values fall substantially short of those achieved through the use of single or multilayer coatings, an important advantage of PCNs is that their physical (*i.e.*, mechanical and flammability-resistant) properties are concurrently and substantially improved upon incorporation of the clay nanoparticles.

The theoretical models introduced earlier for PCNs provide valuable guidance with regard to the factors influencing barrier performance. Deviations from model predictions are often attributable to two unrealistic model assumptions: complete exfoliation and invariant orientation (parallel to the substrate surface). As Shah et al. [58] have demonstrated in Figure 2.14a, predictions from the Nielsen tortuosity model (Eq. 7), which implicitly invokes the first assumption, agree favorably with experimental observations for O₂, N₂ and CO₂ in the case of melt processed LDPE containing 1 wt% organically-modified MMT possessing an aspect ratio of 120. At higher MMT loading levels, however, the predictions underestimate the relative permeability. Deviation from the second assumption can be taken into account through the use of an order parameter, introduced by Bharadwaj [132] in Eq. 10. In Figure 2.14b, setting $S = 0.92$ yields predictions that fit the experimental data reasonably well, implying that most, but

not all, of the platelets are oriented parallel to the substrate surface. Since complete parallel orientation of the platelets corresponds to $S = 1.0$, this relatively minor reduction in S explains why the original Nielsen model not only helps to explain experimental results (especially at low loading levels where the first assumption is likely to be valid) but also remains a widely used predictive tool [133].

2.7. Conclusions and Outlook

Improving the barrier properties of commodity and engineering thermoplastics commonly used in food packaging applications to contend with growing economic demands for increased shelf life and decreased weight (and energy costs associated with transportation) has been achieved through the development of various inorganic surface coatings and polymer nanocomposite designs. Single-layer metal and metal oxide coatings are routinely deposited by PVD and CVD methods, with the latter providing more conformal coatings on rough surfaces or nonplanar (three-dimensional) objects. In addition, PVD coatings are generally less effective as barrier materials than CVD coatings due to a relatively higher defect density caused by lower mechanical flexibility and the absence of an interphase layer. Silicon-based CVD coatings are, however, prone to cracking as a consequence of the stresses that develop in the system. Attempts to increase the coating thickness to reduce transverse defects and improve barrier performance fail beyond an optimum thickness because of stress mismatch between the coating and substrate. Atomic layer deposition constitutes a very attractive emerging technology designed to overcome the drawbacks associated with single-layer deposition processes. Recent studies have demonstrated that thin, nearly defect-free ALD coatings

measuring only 5 nm thick exhibit OTR values below the detectable limit of conventional permeation measurements. Although ALD is classified here as a single-layer process because the result is a chemically homogeneous coating, ALD coatings actually consist of numerous layers that are deposited step-by-step at atomic dimensions by controlled reaction and purge sequences. Since the resulting coating is nearly defect-free, it comes closest to serving as an idealized impenetrable barrier intended to prevent (not hinder) diffusion. In similar fashion but at larger length scales, LBL deposition is a true multilayer process that likewise holds immense commercial promise for the barrier enhancement of polymer substrates by introducing extensive tortuosity into the diffusion pathway of permeating gases. Because the nanoscale brick wall composed of oppositely charged clay "bricks" and polymer "mortar" is fabricated by repeated alternating immersion into a clay suspension and a polymer solution, the clay layers comprising these transparent coatings are highly oriented. This deposition process can be performed at ambient temperature and pressure, and yields coatings that exhibit OTR levels below $0.005 \text{ cm}^3/(\text{m}^2\text{-day-atm})$.

An appealing alternative to deposition methods involves PCNs, in which a natural or organically-modified clay is introduced into a polymer matrix. A very important commercial consideration is that this approach is capable of generating large volumes of products with various shapes and sizes through the use of conventional polymer processing technologies, such as extrusion or blow/injection molding, which are routinely employed in today's food packaging industry. Since exfoliation is required to achieve barrier improvement in PCNs and since most polymers employed in the preparation of PCNs are nonpolar, natural clays have been chemically modified with organic surfactants or physically modified with compatibilizing

agents to improve the dispersability of the clay platelets within the polymer matrix. At high levels of exfoliation with about 5 wt% clay, the barrier improvement factor is $\approx 3x$, which pales in comparison to CVD, ALD and LBL deposition methods with improvement factors in excess of 2-3 orders of magnitude. Due largely to their relatively facile processability, mechanical robustness and lengthy stability, however, PCNs remain a commercially important class of polymer-based barrier materials, and several theoretical formalisms have been developed to predict the barrier efficacy of PCNs. The original Nielsen model, as well as its later versions proposed to account for variations in platelet orientation, and the Cussler model account for the high aspect ratio of clay platelets and other geometric factors that influence the diffusion pathway of permeating molecules. All the methods discussed in this chapter are intended to improve the barrier performance of food packaging through the enlightened use of hybrid materials in which polymeric substrates/matrices are coupled with impermeable inorganic coatings or additives. Alternate material designs capable of providing comparable or superior barrier performance in economical and sustainable fashion are of tremendous fundamental and technological interest.

2.8. Acknowledgments

We express our sincere gratitude to the United Resource Recovery Corporation (Spartanburg, SC, USA) for supporting this work.

Tables

Table 2.1. Comparison between the barrier properties of different polymer-based materials. ^a

Deposition ^b	Polymer	Coating	P_m (cm ³ /m ² -day-atm)	P_c (cm ³ /m ² -day-atm)	BIF	T (°C)	Ref.
Sputtering	PET	80 nm AlO _x N _y	1.8x10 ⁻³	5.0x10 ⁻⁵	36	23	Erlat et al. 2001
Evaporation	PET ^{d)}	17 nm Al ₂ O ₃	2.1x10 ⁻³	5.6x10 ⁻⁵	38	30	Roberts et al. 2002
PECVD	PET	100 nm SiO _x	1.7x10 ⁻⁵	3.8x10 ⁻⁶	440	30	Inagaki et al. 1999
PECVD	PET	20-200 nm SiO _x	2.0x10 ⁻³	4.5x10 ⁻⁶	444	30	Erlat et al. 1999
ALD	PET	10 nm Al ₂ O ₃	—	<2.510 ⁻⁷	—	23	Carcia et al. 2009
Al ₂ O ₃	PET	1.25 μm	6.0x10 ⁻²	<3.1x10 ⁻⁵	>1935	—	Affinito et al. 1996
LBL (30)	PET	571 nm	1.5x10 ⁻³	<9x10 ⁻⁷	>1700	23	Jang et al. 2008
LBL (30)	PET	118nm	1.5x10 ⁻³	<9x10 ⁻⁷	>1700	23	Yang et al. 2010
LBL (70)	PET	231nm	1.5x10 ⁻³	<9x10 ⁻⁷	>1700	23	Priolo et al. 2010a
LBL (24)	PET	120 nm	1.5x10 ⁻³	<9x10 ⁻⁷	>1700	23	Priolo et al. 2011
PNC	Epoxy	5 vol%	1.5x10 ⁻³	4.2x10 ⁻⁴	3.6	23	Osman et al. 2004
PNC	PLA	4 wt%	2.0x10 ⁻²	1.8x10 ⁻²	1.13	20	Ray et al. 2002
PNC	HDPE	5 wt%	4.1x10 ⁻¹	2.46x10 ⁻¹	1.68	20	Jacquelot et al. 2006

^a Except for the CO₂ data of Jacquelot et al. (2006), all other data are provided for O₂.

^b In the case of LBL deposition, the number in parentheses identifies the number of bilayers.

Figures

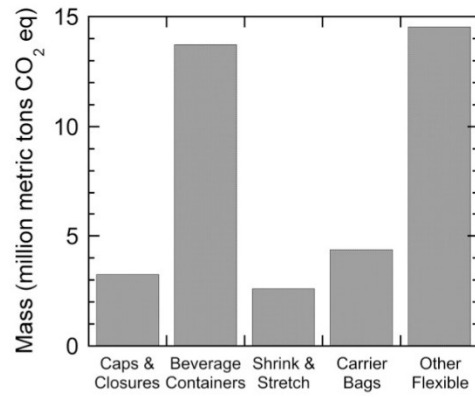


Figure 2.1. The 2014 mass quantities (on a CO₂ equivalent basis) of various polymeric materials employed in various food packaging functions in the U.S (adapted from Franklin Associates with permission) [1].

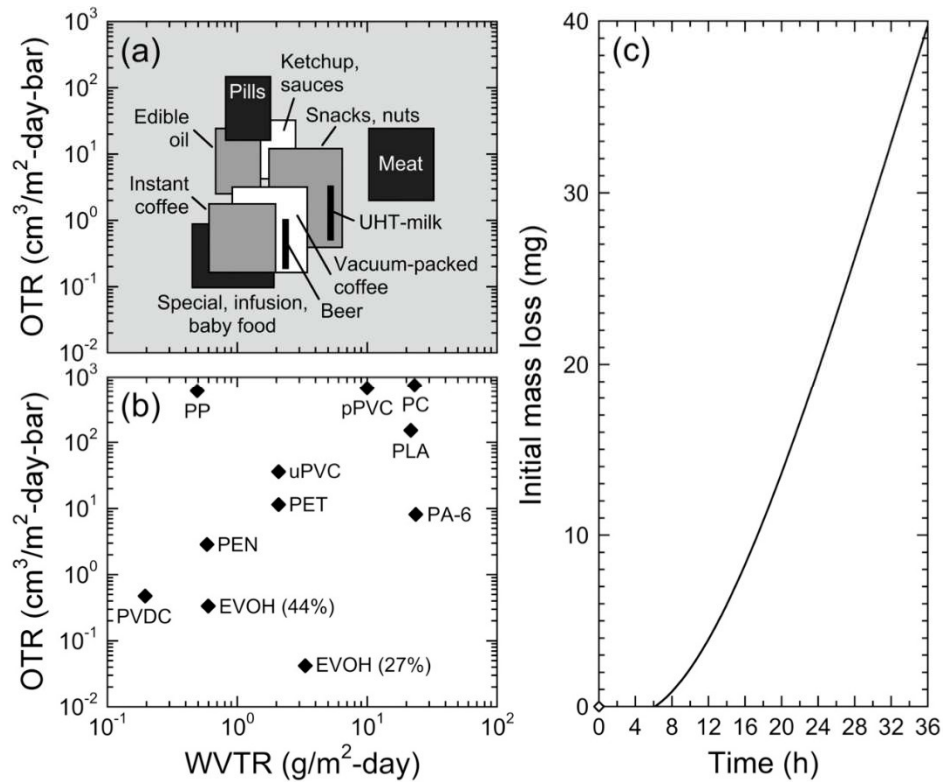


Figure 2.2. (a) Oxygen barrier requirements for various food packaging at 23°C and (b) typical OTR values of commercially relevant polymer films measuring 100 μm thick at 23 °C as functions of the WVTR (adapted from Hanika et al. 2003 with permission from Wiley) [6]. Included here are ethylene vinyl alcohol (EVOH) with two different degrees of substitution, poly(vinylidene chloride) (PVDC), poly(ethylene naphthalate) (PEN), poly(ethylene terephthalate) (PET), nylon-6 (PA-6), unplasticized poly(vinyl chloride) (uPVC), plasticized poly(vinyl chloride) (pPVC), poly(lactic acid) (PLA), polycarbonate (PC), and polypropylene (PP). (c) The initial loss of CO₂ from a PET bottle containing a carbonated soft drink measured at 24 °C and a gas pressure of 3 bar (adapted with permission from the Composite Agency) [62].

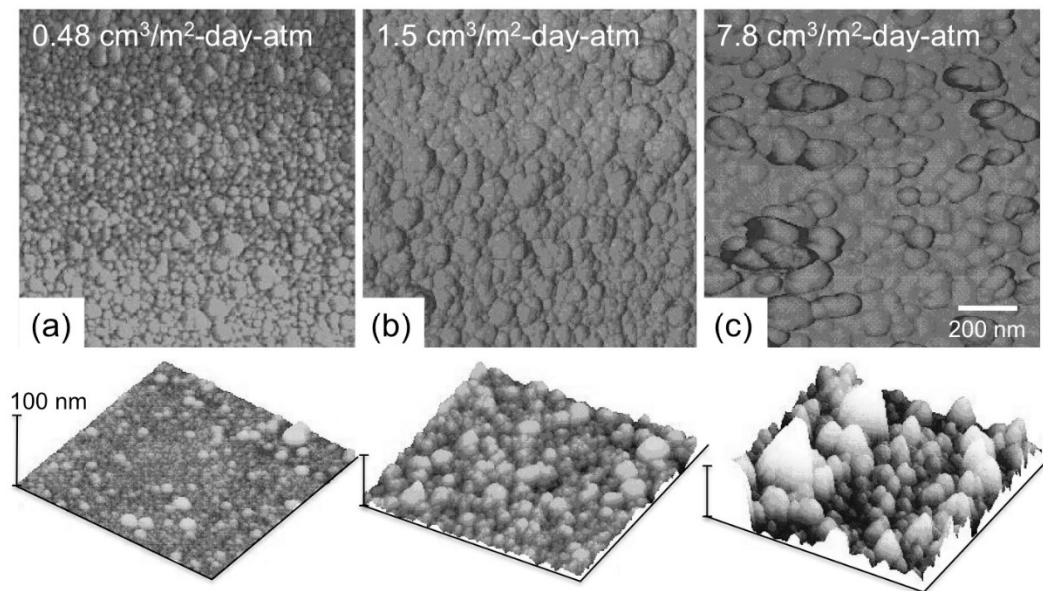


Figure 2.3. A series of two- and three-dimensional AFM height images (top and bottom rows, respectively) acquired from SiO_x coatings varying in OTR (labeled) on PET substrates at 30°C (adapted from Erlat et al. 1999 with permission from the American Chemical Society) [16].

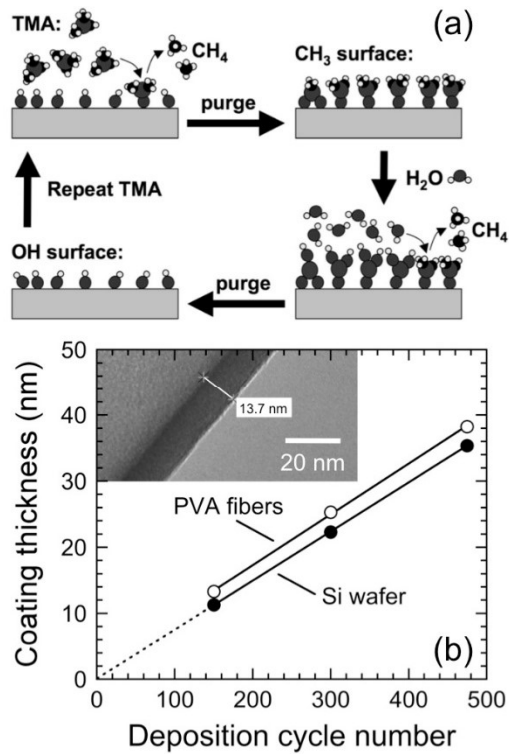


Figure 2.4. (a) The sequence of events corresponding to ALD conducted over a single cycle using TMA as the reactive precursor to generate an Al₂O₃ coating. (b) Thickness as a function of deposition cycle number for Al₂O₃ coatings on PVA fibers and silicon wafers (labeled). The lines are linear regressions to the data. The inset is a TEM image of the coating (about 14 nm thick) on a PVA fiber (adapted from Peng et al. 2007 with permission from the American Chemical Society)[40].

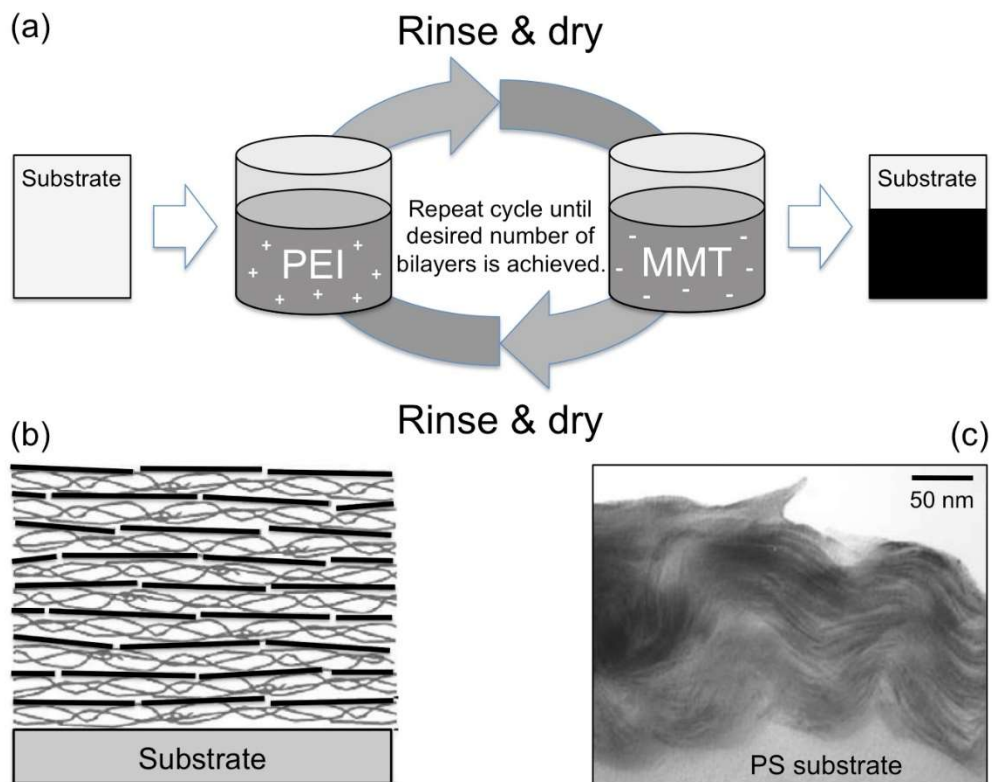


Figure 2.5. (a) The sequence of events corresponding to LBL deposition conducted with alternating immersions of the substrate in an aqueous poly(ethylene imine) (PEI) polycation solution and an aqueous MMT suspension. (b) Schematic illustration of the bilayers formed by LBL deposition onto a polymeric substrate. (c) Cross-sectional TEM image confirming the existence of numerous layers of clay platelets on the surface of a PS substrate (all adapted from Priolo et al. 2010a with permission from the American Chemical Society) [11].

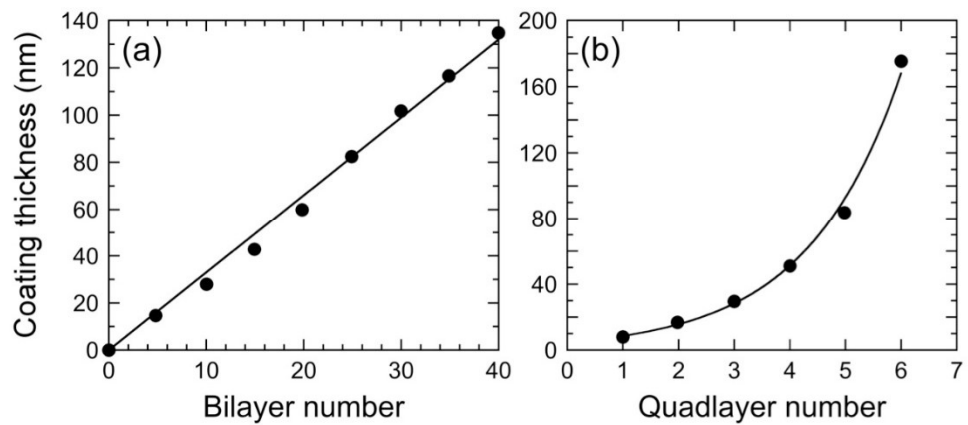


Figure 2.6. LBL coating thickness presented as a function of the number of (a) bilayers and (b) quadlayers for depositions employing either PEI alone or alternating immersions in PEI and poly(acrylic acid). The lines correspond to linear (a) and exponential (b) regressions of the data from Priolo et al. 2010a [11] and 2010b [34], respectively.

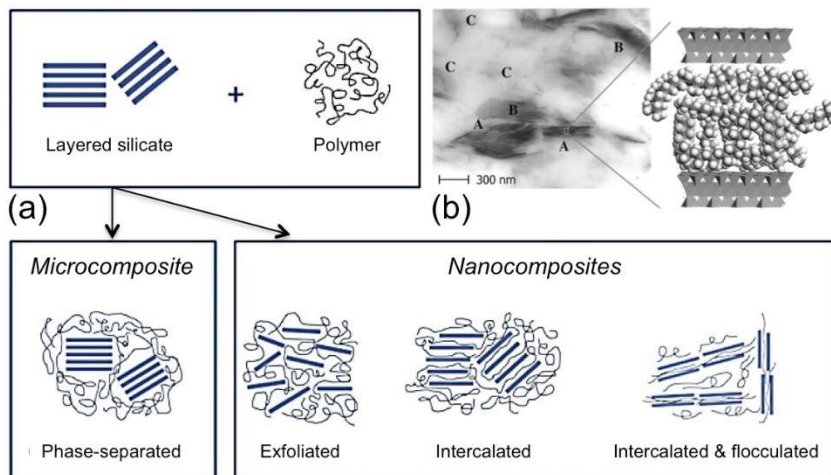


Figure 2.7. (a) Schematic illustration showing the results of incorporating layered silicates into polymeric matrices to yield either phase-separated microcomposites or different types of nanocomposites (labeled), depending on the level of dispersion achieved (adapted from Galimberti 2012) [110]. (b) TEM image of a nanocomposite composed of dispersed clay platelets in a PP matrix. Here, A, B and C identify intercalated stacks, disordered intercalated tactoids and exfoliated platelets, respectively. A schematic representation of an intercalated clay stack wherein parallel platelets are separated by PP chains (reproduced from Manias 2001 with permission from the Materials Research Society) [111].

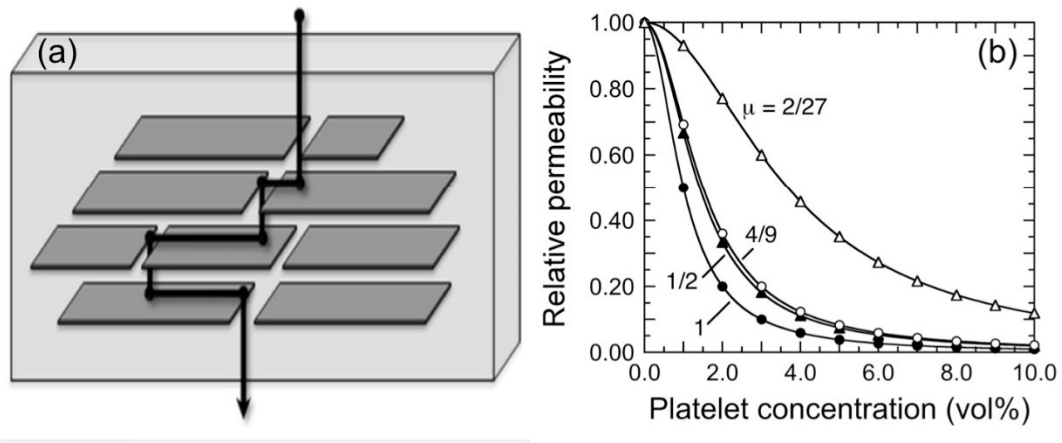


Figure 2.8. (a) Schematic diagram illustrating the diffusion pathway for a penetrant species through platelet-shaped nanoscale fillers embedded in a polymer matrix (adapted from Galimberti 2012)[110]. (b) Predictions of the relative permeability of PCNs as a function of plate concentration according to the Cussler model (Eq. 8) in which $\alpha = 100$ and μ is assigned discrete values (labeled) according to the spatial arrangements and platelet descriptions discussed in the text.

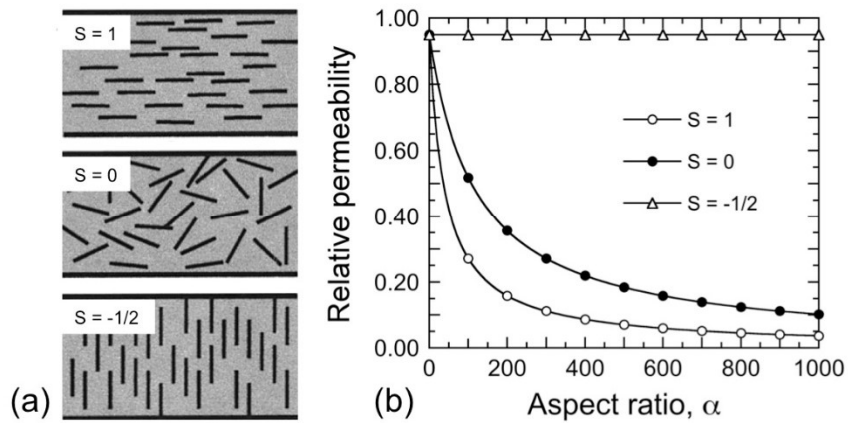


Figure 2.9. (a) Graphical representations of three different orientations (labeled with the corresponding order parameter, S) that clay platelets can adopt in a PCN (adapted from Bharadwaj 2001 with permission from the American Chemical Society) [132]. (b) Predictions for the relative permeability of PCNs containing 5 vol% clay as a function of the platelet aspect ratio for the three values of S (labeled) that are schematically depicted in (a).

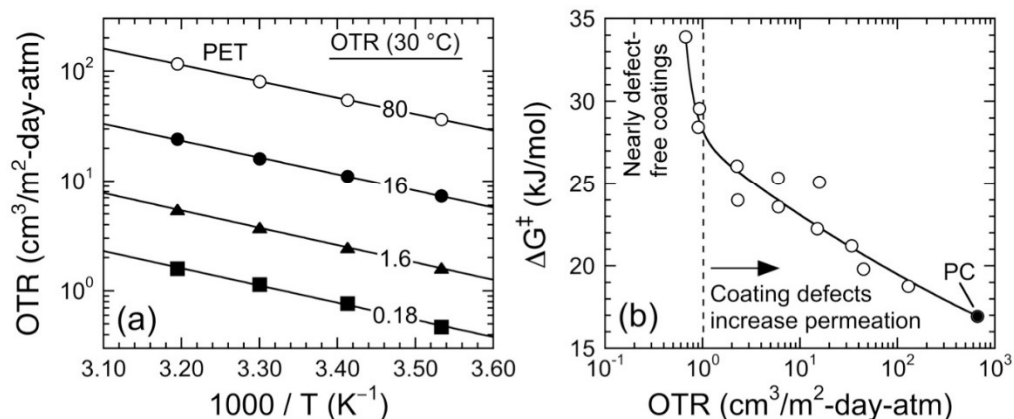


Figure 2.10. (a) Arrhenius-type temperature dependence of the OTR of four SiOx coatings (labeled) deposited by PECVD on PET substrates (reproduced from Erlat et al. 1999 with permission from the American Chemical Society) [16]. The regressed lines correspond to Eq. 11, and the resulting slopes yield the thermal activation energy, which is provided as a function of OTR for SiOx coatings deposited on PC substrates in (b). The solid line serves as a guide for the eye, whereas the dashed line approximates the position of the abrupt change in slope (adapted from Erlat et al. 2000 with permission from the Materials Research Society) [17].

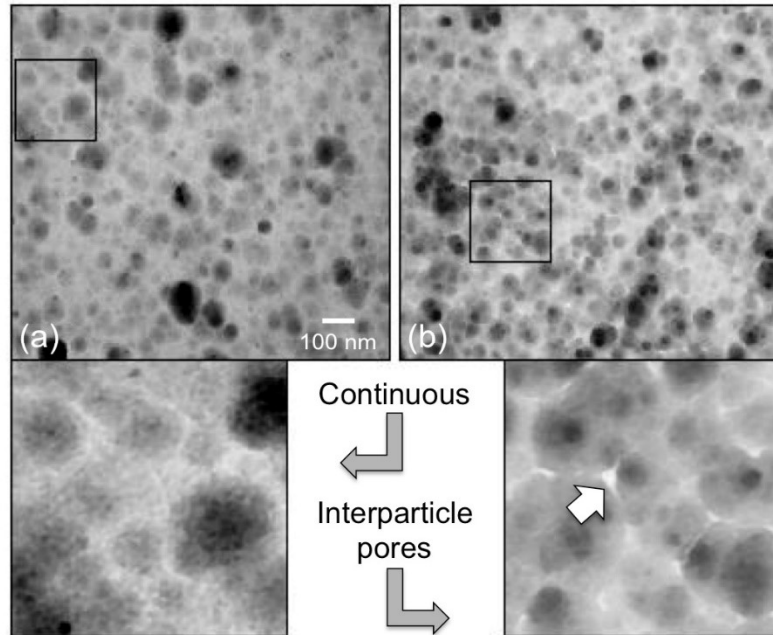


Figure 2.11. A pair of TEM images collected from SiO_x coatings deposited by PECVD on PET substrates and varying in OTR(in cm³/m²-day-atm): (a) 0.52 and (b) 16. The enlargements of the boxed regions reveal the contiguity of the coatings, with interparticle pore defects clearly visible (adapted from Erlat et al. 1999 with permission from the American Chemical Society) [16].

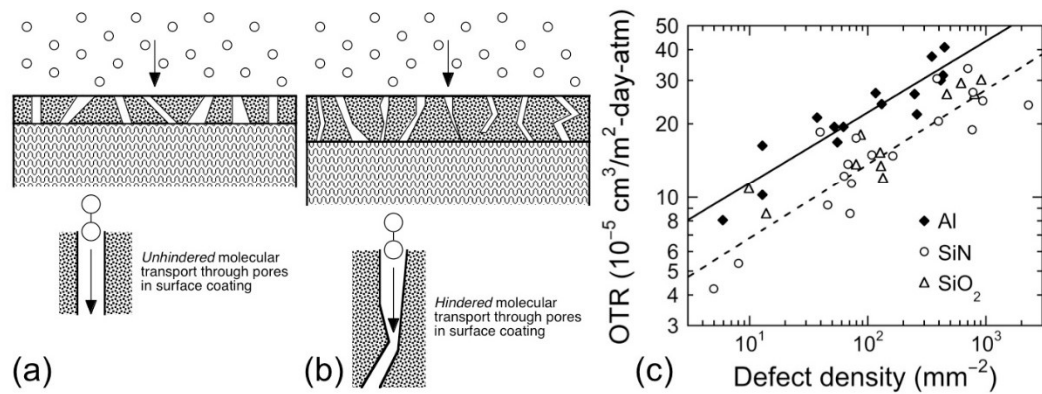


Figure 2.12. Schematic diagrams of molecular transport through (a) thin and (b) thick single-layer coatings illustrating the effect of defect size and shape (adapted from Erlat et al. 2000 with permission from the Materials Research Society) [17]. In (c), OTR values are provided as a function of defect density for three different single-layer coatings (labeled) measured above their critical thicknesses by da Silva Sobrinho et al. (2000) [4]. The solid lines are power-law regressions to the data and are provided as guides for the eye.

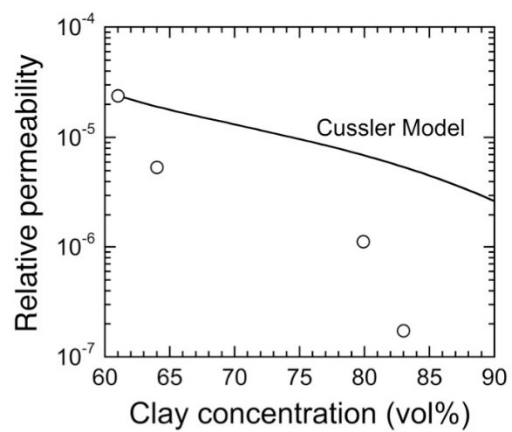


Figure 2.13. Experimental relative permeability values of LBL multilayer coatings as a function of clay concentration, as well as corresponding predictions from the Cussler model (adapted from Priolo et al. 2011 with permission from the American Chemical Society) [86].

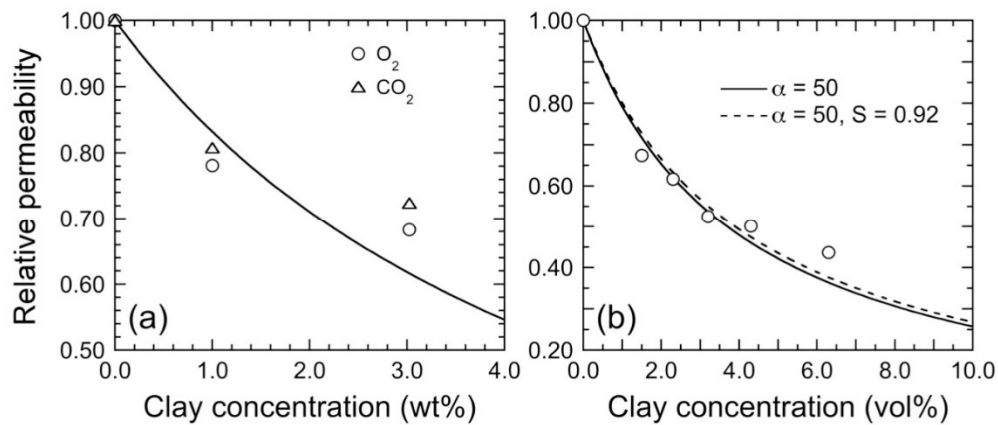


Figure 2.14. (a) Relative permeabilities of O₂ and CO₂ (labeled) in LDPE PCNs as a function of MMT concentration. The solid line corresponds to predictions from the Nielsen model in which $\alpha = 120$ (adapted from Shah et al. 2006 with permission from Elsevier) [58]. (b) Relative permeability of O₂ in PCNs prepared from hydrogenated acrylonitrile butadiene rubber with predictions from the original Nielsen model (solid line with $\alpha = 50$) and the Bharadwaj modification (dashed line with $\alpha = 50$ and $S = 0.92$) illustrating the marginal improvement achieved by adding the order parameter (adapted from Gatos & Karger-Kocsis 2007 with permission from Elsevier) [133].

References

- [1] Franklin Associates, Impacts of plastics packaging on life cycle energy consumption & greenhouse gas emissions in the United States and Canada, 2014. www.plastics.americanchemistry.com.
- [2] R. Lilienfeld, The ULS Report: Packaging Myths and Mantras, 2014. www.use-less-stuff.com.
- [3] N. Inagaki, S. Tasaka, H. Hiramatsu, Preparation of oxygen gas barrier poly (ethylene terephthalate) films by deposition of silicon oxide films plasma-polymerized from a mixture of tetramethoxysilane and oxygen, *J. Appl. Polym. Sci.* 71 (1999) 2091–2100.
- [4] A.S. da Silva Sobrinho, G. Czeremuskin, M. Latreche, M.R. Wertheimer, Defect-permeation correlation for ultrathin transparent barrier coatings on polymers, *J. Vac. Sci. Technol. A Vacuum, Surfaces, Film.* 18 (2000) 149–157.
- [5] G. Czeremuskin, M. Latrèche, M.R. Wertheimer, a. S. da Silva Sobrinho, M. Latreche, M.R. Wertheimer, et al., Ultrathin silicon-compound barrier coatings for polymeric packaging materials: An industrial perspective, *Plasmas Polym.* 6 (2001) 107–120.
- [6] M. Hanika, H.C. Langowski, U. Moosheimer, W. Peukert, Inorganic layers on polymeric films—Influence of defects and morphology on barrier properties, *Chem. Eng. Technol.* 26 (2003) 605–614.
- [7] J. Lewis, Material challenge for flexible organic devices, *Mater. Today.* 9 (2006) 38–45.
- [8] J. Jiang, M. Benter, R. Taboryski, K. Bechgaard, Oxygen barrier coating deposited by novel plasma-enhanced chemical vapor deposition, *J. Appl. Polym. Sci.* 115 (2010) 2767–2772.
- [9] P.F. Carcia, R.S. McLean, M.D. Groner, A.A. Dameron, S.M. George, Gas diffusion ultrabarriers on polymer substrates using Al₂O₃ atomic layer deposition and SiN plasma-enhanced chemical vapor deposition, *J. Appl. Phys.* 106 (2009) 23533.
- [10] H. Zhang, Scale-Up of Extrusion Foaming Process for Manufacture of Polystyrene Foams Using Carbon Dioxide, University of Toronto, 2010.
- [11] M.A. Priolo, D. Gamboa, J.C. Grunlan, Transparent clay–polymer nano brick wall assemblies with tailorable oxygen barrier, *ACS Appl. Mater. Interfaces.* 2 (2010) 312–320.

- [12] H. Chatham, Oxygen diffusion barrier properties of transparent oxide coatings on polymeric substrates, *Surf. Coatings Technol.* 78 (1996) 1–9.
- [13] R. Cueff, G. Baud, M. Benmalek, J.P. Besse, J.R. Butruille, H.M. Dunlop, et al., Characterization and adhesion study of thin alumina coatings sputtered on PET, *Thin Solid Films.* 270 (1995) 230–236.
- [14] N. Imai, M. Sekiguchi, M. Kano, T. Krug, G. Steiniger, A. Meier, Evaporation method of forming transparent barrier film, U.S. Patent and Trademark Office, 1995.
- [15] C. Deng, H.E. Assender, F. Dinelli, O. V Kolosov, G.A.D. Briggs, T. Miyamoto, et al., Nucleation and growth of gas barrier aluminium oxide on surfaces of poly (ethylene terephthalate) and polypropylene: effects of the polymer surface properties, *J. Polym. Sci. Part B Polym. Phys.* 38 (2000) 3151–3162.
- [16] A.G. Erlat, R.J. Spontak, R.P. Clarke, T.C. Robinson, P.D. Haaland, Y. Tropsha, et al., SiO_x gas barrier coatings on polymer substrates: morphology and gas transport considerations, *J. Phys. Chem. B.* 103 (1999) 6047–6055.
- [17] A.G. Erlat, B.-C. Wang, R.J. Spontak, Y. Tropsha, K.D. Mar, D.B. Montgomery, et al., Morphology and gas barrier properties of thin SiO_x coatings on polycarbonate: Correlations with plasma-enhanced chemical vapor deposition conditions, *J. Mater. Res. Pittsburgh.* 15 (2000) 704–717.
- [18] Y. Leterrier, Durability of nanosized oxygen-barrier coatings on polymers, *Prog. Mater. Sci.* 48 (2003) 1–55.
- [19] H. Low, Y. Xu, Moisture barrier of Al_xO_y coating on poly(ethylene terephthalate), poly(ethylene naphthalate) and poly(carbonate) substrates, *Appl. Surf. Sci.* 250 (2005) 135–145.
- [20] S.W. Keller, S.A. Johnson, E.S. Brigham, E.H. Yonemoto, T.E. Mallouk, Photoinduced charge separation in multilayer thin films grown by sequential adsorption of polyelectrolytes, *J. Am. Chem. Soc.* 117 (1995) 12879–12880.
- [21] Y. Lvov, K. Ariga, I. Ichinose, T. Kunitake, Molecular film assembly via layer-by-layer adsorption of oppositely charged macromolecules (linear polymer, protein and clay) and concanavalin A and glycogen, *Thin Solid Films.* 284 (1996) 797–801.
- [22] J.D. Affinito, M.E. Gross, C.A. Coronado, G.L. Graff, E.N. Greenwell, P.M. Martin, A new method for fabricating transparent barrier layers, *Thin Solid Films.* 290-291 (1996) 63–67.
- [23] R.K. Iler, Multilayers of colloidal particles, *J. Colloid Interface Sci.* 21 (1966) 569–594.

- [24] J.D. Affinito, S. Eufinger, M.E. Gross, G.L. Graff, P.M. Martin, PML/oxide/PML barrier layer performance differences arising from use of UV or electron beam polymerization of the PML layers, *Thin Solid Films*. 308 (1997) 19–25.
- [25] N.A. Kotov, Layer-by-layer self-assembly: The contribution of hydrophobic interactions, *Nanostructured Mater.* 12 (1999) 789–796.
- [26] P.T. Hammond, Form and function in multilayer assembly: New applications at the nanoscale, *Adv. Mater.* 16 (2004) 1271–1293.
- [27] P. He, N. Hu, J.F. Rusling, Driving forces for layer-by-layer self-assembly of films of SiO₂ nanoparticles and heme proteins, *Langmuir*. 20 (2004) 722–729.
- [28] W.-S. Jang, J.C. Grunlan, Robotic dipping system for layer-by-layer assembly of multifunctional thin films, *Rev. Sci. Instrum.* 76 (2005) 103904.
- [29] X. Zhang, H. Chen, H. Zhang, Layer-by-layer assembly: from conventional to unconventional methods, *Chem. Commun.* (2007) 1395–1405.
- [30] W.-S. Jang, I. Rawson, J.C. Grunlan, Layer-by-layer assembly of thin film oxygen barrier, *Thin Solid Films*. 516 (2008) 4819–4825.
- [31] N. Cini, T. Tulun, G. Decher, V. Ball, Step-by-step assembly of self-patterning polyelectrolyte films violating (almost) all rules of layer-by-layer deposition, *J. Am. Chem. Soc.* 132 (2010) 8264–8265.
- [32] V.H. Orozco, V. Kozlovskaya, E. Kharlampieva, B.L. López, V. V Tsukruk, Biodegradable self-reporting nanocomposite films of poly (lactic acid) nanoparticles engineered by layer-by-layer assembly, *Polymer* 51 (2010) 4127–4139.
- [33] Y.-H. Yang, F.A. Malek, J.C. Grunlan, Influence of deposition time on layer-by-layer growth of clay-based thin films, *Ind. Eng. Chem. Res.* 49 (2010) 8501–8509.
- [34] M.A. Priolo, D. Gamboa, K.M. Holder, J.C. Grunlan, Super gas barrier of transparent polymer–clay multilayer ultrathin films, *Nano Lett.* 10 (2010) 4970–4974.
- [35] O. Shchepelina, I. Drachuk, M.K. Gupta, J. Lin, V. V Tsukruk, Silk on Silk Layer by Layer Microcapsules, *Adv. Mater.* 23 (2011) 4655–4660.
- [36] J.W. Elam, C.A. Wilson, M. Schuisky, Z.A. Sechrist, S.M. George, Improved nucleation of TiN atomic layer deposition films on SiLK low-k polymer dielectric using an Al₂O₃ atomic layer deposition adhesion layer, *J. Vac. Sci. Technol. B Microelectron. Nanom. Struct.* 21 (2003) 1099–1107.

- [37] C.A. Wilson, R.K. Grubbs, S.M. George, Nucleation and growth during Al₂O₃ atomic layer deposition on polymers, *Chem. Mater.* 17 (2005) 5625–5634.
- [38] M.D. Groner, S.M. George, R.S. McLean, P.F. Carcia, Gas diffusion barriers on polymers using Al₂O₃ atomic layer deposition, *Appl. Phys. Lett.* 88 (2006) 51903–51907.
- [39] E. Langereis, M. Creatore, S.B.S. Heil, M.C.M. Van de Sanden, W.M.M. Kessels, Plasma-assisted atomic layer deposition of Al₂O₃ moisture permeation barriers on polymers, *Appl. Phys. Lett.* 89 (2006) 81915.
- [40] Q. Peng, X.-Y. Sun, J.C. Spagnola, G.K. Hyde, R.J. Spontak, G.N. Parsons, Atomic layer deposition on electrospun polymer fibers as a direct route to Al₂O₃ microtubes with precise wall thickness control, *Nano Lett.* 7 (2007) 719–722.
- [41] C.A. Wilson, J.A. McCormick, A.S. Cavanagh, D.N. Goldstein, A.W. Weimer, S.M.M. George, Tungsten atomic layer deposition on polymers, *Thin Solid Films.* 516 (2008) 6175–6185.
- [42] P.F. Carcia, R.S. McLean, M.H. Reilly, Permeation measurements and modeling of highly defective Al₂O₃ thin films grown by atomic layer deposition on polymers, *Appl. Phys. Lett.* 97 (2010) 221901–221903.
- [43] S.M. George, Atomic layer deposition: an overview, *Chem. Rev.* 110 (2010) 111–131.
- [44] J.C. Spagnola, B. Gong, S.A. Arvidson, J.S. Jur, S.A. Khan, G.N. Parsons, Surface and sub-surface reactions during low temperature aluminium oxide atomic layer deposition on fiber-forming polymers, *J. Mater. Chem.* 20 (2010) 4213–4222.
- [45] M. Alexandre, P. Dubois, Polymer-layered silicate nanocomposites: preparation, properties and uses of a new class of materials, *Mater. Sci. Eng. R Reports.* 28 (2000) 1–63.
- [46] C. Zeng, L.J. Lee, Poly (methyl methacrylate) and polystyrene/clay nanocomposites prepared by in-situ polymerization, *Macromolecules.* 34 (2001) 4098–4103.
- [47] S.S. Ray, K. Yamada, M. Okamoto, K. Ueda, S. Sinha Ray, K. Yamada, et al., Polylactide-layered silicate nanocomposite: a novel biodegradable material, *Nano Lett.* 2 (2002) 1093–1096.
- [48] J. Li, C. Zhou, G. Wang, D. Zhao, Study on rheological behavior of polypropylene/clay nanocomposites, *J. Appl. Polym. Sci.* 89 (2003) 3609–3617.
- [49] R.K. Shah, D.R. Paul, Nylon 6 nanocomposites prepared by a melt mixing masterbatch process, *Polymer.* 45 (2004) 2991–3000.

- [50] W. Lertwimolnun, B. Vergnes, Influence of compatibilizer and processing conditions on the dispersion of nanoclay in a polypropylene matrix, *Polymer* 46 (2005) 3462–3471.
- [51] Y. Zhong, Z. Zhu, S.-Q. Wang, Synthesis and Rheological Properties of Polystyrene/Layered Silicate Nanocomposite, *Polymer* 46 (2005) 3006–3013.
- [52] S.S. Ray, Rheology of polymer/layered silicate nanocomposites, *J. Ind. Eng. Chem.* 12 (2006) 811.
- [53] M. Bousmina, Study of intercalation and exfoliation processes in polymer nanocomposites, *Macromolecules*. 39 (2006) 4259–4263.
- [54] M. Tokihisa, K. Yakemoto, T. Sakai, L.A. Utracki, M. Sepehr, J. Li, et al., Extensional flow mixer for polymer nanocomposites, *Polym. Eng. Sci.* 46 (2006) 1040–1050.
- [55] L.A. Utracki, M. Sepehr, J. Li, Melt compounding of polymeric nanocomposites, *Int. Polym. Process.* 21 (2006) 3–16.
- [56] S. Ray, S.Y. Quek, A. Eastal, X.D. Chen, The potential use of polymer-clay nanocomposites in food packaging, *Int. J. Food Eng.* 2 (2006).
- [57] E. Jacquelot, E. Espuche, J.F. Gérard, J. Duchet, P. Mazabraud, Morphology and gas barrier properties of polyethylene-based nanocomposites, *J. Polym. Sci. Part B Polym. Phys.* 44 (2006) 431–440.
- [58] R.K. Shah, R.K. Krishnaswamy, S. Takahashi, D.R. Paul, Blown films of nanocomposites prepared from low density polyethylene and a sodium ionomer of poly(ethylene-*co*-methacrylic acid), *Polymer* 47 (2006) 6187–6201.
- [59] S. Hamzehlou, A.A. Katbab, Bottle-to-bottle recycling of PET via nanostructure formation by melt intercalation in twin screw compounder: Improved thermal, barrier, and microbiological properties, *J. Appl. Polym. Sci.* 106 (2007) 1375–1382.
- [60] E. Moncada, R. Quijada, J. Retuert, Comparative effect of metallocene and Ziegler-Natta polypropylene on the exfoliation of montmorillonite and hectorite clays to obtain nanocomposites, *J. Appl. Polym. Sci.* 103 (2007) 698–706.
- [61] A. Schechter, N. Malik, D. Haffner, S. Smith, T.R. Harris, O. Paepke, et al., Bisphenol A (BPA) in U.S. Food Environmental Science and Technology, 44 (2010) 9425–9430.
- [62] Composite Agency, Carbon Dioxide Diffusion Loss from PET Bottle, <http://www.composite-agency.com/archive/Carbon-Dioxide-Diffusion-PET.pdf> (accessed October 1, 2013).
- [63] J.R. Fried, H.C. Liu, C. Zhang, Effect of sorbed carbon dioxide on the dynamic

- mechanical properties of glassy polymers, *J. Polym. Sci. C Polym. Lett.* 27 (1989) 385–392.
- [64] R. Boyer, J. McKinney, *Food Storage Guidelines for Consumers*, Virginia Coop. Ext. 2013 (2013) 1–12.
- [65] *Nanocomposite Plastic Technologies*, 2003. www.ip.research.sc.edu.
- [66] E. Aionicesei, M. Škerget, Ž. Knez, Measurement of CO₂ solubility and diffusivity in poly (L-lactide) and poly (D,L-lactide- co-glycolide) by magnetic suspension balance, *J. Supercrit. Fluids.* 47 (2008) 296–301.
- [67] A.E. Özçam, *Surface Modification and Characterization of Polymeric Materials for Targeted Functionality*, Ph.D. Dissertation, North Carolina State University, 2011.
- [68] E. Markočič, M. Škerget, Ž. Knez, Solubility and diffusivity of CO₂ in poly (l-lactide)–hydroxyapatite and poly(d,l-lactide-co-glycolide)–hydroxyapatite composite biomaterials, *J. Supercrit. Fluids.* 55 (2011) 1046–1051.
- [69] A. Sorrentino, M. Tortora, V. Vittoria, Diffusion behavior in polymer-clay nanocomposites, *J. Polym. Sci. Part B Polym. Phys.* 44 (2006) 265–274.
- [70] V. Mittal, Barrier Resistance Generation in Polymer Nanocomposites, in: V. Mittal (Ed.), *Optim. Polym. Nanocomposite Prop.*, 1st ed., Wiley-VCH, Weinheim, Germany, 2010: pp. 173–194.
- [71] G.L. Graff, P.E. Burrows, R.E. Williford, R.F. Praino, Barrier layer technology for flexible displays, in: G. Crawford (Ed.), *Flex. Flat Panel Displays*, John Wiley & Sons, Hoboken, NJ, 2005: pp. 57–77.
- [72] E.H. Jamieson, a. H. Windle, Structure and oxygen-barrier properties of metallized polymer film, *J. Mater. Sci.* 18 (1983) 64–80.
- [73] J.F. Silvain, A. Veyrat, J.J. Ehrhardt, Effect of the temperature on the adhesion and the morphology of thin metal films evaporated on polyethylene terephthalate, *Thin Solid Films.* 221 (1992) 114–119.
- [74] F. Milde, K. Goedicke, M. Fahland, Adhesion behavior of PVD coatings on ECR plasma and ion beam treated polymer films, *Thin Solid Films.* 279 (1996) 169–173.
- [75] P. Gonzalez, E. Garcia, J. Pou, D. Fernandez, J. Serra, B. Leon, et al., Silicon oxide thin films grown by Xe₂ excimer lamp chemical vapour deposition: the role of the substrate temperature and the window-substrate distance, *Thin Solid Films.* 241 (1994) 348–351.
- [76] A.S. da Silva Sobrinho, M. Latreche, G. Czeremuskin, J.E. Klemberg-Sapieha, M.R.

Wertheimer, Transparent Barrier coatings on polyethylene terephthalate by single-and dual-frequency plasma-enhanced chemical vapor deposition, *J. Vac. Sci. Technol. A Vacuum, Surfaces, Film.* 16 (1998) 3190–3198.

- [77] T. Suntola, J. Autson, Method for producing compound thin films, 4 058 430, 1977.
- [78] J.C. Spagnola, Atomic layer deposition on fiber forming polymers and nonwoven fiber structures, NCSU, 2010.
- [79] K.B. Blodgett, I. Langmuir, Built-up films of barium stearate and their optical properties, *Phys. Rev.* 51 (1937) 964.
- [80] H. Kuhn, D. Möbius, Systems of Monomolecular Layers Assembling and Physicochemical Behavior, *Angew. Chemie Int. Ed. English.* 10 (1971) 620–637.
- [81] G. Decher, Layer-by-Layer Assembly, in: G. Decher, J.B. Schlenoff (Eds.), *Multilayer Thin Film.*, Wiley-VCH, Weinheim, Germany, 2012: pp. 1–22.
- [82] G. Decher, J.-D. Hong, Buildup of ultrathin multilayer films by a self-assembly process, I. consecutive adsorption of anionic and cationic bipolar amphiphiles on charged surfaces, in: *Makromol. Chemie. Macromol. Symp.*, Hüthig & Wepf Verlag, 1991: pp. 321–327.
- [83] G. Decher, J.D. Hong, Buildup of ultrathin multilayer films by a self-assembly process: II. Consecutive adsorption of anionic and cationic bipolar amphiphiles and polyelectrolytes on charged surfaces, in: *Berichte Der Bunsengesellschaft Für Phys. Chemie*, Wiley Online Library, 1991: pp. 1430–1434.
- [84] G. Decher, J.D. Hong, J. Schmitt, Buildup of ultrathin multilayer films by a self-assembly process: III. Consecutively alternating adsorption of anionic and cationic polyelectrolytes on charged surfaces, *Thin Solid Films.* 210 (1992) 831–835.
- [85] G. Decher, Fuzzy nanoassemblies: toward layered polymeric multicomposites, *Science* 277 (1997) 1232–1237.
- [86] M.A. Priolo, K.M. Holder, D. Gamboa, J.C. Grunlan, Influence of clay concentration on the gas barrier of clay–polymer nanobrick wall thin film assemblies, *Langmuir.* 27 (2011) 12106–12114.
- [87] J.B. Schlenoff, S.T. Dubas, T. Farhat, Sprayed polyelectrolyte multilayers, *Langmuir.* 16 (2000) 9968–9969.
- [88] P.A. Chiarelli, M.S. Johal, J.L. Casson, J.B. Roberts, J.M. Robinson, H. Wang, Controlled fabrication of polyelectrolyte multilayer thin films using spin-assembly, *Adv. Mater.* 13 (2001) 1167–1171.

- [89] P.A. Chiarelli, M.S. Johal, D.J. Holmes, J.L. Casson, J.M. Robinson, H.-L. Wang, Polyelectrolyte spin-assembly, *Langmuir*. 18 (2002) 168–173.
- [90] C. Jiang, S. Markutsya, V. V Tsukruk, Compliant, robust, and truly nanoscale free standing multilayer films fabricated using spin assisted layer by layer assembly, *Adv. Mater.* 16 (2004) 157–161.
- [91] R. von Klitzing, R. Kohler, C. Chenigny, Neutron Reflectometry at Polyelectrolyte Multilayers, in: G. Decher, J.B. Schlenoff (Eds.), *Multilayer Thin Film.*, Willey-VCH, Weinheim, Germany, 2012: pp. 219–268.
- [92] O. Félix, Z. Zheng, F. Cousin, G. Decher, Are sprayed LbL-films stratified? A first assessment of the nanostructure of spray-assembled multilayers by neutron reflectometry, *Comptes Rendus Chim.* 12 (2009) 225–234.
- [93] A.G. Erlat, B.M. Henry, J.J. Ingram, D.B. Mountain, A. McGuigan, R.P. Howson, et al., Characterisation of aluminium oxynitride gas barrier films, *Thin Solid Films*. 388 (2001) 78–86.
- [94] U. of South Carolina Research Foundation, Polymer Nanocomposite Technology Brief, 2013 (2003) [http://ip.research.sc.edu/PDF/Polymer Nanocomposite Technology Brief v1.pdf](http://ip.research.sc.edu/PDF/Polymer%20Nanocomposite%20Technology%20Brief%20v1.pdf) (accessed January 1, 2014).
- [95] S.S. Ray, M. Okamoto, S. Sinha Ray, M. Okamoto, Polymer/layered silicate nanocomposites: a review from preparation to processing, *Prog. Polym. Sci.* 28 (2003) 1539–1641.
- [96] M.A. Osman, V. Mittal, M. Morbidelli, U.W. Suter, Epoxy-layered silicate nanocomposites and their gas permeation properties, *Macromolecules*. 37 (2004) 7250–7257.
- [97] R. Krishnamoorti, K. Yurekli, Rheology of polymer layered silicate nanocomposites, *Curr. Opin. Colloid Interface Sci.* 6 (2001) 464–470.
- [98] Y.T. Lim, O.O. Park, Phase morphology and rheological behavior of polymer/layered silicate nanocomposites, *Rheol. Acta.* 40 (2001) 220–229.
- [99] T.H. Kim, S.T. Lim, C.H. Lee, H.J. Choi, M.S. Jhon, Preparation and rheological characterization of intercalated polystyrene/organophilic montmorillonite nanocomposite, *J. Appl. Polym. Sci.* 87 (2003) 2106–2112.
- [100] L. Shen, Y. Lin, Q. Du, W. Zhong, Y. Yang, Preparation and rheology of polyamide-6/attapulgite nanocomposites and studies on their percolated structure, *Polymer* 46 (2005) 5758–5766.

- [101] M. Kráčalík, M. Studenovský, J. Mikešová, A. Sikora, R. Thomann, C. Friedrich, et al., Recycled PET Nanocomposites Improved by Silanization of Organoclays, *J. Appl. Polym. Sci.* 106 (2007) 926–937.
- [102] S.N. Bhattacharya, M.R. Kamal, R.K. Gupta, *Polymeric nanocomposites: theory and practice*, Carl Hanser Publishers, Munich, 2008.
- [103] M. Song, J. Jin, Rheological behavior of polymer nanocomposites, in: V. Mittal (Ed.), *Optim. Polym. Nanocomposite Prop.*, 1st ed., Wiley-VCH, Weinheim, Germany, 2010: pp. 93–122.
- [104] G.W. Beall, C.E. Powell, *Fundamentals of Polymer-Clay Nanocomposites*, 1st ed., Cambridge University Press, Cambridge, UK, 2011.
- [105] V. Mittal, Polymer nanocomposites: synthesis, microstructure, and properties, in: V. Mittal (Ed.), *Optim. Polym. Nanocomposite Prop.*, 1st ed., Wiley-VCH, Weinheim, Germany, 2010: pp. 1–20.
- [106] L.C. Sawyer, D.T. Grubb, G.F. Meyers, *Polymer microscopy*, 3rd ed., Springer, New York, NY, USA, 2007.
- [107] A. Okada, A. Usuki, Twenty years of polymer-clay nanocomposites. *Macromolecular Materials and Engineering*, *Macromol. Mater. Eng.* 291 (2006) 1449–1476.
- [108] M. Kawasumi, The discovery of polymer clay hybrids, *J. Polym. Sci. Part A Polym. Chem.* 42 (2004) 819–824.
- [109] F. Hussain, M. Hojjati, M. Okamoto, R.E. Gorga, Review article: polymer-matrix nanocomposites, processing, manufacturing, and application: an overview, *J. Compos. Mater.* 40 (2006) 1511–1575.
- [110] M. Galimberti, Rubber Clay Nanocomposites, *Adv. Elastomers – Technol. Prop. Appl.* (2012).
- [111] E. Manias, A direct-blending approach for polypropylene/clay nanocomposites enhances properties, *Mater. Res. Soc. Bull.* 26 (2001) 862–863.
- [112] M. Fujiyama, Morphology development in polyolefin nanocomposites, in: V. Mittal (Ed.), *Optim. Polym. Nanocomposite Prop.*, 1st ed., Wiley-VCH, Weinheim, Germany, 2010: pp. 67–92.
- [113] E.P. Giannelis, R. Krishnamoorti, E. Manias, *Polymer-Silicate Nanocomposites: Model Systems for Confined Polymers and Polymer Brushes*, in: S. Granick (Ed.), *Polym. Confin. Environ.*, Springer, Berlin Heidelberg, 1999: pp. 107–147.

- [114] D.J. Frankowski, M.D. Capracotta, J.D. Martin, S. a. Khan, R.J. Spontak, Stability of organically modified montmorillonites and their polystyrene nanocomposites after prolonged thermal treatment, *Chem. Mater.* 19 (2007) 2757–2767.
- [115] P.B. Messersmith, E.P. Giannelis, Polymer-layered silicate nanocomposites: in situ intercalative polymerization of. epsilon.-caprolactone in layered silicates, *Chem. Mater.* 5 (1993) 1064–1066.
- [116] U. Yilmazer, G. Ozden, Polystyrene–organoclay nanocomposites prepared by melt intercalation, in situ, and masterbatch methods, *Polym. Compos.* 27 (2006) 249–255.
- [117] A. Ammala, C. Bell, K. Dean, Poly (ethylene terephthalate) clay nanocomposites: improved dispersion based on an aqueous ionomer, *Compos. Sci. Technol.* 68 (2008) 1328–1337.
- [118] D.J. Rousseaux, N. Sallem-Idrissi, A.-C. Baudouin, J. Devaux, P. Godard, J. Marchand-Brynaert, et al., Water-assisted extrusion of polypropylene/clay nanocomposites: A comprehensive study, *Polymer* 52 (2011) 443–451.
- [119] A.B. Morgan, J.W. Gilman, Characterization of polymer layered silicate (clay) nanocomposites by transmission electron microscopy and x-ray diffraction: A comparative study, *J. Appl. Polym. Sci.* 87 (2003) 1329–1338.
- [120] J. Comyn, Introduction to Polymer Permeability and the Mathematics of Diffusion, in: J. Comyn (Ed.), *Polym. Permeability*, 1st ed., Elsevier, London and New York, 1985: pp. 1–10.
- [121] N.P. Patel, A.C. Miller, R.J. Spontak, Highly CO₂-permeable and selective polymer nanocomposite membranes, *Adv. Mater.* 15 (2003) 729–733.
- [122] M. Perez-Blanco, J.R. Hammons, R.P. Danner, Measurement of the solubility and diffusivity of blowing agents in polystyrene, *J. Appl. Polym. Sci.* 116 (2010) 2359–2365.
- [123] T.C. Merkel, B.D. Freeman, R.J. Spontak, Z. He, I. Pinnau, P. Meakin, et al., Ultraparpermeable, reverse-selective nanocomposite membranes, 296 (2002) 519–522.
- [124] X. Hu, J. Tang, A. Blasig, Y. Shen, M. Radosz, CO₂ permeability, diffusivity and solubility in polyethylene glycol-grafted polyionic membranes and their CO₂ selectivity relative to methane and nitrogen, *J. Memb. Sci.* 281 (2006) 130–138.
- [125] C.H. Klute, Diffusion of small molecules in semicrystalline polymers: water in polyethylene, *J. Appl. Polym. Sci.* 1 (1959) 340–350.
- [126] L.E. Nielsen, Models for the permeability of filled polymer systems, *J. Macromol. Sci.*

1 (1967) 929–942.

- [127] G.H. Fredrickson, J. Bicerano, Barrier properties of oriented disk composites, *J. Chem. Phys.* 110 (1999) 2181–2188.
- [128] J.P. DeRocher, B.T. Gettelfinger, J. Wang, E.E. Nuxoll, E.L. Cussler, Barrier membranes with different sizes of aligned flakes, *J. Memb. Sci.* 254 (2005) 21–30.
- [129] E.L. Cussler, S.E. Hughes, W.J. Ward III, R. Aris, Barrier membranes, *J. Memb. Sci.* 38 (1988) 161–174.
- [130] G.D. Moggridge, N.K. Lape, C. Yang, E.L. Cussler, Barrier films using flakes and reactive additives, *Prog. Org. Coatings.* 46 (2003) 231–240.
- [131] W.-S. Jang, Layer-by-layer assembly of clay-filled polymer nanocomposite thin films, Texas A&M University, 2008.
- [132] R.K. Bharadwaj, Modeling the barrier properties of polymer-layered silicate nanocomposites, *Macromolecules.* 34 (2001) 9189–9192.
- [133] K.G. Gatos, J. Karger-Kocsis, Effect of the aspect ratio of silicate platelets on the mechanical and barrier properties of hydrogenated acrylonitrile butadiene rubber (HNBR)/layered silicate nanocomposites, *Eur. Polym. J.* 43 (2007) 1097–1104.
- [134] A.P. Roberts, B.M. Henry, A.P. Sutton, C.R.M. Grovenor, G.A.D. Briggs, T. Miyamoto, et al., Gas permeation in silicon-oxide/polymer (SiO_x/PET) barrier films: role of the oxide lattice, nano-defects and macro-defects, *J. Memb. Sci.* 208 (2002) 75–88.
- [135] N. Hasegawa, H. Okamoto, M. Kato, A. Usuki, N. Sato, Nylon 6/Na-montmorillonite nanocomposites prepared by compounding nylon 6 with Na-montmorillonite slurry, *Polymer* 44 (2003) 2933–2937.
- [136] S. Nazarenko, P. Meneghetti, P. Julmon, B.G. Olson, S. Qutubuddin, Gas barrier of polystyrene montmorillonite clay nanocomposites: Effect of mineral layer aggregation, *J. Polym. Sci. Part B Polym. Phys.* 45 (2007) 1733–1753.
- [137] J. Golebiewski, A. Galeski, Thermal stability of nanoclay polypropylene composites by simultaneous DSC and TGA, *Compos. Sci. Technol.* 67 (2007) 3442–3447.

CHAPTER 3

Investigating Morphology of Layer-by-Layer Coated Polystyrene-Based Membranes, Using Clay with Alternative Interlayers of Polyethyleneimine or Polyethyleneterephthalate Ionomer

Abstract

Due to being easy, cheap, environmental friendly, and still highly efficient, layer-by-layer (LBL) coating can be considered as one of new popular approaches for improving barrier properties of polymeric membranes against gases. In this research, generating LBL assemblies, based on natural clay and alternative cationic polyelectrolyte (PE) interlayers of polyethyleneimine (PEI) or anionic polyethyleneterephthalate ionomer (PETi), and their morphology and barrier properties were investigated. In fact, transmission electron microscopy (TEM) and scanning electron microscopy (SEM) images of the built-up LBL coatings showed the formation of tortuous networks of galleries built between intercalated rows of high aspect ratio clay platelet layers, oriented parallel to the polymeric substrate surface line, when appropriate contents of macromolecular glue and clay in their solution and well-dispersed suspensions in deionized water, respectively, were used. Then, x-ray diffractometry (XRD) results confirmed the increased intercalation occurred in aforementioned LBL assemblies and showed how the level of intercalation can vary with change in the content of their mentioned ingredients. Also, permeation tests results showed significant decreases in permeability of LBL-coated films, based on polystyrene, that have never been reported in the literature for this hydrophobic polymer. These findings confirmed the formation of above explained tortuous barrier coatings, as a result of appropriate interactions between clay and polyelectrolyte and

oriented layout of LBL assemblies. The other suggested reasons for barrier improvement in these LBL-coated membranes might be the plasma treatment of the substrate to promote a firm contact between coating and substrate. Also, with the increase in clay content in suspension, decreasing trend of permeability leveled off at clay content of 3-5wt% in suspension, possibly due to lack of its exfoliation in suspension and its increased viscosity, resulting in the lack of orientation in made LBL assembly. Similarly, increasing the content of PEI in DIW, above a limiting point, posed increased non-orientation and waviness and the decrease in intercalation. To sum up, resulted membranes could provide a decent potential for barrier improvement demands in food packaging industry.

3.1. Introduction

Lower weight and costs of polymeric materials have made them an appropriate alternative for traditional materials in different applications, including packaging industries. However, to improve shelf life of contained materials, barrier properties of polymer packagings needs to increase. Coating of the polymeric membranes with thin, to remain flexible, and still barrier films have been attempted by scientists to answer this demand [1–3]. Despite initial concentrated attempts on using single coating layers [4–6], gradually multilayer coatings, due to their spontaneously higher flawlessness, attracted much attention, amongst which layer-by-layer deposition, due to its features, like easy processing, low costs, and environmentally safe, was considered as an appropriate choice [1,7–13]. Layer-by-layer (LBL) deposition, which is mainly done through alternating immersion of substrates in oppositely charged solutions, can have a variation in chemistry, molecular weight, and ionic strength of its components, resulting

in multilayer films with thickness of only a few nm to a few hundreds of nm [14–16]. In fact, different from traditional compounding, where the small entropic force of polymeric chains made their homogeneous mixing challenging [17,18], in LBL, the strong electrostatic attraction between charged groups of alternating layers makes their molecular level blending possible. LBL assemblies made through electrostatic forces between polycations and clay, in the form of flexible nanobrick walls of clay platelets, mainly montmorillonite (MMT), through increasing the tortuosity and increasing the path of permeating species, turned out to result in significant barrier improvements [14,19]. Nevertheless, to improve the wettability of nonpolar polymer substrates with an inorganic coating, their surface treatments through different methods like corona, ultraviolet ozone (UVO) irradiation, oxygen plasma, flame, and chemical methods are needed [14,20–23].

Despite previous studies on morphology and oxygen barrier properties of PEI, MMT LBL assemblies, the permeation properties, for challenging nonpolar substrates, have not been investigated yet. So, this study, in addition to studying the morphology of such LBL assemblies, would embark on investigating their barrier properties, for disputing PS substrate as a superhydrophobic polymer. Also, using polyethyleneterephthalate ionomer (PETi) interlayers as a potential alternative for PEI interlayer, and morphology and barrier properties of resulted LBL assemblies would be discussed. It should be mentioned that different from previously used polyelectrolytes that are positively-charged to interact with negative charges on the surface of MMT layers, PETi is negatively charged and would possibly interact with positive charges on the edge of MMT platelets [24–26].

3.2. Experimental

3.2.1. Materials

Polystyrene (PS) ($M_n=100\text{kDa}$, PDI: 1.01) was kindly granted by Proctor & Gamble, and due to ease of sectioning, was used as the substrate for transmission electron microscopy images. Poly (styrene-co-butadiene) (PS*) (density= 1.04g/cm^3 at 25°C , butadiene=4wt%) was supplied by Sigma-Aldrich (St Louis, MO). Branched polyethyleneimine (PEI) ($M_n=60\text{kDa}$, $M_w=750\text{kDa}$, density= 1.07 g/cm^3 (at 20°C)) in DIW (50wt%), was purchased from Scientific Polymer Products (Ontario, NY). This grade had showed higher thermal stability compared with, other researchers choice [13,14], polyethyleneimine ($M_w=25\text{kDa}$, $M_n=10\text{kDa}$), according to the previous study conducted in this group [24]. Polyethylene terephthalate ionomer (AQ55S) (PETi) (density= 0.82g/cm^3) was generously donated by Eastman Chemical Company (Kingsport, TN). The purified nanoclay, Cloisite Na^+ , was obtained from Southern Clay Products (SCP) (Gonzales, TX). Cation exchange capacity of this natural clay is 92mequiv/100g [27,28], and their specific gravity is 2.86g/cm^3 [28]. Deionized water (DIW) used, mainly as a media for PEI and MMT, had a water resistivity of $18.2\text{M}\Omega$ at 25°C and was made by Direct-Q 3 UV water purification system of Millipore [7,8,14]. Ultra high purity (99.999% purity) O_2 was purchased from National Welders Supply Co. (Charlotte, NC) and Air Liquid America Specialty Gases LLC. (Plumsteadville, PA). High purity CO_2 (99.99% purity) was obtained from National Welders Supply Co. (Charlotte, NC). High purity CO_2 (99.9% purity) was obtained from National Welders Supply Co. (Charlotte, NC) and Air Liquide America Specialty Gases LLC. (Houston, TX). Ultra high purity (99.999% purity) He was purchased from Air Gas Inc. (Radnor Township, PA).

3.2.2. Thin Film Preparation

Thin films of PS* and PS were prepared by solution casting from toluene at room temperature on crystallization plates, which were previously cleaned with acetone and methanol, before being rinsed by DIW, respectively. PS* (butadiene=4wt%) was used as an alternative for pure polystyrene (PS), which its resulted thin films are too brittle to be mounted and be sealed appropriately on the permeation cell equipment. The resulted films were heated up to 110°C (above PS glass transition temperature), under vacuum, in order to assure complete removal of toluene.

3.2.3. Plasma Treatment

Oxygen plasma exposure of solution cast PS and PS* films, with the typical thickness of 100 µm, was done by a laboratory and small-scale production plasma system FEMTO (low-pressure plasma), manufactured by Diener Electronics (Germany) at power of 10W/cm², and gas flow rate of 20 sccm (standard cubic centimeters per minute), or intensity of 0.5W/sccm, for 60s, to induce polar groups such as carbonyl and carboxylic acid to increase the hydrophilicity and surface adhesion properties of PS*. Thus, it promotes the attraction and attachment of later on deposited polycations to its surface [21,22,29].

3.2.4. Layer-by-Layer (LBL) Coating of Thin Films

Polyelectrolyte solutions were prepared by dissolving PEI in DIW at different concentrations of 0.1, 0.5, 1, and 10wt% at room temperature. Na⁺MMT suspensions, with various concentrations of 0.1, 1, 3, and 5%wt% in DIW, were prepared by 20 min ultrasonication, followed by intensive stirring, at about 600 rpm, of the suspension over the

extended time of 24 h, in order to achieve stable exfoliation and homogeneity. Each plasma treated film was immersed in PEI solution for 5 min, rinsed with DIW, and dried with filtered air. Then in a similar procedure, a layer of MMT platelets was deposited on the already PEI-coated film, to build the first bilayer of the coating. This operation was repeated in order to reach the desired number of bilayer coatings. Due to the nature of the immersion process, bilayers are deposited on both sides of the polymeric substrate, but for simplicity, from now on we only count the number of bilayers (BLs) deposited on one side of the substrate in our remarks.

Also, PETi, containing random anionic functionalities on the backbone of PET, which had been investigated for making PNCs, successfully [26,30,31], were tried, as a proposed alternative for PEI, to build up LBL assemblies. Thus, as an alternative to PEI solutions, solutions of PETi in DIW were stirred similarly, but at 60°C, almost above PETi glass transition temperature [26,30], and used for alternating LBL deposition with clay, in a similar way.

3.2.5. Transmission Electron Microscopy (TEM)

LBL-coated films were embedded in epoxy and sectioned with a Leica Ultracut 7 at ambient condition, yielding sections of approximately 120 nm thin, floated onto DIW, before being picked up on carbon coated 200 mesh copper TEM grids [32]. A series of microscopic images were acquired from the microtomed thin sections, using a JEOL 2000 FX (Parbody, MA) TEM at an accelerating voltage of 200kV and calibrated magnification.

3.2.6. Scanning Electron Microscopy (SEM)

Alternative to TEM images, a JEOL JSM-6400F FESEM (Parbody, MA), operated at an accelerating voltage of 10kV, was used to investigate the morphology of LBL-coated films cross-sections, after sputter coating a thin layer of Au-Pd ($\approx 10\text{nm}$) on them [24].

3.2.7. X-Ray Diffractometry (XRD)

Wide angle x-ray diffractometry was performed at ambient temperature on an Inel XRG 3000 diffractometer (Artenay, France) with $\text{CuK}\alpha$ radiation (wavelength $\lambda=0.15405\text{ nm}$) at 35kV and 30mA. XRD samples were tested in reflection mode using the Bragg-Brentano para-focusing geometry (powders and films), and diffraction intensity data were usually recorded in diffraction angle range of 3.0° to about 40.0° [33,34]. Samples were dried in vacuum oven at 50°C for 48 h and stored in desiccator before performing characterizations.

3.2.8. Gas Permeation

Gas permeation experiments on neat as well as LBL-coated films were carried out with a constant-volume/ variable-pressure technique, shown in the schematic Figure 4.1.e. at about 20°C and atmospheric pressure for oxygen and carbon dioxide and helium gases. Samples were dried in vacuum oven at 50°C for 48h and stored in desiccator before performing characterizations [35,36]. Accordingly, each polymeric membrane, with thickness L , was covered by two tapes of Aluminum, with an exposure area of A (2.27cm^2), which gas can pass through. Then, after the evacuation of the whole system, the desired gas, with a determined upstream pressure of typically 1 atm was permeated through the membrane into the vessel of

known volume (V) in the downstream, and pressure in the downstream was recorded, by a pressure transducer connected to a computer.[37,38]

Therefore, the permeability of the gases through a membrane were measured by the following equation.

$$P = \frac{VL}{ART\Delta P} \frac{dP}{dt} \quad (1)$$

where V, L, A, R, ΔP , and $\frac{dP}{dt}$ are the downstream volume, membrane thickness, membrane exposure area, universal gas constant, the difference between constant upstream and initial downstream pressures, and steady rate of increase in gas pressure in downstream, respectively [37,38].

3.3. Results and Discussion

3.3.1. Proposed Mechanism of Formation and Morphology of Nanobrick LBL

Assemblies

According to the following schematics (Figures 3.1), it is proposed that MMT clay is exfoliated by stirring at high speeds over extended time, to reach a semi-exfoliated state, where water molecules can diffuse in the space between clay platelets and increase their interplanar spacing. Then, after deposition of this clay on an already polyelectrolyte-coated polymeric substrate, through occurring electrostatic interactions between counterions, the chains of polyelectrolyte can possibly intercalate between deposited clay platelets. With repeating these alternating deposition steps, a multilayer nanobrick wall conforming oriented platelets and polyelectrolyte mortar can be built that could theoretically provide superior barrier properties

if both the interfaces between clay platelets and polymeric interlayers and also between LBL assemblies and substrates would be strong enough [1,7,8,14,28,39].

3.3.2. TEM Results for PEI-MMT LBL Assemblies

TEM micrographs show the cross-section of LBL assemblies deposited on PS substrate, where mostly individual clay platelets rows, as dark lines, can be differentiated from lighter polyelectrolyte layers. Figure 3.2 shows assemblies of 30BL's, alternatingly deposited from a solution of 0.5wt% PEI and suspension of 1wt% Na⁺MMT, both in DIW, respectively. As it was reported by other authors [1,7,8,14], it can be observed (particularly in images with higher magnifications) that, due to existing electrostatic attractions between PEI chains and clay platelets surfaces, mainly exfoliated clay platelets deposit parallel to the PS substrate surface line, and form a well-ordered nanobrick wall of single sheets, where mortar polyelectrolyte chains are intercalated in between them.

The reason for the slight waviness evident in such neatly ordered LBL assemblies can be sought in relieved stresses through cutting such thin sections with ultramicrotomy, in addition to low topographical uniformity, as a feature of natural clays [7]. Also, cutting of cross-sections with small angles, is another reason for both disparity in the nanobrick structure of LBL assemblies and an apparent thickness, which is typically higher than their real thickness [7,8,14].

The high level of orientation, exfoliation, and tightly packing seen in TEM micrographs is the unique feature of the LBL structures. In fact, owing to the strong electrostatic attraction of positively-charged PEI, negatively charged clay platelets are absorbed mainly oriented with

their largest dimensions parallel to the surface of the film. Thus, a highly laminar, oriented and tightly packed structure of highly exfoliated clay platelets layers is constructed, which are not achievable with any other method of direct mixing of polymers and clays [8].

With the increase in the concentration of MMT in DIW to 5wt%, reaching to an exfoliated suspension in that high level of viscosity is not possible anymore. As a result, instead of mainly individually depositing of clay platelets parallel to the substrate surface, mass deposition of aggregated clay stacks occur, and an amorphous coating is formed, instead of otherwise oriented and packed LBL assemblies, in lower contents of clay in DIW (Figure 3.3.a) [14].

Also, Figures 3.3b and 3.3c show the LBL assemblies for suspension of 3wt% MMT in DIW, when the content of PEI in DIW increases from 0.1wt% to 10wt%. It can be seen that lower concentration of PEI in DIW can have a decreasing effect on the thickness of their interlayers in LBL assembly, to promote densely pack appearance of resulted coating (Figure 3.3b). On the other hand, very high concentration of PEI in DIW (Figure 3.3c), due to increasing its interlayers thickness, decreases packed order and increases the disparity in the LBL assembly layout, regionally resulting in higher apparent waviness [8].

3.3.3. SEM Results for PEI-MMT LBL Assemblies

In a parallel attempt, similar to TEM images, SEM micrographs show a proper level of orientation for intercalated clay platelets, deposited individually on PEI mortar, forming densely packed nanobrick wall of LBL assemblies. However, in SEM images instead of merely following the same sample trend as of TEM, it was tried to show some other complementary trends in LBL morphology, with the change in the concentration of its ingredients. It should

be mentioned that in dark-field images of SEM, different from bright-field TEM images, clay particles look brighter, and polymer seems darker (Figure 3.4).

With increased clay content in DIW to 3wt% (Figure 3.5.a), no significant change in the oriented and compact layout of LBL assemblies is noticed, except a slight increase in the thickness of clay layers, which might be due to a slight decrease in MMT suspension exfoliation. Hence, a low rise in the number of platelets deposited in each immersion cycle occurs.

Also, the SEM image obtained for a lower amount of PEI in DIW (0.1 wt%) shows a slightly lower thickness of PEI interlayers in the resulted LBL assemblies, while the orientation is kept at a proper level. Again, like for TEM images, in SEM micrographs, cutting of cross-sections with small angles, is another reason for the disparity in the nanobrick structure of LBL assemblies and an apparent thickness, which is typically higher than their actual thickness (Figure 3.5.b) [14].

3.3.4. TEM Results for PETi-MMT LBL Assemblies

TEM images from the cross-section of LBL assemblies made from the solution of 0.5wt% PETi in DIW and 1wt% MMT in DIW, almost similar with those containing PEI, show a decent level of orientation of intercalated clay rows, which along with PETi interlayers, form densely packed nanobrick walls (Figure 3.6). It should be mentioned that there are two separate LBL assemblies observed, where the second one might be a delamination of the LBL under the applied stresses, mainly through cutting, or another LBL assembly that just by coincidence has been dropped beside the first one. In the higher magnification scale of the image (Figure 3.6b)

exfoliated tactoids of clay platelets are clearly observable. When the clay content in DIW is increased to 3 and 5wt%, the oriented LBL assembly is not observable anymore. This amorphous shape of the coating is particularly evident in the latter one, with 5wt% MMT in suspension (Figures 3.7a and 3.7b). On the other hand, with the increase in the PETi content in solution to 10wt%, despite the occurrence of some irregularities, still a moderate level of orientation in the LBL assembly of intercalated clay platelets is observed (Figure 3.7c). To sum up, microscopy results from LBL assemblies including proposed PETi, with random anionic functional incorporations on the backbone of PET, show qualitative similarities with the one made from cationic PEI interlayers.

3.3.5. Quantifying Intercalation of Polymeric Interlayers between Clay Platelets in LBL Assemblies through X-Ray Diffractometry (XRD)

XRD patterns show neat MMT powder exhibiting a peak at 8.37° that corresponds to a basal (001) distance (d_{001}) of 1.056 nm. This value falls correctly in the range reported by other authors for this type of clay [7,8]. In the LBL assemblies, due to intercalation of polymeric chains between clay platelets, the basal planar spacing show some increase, resulting in the shift of the corresponding peak to lower diffraction angles (Figure 3.8).

3.3.5.1. XRD Experiment for PEI-MMT LBL Assemblies

For the LBL assemblies made at constant PEI solutions of 0.1 and 1 wt% in DIW, variations in MMT content in DIW cause significant changes in gallery spacing between clay layers. In fact, at 0.1wt % PEI in DIW, with increasing MMT content in DIW from 1 to 3 wt%, obtained peaks move from 6.73° to 7.07° , resulting interplanar spacing values of 1.312 nm and 1.250nm,

respectively (Figure 3.8.a, Table 3.1). Also, at 1wt% PEI in DIW, increasing MMT content in DIW from 1 to 3wt%, resulted in diffraction peaks at 6.51° and 6.67° , which are corresponding to 1.357nm and 1.323 nm, respectively (Figure 3.8.b, Table 3.1). It means that generally with increase the MMT content in DIW, interplanar spacing shows less increase. Thus, it implies lower intercalation occurred, which may be related to the lower level of exfoliation of MMT in DIW suspension when its content increases [7,8,14].

On the other hand, for the LBL assemblies made from 0.5wt% PEI in solution, when the MMT contents in suspension varies from 0.1wt% to 1, and 3wt%, the corresponding peaks display at 6.43° , 6.38° , and 6.44° , which shows interplanar spacing values of 1.374nm, 1.384nm, and 1.370 nm. The reason for this slight change in interplanar distance with clay content variation at constant content of PEI in solution might reflect the optimized level of 0.5wt% for PEI in DIW, from the point of view of electrostatic interaction and chains motion, for intercalation between clay platelets. In fact, the highest interplanar spacing in the examined range occurs at this level of PEI in DIW. Thus, the applied change in MMT concentration, in the experimented range, does not alter this optimum interplanar spacing significantly [14] (Figure 3.8,c, Table 3.1). In fact, in both mentioned contents of 1 and 3wt% of MMT in suspension, resulted LBL, built from solutions of 0.5wt% PEI in DIW shows the relatively highest interplanar spacings.

This good level of quantitative XRD result for intercalation at 0.5wt% PEI and 1wt% MMT in DIW can be confirmed with corresponding TEM and SEM images that qualitatively showed decent intercalations for LBL assembly of well-oriented clay rows. Also, as it was expected

from the amorphous coating imaged by TEM, the surface of the sample made of 5wt% MMT in DIW was too rough to provide an appropriate XRD peak (Figure 3.3.a).

It should be added that samples made of 10wt% PEI in DIW showed too much surface roughness to give appropriate XRD peaks, confirmed by too much waviness of corresponding TEM images. Also, it should be mentioned that the highest interplanar spacing values reported in this study (above 0.30 nm), are superior to values reported in previous studies on these LBL assemblies, (about 0.20nm) [7,8,14]. It might be related to the higher exfoliation of clay, reached at very high stirring rates, over extended times.

3.3.5.2. XRD Experiment for PETi-MMT LBL Assemblies

Looking at the XRD patterns obtained for LBL assemblies made from the solution of PETi in DIW and suspension of MMT in DIW, significant shifts in diffraction peaks, related to the interlayer spacing of MMT platelets (d_{001}) to lower diffraction angle areas, are observed.

For the LBL assemblies made from solutions with constant PETi content in DIW of 0.5 and 10wt%, with increasing the MMT content in suspension from 0.1 to 1wt%, the diffraction peak of interplanar spacing shifts from 6.12° to 6.51° , and from 6.13° to 6.56° , respectively. Thus, the corresponding interplanar spacing would change from 1.428 nm to 1.357 nm and from 1.442 nm to 1.346 nm, severally. The decreased interplanar spacing with increasing the MMT content can entail the decline in intercalation occurred in the pertaining LBL assemblies. As it was previously explained for PEI-containing LBL assemblies, it might be related to the decreased exfoliation, at the higher content of MMT in suspension (Figure 3.9).

Compared with PEI derived LBL assemblies that showed appropriate XRD peak at 3wt% MMT in DIW, when PETi is used as the macromolecular glue, no appropriate XRD diffraction peak is obtained, due to the significant surface roughness of the prepared samples. It was confirmed by the lack of laminary oriented LBL assemblies at this level of MMT in their TEM images. Thus, when MMT content and its viscosity is higher, PEI is more efficient in attracting their particles in a less aggregated way and oriented parallel to the substrate surface. Nevertheless, then PETi might promote wider gallery spaces between (deposited) clay platelets when MMT% in DIW is low. Therefore, it might be conjectured that since negative ions on PETi mainly attract the positively-charged edges of clay platelets, rather than their negatively charged surfaces, initially clay platelets approach the substrate surface with their edge sides. Then, gradually as a combinative result of clay interaction with PETi chains, and the effect of the center of gravity of high aspect ratio clay platelets, they tend to lie down horizontally on the substrate surface. So, when the clay concentration is relatively low (e.g. 0.1 or 1wt% in DIW), possibly there is enough vacant space around each deposited clay platelet, letting it lie down parallel to the surface. On the other hand, when the clay content is high (e.g. 3 or 5 wt% in DIW), the numerous adjacent clay platelets deposited probably impede the laminar lying down of each other, to form a rather angled orientation of clay platelets on the substrate.

In addition, wider galleries between clay platelets developed by PETi intercalated chains, when the clay concentration is relatively low (0.1wt%), might be due to the repulsion between negative charges on both intercalated mobile chain segments of PETi between clay galleries and clay platelets surfaces.

Also, with a change in PETi content at DIW, while MMT content in DIW is kept constant at 0.1 and 1wt%, respectively, interplanar spacings show no significant variation. So, in the PETi content range of 0.5 to 10wt % in DIW, mainly MMT% is the determining factor for obtained level of intercalation in resulted LBL assemblies. Therefore, PETi in this content range in DIW shows a really good level of intercalation between clay platelets, significantly better than its alternative, PEI.

3.3.6. Transport Properties in LBL Assemblies

Results of oxygen permeation experiments at room temperature for LBL assemblies from either of polyelectrolytes, PEI or PETi, (0.5wt% in DIW) for a range of different contents of clay in suspension are displayed. In addition, the term barrier improvement factor can be used to show clearer the efficiency of LBL coatings in improving barrier properties of polymeric substrates (Equation 3.2, Figure 3.10)

$$\text{Barrier Improvement Factor (BIF)} = \frac{\text{Permeation rate of neat polymer film}}{\text{Permeation rate of coated polymer}} \quad (2)$$

Considering only five bilayer deposition cycles and hydrophobic nature of the substrate polymer, reaching to around 500 times barrier improvement (for LBL assemblies containing PEI interlayers), may look impressive. In fact, the group of following reasons may be responsible for achieving these results. First, intensive stirring of clay suspensions over extended times promotes their intercalation and exfoliations. Then, deposition of clay platelets parallel to the substrate baseline and intercalation of polyelectrolyte chains between their galleries may provide tortuous nanobrick walls against the transport of permeant species, to increase their diffusion path dramatically. In addition, the effect of plasma treatment for

improving the interaction of otherwise hydrophobic polymeric substrate and LBL coating should not be overlooked.

For both LBL coatings, with increasing the concentration of clay in suspension, gradually their efficiency for improving barrier resistance against oxygen decrease, which can be related to decreasing the exfoliation level of clay in DIW and increase in its viscosity. However, two LBL assemblies show deviations in their performance results. Although in the similar combinations of 1wt% MMT in DIW and 0.5wt% polyelectrolyte in DIW for either PEI or PETi, both LBL assemblies show close barrier improvement results against O₂, with increase in content of MMT in DIW from 0.1wt% to 3wt%, PETi-containing coatings show less steep decrease in oxygen permeation, followed by an increasing trend, with further increase in MMT content in DIW of up to 5wt%. These results show the relatively higher efficiency of PEI as an interlayer to interact with clay particles for making lamellarly oriented and exfoliated LBL assemblies when the initial concentration of clay and its viscosity are higher. This confirms the morphological results already discussed. On the other hand, for LBL assemblies made from thinner suspensions of MMT in DIW (0.1wt%), PETi-containing coatings show relatively higher barrier improvement, which may perhaps be related to their aforementioned higher intercalations, promoted by the repulsion between evenly charged clay platelets surfaces and intercalated mobile segments of PETi molecular chains.

3.4. Proposed Mechanism of Deposition for PETi-Containing LBL Assemblies

Based on morphological investigation and barrier properties of LBL assemblies formed with PETi interlayers it is postulated that clay platelets already intercalated and exfoliated in

water are attracted from their positively-charged edges, by the negative charges on PETi backbone. Thus, possibly they approach and deposit on the substrate in tilted or sometimes perpendicular directions (Figures 3.11a, 3.11b), relative to the previous assemblies, containing the positively-charged PEI layers, where MMT platelets were mainly deposited parallel to the substrate. However, probably as a result of diffusion of PETi chains segments between clay platelets galleries, and effect of the center of gravity of clay platelets with high aspect-ratios, they gradually lie down almost horizontally to the substrate surface (Figures 3.11c, 3.11e). The horizontal layout of deposited clay platelets on the substrate surface is promoted when their number is few, leaving free side space for them to lie down. This condition may perhaps occur when the clay concentration in DIW is low enough (e.g. 1wt% or lower). As mentioned before TEM images from their cross-section demonstrated this laminar oriented layout of their LBL assemblies.

On the other hand, when clay concentration in DIW is high, the number of clay platelets deposited is large. Thus, the horizontal lying down of deposited clay platelets is impeded by the existence of the other adjacent clay platelets deposited close to them (Figures 3.11d, 3.11f). As TEM images showed, when clay content in DIW increases, a significant decrease in clay laminar orientation occurs. These results were confirmed by occurring layoff in their barrier improvement.

3.5. Conclusions

Cumulative results of TEM, SEM, XRD, and permeation measurements done for LBL coatings made of two alternative types of macromolecular glues of PEI and PETi, with MMT,

demonstrated the formation of tortuous networks of galleries formed between intercalated layers of high aspect ratio clay platelet layers, oriented parallel to the polymeric substrate surface line. Thus, through increasing the permeant path distance, the barrier properties of resulted coated membrane against gases increased significantly.

In fact, reaching to BIF of around 500 times against O₂ for only 5 times immersion in clay suspension, for hydrophobic polystyrene-based polymers is a record that has never been reported before. It can be related to various reasons including, high level of clay exfoliation reached by high stirring rates over extended times, efficient performance of the polyelectrolyte, both for attracting clay platelets to the substrate and then for intercalating appropriately between their layers to make an oriented and intercalated LBL assembly. Also, the effect of plasma treatment for attaching the LBL firmly to the polymeric substrate, should not be overlooked.

Both TEM and XRD results showed that with increasing the content of MMT in DIW, orientation and intercalation of resulted assemblies decreased, possibly due to the lack of exfoliation in their highly viscous suspensions. Similarly, permeability values leveled out with the increase in MMT in DIW, between 3-5wt%. Similarly, increasing polymer interlayer content in DIW, above a limiting point resulted in the negative effect on orientation and intercalation of LBL assemblies, which is more significant for LBL assemblies built from PEI interlayers.

To sum up, from the point of view of making more oriented and regular LBL assemblies to provide higher barrier improvements, PEI worked more efficiently for higher content of clay

in suspension, with higher viscosity. This variation may root back in the difference between charges on PEI and PETi chains. In fact, different from the cationic PEI, which adsorb clay platelets from their negatively charged surfaces, anionic PETi mainly attracts positively-charged edges of platelets. Thus, in the case of PETi interlayers, for high contents of clay in suspensions, clay platelets initially landed in a tilted direction cannot lie down horizontally, since they are surrounded by many other depositing clay platelets, resulting in a tilted layout of LBL, with inferior barrier improvements. On the other hand, PETi showed better intercalation and barrier improvement, when dilute suspensions of clay were used. It might be a side effect of repulsion between even charges on clay platelets surfaces and intercalated PETi chains in galleries between platelets to promote LBL assemblies tortuosity.

Tables

Table 3.1. Interplanar spacings of 001 crystallographic planes in clay and location of their corresponding diffraction angle peaks for neat Na⁺MMT and its 30BL assemblies with PEI, for corresponding contents of PEI and MMT in DIW.

Material	Diffraction Angle 2θ (°)	Interplanar spacing (nm)
Na ⁺ MMT	8.370	1.056
LBL(0.1wt%PEI,1wt%MMT)	6.730	1.312
LBL(0.1wt%PEI,3wt%MMT)	7.065	1.250
LBL(0.5wt%PEI,0.1wt%MMT)	6.427	1.374
LBL(0.5wt%PEI,1wt%MMT)	6.380	1.384
LBL(0.5wt%PEI,3wt%MMT)	6.445	1.370
LBL(1wt%PEI,1wt%MMT)	6.510	1.357
LBL(1wt%PEI,3wt%MMT)	6.673	1.323

Table 3.2. Interplanar spacings of 001 crystallographic planes in clay and location of their corresponding diffraction angle peaks for neat Na⁺MMT and its 30BL assemblies with PETi, for corresponding contents of PETi and MMT in DIW.

Material	Diffraction Angle 2θ (°)	Interplanar spacing (nm)
Na ⁺ MMT	8.37	1.056
LBL(0.5wt%PETi,0.1wt%MMT)	6.119	1.428
LBL(0.5wt%PETi,1wt%MMT)	6.511	1.357
LBL(10wt%PETi,0.1wt%MMT)	6.129	1.442
LBL(10wt%PETi,1wt%MMT)	6.562	1.346

Figures

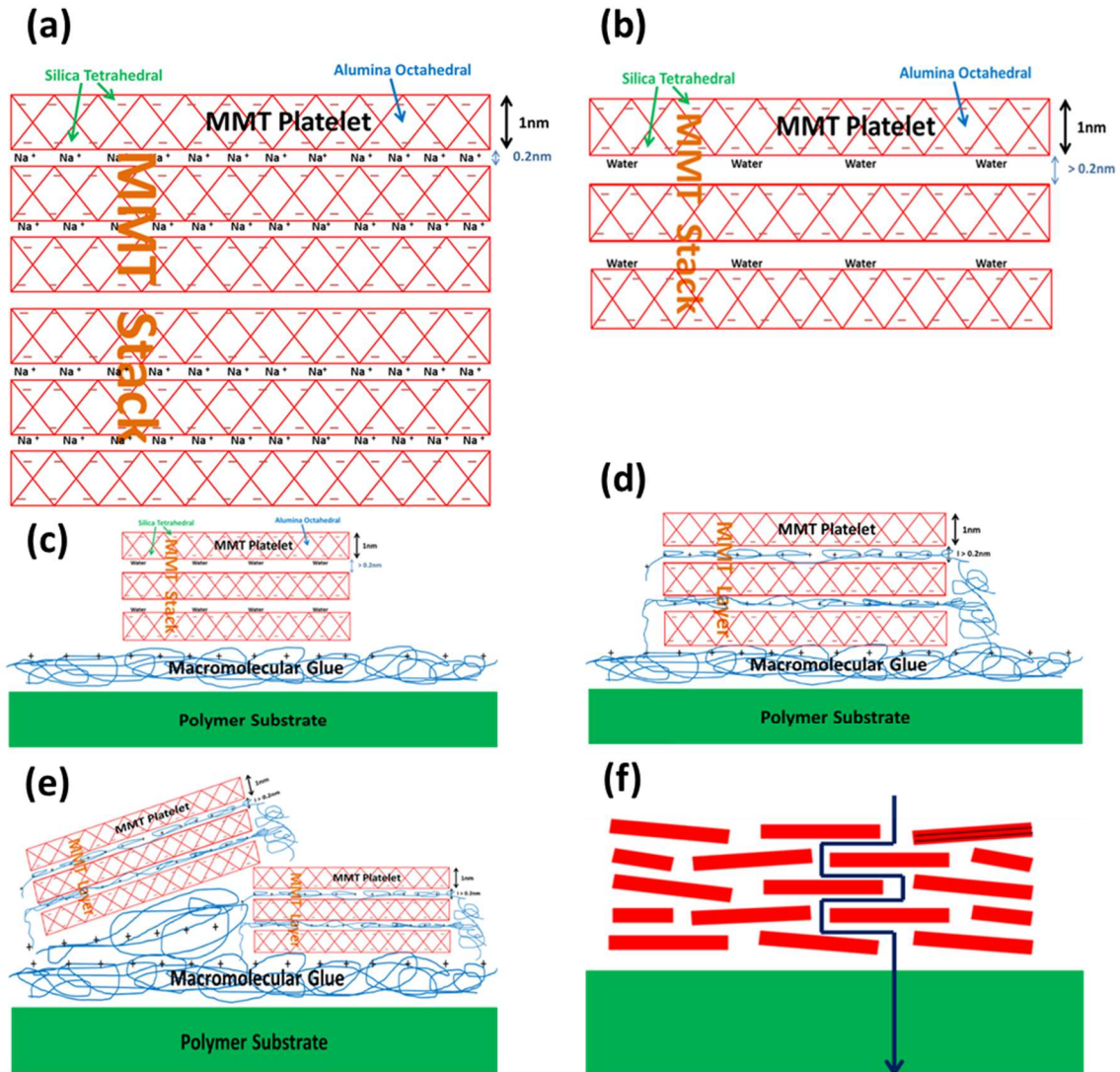


Figure 3.1. (a) Neat MMT (stack), where exchangeable Na⁺ cations keep MMT platelets close to each other (0.2nm) in agglomerated stacks. (b) Exfoliated MMT in DIW, where only a few MMT platelets are in parallel order close to each other (almost stack) and water molecules diffuse in the space between platelets, negatively charged on the surface, and increases the size of d (basal planar spacing). (c) Deposition of negatively charged MMT layers, in DIW media, on the substrate film, already coated by positively-charged PE. (d,e) Intercalation of positively-charged PE chains in between negatively charged MMT platelets in a layer. (f) LBL deposited assemblies, with increased tortuosity in their nanobrick wall structure, and schematic of the tortuous path made in LBL assemblies against permeant molecules.

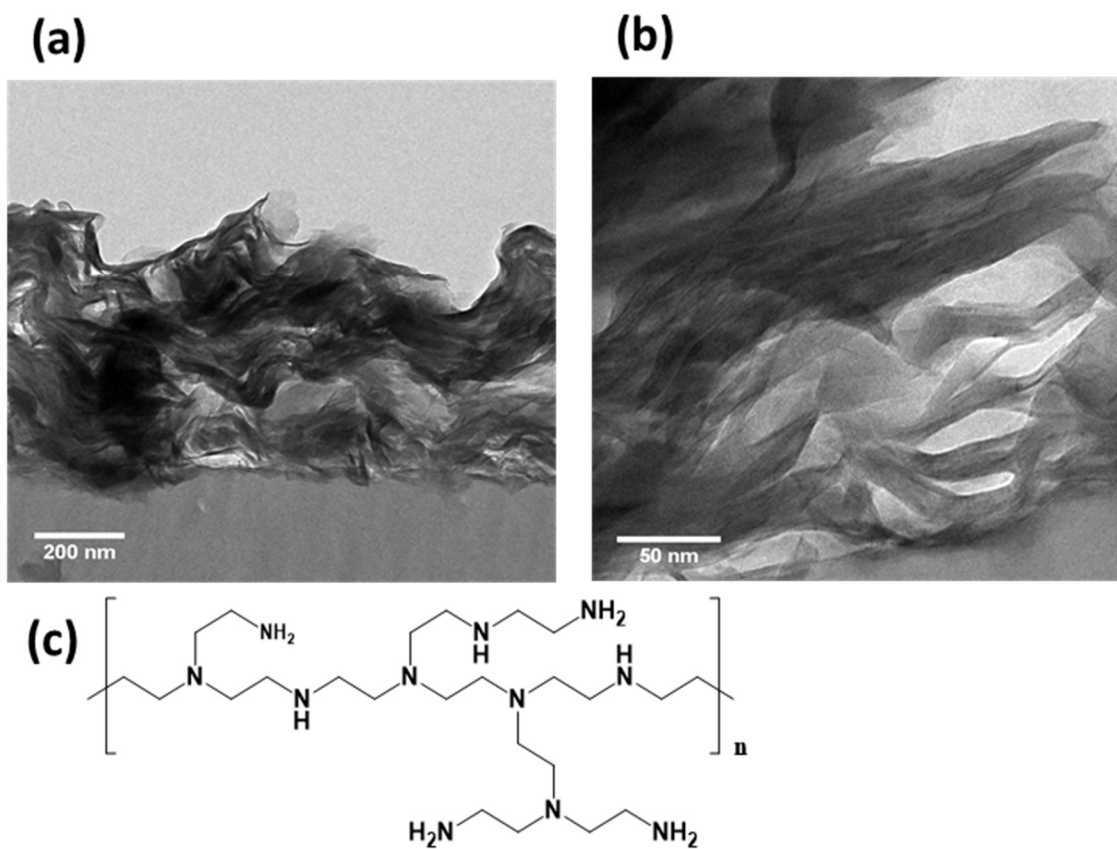


Figure 3.2. Cross-sectional image of 30-bilayer assemblies made from PEI solution (0.5wt%) and MMT suspension (1wt%), respectively, in different magnification scales, of (a)10,000X, (b)40,000X.(c) structural representation of branched PEI.

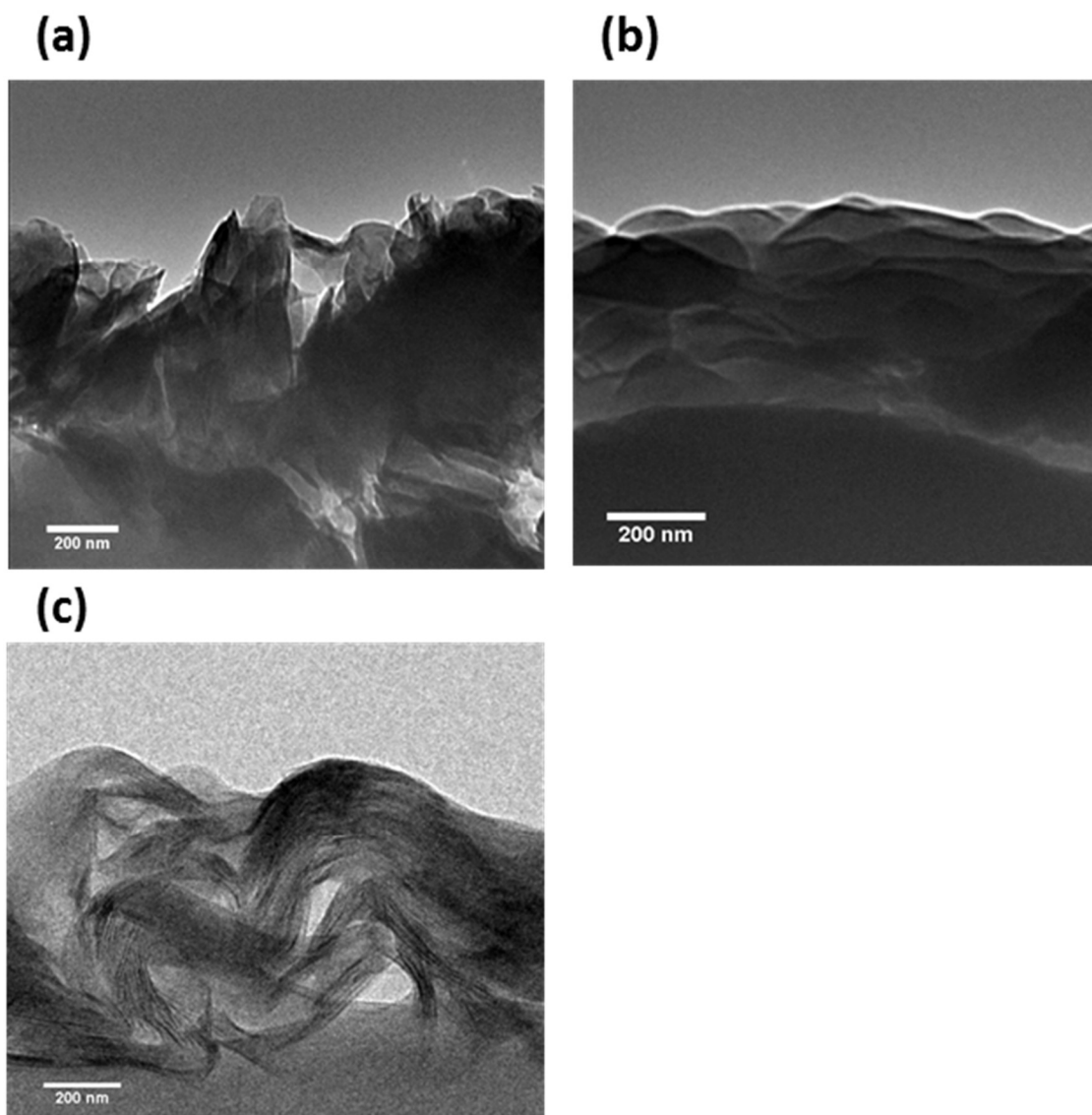


Figure 3.3. Cross-sectional image of 30-bilayer assemblies made from PEI solution and MMT suspension of (a) 0.5wt% and 5wt%, (b) 0.1wt% and 3wt%, (c) 10wt% and 3wt%, respectively.

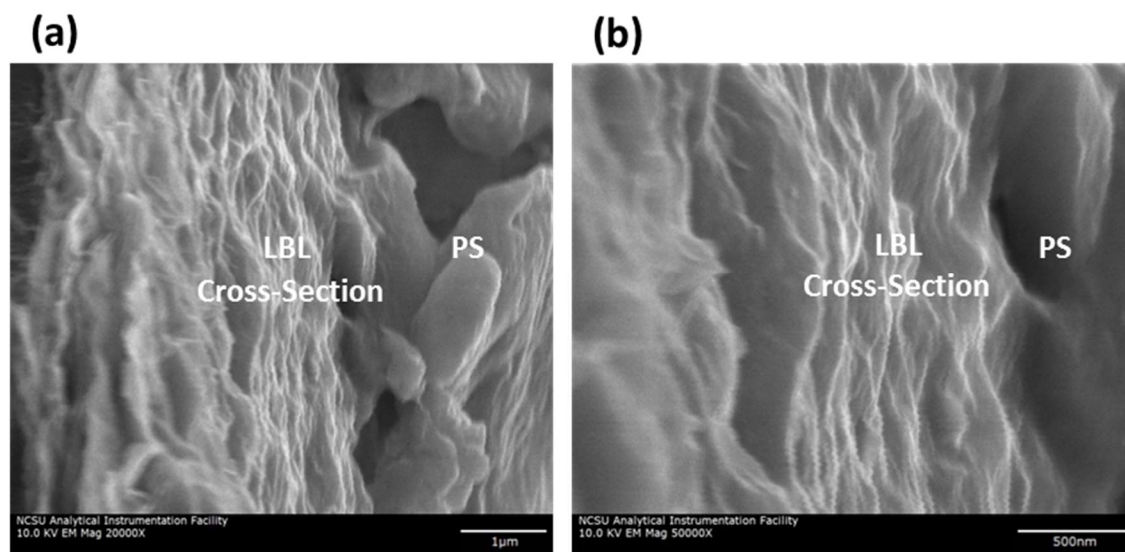


Figure 3.4. Cross-sectional images of 20-bilayer assemblies made from PEI solution (0.5wt%) and MMT suspension (1wt%), respectively, in two different magnification scales of (a) 20,000X and (b) 50,000X. The gray sides on the right are PS substrate.

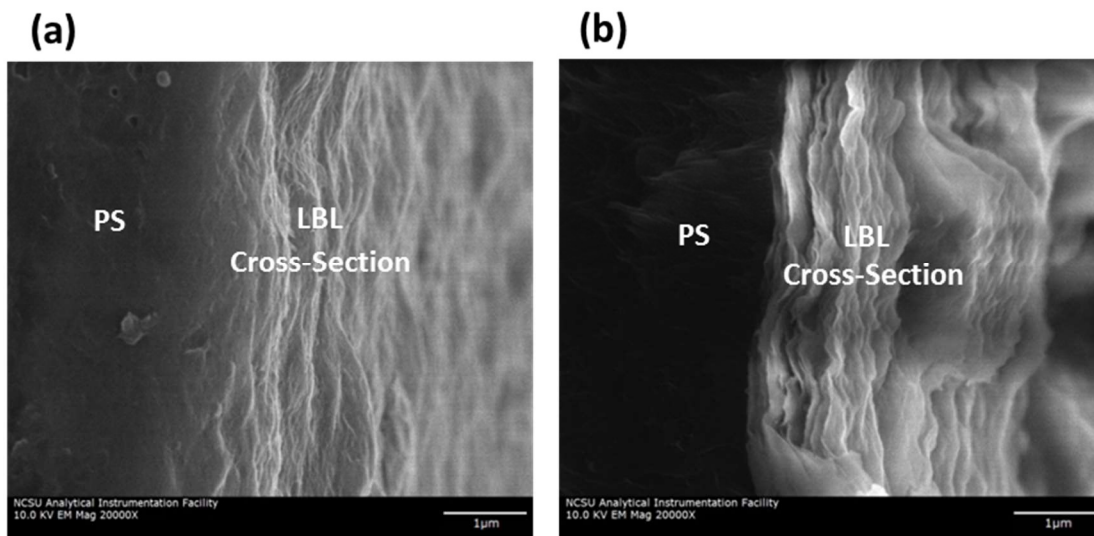


Figure 3.5. Cross-sectional image of 20-bilayer assemblies made from PEI solution and MMT suspension of (a) 0.5wt% and 3wt% (b) 0.1wt% and 1wt%, respectively. The left dark side is PS substrate.

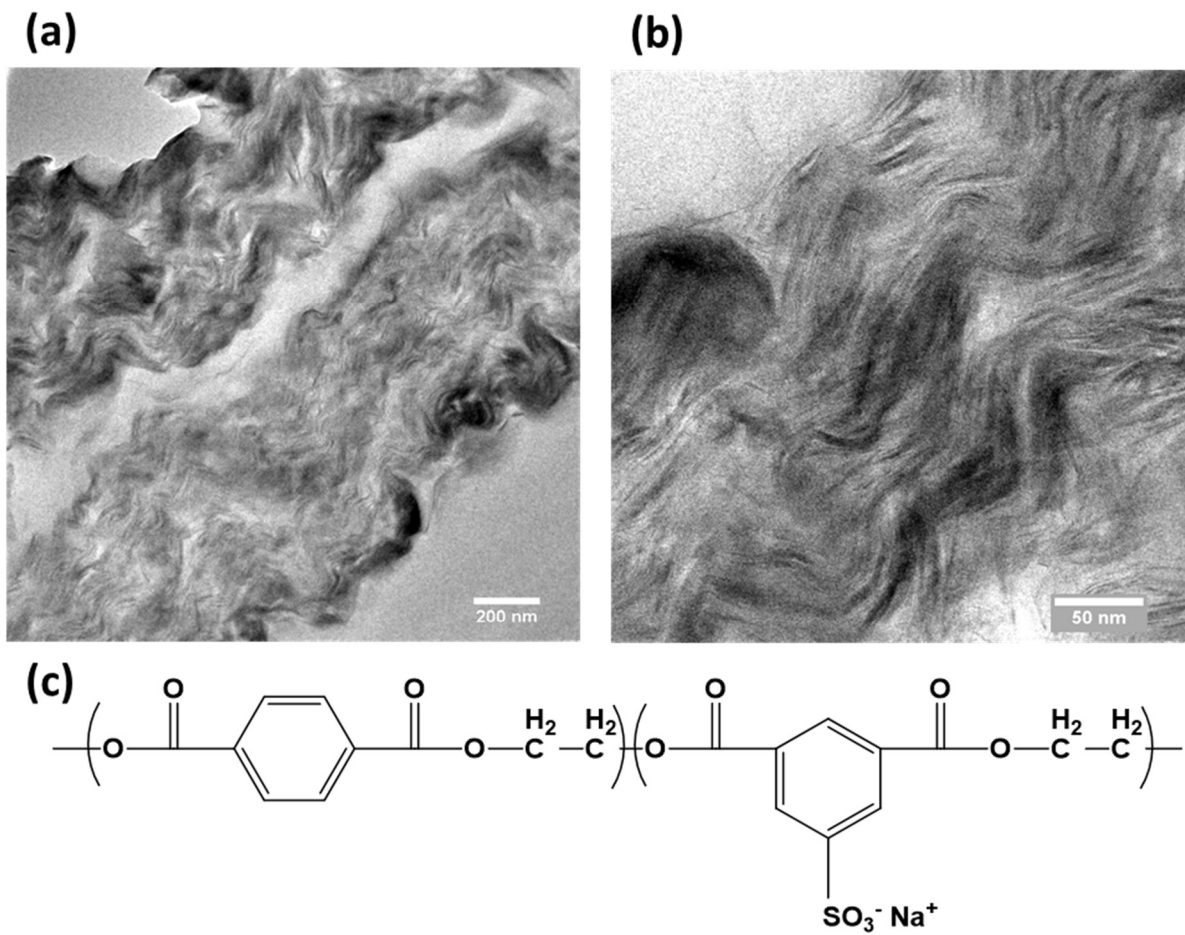


Figure 3.6. (a), (b) Cross-sectional images of 30-bilayer assemblies made from PETi solution (0.5wt%) and MMT suspension (1wt%), respectively, at two different magnification scales. (c) The chemical representation of PETi.

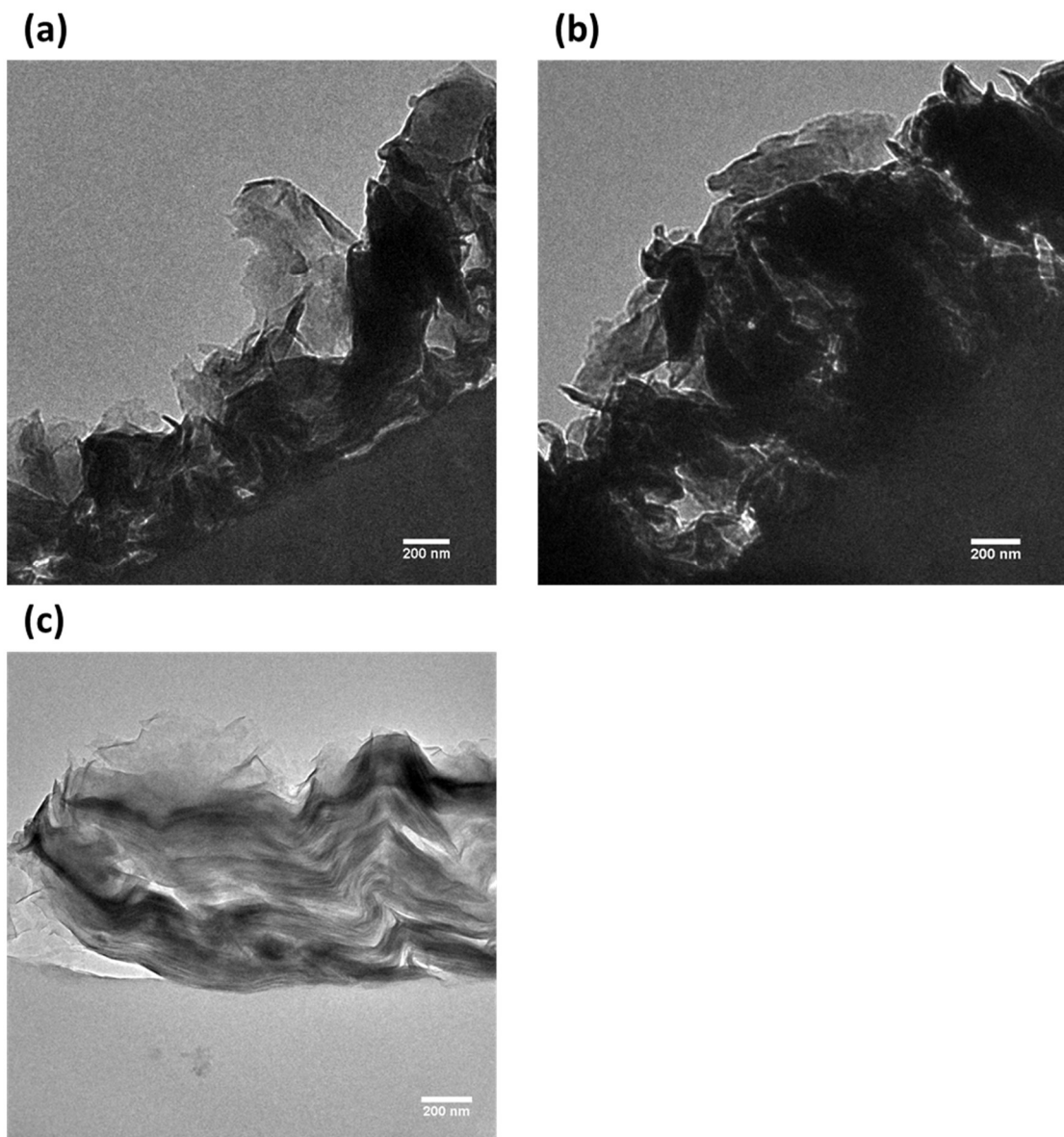


Figure 3.7. Cross-sectional images of 30-bilayer assemblies made from PETi solution and MMT suspension of (a) 0.5wt% and 3wt%, (b) 0.5wt% and 5wt%, and (c) 10wt% and 1wt%, respectively.

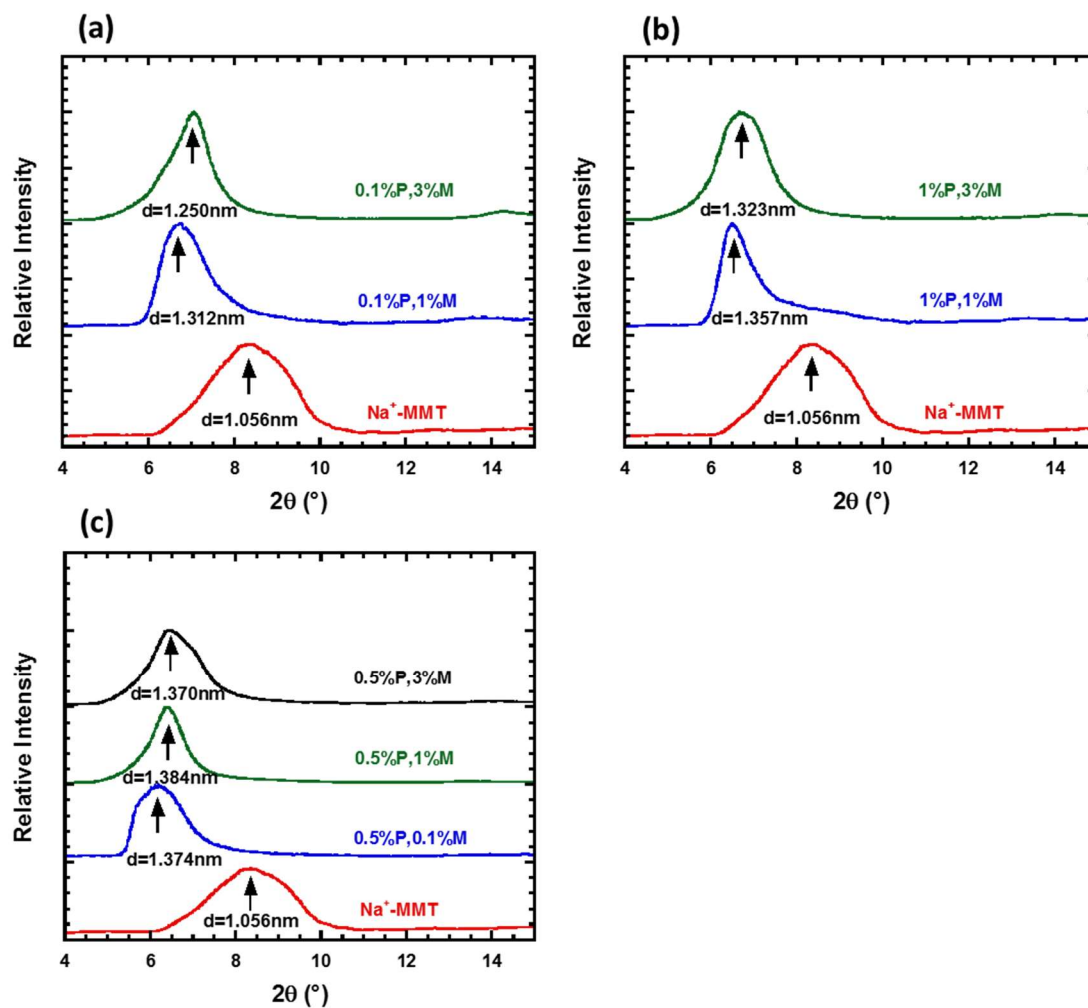


Figure 3.8. XRD patterns for neat Na⁺MMT and 30-BL films made from varying MMT content in suspension of 0.1, 1, and 3 wt%, for constant (a) 0.1wt%, (b) 1wt%, and (c) 0.5wt% PEI solution in DIW.

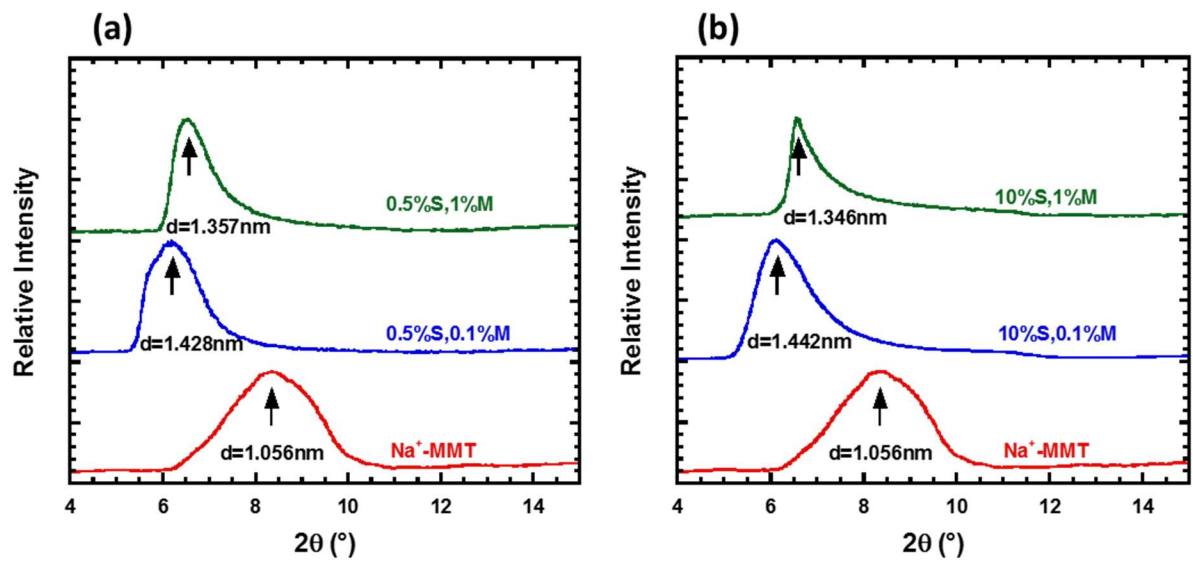


Figure 3.9. XRD patterns for neat Na⁺-MMT and 30-BL films made from varying MMT content in suspension of 0.1 and 1wt% for constant (a) 0.5wt% and (b) 10wt% PETi(S) solution in DIW.

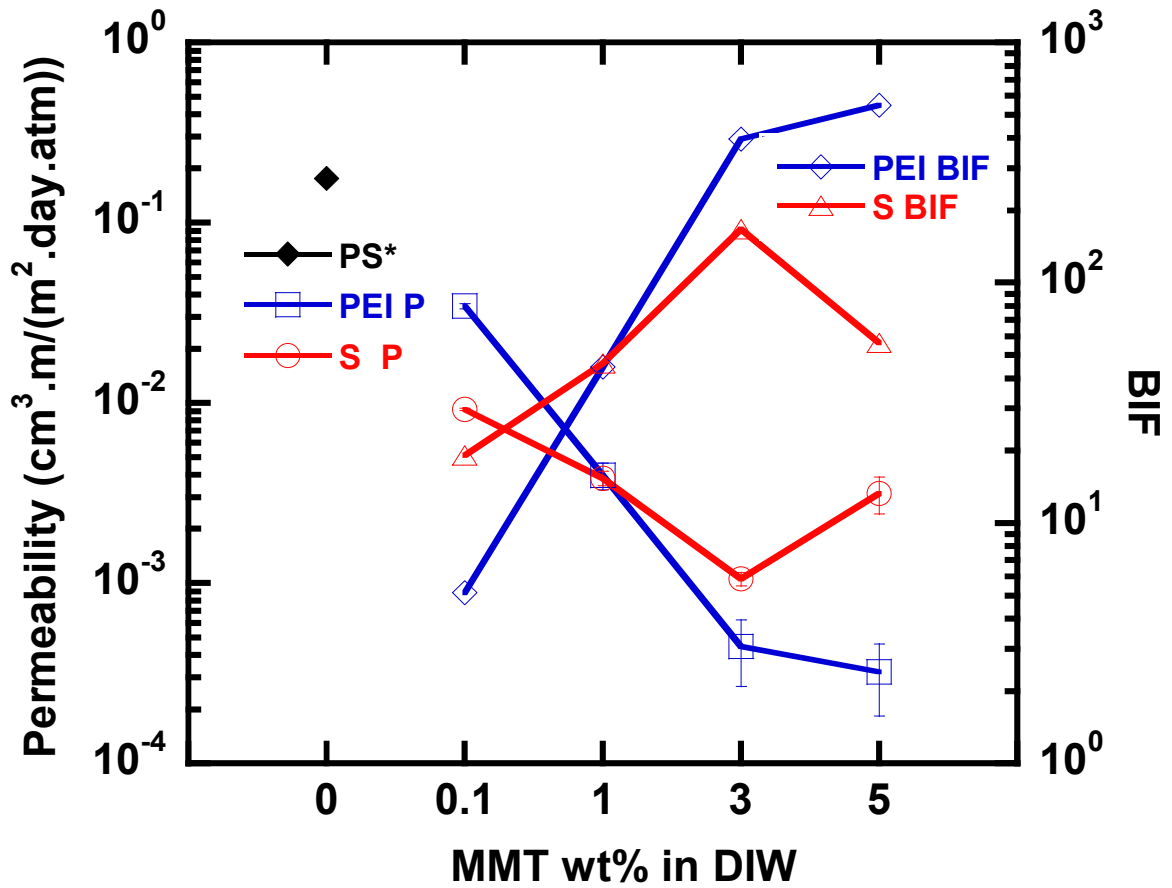


Figure 3.10. A comparison of oxygen permeability and BIF values, for 5 times deposition of two type of BL coatings, containing interlayers of PEI and PETi (S) (both 0.5wt% in DIW), when the clay concentration varies from 0.1wt% to 5wt% in its suspensions. Lines are guides for eyes.

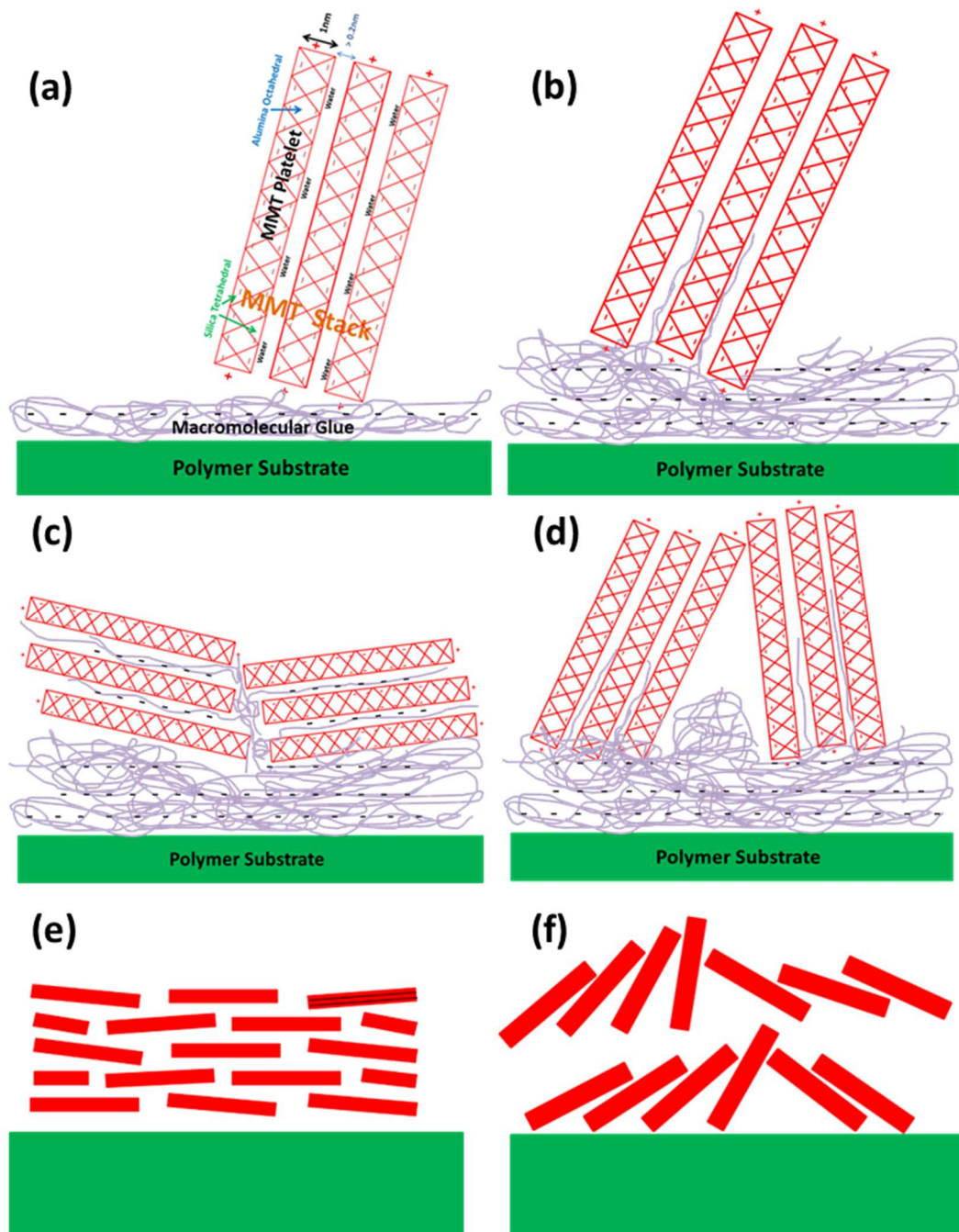


Figure 3.11. (a) Deposition of MMT layers, with positive charges on their edges, on a substrate film, already coated by negatively charged PE. (b) The intercalation of mobile chain segment of PE between clay galleries. (c,e) Laminar layout and (d,f) tilted layout of deposited clay platelets, in low and high concentrations of MMT in its suspensions, respectively.

References

- [1] W.-S. Jang, I. Rawson, J.C. Grunlan, Layer-by-layer assembly of thin film oxygen barrier, *Thin Solid Films*. 516 (2008) 4819–4825.
- [2] J. Lewis, Material challenge for flexible organic devices, *Mater. Today*. 9 (2006) 38–45.
- [3] J. Jiang, M. Benter, R. Taboryski, K. Bechgaard, Oxygen barrier coating deposited by novel plasma-enhanced chemical vapor deposition, *J. Appl. Polym. Sci.* 115 (2010) 2767–2772.
- [4] A.P. Roberts, B.M. Henry, A.P. Sutton, C.R.M. Grovenor, G.A.D. Briggs, T. Miyamoto, et al., Gas permeation in silicon-oxide/polymer (SiO_x/PET) barrier films: role of the oxide lattice, nano-defects and macro-defects, *J. Memb. Sci.* 208 (2002) 75–88.
- [5] H.Y. Low, Y. Xu, Moisture barrier of Al_xO_y coating on poly(ethylene terephthalate), poly(ethylene naphthalate) and poly(carbonate) substrates, *Appl. Surf. Sci.* 250 (2005) 135–145.
- [6] Y. Leterrier, Durability of nanosized oxygen-barrier coatings on polymers, *Prog. Mater. Sci.* 48 (2003) 1–55.
- [7] Y.-H. Yang, F.A. Malek, J.C. Grunlan, Influence of deposition time on layer-by-layer growth of clay-based thin films, *Ind. Eng. Chem. Res.* 49 (2010) 8501–8509.
- [8] M.A. Priolo, D. Gamboa, J.C. Grunlan, Transparent clay-polymer nano brick wall assemblies with tailorable oxygen barrier, *ACS Appl. Mater. Interfaces*. 2 (2010) 312–320.
- [9] N. Cini, T. Tulun, G. Decher, V. Ball, Step-by-step assembly of self-patterning polyelectrolyte films violating (almost) all rules of layer-by-layer deposition, *J. Am. Chem. Soc.* 132 (2010) 8264–8265.
- [10] P.T. Hammond, Form and function in multilayer assembly: New applications at the nanoscale, *Adv. Mater.* 16 (2004) 1271–1293.
- [11] X. Zhang, H. Chen, H. Zhang, Layer-by-layer assembly: from conventional to unconventional methods, *Chem. Commun.* (2007) 1395–1405.
- [12] O. Shchepelina, I. Drachuk, M.K. Gupta, J. Lin, V. V Tsukruk, Silk on Silk Layer by Layer Microcapsules, *Adv. Mater.* 23 (2011) 4655–4660.

- [13] Y.-H. Yang, L. Bolling, M. Haile, J.C. Grunlan, Improving oxygen barrier and reducing moisture sensitivity of weak polyelectrolyte multilayer thin films with crosslinking, *RSC Adv.* (2012) 12355–12363.
- [14] M.A. Priolo, K.M. Holder, D. Gamboa, J.C. Grunlan, Influence of clay concentration on the gas barrier of clay–polymer nanobrick wall thin film assemblies, *Langmuir.* 27 (2011) 12106–12114.
- [15] Y. Yang, M. Haile, A. Malek, J.C. Grunlan, Super Gas Barrier of All-Polymer Layer-by-Layer Assemblies, *Acs Spring* 2011. 1 (2011) 156–157.
- [16] G. Decher, Layer-by-Layer Assembly, in: G. Decher, J.B. Schlenoff (Eds.), *Multilayer Thin Film.*, Willey-VCH, Weinheim, Germany, 2012: pp. 1–22.
- [17] I. Soltani, M.E. Zeynali, A.A. Yousefi, Toughening of glass fiber reinforced Nylon 66 with EPDM-MAH: Dynamic mechanical, rheological, and morphological investigations, *E-Polymers.* (2012) 1–14.
- [18] M.E. Zeynali, A. A. Yousefi, I. Soltani, Effects of Malienated Ethylene Propylene Diene Monomer (EPDM) Rubber on Dynamic-Mechanical and Rheological Properties of Polyamide 66 (PA 66) Composites, *Polym. Plast. Technol. Eng.* 48 (2008) 42–47.
- [19] M.A. Priolo, D. Gamboa, K.M. Holder, J.C. Grunlan, Super gas barrier of transparent polymer– clay multilayer ultrathin films, *Nano Lett.* 10 (2010) 4970–4974.
- [20] M. Dhayal, M.R. Alexander, J.W. Bradley, The surface chemistry resulting from low-pressure plasma treatment of polystyrene: The effect of residual vessel bound oxygen, *Appl. Surf. Sci.* 252 (2006) 7957–7963.
- [21] C. Chaiwong, P. Rachtanapun, P. Wongchaiya, R. Auras, D. Boonyawan, Effect of plasma treatment on hydrophobicity and barrier property of polylactic acid, *Surf. Coatings Technol.* 204 (2010) 2933–2939.
- [22] I. Beaulieu, M. Geissler, J. Mauzeroll, Oxygen plasma treatment of polystyrene and zeonor: Substrates for adhesion of patterned cells, *Langmuir.* 25 (2009) 7169–7176.
- [23] E. Bonaccorso, K. Graf, Nanostructuring effect of plasma and solvent treatment on polystyrene, *Langmuir.* 20 (2004) 11183–11190.
- [24] A.E. Özçam, *Surface Modification and Characterization of Polymeric Materials for Targeted Functionality*, North Carolina State University, 2011.
- [25] G.W. Beall, C.E. Powell, *Fundamentals of Polymer-Clay Nanocomposites*, 1st ed., Cambridge University Press, Cambridge, UK, 2011.

- [26] A. Ammala, C. Bell, K. Dean, Poly (ethylene terephthalate) clay nanocomposites: improved dispersion based on an aqueous ionomer, *Compos. Sci. Technol.* 68 (2008) 1328–1337.
- [27] M. Pluta, A. Galeski, M. Alexandre, M. a. Paul, P. Dubois, Polylactide/montmorillonite nanocomposites and microcomposites prepared by melt blending: Structure and some physical properties, *J. Appl. Polym. Sci.* 86 (2002) 1497–1506.
- [28] M.N. Muralidharan, S.A. Kumar, S. Thomas, Morphology and transport characteristics of poly(ethylene-co-vinyl acetate)/clay nanocomposites, *J. Memb. Sci.* 315 (2008) 147–154.
- [29] S. Guruvenket, G.M. Rao, M. Komath, A.M. Raichur, Plasma surface modification of polystyrene and polyethylene, *Appl. Surf. Sci.* 236 (2004) 278–284.
- [30] A. Ghanbari, M.-C.C. Heuzey, P.J. Carreau, M.-T.T. Ton-That, Morphology and properties of polymer/organoclay nanocomposites based on poly(ethylene terephthalate) and sulfopolyester blends, *Polym. Int.* 62 (2013) 439–448.
- [31] X.F. Xu, A. Ghanbari, W. Leelapornpisit, M.C. Heuzey, P. Carreau, Effect of Ionomer on Barrier and Mechanical Properties of PET/Organoclay Nanocomposites Prepared by Melt Compounding, *Int. Polym. Process.* 26 (2011) 444–455.
- [32] D. Wang, C. Wilkie, In-situ reactive blending to prepare polystyrene–clay and polypropylene–clay nanocomposites, *Polym. Degrad. Stab.* 80 (2003) 171–182.
- [33] D.J. Frankowski, S. a. Khan, R.J. Spontak, Chain-scission-induced intercalation as a facile route to polymer nanocomposites, *Adv. Mater.* 19 (2007) 1286–1290.
- [34] D.J. Frankowski, M.D. Capracotta, J.D. Martin, S. a. Khan, R.J. Spontak, Stability of organically modified montmorillonites and their polystyrene nanocomposites after prolonged thermal treatment, *Chem. Mater.* 19 (2007) 2757–2767.
- [35] C.A. Wilson, J.A. McCormick, A.S. Cavanagh, D.N. Goldstein, A.W. Weimer, S.M. George, Tungsten atomic layer deposition on polymers, *Thin Solid Films.* 516 (2008) 6175–6185.
- [36] P.F. Carcia, R.S. McLean, M.H. Reilly, Permeation measurements and modeling of highly defective Al₂O₃ thin films grown by atomic layer deposition on polymers, *Appl. Phys. Lett.* 97 (2010) 221901–221903.
- [37] X. Hu, J. Tang, A. Blasig, Y. Shen, M. Radosz, CO₂ permeability, diffusivity and solubility in polyethylene glycol-grafted polyionic membranes and their CO₂ selectivity relative to methane and nitrogen, *J. Memb. Sci.* 281 (2006) 130–138.

- [38] N.P. Patel, A.C. Miller, R.J. Spontak, Highly CO₂-Permeable and Selective Polymer Nanocomposite Membranes, *Adv. Mater.* 15 (2003) 729–733.
- [39] D.R. Paul, L.M. Robeson, Polymer nanotechnology: Nanocomposites, *Polymer* 49 (2008) 3187–3204.

CHAPTER 4

Effect of Polyelectrolyte on the Barrier Properties of Layer-by-Layer Nanoclay Coatings

Abstract

The development of effective barrier materials is becoming increasingly important, particularly as microelectronic devices and food supplies must be protected for extended periods of time from atmospheric gases and water vapor. One of the most effective, facile, eco-friendly, and inexpensive strategies introduced in this spirit is the sequential buildup of layer-by-layer (LBL) surface coatings. This technology relies on the repeated, alternating deposition of impermeable nanoclay platelets possessing a large diameter-to-thickness aspect ratio and a polyelectrolyte adhesive. Previous studies have focused extensively on the use of polycations for this purpose since they are attracted by the negative charges inherently present on the face of natural nanoclays, such as montmorillonite (MMT). In this work, we compare the barrier properties of LBL coatings prepared with a common polycation and a polyester-based polyanion, which selectively interacts with the positive charges that accumulate on the edges of nanoclay platelets. Deposition of these coatings on a hydrophobic styrenic copolymer is reported here to promote dramatic reductions in the measured permeabilities of oxygen and carbon dioxide. This study, which systematically explores the dependence of single-gas permeability on factors such as MMT suspension concentration, bilayer (BL) coating number and temperature, aims to expand the understanding and utility of LBL coatings.

Keywords: Barrier, LBL assembly, nanocomposite, packaging, multilayer coating

4.1. Introduction

Despite their generally low cost, weight and expense, polymers frequently employed to meet the demands of the packaging industry possess barrier properties that remain unacceptably low and vastly inferior to their inorganic counterparts [1,2]. For this reason, hybrid material and multistep processing strategies [3–5], resulting in single/multiple surface coatings and bulk nanocomposite formulations, have been introduced in response to this growing need especially in the microelectronics, biomedical and food packaging industries. According to recent assessments [6], the global worth of flexible packaging is projected to reach \$293 billion by 2022, and the largest share of global packaging consumption is expected to involve food and beverages (it accounted for 80% in 2014). Single surface coatings on polymer substrates can be achieved by chemical vapor deposition [2] and atomic layer deposition [4,5,7], respectively, whereas nanocomposites rely on the dispersion of nanoscale objects in a polymer matrix [8–10]. While thin solid coatings generally provide the greatest barrier efficacy (by reducing permeability by several orders of magnitude), they require specialized chemical precursors and deposition chambers, and they are prone to defects and cracking [11–14]. In contrast, the incorporation of nanoclay in polymer nanocomposites is much less effective at decreasing gas permeability, but tends to augment mechanical properties such as modulus and toughness [8,10,15–17]. Among the tactics proposed for enhancing the barrier performance of polymer substrates, layer-by-layer (LBL) coatings [18–25] have emerged as one of the most facile, inexpensive, eco-friendly, and effective multilayer approaches capable of providing significant barrier improvement.

To be effective, LBL coatings require electrostatic attraction between a polyelectrolyte and

an oppositely charged, impermeable nanoparticle [25]. Repeated alternating deposition of these constituents results in a loosely arranged "brick and mortar" nanolaminate morphology, illustrated in **Figure 4.1**. Because of their disk-like shape with a generally high diameter-to-thickness aspect ratio, natural nanoclays, such as montmorillonite (MMT), with a negative charge on each platelet face are commonly utilized in LBL coatings. As a consequence, most of the polyelectrolytes reported thus far are polycations, such as polyethyleneimine (PEI), which can complex with the platelets and thereby stabilize the coating. Such coatings exhibit remarkable barrier properties, with reductions in O₂ permeability of over 3 orders of magnitude reported [26] for LBL coatings composed of 24 bilayers (where *bilayer*, BL, refers to one polyelectrolyte layer and an adjacent nanoclay layer). Most commercial polymers employed in packaging are inherently hydrophobic, in which case their surfaces are often modified by different treatment methods (e.g., O₂ plasma, coronal discharge, ultraviolet ozone, and chemical reactions) to introduce polar moieties and improve surface wettability [20,27,28]. Although the barrier properties of LBL coatings have been the subject of numerous studies (primarily focusing on O₂ permeation), the present work aims to extend the current understanding of such coatings by investigating the effect of temperature on both O₂ and CO₂ permeation. In addition, the barrier efficacy of a polyanion that can complex with the positive charges that accumulate on the edges of MMT platelets [29–31] is examined and quantitatively compared with that of PEI.

4.2. Experimental

4.2.1. Materials

A polystyrene (PS) homopolymer with a number-average molecular weight (\bar{M}_n) of 100 kDa and a polydispersity index (PDI) of 1.01 was synthesized by living anionic polymerization (Dr. S. D. Smith of the Procter & Gamble Co.) and was utilized as the substrate for LBL coatings in transmission electron microscopy (TEM) images due to ease of sectioning at ambient temperature. A commercial random poly(styrene-*co*-butadiene) (SB) copolymer ($\bar{M}_n = 95.4$ kDa and PDI = 1.85 from size-exclusion chromatography) containing 4.0 wt% B was purchased from Sigma-Aldrich (St. Louis, MO) and used as the substrate for LBL coatings in permeation tests due to its rubber-improved fracture resistance. A branched PEI ($\bar{M}_n = 60$ kDa and PDI = 12.5, according to the manufacturer) with good thermal stability [32,33] was obtained from Scientific Polymer Products (Ontario, NY), whereas an AQ55S poly(ethylene terephthalate) ionomer (PETi) ($\bar{M}_n = 7-8$ kDa [34]) was generously donated by Eastman Chemical Company (Kingsport, TN). The chemical structures of these two polyelectrolytes are depicted in **Figure 4.2**. Purified Na⁺MMT nanoclay with a cation exchange capacity [29] of 0.92 meq/g was procured from Southern Clay Products (Gonzales, TX). Ultrahigh-purity (99.999%) O₂ and high-purity (at least 99.9%) CO₂ were purchased from National Welders Supply Co. (Charlotte, NC) and Air Liquid America Specialty Gases (Plumsteadville, PA), respectively. The resistivity of deionized water (DIW), prepared with the Millipore Direct-Q 3 UV purification system and used primarily as the liquid medium for polyelectrolyte solutions and MMT suspensions, was 18.2 MΩ at 25°C.

4.2.2. Specimen Preparation

Polymer films typically measuring 100 μm thick were prepared on crystallization plates by solution casting from toluene at ambient temperature. Resultant films were annealed under vacuum for 24 h in the melt at 110°C (above the PS glass transition temperature, T_g , of 100°C) to ensure complete solvent removal. The films were then exposed to O_2 plasma generated in a low-pressure FEMTO plasma system (Diener Electronic GmbH, Ebhausen, Germany) operated at a power of 10 W/cm^2 and a gas flow rate of 20 sccm (standard cm^3/min) for 60 s to introduce polar organic moieties and thus enhance surface hydrophilicity. A polyelectrolyte solution was prepared by dissolving PEI at 0.5 wt% in DIW by continuous stirring at ambient temperature. In the case of PETi, an identical solution was produced for comparison, but dissolution was conducted at 60°C (above the PETi T_g of 52°C). Four MMT suspensions at 0.1, 1.0, 3.0, and 5.0 wt% in DIW were ultrasonicated for 20 min, followed by continuous stirring at ~ 600 rpm for 24 h, to achieve stable exfoliation and homogeneity. Each plasma-treated film was immersed in a predetermined polyelectrolyte solution for 5 min, rinsed with DIW to remove excess polymer and dried with filtered air. The polyelectrolyte-coated film was subsequently immersed in one of the MMT suspensions to deposit a layer of MMT platelets and produce the first BL. This sequence of events, conducted at ambient temperature, was repeated until a desired number of BLs accumulated on each specimen.

4.2.3. Specimen Characterization

Electron-transparent sections for TEM analysis were generated by first embedding LBL-coated PS films in epoxy and then microtoming the resulting composites in a Leica Ultracut 7

at ambient temperature. Digital TEM images of sections measuring ~120 nm thick and floated onto carbon-coated copper grids were acquired on a JEOL 2000-FX microscope operated at an accelerating voltage of 200 kV. Single-gas permeation tests were performed on both uncoated and LBL-coated SB films in a constant-volume/variable-pressure cell. Specimens were held under vacuum at 50°C for 48 h and stored in a desiccator before analysis [5,35]. Each membrane of measured thickness (L) and exposure area (A) was inserted into the permeation cell [36,37], which was subsequently evacuated. A desired gas with an upstream pressure (p_u) of typically 1 atm was introduced into the system and permitted to permeate through the membrane into a downstream vessel of known volume (V). The downstream pressure (p_d) was recorded as a function of time (t) by a transducer connected to a computer for automated data acquisition. The permeability (P) of each gas tested was given by

$$P = \frac{VL}{ART(p_u - p_d)} \frac{dp_d}{dt} \quad (1)$$

where R is the universal gas constant and T denotes absolute temperature. While most permeation tests were conducted at ambient temperature, a limited number of experiments were likewise performed at elevated temperatures below the upper T_g of the SB substrate (to avoid membrane distortion).

4.3. Results and Discussion

As discussed earlier, electrostatic attraction between alternating layers of polyelectrolyte and nanoclay platelets yields "nanobrick" coatings that effectively serve as impermeable surface barriers to gas transport. Although the present work focuses primarily on aspects of LBL coatings that influence molecular transport (a forthcoming companion study addresses

associated morphological considerations), we first examine the LBL coatings generated here to discern if they exhibit the expected nanobrick morphology. The TEM image acquired from a PEI/MMT coating with 30 BLs (deposited from 0.5 wt% PEI and 1.0 wt% MMT) and presented in **Figure 4.3** confirms that the coating is a nanolaminate with a large population of electron-opaque MMT platelets oriented nearly parallel to the substrate surface. Variations in platelet orientation are attributed to platelet overlap that can occur during the deposition process schematically depicted in **Figure 4.4**. In the same fashion as thick, vapor-deposited single-layer coatings, defects that develop with a small number of deposited BLs become exaggerated as the number of BLs is increased. Since the average thickness of the coating measured from cross-sectional TEM images such as the one displayed in **Figure 4.3** is ~500 nm, it immediately follows that each BL contributes ~17 nm. Since each freestanding membrane is fully immersed in the polyelectrolyte solutions and MMT suspensions, a BL is deposited on both film sides during each dipping cycle, in which case the total number of BLs accumulated on a membrane is actually twice the number of BLs reported. Another important consideration here is that the polymer substrate visible in the TEM image shown in **Figure 4.3** is PS, but the permeation results reported below are measured from membranes with SB substrates. Oxygen permeabilities determined from uncoated PS and SB substrates at ambient temperature are 0.14 and 0.18 cm³-m/m²-day-atm, respectively, in quantitative agreement with previous findings (0.14 cm³-m/m²-day-atm at 25°C [38,39]) and each other, confirming that these two substrates possess comparable gas-transport properties.

4.3.2. Effect of Plasma Treatment

Independent prior studies have established that O₂ plasma treatment of hydrophobic polymer surfaces introduces the polar functional groups required for the success of various coating technologies [27,28,38]. Extension of this procedure to the neat SB copolymer with 4.0 wt% rubber yields the O₂ and CO₂ permeabilities (P_{O₂} and P_{CO₂}, respectively) presented for comparison in **Figure 4.5**. With and without plasma treatment, P_{CO₂} is higher than P_{O₂} through the uncoated polymer membranes even though the molecular size of CO₂ is larger than that of O₂. This observed behavior most likely reflects the ability of CO₂ to plasticize the glassy copolymer and correspondingly increase the free volume responsible for governing molecular transport. This explanation is consistent with the observation that plasma treatment serves to improve P_{O₂} by 66%, but has less impact (23% increase) on P_{CO₂}. Deposition of 5 PEI/MMT BLs on the untreated substrate promotes noticeable reductions in both permeabilities in **Figure 4.5**. A measure of barrier efficacy for a given penetrant gas is the barrier improvement factor (BIF) calculated from the ratio of gas permeability through the untreated polymer film to that through the LBL-coated membrane. Corresponding integer BIF values are 3 for O₂ and 44 for CO₂. If the substrate surface is plasma-treated prior to deposition of 5 PEI/MMT BLs, however, P_{O₂} and P_{CO₂} decrease more significantly, resulting in BIF values of 45 and 94, respectively. In light of the substantial improvement in barrier performance achieved by surface plasma treatment, we conclude that plasma-pretreatment of the SB surface benefits LBL coating fabrication by promoting adhesion of the PEI polycation and nanoclay platelets (since the platelet edges are positively charged), in which case all specimens produced and characterized

here are plasma-treated under the same experimental conditions prior to LBL coating deposition.

4.3.3. Effect of Suspension Concentration

The first LBL coating parameter to be explored is the MMT concentration in DIW suspensions. An increase in MMT concentration in an aqueous suspension is expected to increase (i) the population of nanoclay platelets available for deposition, (ii) the propensity of having exfoliated, intercalated and aggregated platelets, (iii) the suspension viscosity, and (iv) the likelihood of achieving conformal and highly oriented coatings with fewer BLs. Measured values of P_{O_2} and P_{CO_2} displayed in **Figure 4.6a** as functions of MMT suspension concentration for membranes with 5 PEI/MMT BLs (0.5 wt% PEI) reveal two important features. The first is that P_{CO_2} remains generally higher than P_{O_2} due presumably to the plasticizing effect of CO_2 . The second is that an increase in MMT concentration is accompanied by pronounced reductions in both P_{O_2} and P_{CO_2} . These decreases are attributed to the extended diffusive pathway (tortuosity) induced by the nanobrick obstacles comprising the LBL coatings. Since $P = S \times D$ in the limit of Fickian diffusion and since both S and D decrease upon addition of impermeable, surface-aligned, high-aspect-ratio nanoclay platelets, gas permeability is anticipated to drop as more platelets are available to accumulate on the substrate surface. While P_{O_2} decreases monotonically over the range of MMT concentrations examined here, P_{CO_2} decreases to a limiting value in the vicinity of $0.002 \text{ cm}^3\text{-m/m}^2\text{-day-atm}$. One plausible reason for this limiting behavior at high MMT concentrations is the deposition of bulky nanoclay aggregates, rather than individual platelets or small tactoids, from aqueous suspension. In this

scenario, tortuosity, and hence permeability, might no longer be affected with regard to the larger CO₂ (relative to O₂) molecules. A similar result is expected for O₂ at higher MMT loading levels, but uniform dispersion of MMT at such concentrations in DIW at ambient temperature becomes problematic.

Interestingly, the corresponding BIF values calculated for both O₂ and CO₂ at high MMT concentrations (3.0-5.0 wt%) range from about 400 to 550, comparing favorably with BIF values reported elsewhere for O₂ through PEI/MMT LBL coatings [26]. In **Figure 4.6b**, analogous O₂ and CO₂ permeabilities are displayed as a function of MMT concentration for membranes with 5 PETi/MMT BLs (0.5 wt% PETi) and likewise confirm that an increase in MMT concentration promotes a similarly profound reduction in gas permeability as the PEI-based LBL coatings (*cf.* **Figure 4.6a**). The highest BIF in this series (about 470) is determined for CO₂ at 3.0 wt% MMT. An obvious difference between LBL coatings prepared with the two polyelectrolytes identified in **Figure 4.2** is that, in the presence of the PETi polyanion, both P_{O₂} and P_{CO₂} increase sharply at MMT concentrations beyond 3.0 wt%. A reason offered for this unexpected observation is depicted in **Figure 4.7**. At low MMT concentrations, single nanoclay platelets and small tactoids attach along their positively charged ends to the PETi layer and flatten when the coated substrates are dried. In this regard, they resemble the process portrayed in **Figure 4.4** for the PEI polycation with the exception that polyelectrolyte intercalation is most likely limited to the edges of tactoids. At sufficiently high MMT concentrations, however, the same nanoclay aggregates discussed earlier with regard to **Figure 4.6a** deposit and pack edgewise onto the PETi layer, thereby forming columnar features wherein the nanoclay platelets are oriented nearly normal to the substrate surface. This

morphology, illustrated in **Figure 4.7** for the PETi polyanion and observed by TEM elsewhere, is less efficient than parallel platelet stacking (as achieved with the PEI polycation) at enhancing barrier performance. Because of this undesirable LBL arrangement, the BIF values for O₂ and CO₂ plummet to 56 and 189, respectively, at 5.0 wt% MMT.

4.3.4. Effect of Bilayer Number

Another important materials design parameter is the BL number, which directly relates to the thickness of the LBL coating. Recall that this number corresponds to the number of bilayers on each side of the freestanding substrate during immersion cycling, and so the total number of BLs deposited is twice this number. The dependence of O₂ and CO₂ permeability on BL number is presented in **Figure 4.8a** for PEI/MMT LBL coatings and **Figure 4.8b** for PETi/MMT LBL coatings wherein the polyelectrolyte and MMT concentrations are 0.5 wt% and 1.0 wt%, respectively (the MMT concentration is selected to avoid columnar platelet stacking). Attempts to improve the barrier effectiveness of these LBL coatings further by depositing additional BLs or increasing the MMT concentration yield permeabilities that approach the detection limit of the permeation cell ($\sim 10^{-5}$ cm³-m/m²-day-atm). Both figures indicate that an increase in BL number is accompanied by systematic reductions in both P_{O₂} and P_{CO₂}, with P_{CO₂} > P_{O₂} as previously observed in **Figure 4.6**. This route to thicker LBL coatings differs from increasing the MMT concentration at constant BL number in that each deposited layer consists of individual nanoclay platelets or small tactoids (rather than suspension aggregates) that remain nearly parallel to the substrate surface. Thickening the LBL nanolaminate while retaining platelet alignment dramatically increases the diffusive pathway,

which is consistent with a reported [26,40] exponential increase in tortuosity with increasing BL number. Two features in **Figure 4.8a** warrant particular attention. First, although P_{CO_2} is generally greater than P_{O_2} due to the plasticizing effect of CO_2 , the two converge for PEI-based LBL coatings with 15 BLs. This observation is attributed to the larger size of CO_2 (relative to O_2) molecules that must navigate through an increasingly tortuous path. The second noteworthy characteristic is that the BIF for CO_2 in this membrane is ~ 2000 (1905). Although the results measured for the PETi-based LBL coatings in **Figure 4.8b** follow the same trend as PEI-based LBL coatings, the barrier is not as effective, with the largest BIF being 524 for CO_2 .

4.3.5. Effect Permeation Temperature

Since $P = S \times D$ and both S and D are thermally-activated processes whose temperature dependence is given by [39]

$$S = S_0 \exp\left(\frac{-\Delta H_S}{RT}\right) \quad (2a)$$

$$\text{and } D = D_0 \exp\left(\frac{E_D}{RT}\right), \quad (2b)$$

respectively, it immediately follows that $P(T)$ can be conveniently expressed as

$$P = P_0 \exp\left(\frac{E_P}{RT}\right) \quad (3)$$

where S_0 , D_0 and P_0 are pre-exponential constants, ΔH_S is the molar enthalpy of sorption, E_D is the molar activation energy for diffusion, and $E_P = (E_D - \Delta H_S)$ is the molar activation energy for permeation. **Equations 4.3** and **4.4** establish that an increase in temperature generally

promotes an increase in diffusion, a decrease in solubility and, if $E_D > \Delta H_S$ (as in the case of non-interacting gases such as O_2) an overall increase in permeation. While the Arrhenius expression employed to describe the thermal dependence of P in **Equation 4.4** has been used to analyze the thermal behavior of gas transport through glass-coated polymer membranes [13,41], its applicability to membranes with an LBL coating has not been previously examined. The utility of **Equation 4.4** lies in the fact that changes in E_P can provide valuable insight into the factors responsible for gas transport. For instance, in the case of glass-coated polymer membranes, an increase in E_P relates to the inability of gas molecules of finite size to diffuse through nanoscale coating defects. Conversely, in the case of polymer nanocomposites containing exfoliated nanoclay platelets, the value of E_P provides a measure of the tortuous path length around impermeable platelets.

The measured permeabilities displayed in **Figure 4.9a** for O_2 and **Figure 4.9b** for CO_2 confirm that both the uncoated and LBL-coated SB membranes obey Arrhenius behavior (**Equation 4.4**). As expected from prior studies, values of E_P extracted from the data for uncoated membranes (15.4 kJ/mol for O_2 and 6.6 kJ/mol for CO_2) indicate that the permeation of CO_2 is more facile than O_2 , in qualitative agreement with the permeability measurements evident in **Figures 4.6** and **4.8**. This behavior is attributed to the well-known ability of CO_2 to plasticize the glassy SB substrate. In the case of the LBL-coated membranes, the concentrations of the polyelectrolytes and MMT are held constant at 0.5 wt% and 3.0 wt%, respectively, to permit direct comparison. We first consider O_2 permeation in **Figure 4.9a**. Deposition of the PETi/MMT LBL coating increases E_P slightly from 15.4 to 20.6 kJ/mol, indicating that the existence of the coating marginally affects the mechanism of O_2 transport.

In the case of the PEI/MMT coating, however, the extent to which O₂ transport is affected is much greater, as E_P is more than doubled to 35.8 kJ/mol. Since O₂ is a relatively non-interacting gas, these findings confirm that a primarily flat nanobrick morphology (afforded by PEI) impedes permeation more effectively than one with columnar tactoids and other defects (introduced by PETi) that ultimately compromise barrier performance. A very different set of results is, however, observed for CO₂ in **Figure 4.9b**. Here, addition of either type of LBL coating promotes a similarly large (~3x) increase in E_P (to 18.1 kJ/mol for PEI-type coatings and 20.8 kJ/mol for PETi-type coatings). Since this change in E_P is surprisingly insensitive to the type of polyelectrolyte employed (and the corresponding nanobrick morphology), we propose that CO₂ plasticizes, and thus swells, not only the SB substrate but also the polyelectrolyte layers, in which case the observed increase in E_P primarily reflects a reduction in diffusivity due to the presence of irregularly oriented nanoclay platelets. It is interesting that the values of E_P for O₂ with a PETi/MMT LBL coating and for CO₂ with any LBL coating are virtually identical, which suggests that CO₂-induced polyelectrolyte swelling might cause the nanoclay platelets to adopt similarly defective morphologies.

4.4. Conclusions

The development of polymer-based packaging materials with improved barrier properties is becoming increasingly important, especially in the microelectronic and food industries. While a variety of different strategies, ranging from single- to multilayer deposition and nanocomposite formulation, have been examined and show tremendous promise, the LBL coating process provides a surprisingly inexpensive and facile approach that is capable of

reducing gas permeability by orders of magnitude without the need for specialized instrumentation. In the present work, we compare the barrier efficacy of LBL coatings prepared with native MMT and one of two chemically dissimilar polyelectrolytes, one a polycation (PEI) and the other a polyanion (PETi). While most investigations of LBL coatings focus extensively on O₂ permeation, this study also examines the molecular transport of CO₂, which is known to plasticize a wide range of polymers, including the polymer substrate and polyelectrolytes employed here. Since the hydrophobic polymer substrate is first activated through the use of O₂ plasma, we first establish the effect of plasma pretreatment on barrier performance. In addition, we interrogate the effects of suspension concentration and bilayer number, and proceed to demonstrate that highly concentrated suspensions can introduce undesirable defects in LBL coatings, especially those fabricated with the PETi polyanion, by compromising their barrier effectiveness. In marked contrast, an increase in the bilayer number at relatively low nanoclay suspension levels is observed to improve barrier performance in systematic fashion. Interestingly, the relatively flat orientation of nanoclay platelets in LBL coatings prepared with PEI does not strongly outperform the more defective morphology of coatings produced with PETi. In fact, the barrier improvement factor for CO₂ in PETi-based LBL coatings exceeds a record ~1900 with 15 deposited bilayers. The temperature-dependent transport behavior of these coatings reveals the effect of polyelectrolyte charge on the activation energy for permeation, which is immensely useful for gleaning insight into the mechanisms and, by inference, the morphological features by which LBL coatings function with respect to different gases. In a forthcoming companion work, we explore the morphologies of these LBL coatings and relate these characteristics to the molecular transport

findings reported herein. In this spirit, we aim to develop further the underlying principles of this gas barrier technology and identify niches in which it can be used effectively in contemporary and emerging applications.

Figures

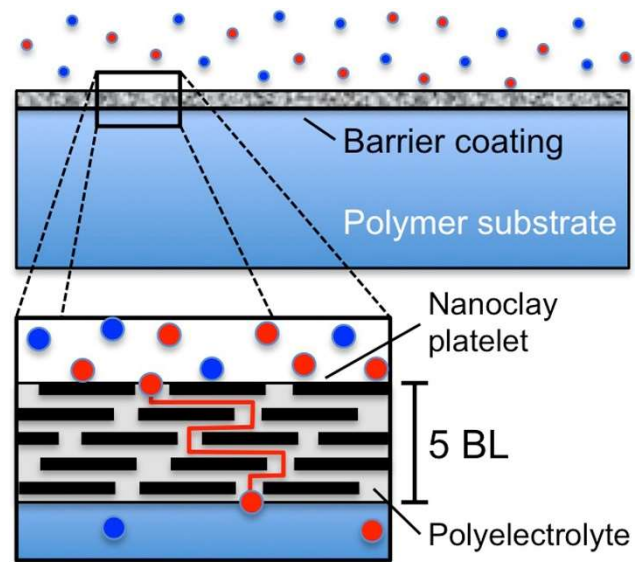


Figure 4.1. Illustration of a layer-by-layer (LBL) coating applied as a gas barrier to the surface of a polymer substrate. Alternating cyclic deposition of a polyelectrolyte and nanoclay platelets generates a "nanobrick" morphology that greatly increases the tortuous pathway for diffusing molecules. The LBL coating depicted here possesses 5 polyelectrolyte/nanoclay bilayers (BLs).

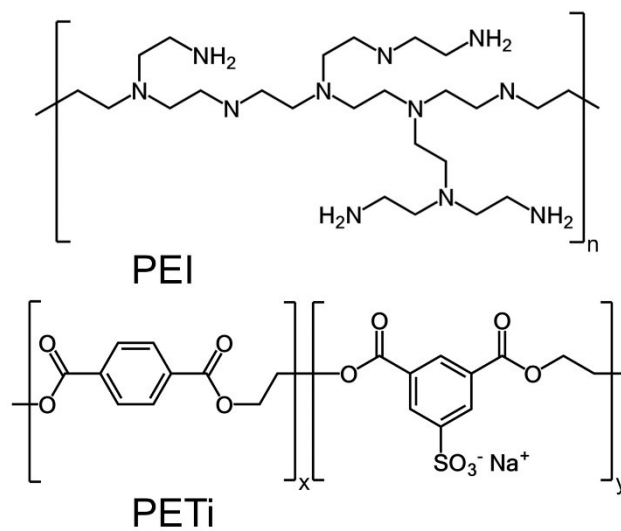


Figure 4.2. Schematic of chemical structures of the two polyelectrolytes employed as adhesives in this study: polyethylenimine (PEI) and poly(ethylene terephthalate) ionomer (PETi).

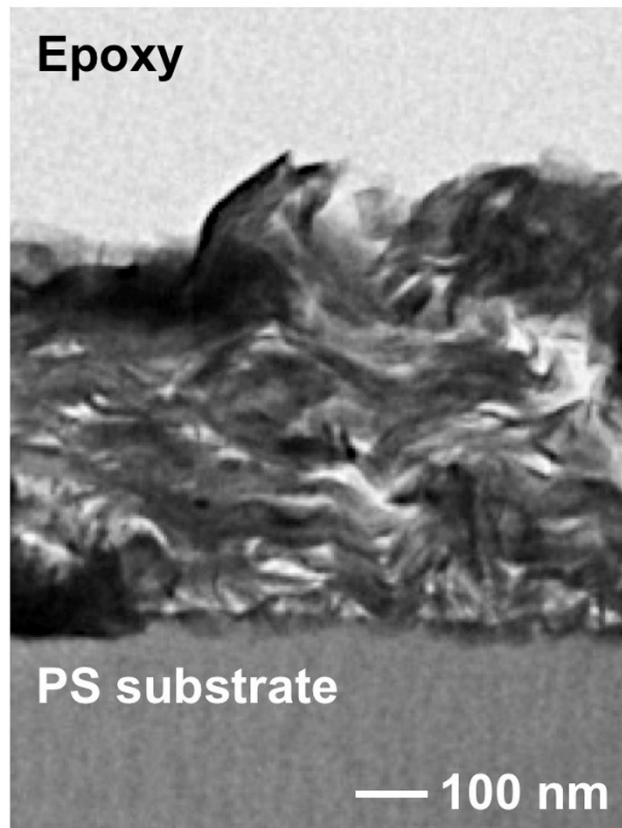


Figure 4.3. Gas Cross-sectional transmission electron microscopy (TEM) image of an LBL coating deposited on PS and embedded in epoxy (to facilitate preparation). The coating was prepared with 30 BLs from a 0.5 wt% PEI aqueous solution and a 1.0 wt% MMT aqueous suspension.

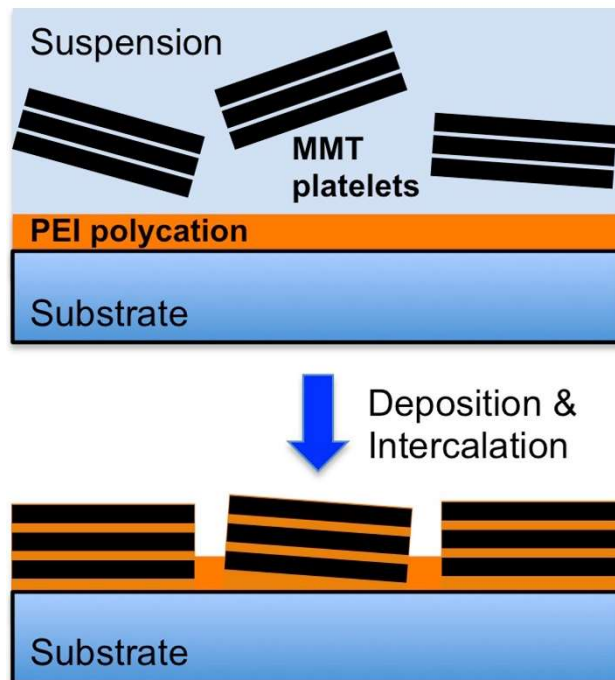


Figure 4.4. Schematic depiction of the mechanism by which MMT nanoclay deposits onto PEI. Platelets with a negative face charge complex with the polycation and arrange themselves in a nearly surface-parallel orientation. The PEI molecules diffuse into the platelet galleries and promote intercalation.

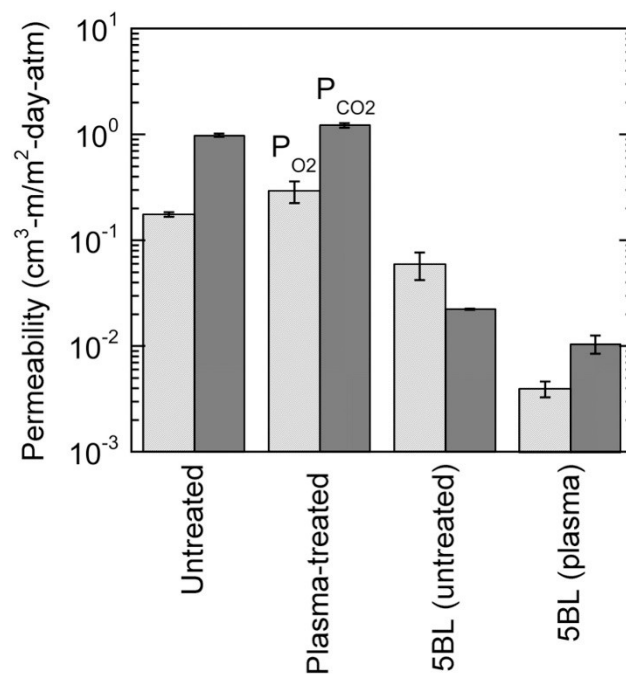


Figure 4.5. Permeability Dependence of O₂ and CO₂ permeabilities (labeled) through a glassy SB film at 20°C on surface O₂ plasma treatment before and after the addition of an LBL coating consisting of 5 BLs prepared from 0.5 wt% PEI and 1.0 wt% MMT in DIW. The error bars denote the standard error in the data.

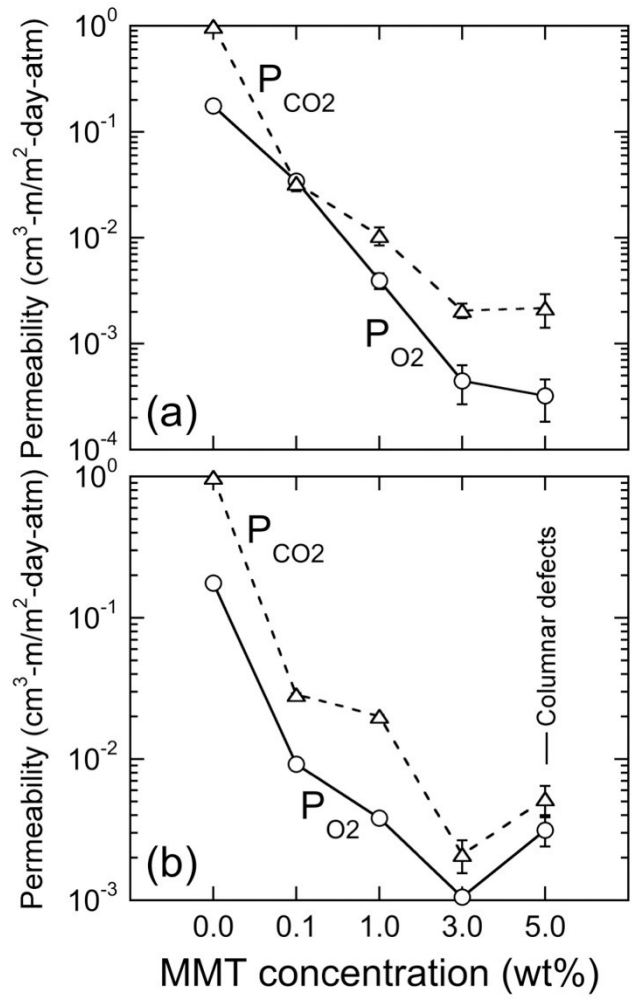


Figure 4.6. Permeabilities of O₂ (o) and CO₂ (Δ) through LBL-coated SB substrates at 20°C presented as a function of MMT concentration in aqueous suspension for 5 BL coatings fabricated from 0.5 wt% PEI (a) or PETi (b) in DIW. The lines serve to connect the data, and the error bars denote the standard error in the data.

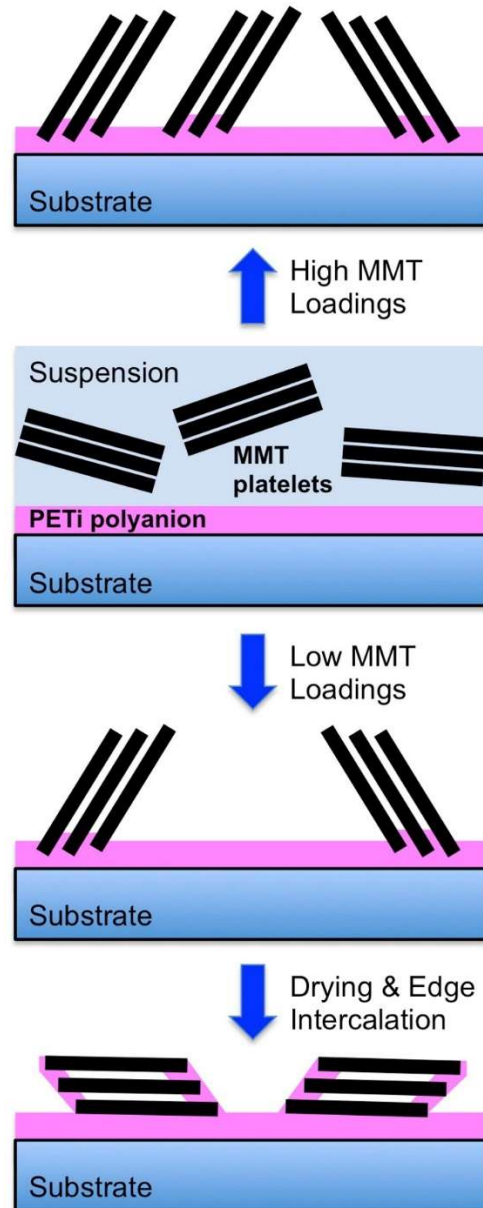


Figure 4.7. Schematic depiction of the mechanism by which MMT nanoclay deposits onto PETi. Platelets with a positive edge charge complex with the polyanion and arrange themselves in a nearly surface-normal orientation. The PETi molecules diffuse into the edges of the platelet galleries and promote limited intercalation. At low MMT suspension concentrations, the platelets subsequently adopt a more surface-parallel orientation upon drying. At high concentrations, however, deposited platelets are crowded and retain a less-effective columnar morphology.

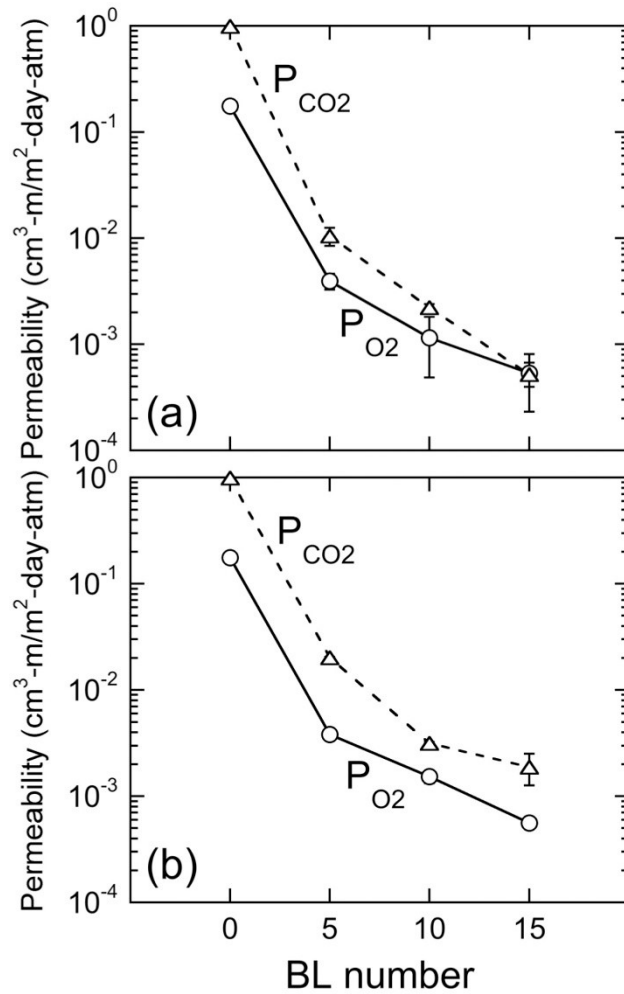


Figure 4.8. Permeabilities of O₂ (o) and CO₂ (Δ) through LBL-coated SB substrates at 20°C presented as a function of BL number for coatings produced from 1.0 wt% MMT and 0.5 wt% PEI (a) or PETi (b) in DIW. The lines serve to connect the data, and the error bars denote the standard error in the data.

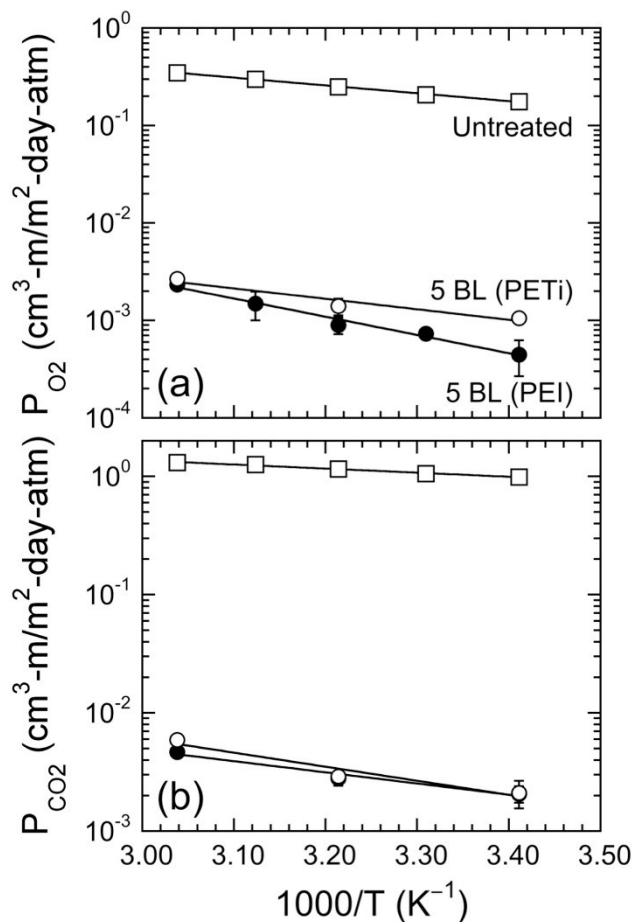


Figure 4.9. Permeabilities of (a) O₂ and (b) CO₂ through LBL-coated SB substrates presented as a function of reciprocal temperature for 5 BL coatings fabricated from 3.0 wt% MMT and 0.5 wt% PEI (a) or PETi (b) in DIW. The lines represent regressions of Eq. 3 to the data, confirming that permeation through uncoated (□) and LBL-coated (PEI, ● ; PETi, ○) SB substrates exhibits Arrhenius behavior. Values of EP extracted from the slopes of the lines are provided in the text.

References

- [1] J. Lewis, Material challenge for flexible organic devices, *Mater. Today* 9 (2006) 38–45.
- [2] J. Jiang, M. Benter, R. Taboryski, K. Bechgaard, Oxygen barrier coating deposited by novel plasma-enhanced chemical vapor deposition, *J. Appl. Polym. Sci.* 115 (2010) 2767–2772.
- [3] H.Y. Low, Y. Xu, Moisture barrier of Al_xO_y coating on poly(ethylene terephthalate), poly(ethylene naphthalate) and poly(carbonate) substrates, *Appl. Surf. Sci.* 250 (2005) 135–145.
- [4] Q. Peng, X.-Y. Sun, J.C. Spagnola, G.K. Hyde, R.J. Spontak, G.N. Parsons, Atomic layer deposition on electrospun polymer fibers as a direct route to Al_2O_3 microtubes with precise wall thickness control, *Nano Lett.* 7 (2007) 719–722.
- [5] P.F. Carcia, R.S. McLean, M.H. Reilly, Permeation measurements and modeling of highly defective Al_2O_3 thin films grown by atomic layer deposition on polymers, *Appl. Phys. Lett.* 97 (2010) 221901.
- [6] Flexible packaging market expected to rocket, *Mater. World* (Nov. 2015) 11.
- [7] P.F. Carcia, R.S. McLean, M.D. Groner, A.A. Dameron, S.M. George, Gas diffusion ultrabarrriers on polymer substrates using Al_2O_3 atomic layer deposition and SiN plasma-enhanced chemical vapor deposition, *J. Appl. Phys.* 106 (2009) 23533.
- [8] S.S. Ray, Recent trends and future outlooks in the field of clay-containing polymer nanocomposites, *Macromol. Chem. Phys.* 215 (2014) 1162–1179.
- [9] D.R. Paul, L.M. Robeson, Polymer nanotechnology: nanocomposites, *Polymer* 49 (2008) 3187–3204.
- [10] A. Giannakas, A. Giannakas, A. Ladavos, Preparation and characterization of polystyrene/ organolaponite nanocomposites, *Polym. Plast. Technol. Eng.* 51 (2012) 1411–1415.
- [11] M. Hanika, H.-C. Langowski, U. Moosheimer, W. Peukert, Inorganic layers on polymeric films—Influence of defects and morphology on barrier properties, *Chem. Eng. Technol.* 26 (2003) 605–614.
- [12] A.P. Roberts, B.M. Henry, A.P. Sutton, C.R.M. Grovenor, G.A.D. Briggs, T. Miyamoto, et al., Gas permeation in silicon-oxide/polymer (SiO_x/PET) barrier films: role of the

oxide lattice, nano-defects and macro-defects, *J. Memb. Sci.* 208 (2002) 75–88.

- [13] A.G. Erlat, B.-C. Wang, R.J. Spontak, Y. Tropsha, K.D. Mar, D.B. Montgomery, et al., Morphology and gas barrier properties of thin SiO_x coatings on polycarbonate: Correlations with plasma-enhanced chemical vapor deposition conditions, *J. Mater. Res.* 15 (2000) 704–717.
- [14] H. Jung, C.H. Jang, I.S. Yeo, T.-H. Song, Investigation of gas permeation through Al-metallized film for vacuum insulation panels, *Int. J. Heat Mass Transf.* 56 (2013) 436–446.
- [15] V. Mittal, Polymer nanocomposites: synthesis, microstructure, and properties, in: V. Mittal (Ed.), *Optimization of Polymer Nanocomposite Properties*, 1st Ed., Wiley-VCH, Weinheim, 2010, pp. 1–20.
- [16] W. Huang, S. Zeng, J. Liu, L. Sun, Bi-axially oriented polystyrene/montmorillonite nanocomposite films, *RSC Adv.* 5 (2015) 58191–58198.
- [17] S. Nazarenko, P. Meneghetti, P. Julmon, B.G. Olson, S. Qutubuddin, Gas barrier of polystyrene montmorillonite clay nanocomposites: Effect of mineral layer aggregation, *J. Polym. Sci. B: Polym. Phys.* 45 (2007) 1733–1753.
- [18] G. Decher, Layer-by-layer assembly, in: G. Decher, J.B. Schlenoff (Eds.), *Multilayer Thin Films: Sequential Assembly of Nanocomposite Materials*, 2nd Ed., Wiley-VCH, Weinheim, 2012, pp. 1–22.
- [19] M.A. Priolo, K.M. Holder, S.M. Greenlee, B.E. Stevens, J.C. Grunlan, Precisely tuning the clay spacing in nanobrick wall gas barrier thin films, *Chem. Mater.* 25 (2013) 1649–1655.
- [20] P. Tzeng, E.L. Lugo, G.D. Mai, B. a Wilhite, J.C. Grunlan, Super hydrogen and helium barrier with polyelectrolyte nanobrick wall thin film., *Macromol. Rapid Commun.* 36 (2015) 96–101.
- [21] K. Apaydin, A. Laachachi, V. Ball, M. Jimenez, S. Bourbigot, V. Toniazzi, et al., Polyallylamine-montmorillonite as super flame retardant coating assemblies by layer-by layer deposition on polyamide, *Polym. Degrad. Stab.* 98 (2013) 627–634.
- [22] A. Laachachi, V. Ball, K. Apaydin, V. Toniazzi, D. Ruch, Diffusion of polyphosphates into (poly(allylamine)-montmorillonite) multilayer films: flame retardant-intumescent films with improved oxygen barrier, *Langmuir* 27 (2011) 13879–13887.
- [23] E.-H. Song, B.-H. Kang, T.-Y. Kim, H.-J. Lee, Y.-W. Park, Y.-C. Kim, et al., Highly

- oriented gold/nanoclay–polymer nanocomposites for flexible gas barrier films, *ACS Appl. Mater. Interfaces* 7 (2015) 4778–4783.
- [24] A.J. Svagan, A. Åkesson, M. Cárdenas, S. Bulut, J.C. Knudsen, J. Risbo, et al., Transparent films based on PLA and montmorillonite with tunable oxygen barrier properties, *Biomacromolecules* 13 (2012) 397–405.
- [25] M.A. Priolo, K.M. Holder, T. Guin, J.C. Grunlan, Recent Advances in gas barrier thin films via layer-by-layer assembly of polymers and platelets, *Macromol. Rapid Commun.* 36 (2015) 866–879.
- [26] M.A. Priolo, K.M. Holder, D. Gamboa, J.C. Grunlan, Influence of clay concentration on the gas barrier of clay–polymer nanobrick wall thin film assemblies, *Langmuir* 27 (2011) 12106–12114.
- [27] C. Chaiwong, P. Rachtanapun, P. Wongchaiya, R. Auras, D. Boonyawan, Effect of plasma treatment on hydrophobicity and barrier property of polylactic acid, *Surf. Coatings Technol.* 204 (2010) 2933–2939.
- [28] I. Beaulieu, M. Geissler, J. Mauzeroll, Oxygen plasma treatment of polystyrene and zeonor: substrates for adhesion of patterned cells, *Langmuir* 25 (2009) 7169–7176.
- [29] G.W. Beall, C.E. Powell, *Fundamentals of Polymer-Clay Nanocomposites*, 1st Ed., Cambridge University Press, Cambridge, 2011.
- [30] A. Ammala, C. Bell, K. Dean, Poly(ethylene terephthalate) clay nanocomposites: improved dispersion based on an aqueous ionomer, *Compos. Sci. Technol.* 68 (2008) 1328–1337.
- [31] G.D. Barber, B.H. Calhoun, R.B. Moore, Poly(ethylene terephthalate) ionomer based clay nanocomposites produced via melt extrusion, *Polymer* 46 (2005) 6706–6714.
- [32] P.S. Srinivasa Rao, B. Smitha, S. Sridhar, A. Krishnaiah, Preparation and performance of poly(vinyl alcohol)/polyethyleneimine blend membranes for the dehydration of 1,4-dioxane by pervaporation: Comparison with glutaraldehyde cross-linked membranes, *Sep. Purif. Technol.* 48 (2006) 244–254.
- [33] X. Xu, C. Song, J.M. Andrésen, B.G. Miller, A.W. Scaroni, Preparation and characterization of novel CO₂ “molecular basket” adsorbents based on polymer-modified mesoporous molecular sieve MCM-41, *Microporous Mesoporous Mater.* 62 (2003) 29–45.
- [34] G.L. Martin, J.A. Ross, S.D. Minter, D.M. Jameson, M.J. Cooney, Fluorescence

characterization of chemical microenvironments in hydrophobically modified chitosan, *Carbohydr. Polym.* 77 (2009) 695–702.

- [35] C.A. Wilson, J.A. McCormick, A.S. Cavanagh, D.N. Goldstein, A.W. Weimer, S.M. George, Tungsten atomic layer deposition on polymers, *Thin Solid Films* 516 (2008) 6175–6185.
- [36] X. Hu, J. Tang, A. Blasig, Y. Shen, M. Radosz, CO₂ permeability, diffusivity and solubility in polyethylene glycol-grafted polyionic membranes and their CO₂ selectivity relative to methane and nitrogen, *J. Memb. Sci.* 281 (2006) 130–138.
- [37] N.P. Patel, A.C. Miller, R.J. Spontak, Highly CO₂-permeable and selective polymer nanocomposite membranes, *Adv. Mater.* 15 (2003) 729–733.
- [38] S.N. Dhoot, Sorption and transport of gases and organic vapors in poly(ethylene terephthalate), Ph.D. Dissertation, University of Texas at Austin, 2004.
- [39] H. Yasuda, V. Stannet, Permeability Coefficients, in: J. Brandrup, E.H. Immergut (Eds.), *Polymer Handbook*, 2nd Ed., Wiley-Interscience, New York, 1975, pp. 229–240.
- [40] Y.-H. Yang, L. Bolling, M. Haile, J. Grunlan, Improving oxygen barrier and reducing moisture sensitivity of weak polyelectrolyte multilayer thin films with crosslinking, *RSC Adv.* 2 (2012) 12355–12363.
- [41] A.G. Erlat, R.J. Spontak, R.P. Clarke, T.C. Robinson, P.D. Haaland, Y. Tropsha, et al., SiO_x gas barrier coatings on polymer substrates: morphology and gas transport considerations, *J. Phys. Chem. B* 103 (1999) 6047–6055.

CHAPTER 5

Morphology of Polymer Nanocomposites Derived From Layer-by-Layer Coated Polystyrene-Based Membranes

Abstract

Particularity of the approach used for preparing these innovative polymer nanocomposites (PNCs) that included initial layer-by-layer (LBL) deposition of clay and polyelectrolyte (PE) on polymeric membranes based on polystyrene, followed by crushing LBL coating into bulk of polymeric membrane through cyclic melt pressing, led to novel morphologies, different from what expected from conventional methods of PNC formation. In fact, as both polarized optical microscopy (POM) and transmission electron microscopy (TEM) micrographs showed, clay particles in prepared PNCs are mostly in the shape of crushed portions of LBL assemblies, with size ranges of up to a few micrometers, which may reflect forming of a microcomposite in the first glance (at low magnification scales). But, further investigations of embedded clay particles in TEM micrographs with higher magnification scales, showed their lamellar structures, comprising swollen intercalated stacks of many montmorillonite (MMT) platelets and flocculated exfoliated tactoids of a few MMT platelets, down to the thickness of about 2nm, to form highly tortuous labyrinths. In fact, these PNCs inherited the initial stable swollen intercalations and exfoliations provided in LBL assemblies. Then, through cyclic melt pressing procedure and applying shear and stress at elevated temperatures on samples, as a result of occurred interaction between LBL assemblies and polymeric matrix, from one side LBL assemblies were broken into smaller particles (macro crashing), and from the other side their

internal expanded intercalation and exfoliation increased (micro crashing). Also, the minor release of individual platelets into the matrix, out of the expanded LBL portions, was observed. The results of x-ray diffractometry (XRD) also demonstrated a noticeable increase in the intercalation between clay platelets, as well as the increase in their interdistance disorderliness, which might be respectively connected to, observed rise in swelling of LBL assemblies in PNCs and crushing LBLs, besides peeling some platelets out of them. This postulated increased exfoliation was more significant for polyethyleneterephthalate ionomer (PETi) containing PNCs, processed over extended times of melt mixing. Nevertheless, considering all morphological investigations, it seems that due to existing fairly strong internal cohesion in LBL assemblies and insufficient intensity of shear stress applied to samples and/or lack of a strong interaction between LBL assemblies and the polymeric matrix, not a significant global nanodispersion of clay platelets occurred throughout the matrix.

5.1. Introduction

Using fillers and inorganic ingredients from the beginning of using polymeric materials in different applications have been considered as one of the main methods to improve their properties for competing with other materials [1,2]. With decreasing the size of those dispersed species, down to micrometer and nanometer scales, their aspect ratio and interfacial contact increase, to surge significantly their effectiveness in low contents, resulting in the emerge of polymer micro and nanocomposites, with improved properties [2–6]. One superiority of composite approaches may be their comprehensive improvement rather than mainly concentrating on one item. For instance, in packaging applications, composite approaches,

show improvement not only in barrier performance, but also in mechanical and thermal properties, in addition to being processable with conventional processing techniques [2,6]; while, coating approaches hold drawbacks for their industrial applications, and they are vulnerable to stress-induced defects and peelings, through their service life [7,8].

Using clay as filler, particularly MMT, due to its low cost, availability and environmentally friendly nature, plus its platelets high aspect ratio, when significantly exfoliated, has been one of the main approaches to synthesize PNCs for different applications, like in automotive [1,2] and packaging industries [2,3,5,9]. Regarding the level of mixing occurred between polymeric matrix and clay particles, morphology of resulted composites are traditionally categorized into groups of, microcomposites or phase-separated, intercalated nanocomposites, where the polymer chains diffuse between platelets of silicate and increase their basal planar spacing, without disorienting their parallel alignment, and exfoliated nanocomposites, where most of clay platelets delaminate from their aggregated stacks to form layers with nanoscale ranges [2,3,10]. Although other subsidiary terms like face-face coagulated intercalated stacks [11] face-edge and edge-edge flocculated exfoliation [11], or skewed tactoids [1] exist as well. In practice, usually most types of morphologies exist in the PNCs, and their morphology is assessed mainly based on the higher value of each of those microstructures [2,3,10,11]. In order to prepare highly exfoliated PNCs of fillers with high aspect ratios, different methods of solution processing [11–13], in-situ polymerization [14,15], melt processing [16–18], and combinations of those methods have been investigated [19,20]. Amongst these methods, melt mixing, due to its more direct features, not using chemicals, and being more compatible with conventional polymer processing methods has attracted more attentions [2]. To overcome

cohesion forces between clay platelets for impeding their intercalation and exfoliation, a significant level of interaction is needed to be made between clay and the polymeric matrix, to exploit the required shear stresses applied during processing, and to peel clay platelets from their aggregated clusters [1,11]. However, hydrophobic nature of polymers, particularly for polymers with nonpolar groups, (e.g. polypropylene, polyethylene, and polystyrene matrices) [1,2] is not in favor of promoting their interaction with the polar surface of the hydrophilic clay. So, organic modification of clay platelets, mainly using alkyl ammonium groups, have been tried to increase their interdistance and hydrophobicity and promote their interaction with polymeric matrix [1,3,13,14,21]. This induced intercalation and exfoliations can be detected through microscopic techniques, like TEM [1,4,11,15,17], in combination with methods like XRD, which mainly detects the increase in galleries between clay platelets through shifting their corresponding diffraction peaks towards lower diffraction angles [1,14,15,17,18]. Nevertheless, downside of such organic modifications, in addition to raising health concerns, which limit their usage to less than 5ppm, was their low thermal stabilities, making their melt processing challenging, particularly for polymers with higher melt processing temperature windows [18,22,23], since the resulted degradations and thermos-oxidations result in lower than expected PNC properties. Accordingly, this study, in a two-step procedure, endeavored to exploit polyelectrolyte (PE) interlayers in LBL assemblies [24,25], to promote intercalation and exfoliation of clay platelets in PNCs.

As mentioned before, through LBL deposition, PE interlayer works to provide stabilized intercalation and exfoliation of clay platelets in LBL coatings. Then, by mixing the intercalated and exfoliated LBL assemblies into the polymeric substrate matrix, with applying shear at

elevated temperatures, it was tried to use the PE interlayers, as providers of intercalation and exfoliation in LBL, for promoting exfoliation of neat MMT inside polymeric matrix (Figure 5.1). In fact, due to PE interaction with both polymeric matrix and MMT, it may potentially work as a bridge to transfer shear stresses applied through melt mixing to the clay phase to improve its dispersion throughout polymeric matrix yet more.

In order to investigate the resulted dispersion and exfoliation in polymer nanocomposites, we used polarized optical microscopy (POM), as a preliminary technique [11,26], and high magnification TEM micrographs [1,11,15,17]. In addition, we used XRD as a complementary investigating approach [1,14,15,17,18], for analyzing intercalation and or exfoliation of our PNCs.

5.2. Experimental

5.2.1. Materials

Poly(styrene-co-butadiene) (PS*) (density=1.04g/cm³ at 25°C, butadiene=4wt.%) was supplied by Sigma-Aldrich (St Louis, MO). Branched polyethyleneimine (PEI) (Mn=60kDa, Mw=750kDa, density=1.07 g/cm³ (at 20 °C)) in DIW (50wt%), was obtained from Scientific Polymer Products (Ontario, NY). The reason for using this grade of PEI instead of the alternative grade (Mw=25kDa, Mn=10kDa) investigated by other researchers [24,25], is its higher thermal stability, based on the previous study conducted in our group [23]. Polyethylene terephthalate ionomer (AQ55S) (PETi) (density =0.82 g/cm³) was generously granted by Eastman Chemical Company (Kingsport, TN). The purified nanoclay, Cloisite Na⁺, was purchased from Southern Clay Products (SCP) (Gonzales, TX), with cation exchange capacity

of 92mequiv/100g [27,28], and specific gravity of 2.86g/cm³ [28]. Irganox 1010, was supplied from Ciba and was used as an antioxidant to avoid thermal oxidation, during cyclic melt pressing procedure. Deionized water (DIW) as a media for PEI and MMT, with water resistivity of 18.2 MΩ at 25°C was prepared by Direct-Q 3 UV water purification system of Millipore [24,25]. Ultra high purity (99.999% purity) oxygen gas was acquired from National Welders Supply Co. (Charlotte, NC) and Air Liquid America Specialty Gases LLC (Plumsteadville, PA). High purity carbon dioxide (99.99% purity) was purchased from National Welders Supply Co. (Charlotte, NC).

5.2.2. Thin Film Preparation

Thin films of PS* were prepared through solution casting from toluene at room temperature, in crystallization plates, cleaned with acetone, methanol, and DIW, respectively. PS* (butadiene= 4wt %) was used as an alternative for pure polystyrene (PS), with too brittle thin films to be mounted and be sealed appropriately on the permeation cell equipment. About 0.1wt % Irganox 1010 was added to the polymer as an antioxidant to prevent samples thermal oxidation, during cyclic melt pressing procedure. The resulted films were heated up to 110°C (above PS glass transition temperature), under reduced air pressure, to assure complete removal of toluene.

5.2.3. Plasma Treatment

Oxygen plasma treatment of solution cast PS* films, with thickness of 100 μm, was done by a laboratory and small-scale production plasma system FEMTO (low-pressure plasma), manufactured by Diener Electronics (Germany) at power of 10W/cm², and gas flow rate of

20sccm (standard cubic centimeters per minute), or intensity of 0.5W/sccm, for 60s, to induce polar groups such as carbonyl and carboxylic acid for promoting hydrophilicity and surface adhesion properties of PS*, and to improve attraction and attachment of later on deposited polycations to its surface [29,30].

5.2.4. Layer-by-Layer (LBL) Coating of Thin Films

Solutions of PEI and PETi in DIW were made at 0.5wt%, which had showed optimum LBL morphology in our previous study (Chapter 3 and Chapter 4), were made through stirring at room temperature and 60°C (above PETi glass transition temperature), respectively. In fact, we used PETi, a PET with random anionic functionalities on its backbone for the first time, as an alternative for cationic PEI, for making LBL assemblies, since it had been used successfully for making polymer nanocomposites [20,31,32]. Slurries of MMT at 1wt% were prepared by 20 min ultrasonication of MMT in DIW, followed by stirring at about 600rpm for 24 hours, to reach to appropriate levels of exfoliation. For coating polymeric films with LBL assemblies, each sample was immersed in either of polyelectrolyte solutions for 5 minutes, followed by being rinsed with DIW and being dried under air flow. Then the same procedure was followed for making a coating of clay platelets on polyelectrolyte layer. This cyclic process was repeated until reaching to the desired number of bilayers (Figure 5.1). Due to the nature of the immersion process, bilayers are deposited on both sides of the polymeric substrate, but for simplicity, from now on we only count the number of bilayers (BLs) deposited on one side of the substrate in our remarks.

5.2.5. Cyclic Melt Pressing

The resulted coated membranes were pressed with a Carver standard hot press in a cyclic manner. To explain it further, each coated membrane was folded three times, and pressed between polyimide (PI) films, covering aluminum sheets, at 200°C, the typical PS melt processing temperature [21,33,34], at 3000 psi, following three minute preheating at pressing temperature. Then, the hot-pressed film was quenched, instantly, between big aluminum sheets, and the next pressing cycle was performed in a similar way. Accordingly, samples were pressed for up to 100 repetitive pressing cycles, like a baker's method.

5.2.6. Thermogravimetry (TGA)

TGA experiments were done for 10mg sample under air flow rate of 25ml/min and with a heating rate of 10C/min up to 700°C and 800°C, with Discovery TGA from TA Instruments in crucible platinum pans with high temperature resistant bails. All samples were dried in reduced pressure for 48h at 80°C before the experiments.

5.2.7. Polarized Optical Microscopy (POM)

Optical microscopy, for membranes of about 50µm thickness, was conducted on a Nikon Optiphot2-Pol polarizing optical microscope, and the pictures were taken with a Canon camera, to visualize the dispersion of clay particles in the composites.

5.2.8. Transmission Electron Microscopy (TEM)

Using freshly prepared glass knives and with a Leica Ultracut 7 at ambient condition, polymer nanocomposites were cut into sections of approximately 80nm thin, floated onto DIW, before being picked up on carbon coated 200 and 400 mesh copper TEM grids [16]. Then using

a JEOL 2000 FX (Parbody, MA) TEM at an accelerating voltage of 200kV and calibrated magnification, series of microscopic images were acquired from the microtomed thin sections.

5.2.9. X-Ray Diffractometry (XRD)

Wide angle x-ray diffractometry investigations for pre-dried samples (at 50°C for 48 h) were conducted at ambient temperature with CuK α radiation (wavelength $\lambda=0.15405$ nm), using either an Inel XRG 3000 diffractometer (Artenay, France) at 35kV and 30mA, or a Rigaku Rapid R-Axis Spider diffractometer (Rigaku, Texas) instrument, at 40kV and 36mA. The samples were probed in reflection mode using the Bragg-Brentano parafofocusing geometry (powders and films), and diffraction intensity data were usually recorded in diffraction angle range of 3.0° to about 40.0° [18].

5.3. Results and Discussion

5.3.1. Polarized Optical Microscopy

So, we used optical microscopy under cross-polarized light condition (POM) for preliminary morphological characterization of our composites, complementary to upcoming TEM and XRD investigations. In fact, despite capability of TEM and XRD for collaborative investigation of the possible occurrence of any exfoliations or intercalations in PNCs, POM micrographs, due to imaging samples in low magnification scales, can give a holistic view of dispersion and distribution of micron-size LBL assemblies' portions throughout polymeric matrix [11,26]. Under polarized light, amorphous polymeric matrix looks dark, while microscale clay inclusions, which scatter and depolarize it, are recognizable as bright spots.

For both PNC types containing PEI and PETi interlayers, it can be seen that with an increase in the number of pressing cycles from 25 to 100 (i.e. increase in time of melt mixing), dispersion (average sizes) and distribution of mashed portions of LBL assemblies in PS* matrix improves. Thus, it can be postulated that certain interactions arise between polymeric matrix and LBL assemblies that along with improve in distribution over extended time of mixing increase their dispersion noticeably [35] (Figures 5.2 and 5.3a, b).

However, with the rise in clay content of composites, by increased number of BL coatings, applied shears efficiency in crushing LBL assemblies into smaller portions decreases [11]. The noticeable reduction in the dispersion level of clay platelets in the matrix, with the increase in the loading towards 5wt% and higher, is a frequently observed problem for melt intercalated PNCs in literature, considered as the downside of this method [2,19]. Thus, in this static cyclic pressing method, insufficiency of global dispersion of clay platelets may be regarded as an inevitable result (Figures 5.2c, 5.2d, 5.3c, 5.3d).

Estimating Clay Content in PNCs. The volume percentages of LBL assemblies portions was determined through image analysis with Image J as an estimation of volume percentages of clay in PNCs [11,36] (Table 5.1). Moreover, as further explained in Chapter 6, by doing the TGA under air flow, clay contents of PNCs containing PEI interlayers in their LBL assemblies were estimated as the residue, after heating up to 600°C [37]. Comparing two data series determined from these two different approaches, showed a good correlation between them (Table 5.1) (i.e. ratio of clay volume, determined by TGA, to LBL assembly volume, estimated from POM images, is about 0.8 for all 3 samples, pointing to about 20% volume content of PE

in their LBL assemblies.), implying on accuracy of image analysis used, which were used with confidence for clay content estimation in PNCs henceforward, where due to thermal stability of PETi, it does not degrade completely at elevated temperatures used for TGA, up to 900°C. The reason for a little lower value for MMT content obtained from TGA (about 80% of image analysis results), might be due to the fact that assemblies observed and analyzed by POM, as TEM micrographs show, contain a fraction of intercalated polymeric interlayers, as well.

Comparing clay content estimated from image analysis of PNCs containing PETi in their LBL assemblies with the former PNCs, showed their relatively lower clay content. As mentioned in the previous study (Chapter 3), it can be a result of more clay platelets deposition during their LBL deposition procedure, due to possibly occurring more efficient interactions between cationic PEI with large negatively charged surfaces of clay platelets in deionized water, compared the interaction between anionic PETi with only positively-charged edges of clay platelets (Table 5.2).

5.3.2. Transmission Electron Microscopy

Since a TEM micrograph reveals the morphology in a very small region, it is usually taken in different magnification scales, from lower to higher, and from various parts of a PNC to be able to form a comprehensive picture of the PNC nanoscale intercalation and exfoliation morphology; complementary to POM images that depict microscale dispersion of clay particles. In bright-field TEM, clay platelets, due to their higher electron density look dark, while polymeric ingredients appear brightly. Accordingly, the dark lines represent cross-sections of clay platelets. It should be mentioned that since TEM images show random cuts

from irregular platelets, the aspect ratio observed is usually less than the real one, which can only be imaged through ideally vertical view at clay platelets. In effect, usually the length and thickness of platelets are observed respectively lower and higher than reality [1]. In our PNCs particularly this issue causes that platelets look thicker than what they are. On the other hand, due to the overlapping of clay platelets in LBL assemblies, usually a skewed agglomerate of them is mistaken as a single platelet with a length of a few times longer than what a single platelet can have [1,24] (Figure 5.4c).

In fact, as both POM (Figures 5.2, 5.3) and TEM micrographs (Figures 5.5, 5.6), in low magnification scales showed, clay particles in PNCs are mostly in the shape of microscale clusters [38], which are in fact, crushed portions of LBL assemblies with size ranges of up to a few micrometers, which may reflect forming of a microcomposite in the first glance [1,37]. Clay aggregations with comparable sizes and shapes had previously been observed for polystyrene-based PNCs in the literature [15,39]. However, further investigations of embedded clay particles, in TEM micrographs with higher magnification scales showed their internal structure comprising, lamellar stacks [37,38] of expanded (and face-face coagulated) intercalations [2,10,38] and (edge-edge and edge-face) flocculated (and skewed) exfoliated [1,2,11] clay platelets tactoids, in form of bundles of nanoclay [40], down to 2nm thick (Figures 5.4, 5.5, 5.6).

It should be mentioned that the reason for such edge to edge bridging, which had already been observed in LBL assemblies, in addition to being a feature of LBL assemblies and electrostatic attractions between consecutive layers, can be sought in interaction between

hydroxyl groups located on clay platelets edges, formed as a result of hydration of silicon oxide (SiO) groups into silicon hydroxide (SiOH) in water [2,15].

In fact, these PNCs inherited the initial stable swollen intercalations and flocculated exfoliations provided in LBL assemblies. Then, through cyclic pressing procedure, and applying shear and stress, at elevated temperatures, on samples, from one side, LBL assemblies are broken into smaller particles (macro crashing), and from the other hand, swelling of their face-face coagulated and intercalated stacks [2,10] and exfoliation of their edge-edge and edge-face flocculated and skewed tactoids increase (micro crashing); in addition, occasionally sole platelets are released into the matrix, out of those expanded LBL portions [38].

The increased interdistance and disorientation of clay layers (tactoids), relative to the initial LBL coatings, can be recognized in both TEM micrographs and XRD plots (decrease in both diffraction angle of peaks corresponding to gallery between clay platelets (increased intercalation) and size of those diffraction peaks (disorientation)). Thus, those expanded and somewhat internally disoriented LBL portions inside polymeric matrix form tortuous labyrinths consisting nanoscale expanded intercalated and edge-edge or face-edge flocculated exfoliated tactoids of a few platelets. So, they may potentially be able to act as scavenging black holes against transport of gases or fluids through the PNC membranes, eventually improving its barrier properties and thermal stabilities (more than what expected from a microcomposite in that low content of clay). In addition, pressing samples into thin films, as an analogy to biaxial stretching, can also direct more split and orientation in already intercalated and exfoliated platelets, respectively, to improve barrier and mechanical properties of prepared PNCs further [16]. Nevertheless, it may be conjectured that due to existing fairly

strong internal cohesion in LBL assemblies, insufficient intensity of shear stress applied on samples, through cyclic hot pressing, and/or lack of a sufficiently strong interaction between LBL assemblies and polymeric matrix [1], no global nanodispersion of LBL assemblies occurs throughout the matrix (Figures 5.4, 5.5, 5.6).

To sum up, investigating TEM micrographs of all samples for PNCs with both interlayer types of PEI and PETi, it can be noticed that despite observing some slight trends, like higher thickness of LBL portions for 15BLs, and lower ones for 5BLs (Figures 5.5 and 5.6), the morphology of each condition is so diverse, comprising all aforementioned morphologies. For instance, for samples pressed for 25cycles, uncrushed long LBL assemblies are observable, while exfoliated individual clay platelets are present as well; or for 100cycle pressing, despite existing exfoliated platelets, some uncrushed LBL assemblies are noticed. Thus, although POM images (and possibly XRD) show some aforementioned qualitative trends in PNCs, with change in time of processing and number of BLs, TEM micrographs demonstrate, in each sample (no matter what condition is), most of possible theoretical morphologies (uncrushed LBL assemblies, intercalation, exfoliation,...) occur.

5.3.3. X-Ray Diffractometry

Mainly XRD is used for crystallographic investigation of clay particles in a composite, particularly to detect shift or possible disappearance of the characteristic peaks corresponding to the basal planar spacing of clay platelets, to discern occurrence of intercalation or exfoliation, in collaboration with microscopic images taken through TEM [2]. As mentioned in Chapter 3, XRD diffractograms showed a peak at 8.37° , corresponding to a basal (001)

distance of 1.056nm for neat MMT [24,25], and LBL assemblies made from MMT and alternative polyelectrolytes of PEI and PETi showed shift in the corresponding diffraction peaks to lower angles, pointing to increase in MMT interplanar spacing, as a result of polyelectrolytes intercalation between clay platelets. In this study, XRD patterns of cyclically pressed PNCs were investigated accordingly.

As a result, XRD plots for cyclically melt pressed PNCs showed slightly increased shifts in the characteristic peak corresponding to the basal planar spacing of clay platelets, compared with LBL coatings. It implies an increase in the distance between clay platelets in their intercalated stacks (Figures 5.7, 5.8). This type of increase in swelling of intercalated stacks, driven by shear stresses applied during cyclic pressing, via occurred interactions between polymeric matrix and LBL assemblies, was already observed through TEM micrographs. Also, it can be seen that with increase in number of melt pressing cycles (i.e. melt mixing time) and decrease in the number of BL coatings (i.e. decrease in clay content), slight shifts in their characteristic peaks towards smaller diffraction angles are observed, to propose their increased intercalations and exfoliations [35]. These results are in accordance with those of aforementioned microscopic investigations.

In the case of PNCs containing PETi, in particular, both shift of characteristic diffraction peaks and their broadening trends towards lower diffraction angles are more noticeable for samples prepared through extended time of mixing (100 melt pressing cycles). It proposes increasing in both value and variation of the average interdistance between their clay platelet inclusions. Thus, it may be conjectured that PETi makes a better interaction with polymeric matrix to transfer the shear stress applied during melt processing to the clay platelets, to

promote their intercalation and exfoliations [35], which might be due to better chemical affinity of PETi with polystyrene-based matrix, relative to that of alternative PEI interlayers (Later on, DMA results (Chapter 6) confirmed the occurrence of this stronger interaction.). Another possible reason for these findings may be the higher thermal stability of PETi, compared with PEI, resulted from their thermogravimetric investigations (Chapter 6).

This broadening and belittling of the intercalation peaks were more significant for PNCs with lower clay content, proposing their higher level of exfoliations [11,22]. So, it might be conjectured that interaction made between polymer and clay is strong enough to overcome the van der Waals forces in galleries between clay layers, to detach clay platelets from each other, into a disrupted exfoliated structure, when the clay content is relatively small. On the other hand, when clay content increases, the aforementioned interaction between polymer and clay can only result in a swollen intercalated state of clay platelets, without disrupting their orientations [2,11,22].

5.4. Conclusions

As almost comprehensive morphological investigations, with polarized optical microscopy (POM), transmission electron microscopy (TEM), and x-ray diffractometry (XRD) showed, the PNCs prepared through cyclic melt pressing of LBL-coated polystyrene-based membranes, are complex combinations of different morphologies; since, cyclically melt pressed portions of LBL assemblies are ground into swollen intercalated (almost oriented) stacks of bilayers and tail-to-tail, face-to-tail flocculated exfoliated (nearly disoriented) tactoids of a few platelets. In addition, there are layers of a few, down to individual, clay platelets, peeled from

LBL assemblies' portions, as dispersions inside the polymeric matrix. In fact, although POM and almost XRD, experiments showed some qualitative trends in PNCs, pointing to improved dispersion, intercalation, and exfoliation, with increase in time of processing and decrease in number of coating BLs (i.e. clay content), TEM micrographs tracked appearance of entire aforementioned morphologies for all PNC samples prepared under various conditions (different contents of clay and time of melt processing).

Also, from increased intercalation and exfoliation of clay platelets in cyclically pressed PNCs, containing either of PEI or PETi alternative polyelectrolyte interlayers in their LBL assemblies, compared with morphologies of initial LBL assemblies coatings, investigated in Chapter 3, it can be postulated that substantial interactions between LBL assemblies and matrix have occurred, as a clue to the compatibilizing role of polyelectrolyte interlayers. Nevertheless, minor extent of global nanodispersion of clay platelets throughout the PS* matrix might conjecture insufficiency of shear stress, applied through cyclic melt pressing, along with the low potential of polyelectrolytes to interact intensely with clay and hydrophobic polymeric matrix, against the existing cohesion in LBL assemblies.

Tables

Table 5.1. Estimation of the clay content in PNCs containing PEI interlayers through both image analysis and TGA residue at 600°C (Inorganic residues of PNC samples after being heated under airflow up to 600°C).

Composition PS*, PEI, MMT, PNC	POM		TGA
	LBL Particle vol%	MMT wt% (600 °C)	MMT vol%
5BL	1	2.2	0.8
10BL	1.47	3.2	1.16
15BL	2.25	5.1	1.85

Table 5.2. Estimation of the clay content in PNCs containing PETi interlayers through image analysis.

Composition PS*, PETi, MMT, PNC	POM LBL Particle vol%
5BL	0.6
10BL	1.25
15BL	1.65

Figures

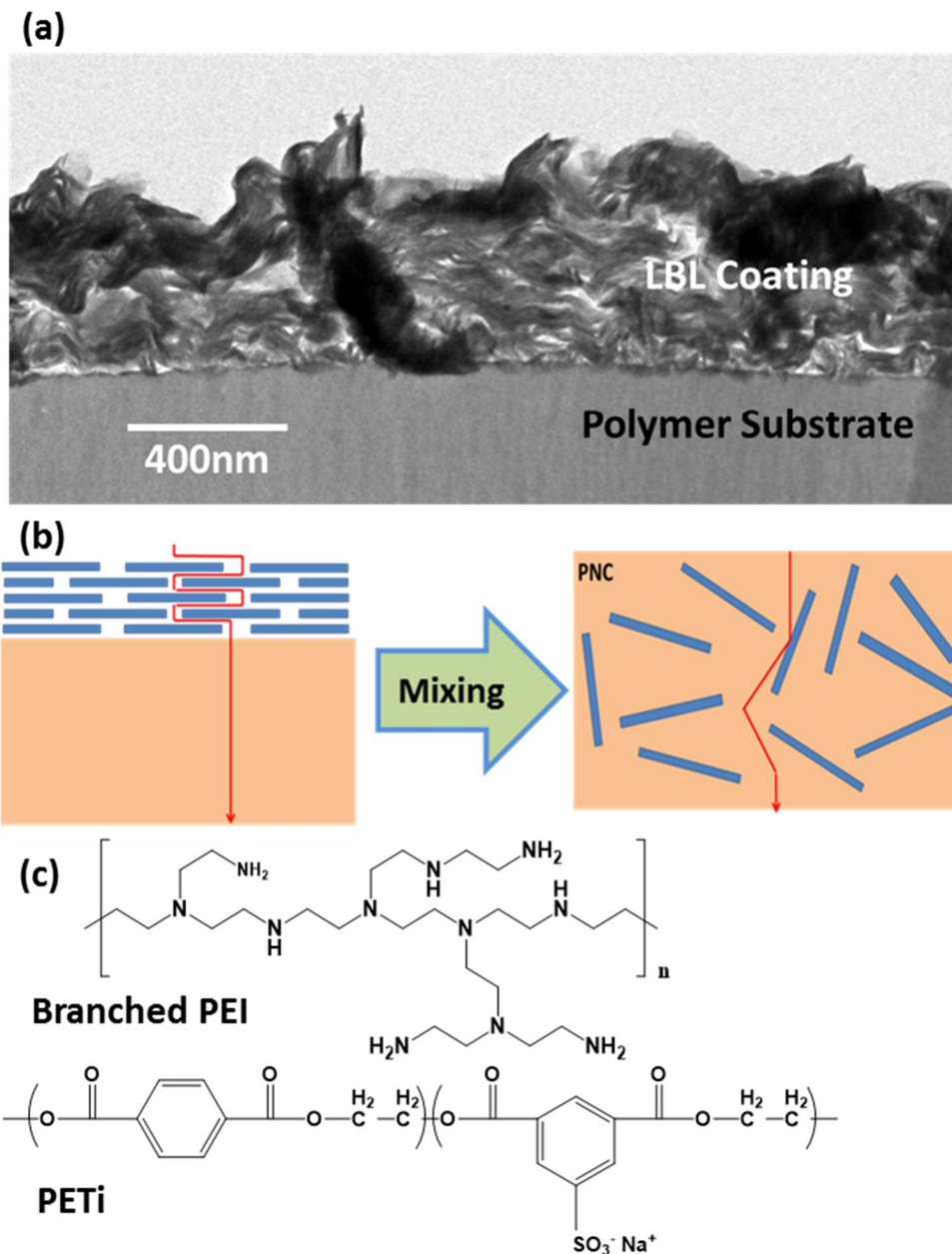


Figure 5.1. (a) Cross-section of a TEM image of a polymeric membrane coated with LBL assemblies of PEI and MMT. (b) Schematic of a polymer layer coated with LBL assemblies, the polymer nanocomposite (PNC) resulted after cyclic hot pressing and gas permeation route in them. (c) Chemical formulae of two alternative polyelectrolyte interlayers, PEI and PETi.

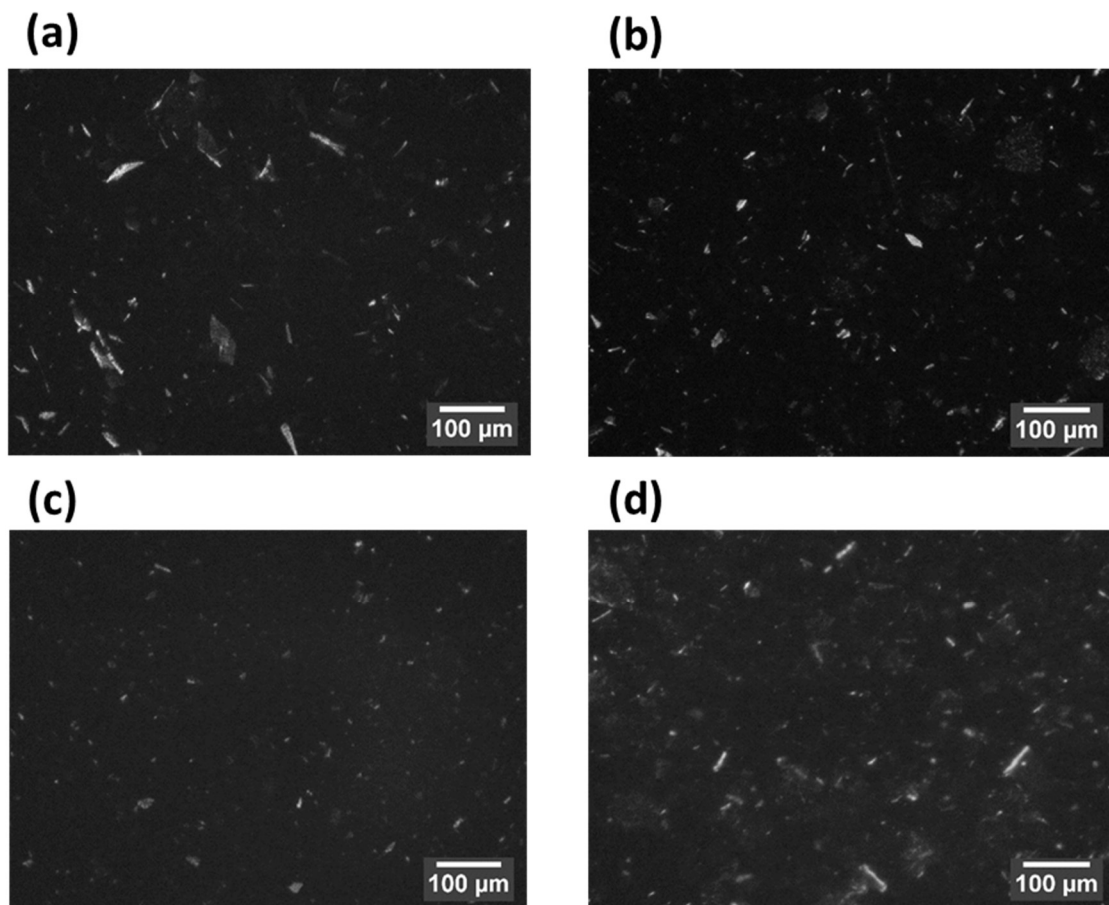


Figure 5.2. Optical microscope images of PNCs of PS* matrix, with PEI and MMT LBL assemblies, for (a) 10 times deposition of BL coating, after 25 cycles of melt pressing, and for 100 cycles pressing when the samples were coated with (b) 10, (c) 5, and (d) 15 times of BL depositions.

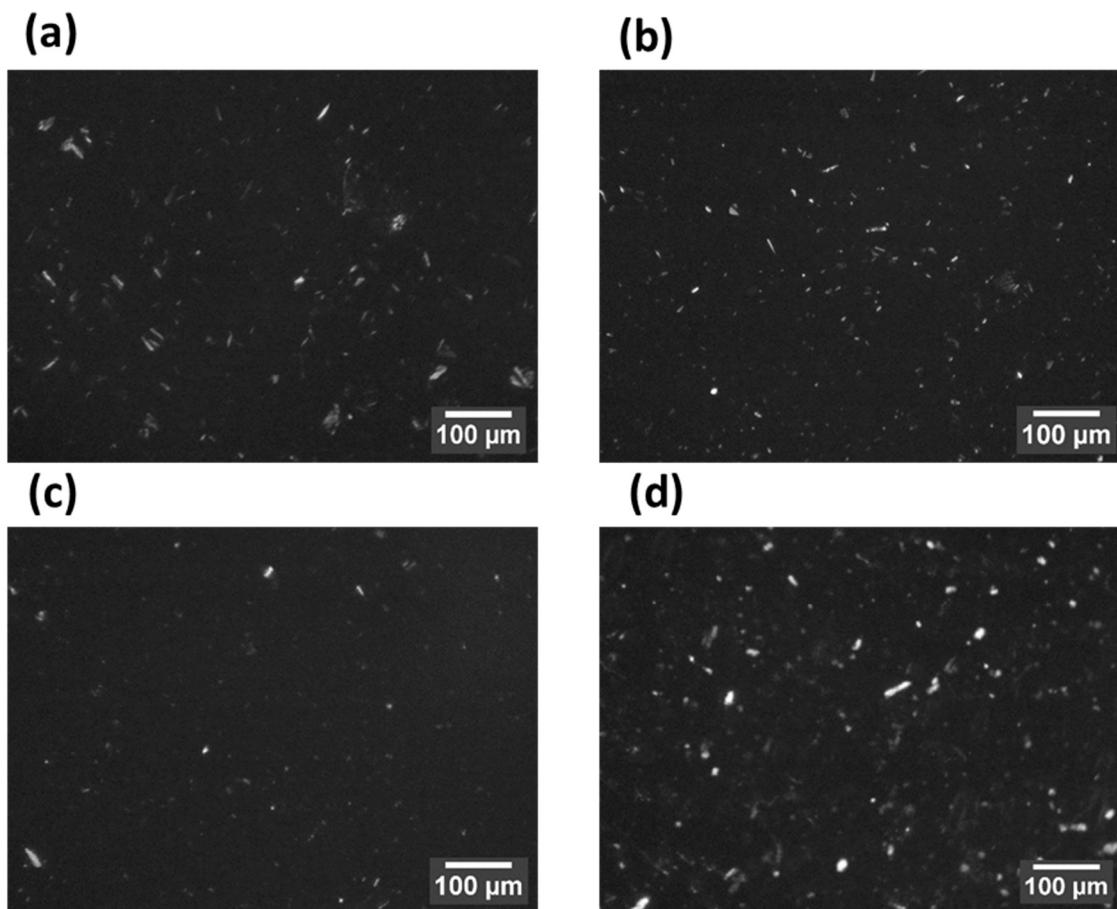


Figure 5.3. Optical microscope images of PNC of PS* matrix, with PETi and MMT LBL assemblies, for (a)10 times deposition of BL coating, after 25 cycles of melt pressing , and for 100 cycles pressing when the samples were coated with (b) 10, (c) 5, and (d)15 times of BL depositions.

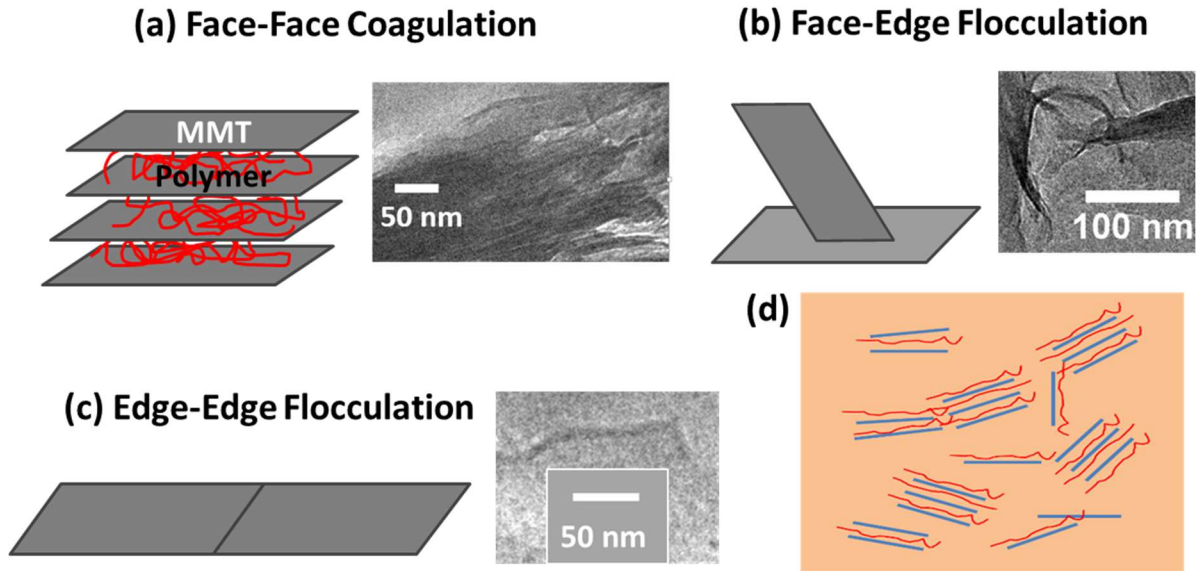


Figure 5.4. Schematic Figures of LBL assemblies' portions in PNC and their typical morphologies: (a) face-face coagulated intercalation of expanded stacks, (b) face-edge and (c) edge-edge flocculated and exfoliated platelets or tactoids of a few platelets, beside their TEM images. (d) Schematic of overall dispersion and distribution of crunched LBL assemblies inside the polymeric matrix.

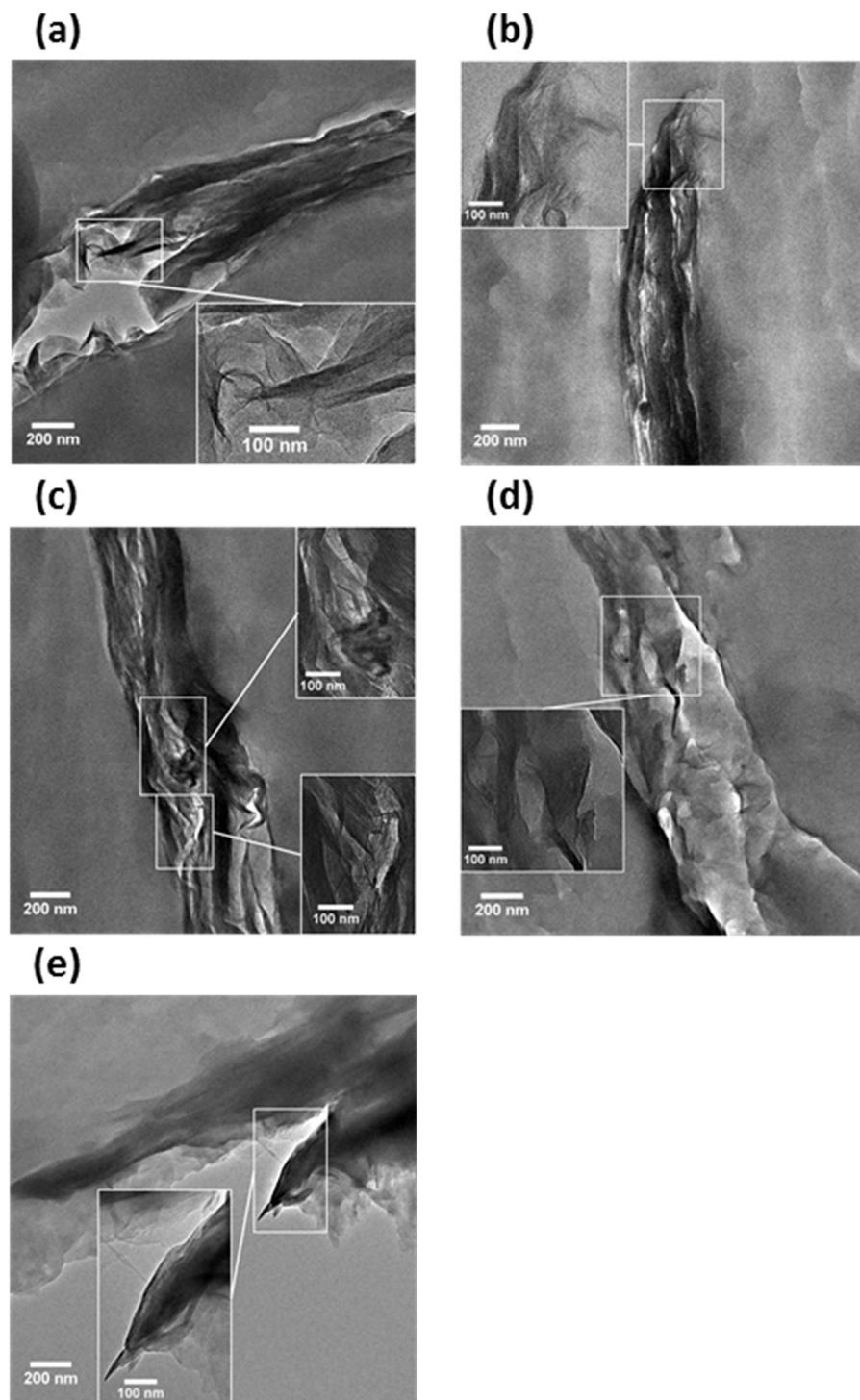


Figure 5.5. TEM micrographs of 100 cycles pressed PNCs containing PEI interlayers in their LBL assemblies portions comprising (a) 5, (b), (c), (d) 10, and (e) 15, -BL coatings.

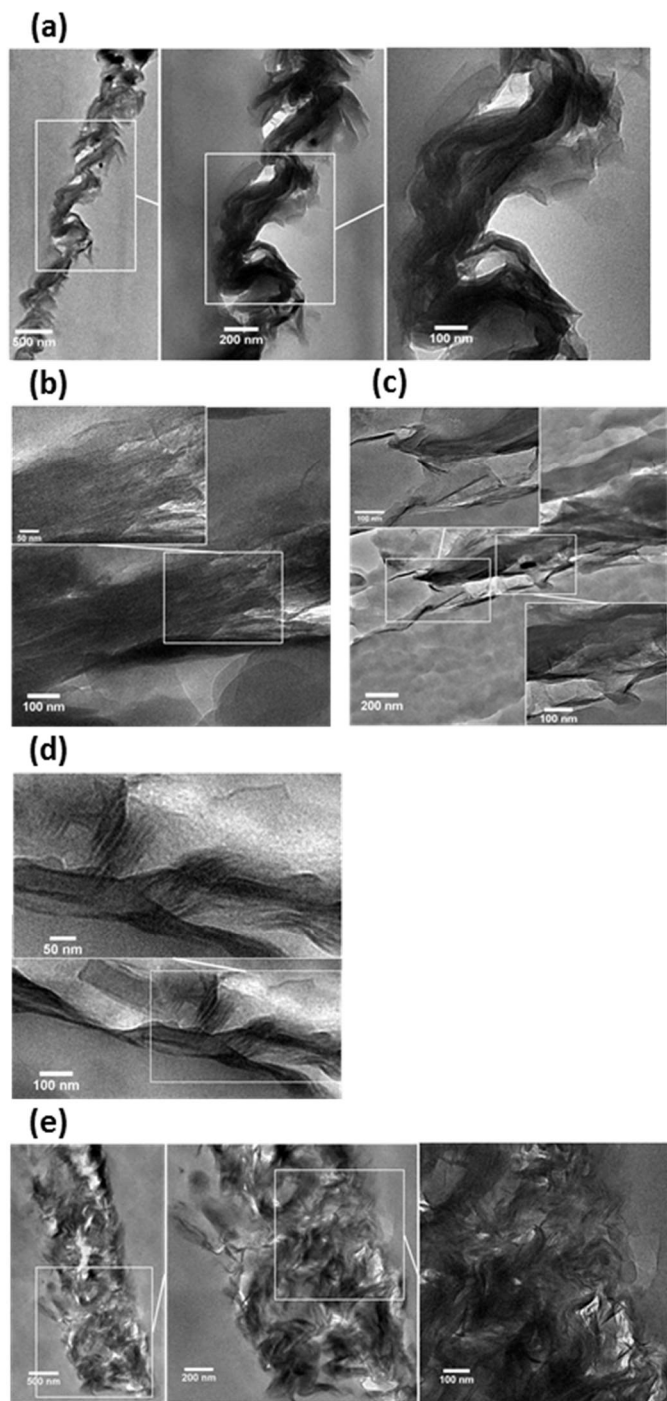


Figure 5.6. TEM micrographs of PNCs containing PETi interlayers in their LBL assemblies portions comprising (a) 10BL coatings, pressed for 25cycles, and (b), (c) 100 cycles; (d) 5BL coatings, (e) 15BL coatings, both pressed for 100 cycles.

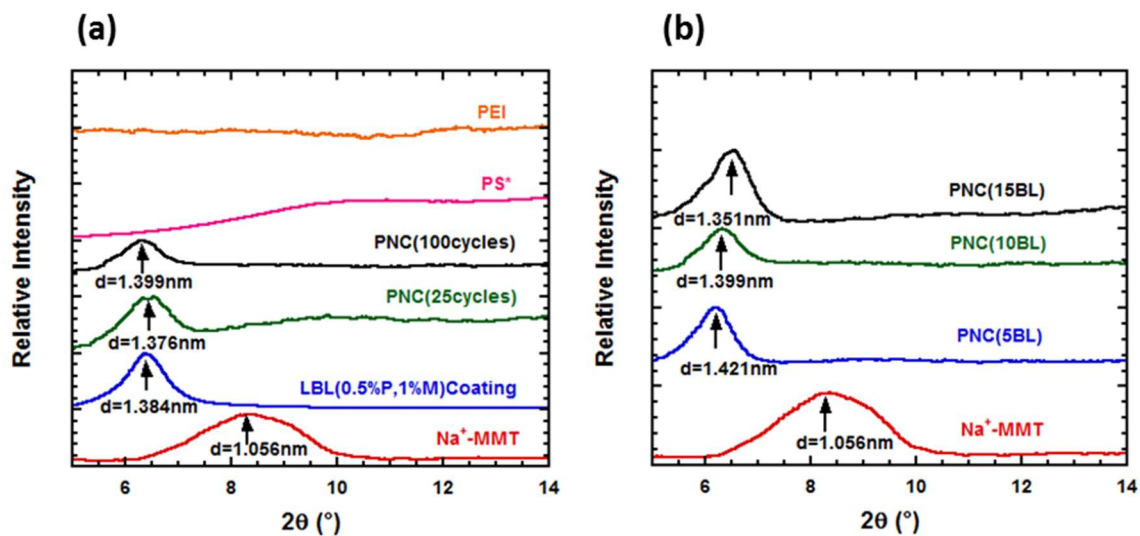


Figure 5.7. XRD patterns for neat MMT, its LBL assemblies coating with PEI, and melt processed PNC with (a) different numbers of pressing cycles of 25 and 100 and (b) different numbers of deposited BL's coatings of 5, 10, and 15.

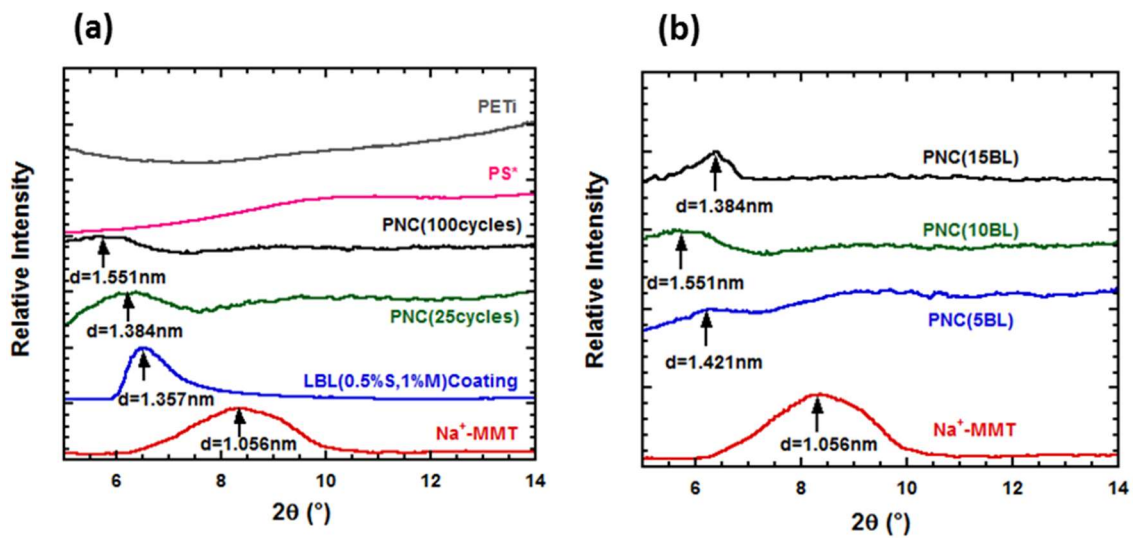


Figure 5.8. XRD patterns for neat MMT, its LBL assemblies coating with PETi, and melt processed PNC with (a) different numbers of pressing cycles of 25 and 100 and (b) different numbers of deposited BLs coatings of 5, 10, and 15.

References

- [1] D.R. Paul, L.M. Robeson, Polymer nanotechnology: Nanocomposites, *Polymer*. 49 (2008) 3187–3204.
- [2] S.S. Ray, Recent Trends and Future Outlooks in the Field of Clay-Containing Polymer Nanocomposites, *Macromol. Chem. Phys.* 215 (2014) 1162–1179.
- [3] V. Mittal, *Optimization of Polymer Nanocomposite Properties*, 1st ed., Wiley-VCH, Weinheim, Germany, 2010.
- [4] L.C. Sawyer, D.T. Grubb, G.F. Meyers, *Polymer microscopy*, 3rd ed., Springer, New York, NY, USA, 2007.
- [5] G.W. Beall, C.E. Powell, *Fundamentals of Polymer-Clay Nanocomposites*, 1st ed., Cambridge University Press, Cambridge, UK, 2011.
- [6] M. Song, J. Jin, Rheological behavior of polymer nanocomposites, in: V. Mittal (Ed.), *Optim. Polym. Nanocomposite Prop.*, 1st ed., Wiley-VCH, Weinheim, Germany, 2010: pp. 93–122.
- [7] M.A. Priolo, D. Gamboa, J.C. Grunlan, Transparent clay– polymer nano brick wall assemblies with tailorable oxygen barrier, *ACS Appl. Mater. Interfaces*. 2 (2010) 312–320.
- [8] P.F. Carcia, R.S. McLean, M.H. Reilly, Permeation measurements and modeling of highly defective Al₂O₃ thin films grown by atomic layer deposition on polymers, *Appl. Phys. Lett.* 97 (2010) 221901–221903.
- [9] S. Ray, S.Y. Quek, A. Eastal, X.D. Chen, The potential use of polymer-clay nanocomposites in food packaging, *Int. J. Food Eng.* 2 (2006).
- [10] M. Galimberti, Rubber Clay Nanocomposites, *Adv. Elastomers – Technol. Prop. Appl.* (2012).
- [11] A. Ranade, N.A. D’Souza, B. Gnade, Exfoliated and intercalated polyamide-imide nanocomposites with montmorillonite, *Polymer* 43 (2002) 3759–3766.
- [12] A. Bansal, H. Yang, C. Li, K. Cho, B.C. Benicewicz, S.K. Kumar, et al., Quantitative equivalence between polymer nanocomposites and thin polymer films., *Nat. Mater.* 4 (2005) 693–698.
- [13] A. Giannakas, A. Giannakas, A. Ladavos, Preparation and Characterization of

Polystyrene/Organolaponite Nanocomposites, *Polym. Plast. Technol. Eng.* 51 (2012) 1411–1415.

- [14] K.J. Lin, C.H. Lee, K.F. Lin, Extraordinary mechanical behavior of exfoliated montmorillonite/polymer nanocomposite films cast from soap-free emulsion polymerized latices, *J. Polym. Sci. Part B Polym. Phys.* 48 (2010) 1064–1069.
- [15] S. Nazarenko, P. Meneghetti, P. Julmon, B.G. Olson, S. Qutubuddin, Gas barrier of polystyrene montmorillonite clay nanocomposites: Effect of mineral layer aggregation, *J. Polym. Sci. Part B Polym. Phys.* 45 (2007) 1733–1753.
- [16] W. Huang, S. Zeng, J. Liu, L. Sun, Bi-axially oriented polystyrene/montmorillonite nanocomposite films, *RSC Adv.* 5 (2015) 58191–58198.
- [17] J. Golebiewski, A. Galeski, Thermal stability of nanoclay polypropylene composites by simultaneous DSC and TGA, *Compos. Sci. Technol.* 67 (2007) 3442–3447.
- [18] D.J. Frankowski, M.D. Capracotta, J.D. Martin, S. a. Khan, R.J. Spontak, Stability of organically modified montmorillonites and their polystyrene nanocomposites after prolonged thermal treatment, *Chem. Mater.* 19 (2007) 2757–2767.
- [19] M. Ziadeh, B. Fischer, J. Schmid, V. Altstädt, J. Breu, On the importance of specific interface area in clay nanocomposites of PMMA filled with synthetic nano-mica, *Polymer* 55 (2014) 3770–3781.
- [20] A. Ammala, C. Bell, K. Dean, Poly (ethylene terephthalate) clay nanocomposites: improved dispersion based on an aqueous ionomer, *Compos. Sci. Technol.* 68 (2008) 1328–1337.
- [21] A. Panwar, V. Choudhary, D.K. Sharma, Review: A review: polystyrene/clay nanocomposites, *J. Reinf. Plast. Compos.* 30 (2011) 446–459.
- [22] N. Greesh, S.S. Ray, J. Bandyopadhyay, S. Sinha Ray, J. Bandyopadhyay, Role of nanoclay shape and surface characteristics on the morphology and thermal properties of polystyrene nanocomposites synthesized via emulsion polymerization, *Ind. Eng. Chem. Res.* 52 (2013) 16220–16231.
- [23] A.E. Özçam, Surface Modification and Characterization of Polymeric Materials for Targeted Functionality. Ph.D. Dissertation, North Carolina State University, 2011.
- [24] M.A. Priolo, K.M. Holder, D. Gamboa, J.C. Grunlan, Influence of clay concentration on the gas barrier of clay–polymer nanobrick wall thin film assemblies, *Langmuir.* 27 (2011) 12106–12114.
- [25] Y.-H. Yang, F.A. Malek, J.C. Grunlan, Influence of deposition time on layer-by-layer

growth of clay-based thin films, *Ind. Eng. Chem. Res.* 49 (2010) 8501–8509.

- [26] S.M. Miriyala, Y.S. Kim, L. Liu, J.C. Grunlan, Segregated Networks of Carbon Black in Poly (vinyl acetate) Latex : Influence of Clay on the Electrical and Mechanical Behavior, *Macromol. Chem. Phys.* 209 (2008) 2399–2409.
- [27] M. Pluta, A. Galeski, M. Alexandre, M. a. Paul, P. Dubois, Polylactide/montmorillonite nanocomposites and microcomposites prepared by melt blending: Structure and some physical properties, *J. Appl. Polym. Sci.* 86 (2002) 1497–1506.
- [28] M.N. Muralidharan, S.A. Kumar, S. Thomas, Morphology and transport characteristics of poly(ethylene-co-vinyl acetate)/clay nanocomposites, *J. Memb. Sci.* 315 (2008) 147–154.
- [29] I. Beaulieu, M. Geissler, J. Mauzeroll, Oxygen plasma treatment of polystyrene and zeonor: Substrates for adhesion of patterned cells, *Langmuir.* 25 (2009) 7169–7176.
- [30] C. Chaiwong, P. Rachtanapun, P. Wongchaiya, R. Auras, D. Boonyawan, Effect of plasma treatment on hydrophobicity and barrier property of polylactic acid, *Surf. Coatings Technol.* 204 (2010) 2933–2939.
- [31] A. Ghanbari, M.-C.C. Heuzey, P.J. Carreau, M.-T.T. Ton-That, Morphology and properties of polymer/organoclay nanocomposites based on poly(ethylene terephthalate) and sulfopolyester blends, *Polym. Int.* 62 (2013) 439–448.
- [32] X.F. Xu, A. Ghanbari, W. Leelapornpisit, M.C. Heuzey, P. Carreau, Effect of Ionomer on Barrier and Mechanical Properties of PET/Organoclay Nanocomposites Prepared by Melt Compounding, *Int. Polym. Process.* 26 (2011) 444–455.
- [33] C. Zeng, L.J. Lee, Poly (methyl methacrylate) and polystyrene/clay nanocomposites prepared by in-situ polymerization, *Macromolecules.* 34 (2001) 4098–4103.
- [34] U. Yilmazer, G. Ozden, Polystyrene–organoclay nanocomposites prepared by melt intercalation, in situ, and masterbatch methods, *Polym. Compos.* 27 (2006) 249–255.
- [35] W. Lertwimolnun, B. Vergnes, Influence of compatibilizer and processing conditions on the dispersion of nanoclay in a polypropylene matrix, *Polymer* 46 (2005) 3462–3471.
- [36] T.D. Fornes, D.R. Paul, Modeling properties of nylon 6/clay nanocomposites using composite theories, *Polymer* 44 (2003) 4993–5013.
- [37] D. Wang, C. Wilkie, In-situ reactive blending to prepare polystyrene–clay and polypropylene–clay nanocomposites, *Polym. Degrad. Stab.* 80 (2003) 171–182.
- [38] F. Bertini, M. Canetti, G. Audisio, G. Costa, L. Falqui, Characterization and thermal

degradation of polypropylene-montmorillonite nanocomposites, *Polym. Degrad. Stab.* 91 (2006) 600–605.

- [39] C. Dazhu, Y. Haiyang, H. Pingsheng, Z. Weian, Rheological and extrusion behavior of intercalated high-impact polystyrene/organomontmorillonite nanocomposites, *Compos. Sci. Technol.* 65 (2005) 1593–1600.
- [40] S.H. Kim, S.C. Kim, Synthesis and Properties of Poly (ethylene terephthalate)/ Clay Nanocomposites by In Situ Polymerization, 103 (2007) 1262–1271.

CHAPTER 6

Transport, Mechanical, and Thermal Properties of Polymer Nanocomposites Derived from Layer-by-Layer Coated Polystyrene-Based Membranes

Abstract

As mentioned in the previous morphological investigations in Chapter 6, particular preparation method of our innovative polymer nanocomposites (PNCs), through initial layer-by-layer (LBL) coating of polymeric samples and then crushing those LBL assemblies inside the polymeric matrix resulted in morphologies, different with the ones expected from more traditional methods of PNC formation, mainly including crushed and expanded portions of LBL assemblies, comprising swollen intercalated stacks of montmorillonite (MMT) platelets and flocculated exfoliated tactoids of a few MMT platelets, down to 2nm thick, along with sole platelets released into the matrix, outside those expanded LBL portions. In this article, dynamic mechanical and thermal, as well as transport properties of these novel PNCs were investigated. In fact, polystyrene-based PNCs, prepared from both alternative polyelectrolyte interlayers, polyethyleneimine (PEI) and polyethyleneterephthalate ionomer (PETi), in their LBL assemblies showed the increase in moduli values that confirmed the occurrence of significant interactions between LBL assemblies and polystyrene-based matrix, induced by the compatibilizing effect of polyelectrolyte interlayers. Also, particularly in the case of PETi interlayers and for an extended time of melt processing, a significant shift in the glassy transition temperature of minor polybutadiene (PB) component of the matrix appeared, towards higher temperatures, which might be related to relatively high compatibility of PETi

and PB. Moreover, barrier improvement resulted for these PNCs, particularly for the ones with PETi interlayers, showed relatively significant improvement, greater than the extent expected from their moderately dispersed morphologies as well as their low content of clay. Thus, it might be conjectured that these tortuous mazes, with high aspect ratios (crushed LBL assemblies' portions), may act as scavengers against transport of gases throughout the PNC membrane. But, their behavior is different from, theoretical models, based on fully dispersed impermeable clay plates in a matrix. Comparing two alternative interlayers, it seems that occurring some slight degradation, during long times of melt mixing at elevated temperatures in PEI, would pose an adverse effect on its efficiency, as a compatibilizer, and consequently on final mechanical and barrier properties of prepared PNCs.

6.1. Introduction

Preparing composites through embedding filler in polymers is one of the main approaches to improve their various properties towards desired aims. In the case of polymer nanocomposites, a decrease in the size of dispersions increases their aspect ratio and their interfaces with the polymeric matrix to intensify its efficiency in the constant level of filler loading [1–3]. For improving barrier properties of polymeric membranes, despite the high efficiency of different single and multilayer coatings, they are prone to defects or being peeled off the substrate [4,5]. On the other hand, polymer nanocomposite approaches, with a global market of one billion dollars in 2012 [6] are usually considered as comprehensive methods for improving various physical and mechanical properties of the pristine polymer, in addition to

improving its barrier properties against gases and fluid. Besides, polymer nanocomposites are processable through conventional polymer processing techniques [2,3].

Polymer-clay nanocomposite, which due to cheap cost, availability, and eco-friendly features of clay are considered as one of the main polymer nanocomposites, are classically divided into categories of phase-separated microcomposites, intercalated nanocomposites, where polymer chains diffuse between clay platelets and separate them, without disordering their orientations, and exfoliated and delaminated polymer nanocomposites. Nevertheless, most real polymer nanocomposites are in fact combinations of these morphologies. Thus, they are labeled by the most plentiful microstructure they possess [2,7,8]. In fact, when the clay platelets are exfoliated appropriately, they can increase the tortuosity of the polymeric matrix significantly [1,9], and increase its barrier properties against gases and fluid [2,10–13], and its thermal stability [2,10,14,15], whereas, aggregated stacks as the centers for heat accumulation may work in favor of a thermal decomposition of polymeric matrix [2]. This increased interfacial area can also raise the moduli of PNCs, more meaningfully than those of conventional composites, considering low contents of clay embedded in their polymeric matrix [16–18]. Besides, nanodispersed clay platelets, when their interdistance is lower than polymer chains gyration radii, through changing the free volume of the polymeric chain, with a mechanism called nanoconfinement effect, depended on the strength of their interactions with polymers, can have increasing or decreasing effect on its glass-rubbery transition temperatures [1,2,17,18].

Between three main methods of preparing the PNCs, solution intercalation [2,13,17], in-situ polymerization, [16,11], and melt intercalation, the last one, due to its compatibility with

conventional polymer processing techniques, and being more ecologically aware, has been practiced more [2,10,15,19]. In addition, there have been studies on different combinations of the aforementioned methods [20,21].

Organic modifications of clay platelets, mainly with alkyl ammonium groups, have frequently been studied to increase the interaction made between hydrophilic clay and polymers, particularly nonpolar polymers, with hydrophobic natures [1,2]. Thus, the shear stress applied through processing would be able to delaminate clay platelets out of their aggregated clusters, into exfoliated polymer nanocomposites. However, low thermal stabilities of these modifying groups make them vulnerable to degradation at high temperatures of melt processing, to pose an adverse effect on properties of resulted PNCs [2,19,22].

Therefore, in this study, as mentioned in the previous one (Chapter 5), it was attempted to promote intercalation and exfoliation of clay platelets through taking advantage of the structure of LBL assemblies [4], where polyelectrolyte (PE) interlayers were intercalated between clay platelets. So, by cyclic pressing of LBL coating on the polystyrene-based substrates, those coating assemblies are crushed into the bulk of polymeric matrix, to make polymer nanocomposite. Thus, PE interlayers can potentially increase interaction of hydrophobic matrix with clay, in order to conduct shear stress applied for dispersing the clay platelets towards forming exfoliated polymer-clay nanocomposites (Figure 6.1).

After morphological investigations made in the previous study (Chapter 5), in this chapter we scrutinized barrier properties, besides performing dynamic mechanical thermal analysis, for our PNCs prepared through two-step approach of LBL coating and cyclic melt pressing, for PS-based matrices. Also, we probed possible trends obtained and their potential correlation

with their morphologies already investigated in Chapter 5. In addition, some minor thermal properties investigations were performed to provide additional support for the accuracy of our barrier and dynamic mechanical measurements [15,17,22].

6.2. Experimental

6.2.1. Materials

Poly(styrene-co-butadiene) (PS*) (density=1.04g/cm³ at 25°C, butadiene=4wt.%) was obtained from Sigma-Aldrich (St Louis, MO). Branched polyethyleneimine (PEI) (Mn=60kDa, Mw=750kDa, density=1.07g/cm³ (at 20°C)) in DIW (50wt%), with demonstrated higher thermal stability, based on the previous investigation conducted in this group [19], relative to its alternative (Mw=25kDa, Mn=10kDa) studied by other scholars [4] was acquired from Scientific Polymer Products (Ontario, NY). Polyethylene terephthalate ionomer (AQ55S) (PETi) (density =0.82 g/cm³) was kindly bestowed by Eastman Chemical Company (Kingsport, TN). The purified nanoclay, Cloisite Na⁺, with the specific gravity of 2.86g/cm³ [23] and cation exchange capacity of 92mequiv/100g [23], was procured from Southern Clay Products (SCP)(Gonzales, TX). Irganox 1010, as antioxidant from Ciba, was used to prevent possible thermal oxidation, via cyclic melt pressing procedure. Deionized water (DIW) with water resistivity of 18.2 MΩ at 25°C, was made by Direct-Q 3 UV water purification system of Millipore, and it was used as a media for PEI and MMT [4]. Ultra high purity (99.999% purity) O₂ was bought from National Welders Supply Co. (Charlotte, NC) and Air Liquid America Specialty Gases LLC. (Plumsteadville, PA). High purity CO₂ (99.99% purity) was purchased from National Welders Supply Co. (Charlotte, NC).

6.2.2. Thin Film Preparation

Thin films of PS* were prepared in pre-cleaned crystallization plates through solution casting from toluene at room temperature. This polymer was used as a tougher alternative to brittle pure PS, which its films would develop significant defects through being mounted and sealed in permeation cell equipment. Irganox 1010 as an antioxidant and in very slight content of 0.1wt% was added to the polymer to prevent its thermal oxidation, during cyclic melt pressing process. In order to completely remove toluene from films, they were evacuated overnight at 110°C (above PS glass transition temperature).

6.2.3. Plasma Treatment

Solution cast PS* films, with average thickness of 100 µm, were plasma treated by a laboratory and small-scale production plasma system FEMTO (low-pressure plasma), manufactured by Diener Electronics (Germany), at gas flow rate of 20sccm (standard cubic centimeters per minute) and 10W/cm² power for 60s, to induce polar groups such as carbonyl and carboxylic acid on films surfaces, and to increase their hydrophilicity and surface adhesion properties, in order to promote attraction and attachment of subsequent deposited polycations to their surfaces [24,25].

6.2.4. Layer-by-Layer (LBL) Coating of Thin Films

After dissolving PEI in DIW to make a 0.5wt% solution, samples were immersed in the solution for 5 minutes, before being rinsed in DIW and letting them dry under air flow. Then the coated samples were immersed for 5 minutes in clay slurry of 1wt% MMT in DIW, prepared through 20min ultrasonication and 24 hours of subsequent stirring at 600 rpm. The

rinsing and drying procedures are similar with that of PEI layer, and this cyclic coating procedure is repeated until reaching to aimed number of bilayers (BLs). Also, PETi, a PET containing random anionic functional incorporations on its backbone, which had showed successful applications for making PNCs [21,26] was used as an alternative for PEI to make LBL assemblies. Thus, PETi was dissolved at DIW at 60°C, above its glass transition temperature, before doing LBL coating of the samples, similar to the aforementioned cyclic approach followed LBL assemblies containing PEI interlayers. Due to the nature of the immersion process, bilayers are deposited on both sides of the polymeric substrate, but for simplicity, from now on we only count the number of bilayers (BLs) deposited on one side of the substrate in our remarks.

6.2.5. Cyclic Melt Pressing

After coating of the polystyrene-based membrane as mentioned before, the coated samples were cyclically hot pressed with a Carver standard press. Accordingly, coated films were three times folded and preheated between aluminum sheets covered by polyimide film at 200°C [12,27], before being pressed at 3000 psi. Then, pressed films were quickly quenched between two big aluminum sheets, and the same pressing procedure is repeated for up to 100 cycles, resembling a baker's method. Then all samples were dried for 48 hours at 80°C and reduced pressure, before conducting following characterization experiments.

6.2.6. Thermogravimetry (TGA)

TGA experiments were done for 10mg samples under both air flow and nitrogen purges of 25ml/min and with heating rate of 10°C/min up to 700°C and 800°C, also, isothermal

experiments for 300min at 200°C, with Discovery TGA from TA Instruments in crucible platinum pans, equipped with high temperature resistant bails.

6.2.7. Differential Scanning Calorimetry (DSC)

DSC measurements for different samples were conducted on Q 2000 and Discovery DSC from TA Instrument with approximately 7mg samples. Scans were performed in nitrogen at a heating and cooling rate of 10 °C/min (Q 2000 temperature range: -90 to 450°C; Discovery temperature range: 25 to 400°C). Glass transition (T_g) and degradation temperature (T_d) were derived from the second heating curve.

6.2.8. Dynamic Mechanical Analysis (DMA)

Dynamic mechanical analysis (DMA) was performed on a DMA Q800 TA Instruments (New Castle DE), in tension mode, with film samples molded in dimensions of 15mmx6.5mmx0.5mm. The samples were tested in constant-frequency mode of 1.0Hz, with a strain of 0.3%, and at heating rate of 3°C/min from -140 to 180°C [16], while the glass transition temperature (T_g) was considered as the peak of loss modulus plot (ASTM 1640-04) [28].

6.2.9. Gas Permeation

A constant-volume/variable-pressure technique, shown in the schematic Figure 4.1e (Chapter 4) was used to perform gas permeation experiments on samples at about 20°C and atmospheric pressure for oxygen and carbon dioxide gases. So, polymeric membranes were covered with aluminum tapes, only exposing a circular area of 2.27cm² in the center to gas permeation. After the evacuation of the whole system, the desired gas, with a determined

upstream pressure of typically 1atm was permeated through the membrane into the vessel of known volume (V) in the downstream, while a pressure transducer connected to a computer recorded the downstream pressure.

Therefore, the permeability values of membranes were measured with the following equation.

$$P = \frac{VL}{ART\Delta P} \frac{dP}{dt} \quad (1)$$

Where V, L, A, R, ΔP , and $\frac{dP}{dt}$ are the downstream volume (transmitted gas volume), membrane thickness, membrane exposure area, universal gas constant, difference between constant upstream and initial downstream pressures, and steady rate of increase in gas pressure in downstream, respectively [29,30].

6.3. Results and Discussion

As explained in the previous chapter, PNCs prepared through cyclic melt pressing of LBL-coated PS* membranes, are in fact complex mixtures of different morphologies, including portions of LBL assemblies comprising aggregated clusters, swollen intercalated (almost oriented) stacks of a few BLs, and tail-to-tail flocculated exfoliated (almost disoriented) tactoids of a few platelets. In addition, there are stacks of a few and even sometimes individual clay platelets, detached from LBL assemblies portions and dispersed inside polymeric matrix (Figure 6.2).

6.3.1. Examining Thermal Stability of Ingredients

6.3.1.1. Temperature Ramp

Since the components are pressed at elevated temperatures and over extended number of cycles (up to 100 pressing cycles), their thermal stabilities, particularly in air media, are needed to be examined, in order to ensure that resulted PNCs would remain free of distinct degradations, which otherwise may affect the resulted properties expected from the embedded clay particles. TGA, which can be performed through heating of a sample material with a usually linear rate, in a controlled atmosphere, e.g. air or N₂, is a quantitative approach for determining the thermal stability of materials as well as their inorganic contents (Although some inorganics like carbon black would decompose under air flow at elevated temperatures.), via its continuous weighing [31]. In order to remove any absorbed moisture or carbon dioxide from the samples, to avoid their desorption through main TGA experiment, particularly for PEI, previously vacuum dried samples were heated at 100°C for 30min under nitrogen purge; then they were cooled down to 25°C, before again being heated up to 700°C under air flow [32].

Na⁺MMT, either under N₂ purge [14,33] (Figure 6.S2) or air flow [19] (Figure 6.3a), showed two degradation steps. The first one finishes by about 100°C, resulting in about 6wt% weight reduction, which might be due to the removal of water molecules, located inside clay galleries [12,34]. The second one, which almost finishes by about 700°C, results in about 88wt% residual. Nevertheless, different from most commercial organically-modified clays with different alkyl ammoniums, which incur significant atmospheric degradation by heating above 200°C [19,22,35,36] (Figure 6.3b), natural clay mostly remains stable and non-

degraded. For PS* matrix, only 2wt% and 10wt% degradation occurred by heating up to 319°C and 374°C, respectively (a little lower than the same degradation results at 380°C and 415°C, respectively, under nitrogen purge (Figure 6.S2)). In case of PEI, a slight weight reduction begins at about 153°C, to decrease the weight by 2% and 10% up to 171.3°C and 293.7°C, respectively; however, the main thermo-oxidation step initiated not lower than about 290°C (Despite some minor differences, like 2% and 10% weight reduction by 203°C and 300°C, respectively, TGA under nitrogen purge shows qualitatively similar results. Figure 6.S2.). Then, at about 370°C, with changing the mechanism of the degradation, the rate of weight decrease lowered. Finally, all PEI was removed as volatiles by about 600°C, and almost nothing remained [37]. Also, PETi did not show the onset of thermo-oxidative degradation before 354°C, which causes 2% weight reduction, followed by 10wt% degradation by heating up to 376.5°C. However, different from other ingredients, PETi would leave about 5wt% residue, even if be heated up to 800°C. It may imply its transform to some more thermally resistant component, as a result of thermal oxidation [21].

6.3.1.2. Isothermal Heating at 200°C

In addition to the aforementioned experiment, isothermal TGA experiments were conducted on both interlayers and a PNC sample containing PEI interlayers, which had shown less thermal stability than other ingredients, at processing temperature of 200°C for 300min, to simulate the extended time of cyclic pressing and obtain their thermal stability under such conditions (Figure 6.3c). PETi, like the temperature ramp experiment, again demonstrated its superior thermal stability, showing almost no degradation. Although PEI showed about 6wt%

degradation, for containing PNC, pressed for 25 cycles at 150°C, weight reduction was negligible (less than 2wt%). All in all, except for PEI that showed a slight thermo-oxidation, yet not normally considered problematic, other ingredients looked completely safe for cyclic pressing at 200°C [34].

6.3.2. Clay Content Estimation in PNCs

Since both PEI and PS* completely degrade upon being heated up to 600°C under airflow, this method [38] was used to estimate the content of inorganic clay content of conforming PNCs, made from LBL deposition of PS* with 0.5wt% and 1wt% solution in DIW of PEI and suspension of MMT, respectively. As it was expected with increased number of BL deposition from 5 to 10 and 15, clay content in PNC increases from about 2.2wt% to 3.2wt% and 5.1wt%, respectively (Figure 6.4b, Table 6.1). Comparing the inorganic content remained after heating up to 600°C and previous estimation of clay particles in PNC, performed by analyzing obtained POM (polarized optical microscopy) images (Chapter 5) [18,35,39], a good level of correlation between results of these two approaches is recognized. In fact, the ratio of clay volume, determined by TGA to LBL assembly volume, estimated from POM images, is about 0.8 for all three samples, pointing to about 20% volume content of PE in their LBL assemblies (Table 6.1).

Thus, due to a good correlation between results of TGA and POM approaches for estimating the clay content in prepared PNCs, plus similarities of LBL assemblies formed for both alternative polyelectrolytes, observed by TEM (i.e. both have almost similar clay to PE ratio in their LBL assemblies.), also high thermal stability of PETi, which would not

completely degrade even upon heating to 950°C, the POM image analysis was chosen to estimate the clay content in PNCs, comprising PETi interlayers in their LBL assemblies (Table 6.2).

Side Analysis for Thermal Stability of PNCs with PEI Interlayers. In addition, from TGA plots, it can be noticed that processed PNCs neither showed any obvious improvement, in thermal stabilities, compared with the pristine PS*, nor a sensible trend in their thermal stabilities could be detected by changing their number of BLs or MMT content in suspension (TGA under nitrogen purge provided almost the same results.). Ideally, if the nanodispersion is achieved through increasing the tortuosity of the matrix, the rate of diffusion of oxygen inside the matrix and diffusion of degraded volatiles out of the sample decrease, which can cause an increase in thermal stability of the PNC, under both air flow and nitrogen purge [15,40]. Thus, the primary reason for observing no improvement in degradation temperature of our PNCs can be on account of the moderate level of dispersion of LBL assemblies portions throughout the matrix, which were observed through POM and TEM experiments, previously. This can be due to the insufficient intensity of cyclic melt pressing and or lack of strong interaction between PS* matrix, PEI, and MMT phases [15].

Also, occurring slight degradation in PEI may induce some degradation in PS* matrix to pose some decreasing effect on the thermal stability of PNC [2,22]. In addition, possible degradation of PEI may have an adverse effect on its interlayer role to transfer applied shear rate to LBL assemblies, to promote their dispersion [34]. Comparing PNCs, a slight increase in degradation temperature with increase in the number of BL coatings, may be connected to

increase in the MMT content in the PNC [35] (Table 6.1, Figure 6.4b). Also, with increasing the number of pressing cycles from 25 to 100, the improvement resulted in thermal stability is negligible, which implies that possible degradation effect might have almost neutralized the potential impact of the increase in dispersion of clay (observed by POM) (Figure 6.4a) [2].

6.3.3. Physical Properties of Interlayers

According to DSC experiments results, PEI shows the glass transition at -42°C (comparable with -47°C , led by Schoolman 1992) and the onset of endothermic degradation (under nitrogen atmosphere) at 318°C . In the case of PETi interlayer, glass transition and beginning of endothermic degradation occur at 52°C and 355°C , respectively (Figure 6.5).

6.3.4. Dynamic Mechanical Investigations

According to DMA experiment, PS* showed two relaxation peaks for its loss modulus plot, the one related to the minor polybutadiene (PB) phase appears at -79.8°C and the one related to the major PS phase appears at 104.8°C (a little higher than 100°C resulted from DSC experiments) [41,42]. Also, at 20°C , the values of storage and loss moduli for pristine PS* are 1566MPa and 24MPa , respectively.

Glassy Transition Temperature. In the case of melt pressed PNCs, glassy transition of PS phase showed some slight decrease, possibly due to plasticizing effect of interlayers [1,2,43]. The additional reason, particularly for PNCs containing PEI, might be slight degradation of PEI that by itself may cause slight PS* degradation [14,22]. This slightly lower T_g for PNCs is in accordance with the aforementioned DSC results, confirming the accuracy of both experiments (Figures 6.6, 6.7, 6.8, 6.9). On the other hand, PB phase showed more sensible

shifts in the glassy transition towards higher temperatures in prepared PNCs, which might be related to occurring stronger interactions between PB and interlayers, possibly due to their higher chemical affinities [1,43]. Also, the small content of PB can be another reason for observing a more significant shift in its T_g peaks (Fox Equation) (Figures 6.6, 6.7, 6.8, and 6.9).

$$\frac{1}{T_g} = \frac{w_1}{T_{g,1}} + \frac{w_2}{T_{g,2}} \quad (2)$$

where, w is the weight fraction of each component in the mixture [44].

It can be seen that with the increase in the number of pressing cycles and number of BL coatings, this interaction increases to increase the glassy transition of PB phase towards higher temperatures. In the former case improve in mixing between interlayer and PB, along the extended mixing time may be the main motivation. While in the latter one, the increase in the interlayer content might pose such improvement.

Particularly, in case of PNCs comprising PETi interlayers in their LBL assemblies, when the number of cyclic melt pressing steps increased towards 100, a pronounced rise in the location and broadness of PB phase was observed, which can postulate noticeable boom in the interaction occurred between PETi and PB phase, possibly as a result of higher chemical affinity between PB with PETi than with PEI. Another reason for this difference may be the higher glassy transition of the PETi, compared with PEI, according to mixing rule for the glassy transition of the compatible components (Fox Equation). Also, slight degradation occurred in PEI through cyclic hot pressing can be conjectured as an additional reason for observing a less

significant increase in glass transition of PB phase in PNCs containing PEI interlayers, when the pressing cycles increase up to 100 steps (Figures 6.6, 6.7, 6.8, and 6.9).

In fact, as observed by TEM and POM micrographs (Figure 6.1), despite reaching to the flocculated exfoliation of clay layers in LBL assemblies portions in the matrix, plus existing divided tactoids of one to a few clay platelets, most LBL assemblies are in micron scales, not to affect the glassy transition of the matrix through nanoscale constraints on polymeric chains, called nano-effect phenomena [1,17,18,39].

Storage Modulus. It can also be seen that for both PNC types elastic modulus evidently increases, compared with pristine PS*, pointing to reinforcement effect of clay dispersions to increase the stiffness of PS* matrix [2,14,16,18]. Comparing two groups of PNCs with different interlayers, it can be seen that resulted increase in PNCs containing PEI is more sensible, particularly when the clay content of PNC, as a result of increased number of BL coatings, increases. It can be postulated as a consequence of a possible stronger interaction occurred between PEI and MMT, as previously demonstrated for their oriented LBL coating (Chapters 3 and 4), to transfer the stress from the matrix to clay particles more efficiently.

Generally with increasing the clay content in PNC, its dispersion level decreases, which poses some negative effect on further improvement in its mechanical properties. In fact, lay off of most properties of PNCs as a result of decreased dispersion level at clay loading of about 5wt% is a typical feature of PNCs prepared through melt intercalation method [2].

In the case of PNCs with PEI interlayers, as mentioned before (Chapters 3 and 4), cationic PEI interacts with all large surfaces of clay platelets. Hence, stronger interfaces are built

between them to transfer the stresses from polymeric matrix to clay particles. Thus, for PNCs containing PEI interlayers, the practiced rise in clay loading poses more significant increasing effect on the clay-matrix interfacial area in the PNC, relative to the reducing influence that may have, by decreasing in dispersion level of clay platelets [20]. While, in the case of PNCs containing anionic PETi interlayer, only the edges of clay platelets interact with interlayers. Thus, the resulted minor interfacial area is less efficient in transferring the applied stresses from polymeric matrix to clay platelets. Hence, with the increase in the clay content, possibly as a result of a significant decrease in clay exfoliation and dispersion, their interfacial area may perhaps decrease rather than increasing. Thus, different from the PNCs comprising PEI interlayers, with the rise in the clay content, via increasing the number of BL coatings, storage modulus for PNCs containing PETi interlayers showed some slight decrease instead of the expected rise [14,20].

On the other hand, it can be noticed that with an increase in the number of pressing cycles from 25 to 100 steps the stiffness of PNCs comprising PETi significantly increased. It is due to increased PNC dispersion, showing that certain interactions exist between LBL assemblies and polymeric matrix [45,46]. However, no significant increase is resulted for PNCs with PEI interlayers, despite observing the growth in the clay dispersion in their POM micrographs. It can be conjectured as a result of slight thermomechanical degradation already detected in PEI through thermogravimetric analysis that may develop to PS* matrix [2,14,22], while more thermally stable PETi is immune from such degradation effect. Since, occurring even a slight degradation around processing temperature (PEI~ 2-3%), especially in the case of processing over extended time, may pose adverse effects on final PNC dispersion and properties [34].

Also, another reason behind relatively lower modulus of PNCs enclosing PETi, compared with the ones comprising PEI ingredient, as POM micrographs showed, might be their relatively lower clay contents.

Loss Modulus. Due to damping effect of clay particles, loss modulus of PNCs, particularly in the peak region of PS phase showed significant boom. It can be seen that with increasing the number of BL coatings, thus increase in clay content, in particular for PNCs containing PEI, such damping increases, similar with the trends observed for their storage moduli [16,18].

6.3.5. Permeation Properties

Permeation test is considered as an indirect investigation of dispersion of clay in the polymeric matrix to make a tortuous network [20], although interfacial strength also can play a significant part in overall barrier properties of a PNC. Through rise in the dispersion of clay platelets in PS* matrix and increase in their aspect ratio, the tortuosity of polymeric matrix proliferates to result in reduced diffusivity of gases like oxygen and carbon dioxide, in a mechanism similar to what mentioned for improving thermal stabilities of such PNCs [2,9,11]. But, as observed in POM and TEM micrographs, possibly owing to insufficient intensity of mixing and/or lack of strong interactions between PS*, PE interlayers, and MMT, despite occurring local flocculated exfoliation of clay platelets inside LBL assemblies portions, most of those portions are still in microscale size, instead of being nanodispersed inside the polymeric matrix. Thus, improvement resulted in barrier properties of PNCs are slight.

Nevertheless, the resulted improvement is more evident than their improvement in thermal stabilities, tested by TGA and DSC experiment. It can be conjectured that those microscale

LBL assemblies portions, work as scavengers for gases to decrease the diffusivity more significantly. Also, due to the particular oriented structure of LBL assemblies, derived by electrostatic forces between oppositely charged polymer and clay layers [4,47] and hydration of clay in DIW, edge-edge flocculation of clay platelets in long and narrow LBL portions [2,11], the aspect ratio of those layers increases, in favor of barrier improvement [9,11]. It might be hypothesized almost similar to the way that high aspect ratio clay platelets like Octect [20] and vermiculite [12,48] increase barrier properties more efficiently than MMT in the same content and dispersion state. The other possible reason for further barrier improvement can be the promotion of splitting and orientation, in intercalated and delaminated clay platelets, respectively [10,20]. In fact, cyclic pressing of PNC samples into thin films may resemble biaxial stretching of PNC samples, which was reported as a reason for the further improvement in the barrier and mechanical properties of PNCs [10]. Such improvement for barrier properties against carbon dioxide is slightly more pronounced than for oxygen. As a reason for that, it may be postulated that larger size of carbon dioxide molecules and their possible interaction with PE interlayers [37] and the surface of clay particle, can grow their potential for being trapped in maze- type networks inside PNCs.

Accordingly, it can be seen that with increased number of BLs and clay content, tortuosity rises to improve barrier properties further. Conversely, it can be seen that with growing number of pressing cycles towards 100, while POM micrographs pointed to improved clay dispersion, only a slight improvement in BIF is provided (from 1.33 to 1.50). As discussed before, it can possibly be a side effect of PEI thermomechanical degradation that may cause a slight degradation in PS* matrix [22] (Figure 6.10). Thus, in case of PNCs containing PETi, due to

higher thermal stability of PETi in increased time of mixing, along with improvement in clay dispersion (POM micrographs), relatively more distinct improvement is resulted, despite slightly lower content of clay in their PNCs (POM image analysis), compared with PNCs comprising PEI interlayers.

On the contrary, with an increase in the number of BL coatings from 10 to 15, BIF values of PNCs comprising PETi interlayers drop back. As mentioned in the discussion of their inferior mechanical properties, it might be due to lower potential of anionic PETi, which might only interact with MMT platelets edges, to interact with clay phase, compared with cationic PEI, which probably interacts with MMT platelets large surfaces. This lower ability of PETi, to attract and interact with clay, relative to PEI, when clay content upturns, had been observed severally before, in both micrographs and barrier properties of LBL coatings. Nevertheless, according to literature, due to the general decrease in the dispersion of PNCs, prepared through melt mixing, when the clay content increases to a certain level (usually 5wt%), turning back in barrier properties is a common issue [2] (Tables 6.3 and 6.4).

Nazarenko and his colleagues [11] conducted intensive studies on oxygen permeability of three different classes of PNCs, based on PS matrix, and prepared through in-situ polymerization method. The first of which included conventional composites using natural MMT. The second one used organically-modified clay with zwitterionic surfactant, octadecyldimethyl betaine (C18DMB), to make intercalated PNCs. In the last category of them there were intercalated and exfoliated PNCs, where vinylbenzyltrimethylammonium chloride (VDAC) was used to modify clay (Figure 6.11). Looking at Nazarenko et al. (one of

few intensive studies on oxygen barrier improvement in polystyrene-based PNCs) permeability results, it can be noticed that in constant content of minerals, our PNCs (even for PEI interlayers) demonstrate more evident barrier improvements, while Nazaranko et al. observed better nanodispersion and interplanar spacing, through their TEM micrographs and XRD plots, respectively. In fact, lower dispersion level in PNCs prepared through melt methods, is a general downside of these approaches, relative to solution and polymerization methods [2,20], resulting in relatively less noticeable barrier improvement in the constant level of clay loading. Thus, it may be postulated that the reason behind higher barrier improvement in our PNCs might be the scavenging effect of swollen intercalated and flocculated exfoliated clay platelets, inside microscale LBL assemblies' portions. Another recent study on PS-based PNCs using organic modified MMT (Cloisite 15A), where already extruded intercalated and exfoliated PNCs were biaxially stretched to increase exfoliation and orientation of clay platelets, showed comparative barrier improvement with our results [10] (Figure 6.11).

6.3.5.1. Modeling Barrier Improvement Results

The theoretical permeation model based on Nielsen equation, modified for randomly oriented disk-shaped and stacked particles with the aspect ratio of L/W [9,11], was used to fit the experimental oxygen permeability data determined for our PNCs.

$$\frac{P_c}{P_0} = \frac{1-\phi_m}{1+\frac{1}{3}\left(\frac{\phi_m L}{2h_m N}\right)} \quad (3)$$

where ϕ_m , L , h , and N , represent clay volume fraction, clay particle (stack) length, one platelet's thickness, and the number of clay platelets in each stack, respectively. In this model aspect ratio of fully dispersed clay platelets was assumed as 240 [1,11].

It can be observed that relative permeability of our PNCs would drop somewhere between theoretical models predicting permeability values for highly dispersed PNCs, with clay aspect ratio (L/W) of 240 and 120. It means that our PNCs perform better than PNCs comprising, 2-platelet stacks, with 240nm length, or 4 platelet stacks, with 480nm length (two stacks edge to edge bridged),....; while their barrier performance is only slightly inferior to PNC models with particle aspect ratio of 240, which means completely exfoliated clay platelets of 240nm long, or stacks of two platelets, which are edge-edge bridged to a second similar 2-platelet stack. These impressive results may point to the aforementioned strong scavenging role of tortuous LBL portions in our samples. The other reason for relatively low oxygen permeability data for our PNCs can be the high length of LBL assemblies' portions, compared with their width, in the form of edge-edge bridged clay platelets in each layer. Thus, their aspect ratios relatively increase, to have an increasing effect on barrier improvement resulted from LBL portions, despite their relatively high widths (Figure 6.11).

To sum up, although insufficient intensity of cyclic pressing, as a melt mixing approach, plus possible low interaction between hydrophobic polymeric matrix, interlayers, and clay particles, in addition to some slight degradation occurred for PNCs containing PEI, may pose adverse effect on dispersion of clay platelets and final properties of our PNCs; still high levels of flocculated exfoliation in those microscale portion of LBL assemblies cause that they behave like scavenging mazes with possibly very high barrier properties, that can improve barrier

properties of PNCs further than expected from the global dispersion of those aggregated assemblies. Thus, if we can increase the mixing intensity through a microscale twin-screw extruder, which is purged with nitrogen, to eliminate thermal degradation of components through mixing, reaching to a more noticeable barrier improvement might be possible.

6.4. Conclusion

Further studies of our novel PNCs through DMA experiments in this article showed noticeable increases in the storage and loss moduli, compared with pristine polymers. It points to the occurrence of significant interaction between clay and polymer matrix, due to effective role of alternative polyelectrolyte interlayers, PEI and PETi, as compatibilizers. In addition, with the increase in the time of melt mixing PETi exhibited noticeably increased interaction with polybutadiene phase of PS* to increase its glass transition to higher temperatures.

Also, considering the moderate level of global nanodispersion and low content of clay in these PNCs, significant improvement in their barrier properties against transport of oxygen and carbon dioxide were resulted through permeability measurement experiments. Thus, it might be postulated that those expanded and somewhat internally disoriented LBL portions inside polymeric matrix can form locally tortuous labyrinths, which might potentially be able to act like scavenging black holes, as both their appearance in high magnification scales and their barrier results resembled, against transport of gases through the PNC membranes. Thus a significant improvement in their barrier properties happens. Also, high aspect ratio of oriented LBL assemblies comprising edge to edge flocculation of clay platelets (which itself is a combinative result of hydration of clay in DIW, electrostatic attraction between oppositely

charged polymer and clay layers, and particular layout of LBL deposition) might be another possible reason for barrier improvement in these innovative PNCs. One additional reason for this improvement may possibly be promoting the orientation of clay platelets perpendicular to the permeation direction, as a result of cyclic pressing of samples into thin films.

Comparing two alternative interlayers, more noticeable improvement in barrier properties and hardness of PNCs containing PETi, with increase in melt processing time, may perhaps be related to its higher thermal resistance, confirmed with TGA experiments; whereas, PEI might incur some slight degradation through extended time of cyclic pressing at high temperatures, to pose negative influence on properties of its conforming PNCs.

Tables

Table 6.1. Estimation of the clay content in PNCs containing PEI interlayers through both image analysis and TGA residue at 600°C.

Composition	POM	TGA	
PS*, PEI, MMT, PNC	LBL Particle vol%	MMT wt%	MMT vol%
5BL	1	2.2	0.8
10BL	1.47	3.2	1.16
15BL	2.25	5.1	1.85

Table 6.2. Estimation of the clay content in PNCs containing PETi interlayers through image analysis.

Composition	POM
PS*, PETi, MMT, PNC	LBL Particle vol%
2x5BL	0.6
2x10BL	1.25
2x15BL	1.65

Table 6.3. Permeability results for O₂, through cyclically melt pressed PNCs, based on LBL-coated PS* membranes at the standard atmospheric conditions.

Thin film assembly	O ₂ Permeability (cm ³ .m/m ² .day.atm)	BIF	MMT Content (vol %)	Temperature (°C)
PS*	0.176			293
Plasma treated PS*	0.293			293
10 2-BL (0.5PEI,1M) (25Cycle,200°C)	0.131	1.34		293
10 2-BL (0.5PEI,1M) (100cycles,200°C)	0.116	1.52	1.16	293
5BL (0.5PEI,1M) (100cycles,200°C)	0.144	1.22	0.8	293
15BL (0.5PEI,1M) (100cycles,200°C)	0.113	1.56	1.85	293
10BL (0.5 PETi,1M) (25cycles,200°C)	0.147	1.20		293
10BL (0.5 PETi,1M) (100Cycle,200°C)	0.101	1.74	1.25	293
5 BL (0.5 PETi,1M) (100cycles,200°C)	0.113	1.57	0.6	293
15BL (0.5 PETi,1M) (100cycles,200°C)	0.116	1.52	1.65	293

Table 6.4. Permeability results for CO₂, through cyclically melt pressed PNCs, based on LBL-coated PS* membranes at the standard atmospheric conditions.

Thin film assembly	CO ₂ Permeability (cm ³ .m/m ² .day.atm)	BIF	MMT Content (vol %)	Temperature (°C)
PS*	0.987			293
Plasma treated PS*	1.218			293
10BL (0.5PEI,1M) (25cycles,200°C)	0.5896	1.67		293
10BL (0.5PEI,1M) (100cycles,200°C)	0.574	1.72	1.16	293
5BL (0.5PEI,1M) (100cycles,200°C)	0.670	1.47	0.8	293
15BL (0.5PEI,1M) (100cycles,200°C)	0.578	1.71	1.85	293
10BL (0.5 PETi,1M) (25cycles,200°C)	0.717	1.38		293
10BL (0.5 PETi,1M) (100cycles,200°C)	0.526	1.88	1.25	293
5BL (0.5 PETi,1M) (100cycles,200°C)	0.680	1.45	0.6	293
15BL (0.5 PETi,1M) (100cycles,200°C)	0.570	1.73	1.65	293

Figures

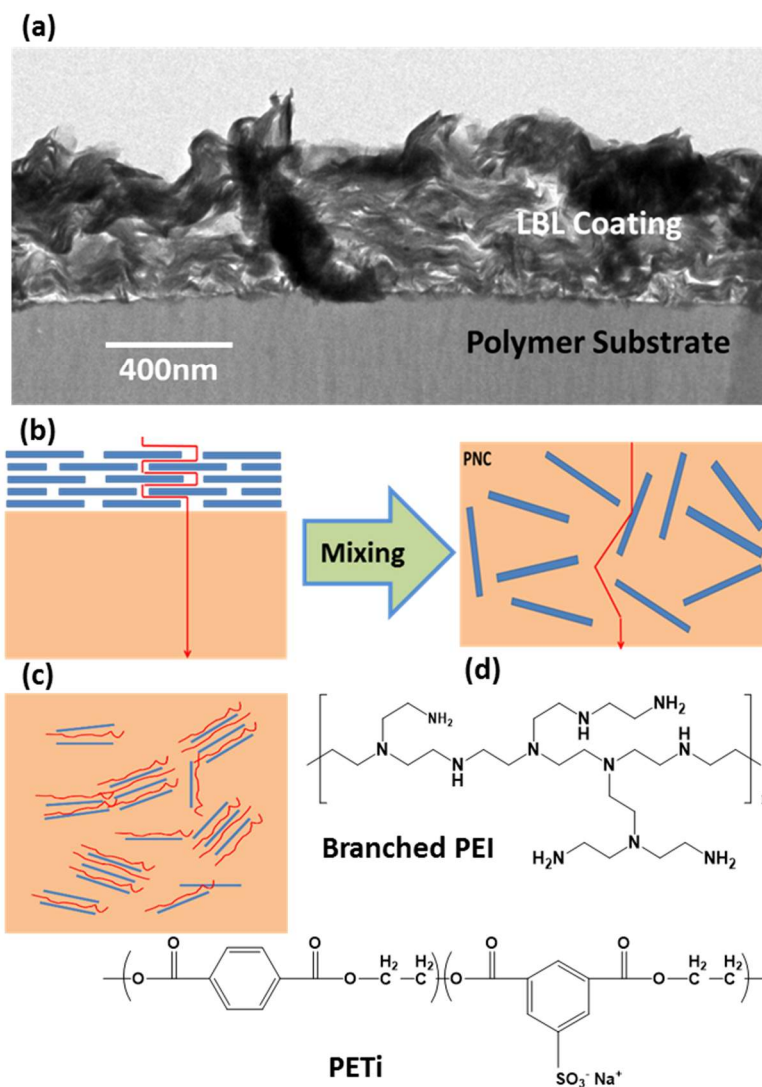


Figure 6.1. (a) Cross-section of a TEM image of a polymeric membrane coated with LBL assemblies of PEI and MMT. (b) Schematic of a polymer film coated with LBL assemblies, the polymer nanocomposite (PNC) resulted after cyclic hot pressing, and gas permeation route in them. (c) Detailed schematic of LBL portions in PNC. (d) Chemical formulae of two alternative polyelectrolyte interlayers, PEI and PETi.

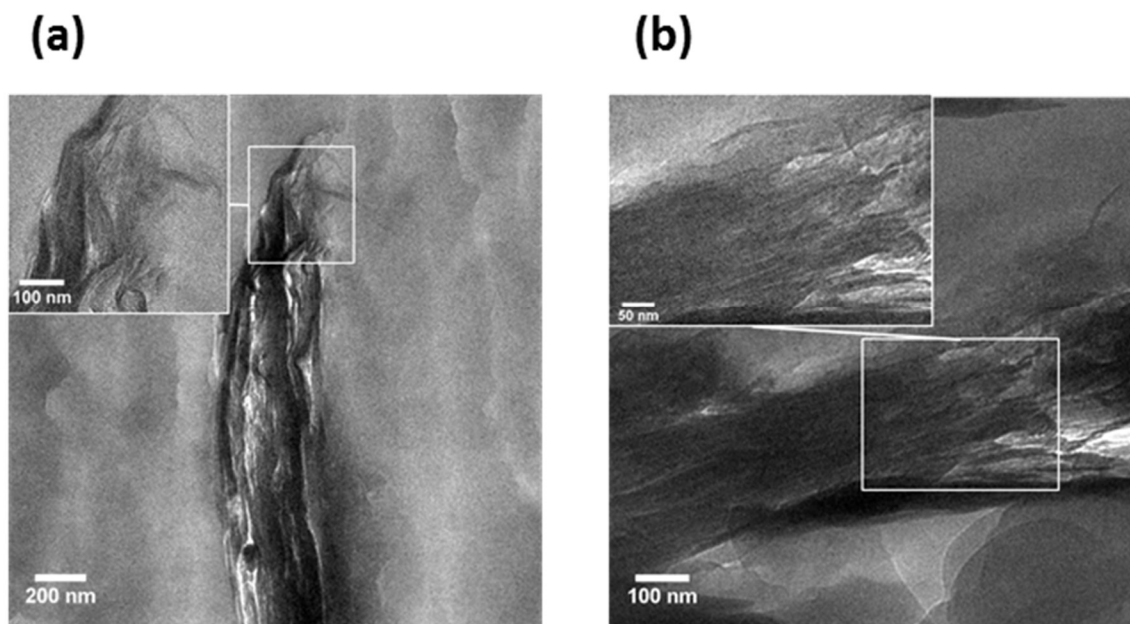


Figure 6.2. LBL portions in PNCs, processed through 100 cycle of melt pressing at 200°C, for LBL coatings deposited from 1wt% suspension of MMT and 0.5wt% solution in deionized water of alternative polyelectrolyte layers (a) PEI and (b) PETi.

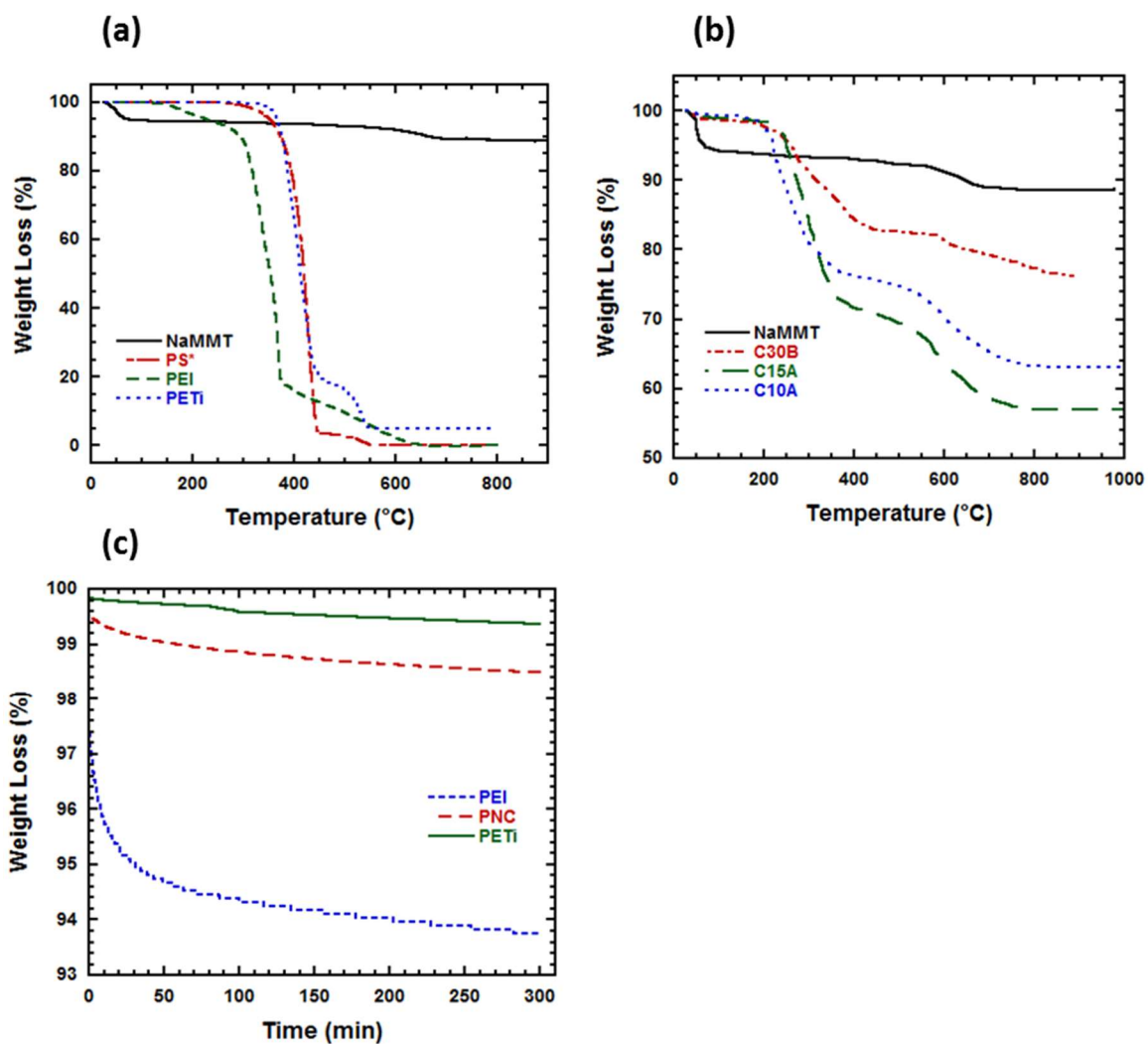


Figure 6.3. TGA thermograms showing degradation behavior under air flow for: (a) Na⁺MMT, PS*, PEI, and PETi. (b) Na⁺MMT in comparison with three conventional organically-modified clays with alkyl ammonium (C30B is Na⁺MMT modified with methyl, tallow, bis-2-hydroxyethyl quaternary ammonium; C15A is Na⁺MMT modified with dimethyl, dehydrogenated tallow quaternary ammonium; C10A is Na⁺MMT modified with dimethyl, benzyl, hydrogenated tallow quaternary ammonium.). (c) Isothermal heating at 200°C of PEI, PETi, and PNC made from 10 bilayer deposition of PEI (0.5wt% in DIW) and MMT (1wt% in DIW) on PS* films, followed by melt pressing for 25 times at 150°C.

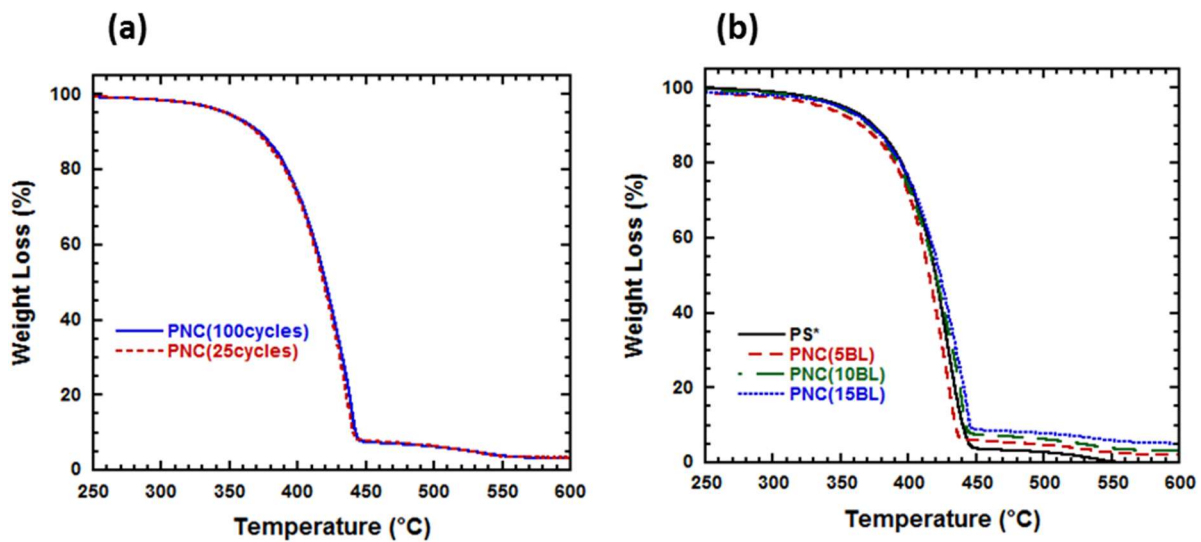


Figure 6.4. TGA thermograms showing degradation behavior under air flow for: (a) PNCs prepared from 10BL deposition of PEI (0.5wt% in DIW) and MMT (1wt% in DIW) on PS* films, followed by melt pressing for 25 and 100 cycles at 200°C. (b) PNCs prepared from 5, 10, 15BL deposition of PEI (0.5wt% in DIW) and MMT (1wt% in DIW) on PS* films, followed by melt pressing for 100 cycles at 200°C.

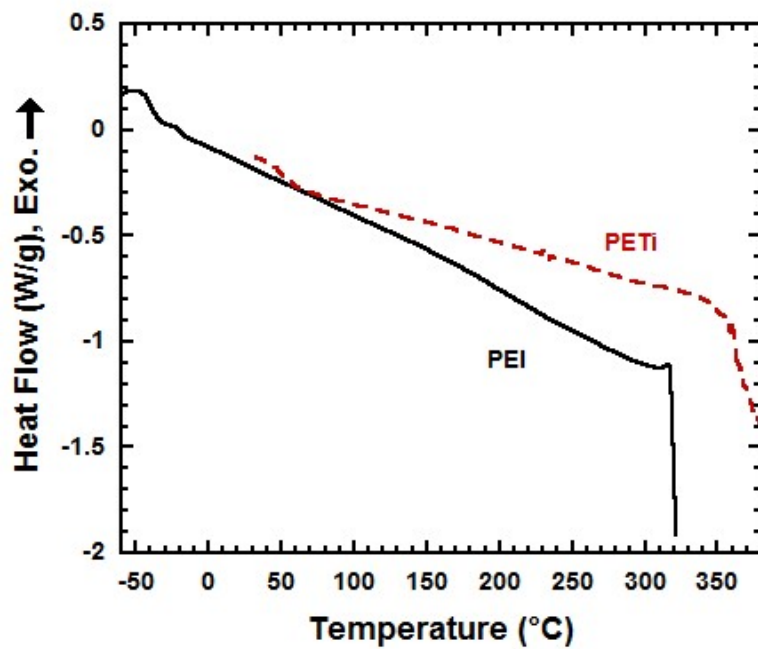


Figure 6.5. DSC plots depicting thermal properties glass transition and degradation temperatures (T_g , T_d) of two different interlayers studied PEI, PETi.

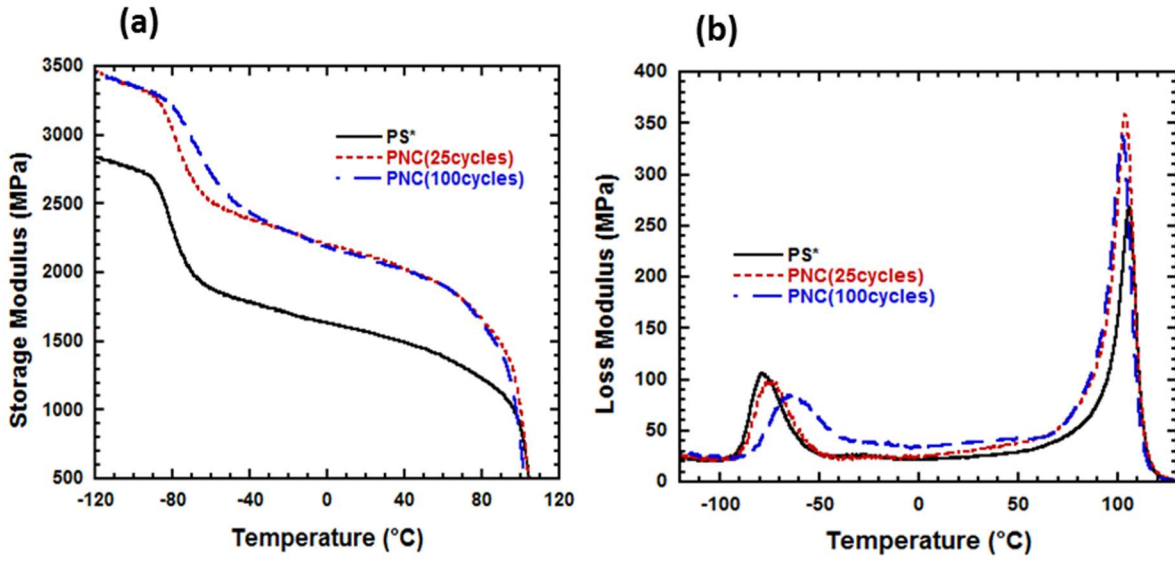


Figure 6.6. (a) Storage and (b) Loss modulus as a function of temperature for PS* and its PNCs made from 10BL deposition of PEI(0.5wt% in DIW) and MMT(1wt% in DIW), followed by 25 and 100 melt pressing cycles at 200°C.

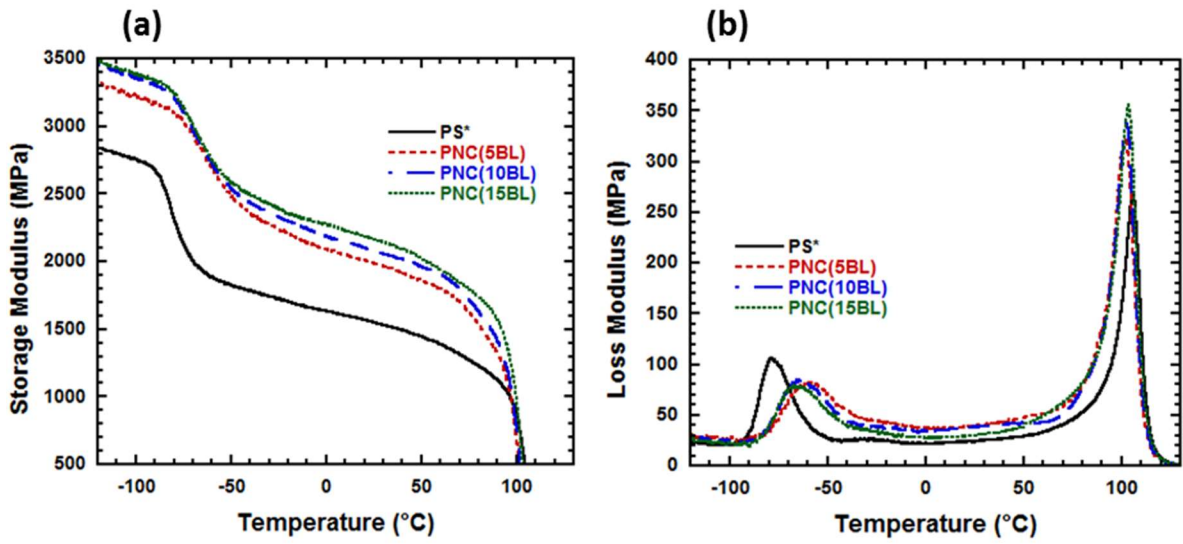


Figure 6.7. (a) Storage and (b) Loss modulus as a function of temperature for PS* and its PNCs made from 5, 10, 15BL deposition of PEI(0.5wt% in DIW) and MMT(1wt% in DIW), followed by 100 melt pressing cycles at 200°C.

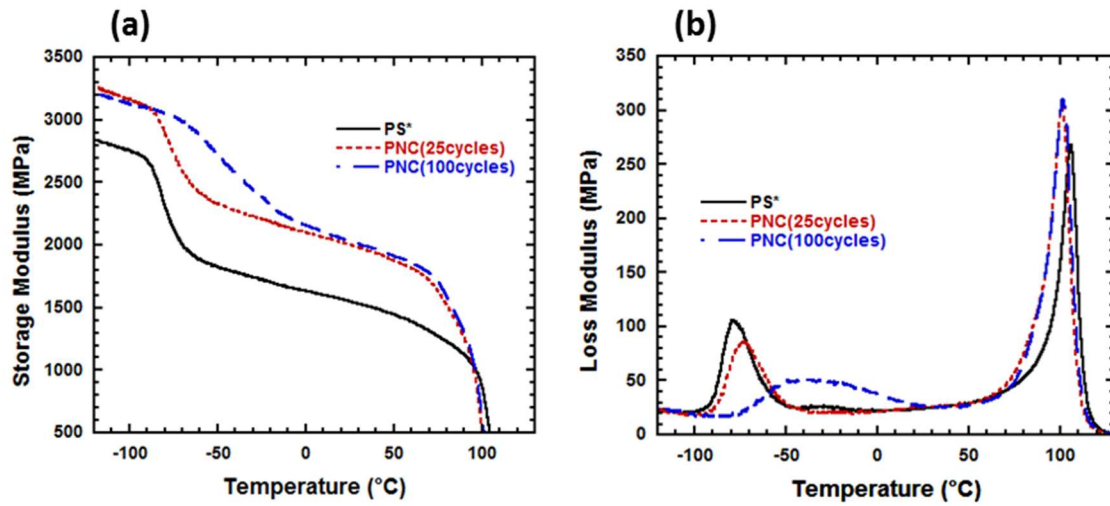


Figure 6.8. (a) Storage and (b) Loss modulus as a function of temperature for PS* and its PNCs made from the 10BL deposition of PETi(0.5wt% in DIW) and MMT(1wt% in DIW), followed by 25 and 100 melt pressing cycles at 200°C.

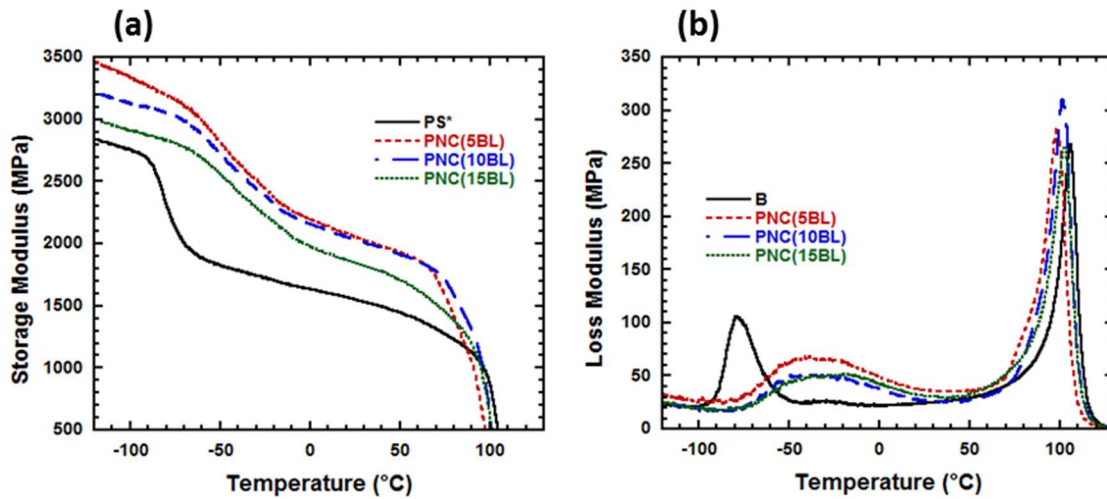


Figure 6.9. (a) Storage and (b) Loss modulus as a function of temperature for PS* and its PNCs made from 5, 10, 15BL deposition of PETi(0.5wt% in DIW) and MMT(1wt% in DIW), followed by 100 melt pressing cycles at 200°C.

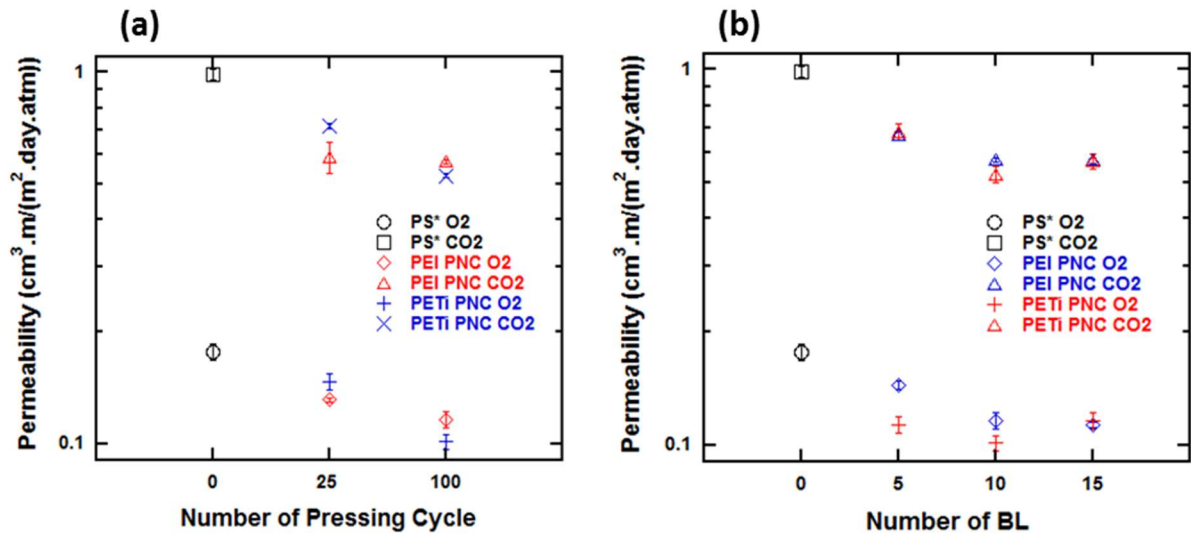


Figure 6.10. Permeation values of oxygen and carbon dioxide at 20°C, in PS* and PNCs, comprising PEI and PETi interlayers, as a function of (a) number of melt pressing cycles, and (b) number of BL coating applied initially on PS* substrate.

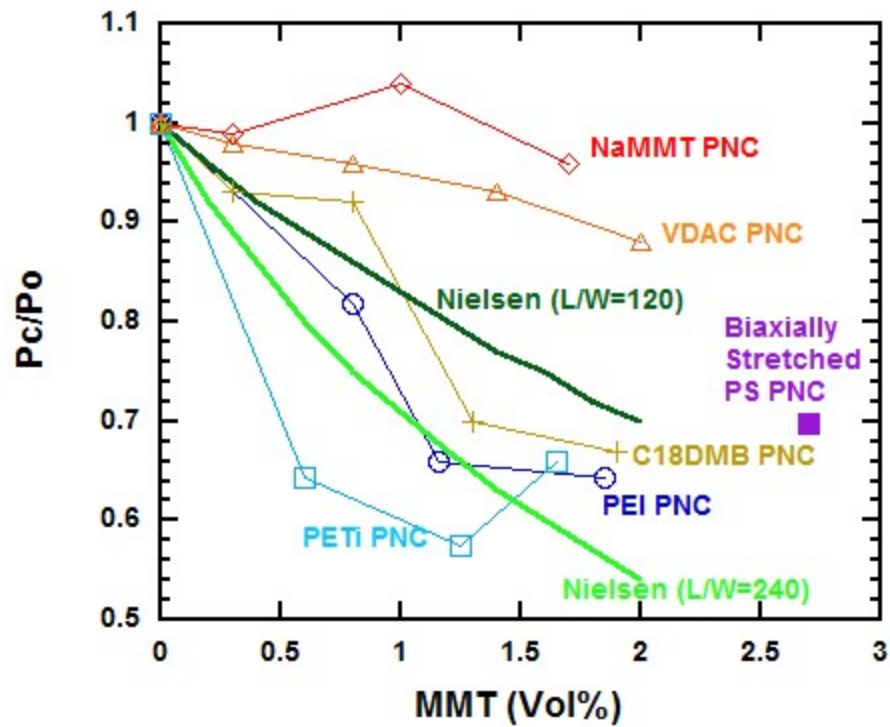


Figure 6.11. Oxygen permeation as a function of MMT volume content, for our novel PNCs compared with theoretical modified Nielsen Model (Bharadwaj 2001) and literature results for PS-based PNCs, Na+MMT PNC, VDAC PNC, C18DMB PNC (Nazarenko et al. 2007), and biaxially stretched PS-based PNCs (Huang et al. 2015). Lines between data points are guides for eyes.

6.5. Supplementary Information

6.5.1. Effect of Initial MMT Content in DIW on PNC's Thermal Stability

With increased content of MMT in DIW from 0.1wt% to 1wt%, and increased clay content in processed PNCs comprising PEI interlayers from 1.9wt% to 3.2wt%, Td values of PNCs showed some slight increase (from 366.7 to 271.4°C for 2wt% degradation). Then it turned back to 367.2°C with more increase in clay content in DIW, up to 3wt%, corresponding to PNC's clay content of 11.8wt%. It can be related to an evident decrease in the dispersion of clay platelets in the matrix, as observed in POM, resulting in its decreased tortuosity, despite increasing its content (Figure 6.S1).

6.5.2. Thermogravimetry under Nitrogen Purge

The TGA under nitrogen purge was performed for PEI, PS*, Na⁺MMT, and their PNCs prepared from 10 and 15 times BL deposition in PEI solution in DIW (0.5wt%) and MMT suspension (1wt%), respectively to examine the thermal stability of components through processing, complementary to the aforementioned TGA under air flow. The results despite minor differences show qualitative correspondence with aforesaid TGA experiment under air flow.

6.5.3. DSC for PNCs Containing PEI Interlayers

The DSC experiment conducted on PS* and its PNCs with PEI and MMT show that glass transition of PS phase of PS* blend occurs at 100°C, which is close to literature result [49], confirming the accuracy of this experiment. In the case of PNCs, glass transitions occur at slightly lower temperatures, which may be due to slight degradation occurred in PEI that may

pose some degradation in PS* matrix [2,22]. The other reason for the decrease in glassy transition temperature of PS phase can be related to plasticizing effect of PEI on matrix chains [43]. These results are in accordance with slightly lower glass transition reported from dynamic mechanical analyses.

Although TGA results did not show any improvement in degradation temperature of the PNCs, from DSC results, it can also be seen that endothermic degradation peaks for PNCs occur at slightly higher temperatures than for PS*. It can be due to the more internal feature of DSC measurement, which is on the basis of heat flux inside the material, compared with TGA, which is based on weight reduction [15]. Nevertheless, due to the moderate level of dispersion of clay platelets, observed through POM and TEM experiments, and possibly occurring some slight degradation [22], the resulted increased thermal stability is negligible. Also, in confirmation of TGA results, it can be seen that with the rise in the number of pressing cycles and number of BL coatings some slight increases in thermal stability are reached, to imply on the rise in matrix tortuosity (Table 6.S3).

Table 6.S1. DSC obtained glass transition and degradation temperatures of PS* and its PNC made from PS* coated with LBL of PEI and MMT, followed by cyclic melt pressing at 200°C. PNCs from Top to down are: 25cycle pressing for PS* with 10BL coating; 100cycles pressing for PS* coated with 5, 10, and 15BL.

DSC	Td(°C) (onset)	Tg (°C) (midpoint)
PS*	366.4	100
PNC(10BL,25cycles)	369.5	97.45
PNC(5BL,100cycles)	366.7	94.3
PNC(10BL,100cycles)	371.8	96.2
PNC(15BL,100cycles)	369.1	93.3

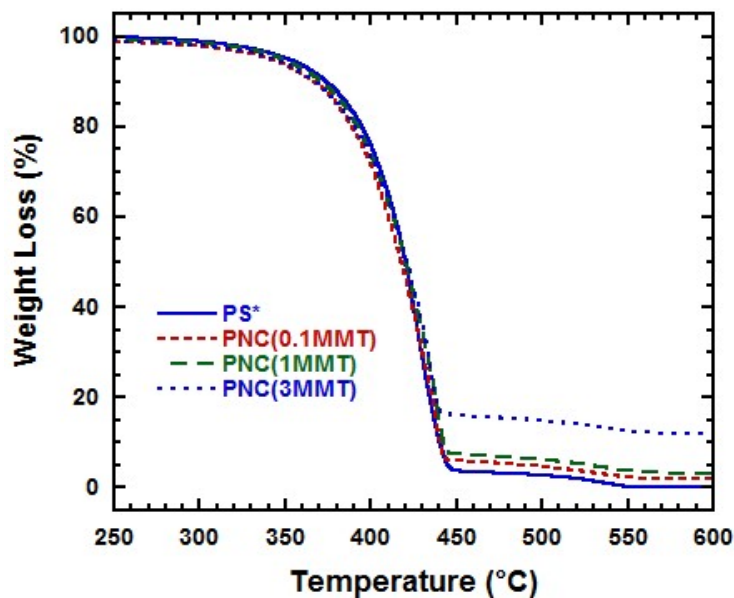


Figure 6.S1. TGA thermograms showing degradation behavior under air flow for: PS* and PNCs prepared from 10BL deposition of PEI (0.5wt% in DIW) and MMT (0.1, 1, and 3wt% in DIW) on PS* films, followed by melt pressing for 100 cycles at 200°C.

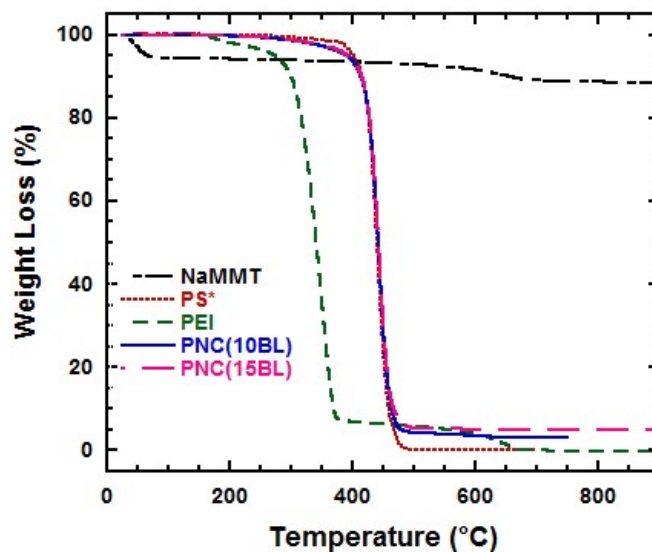


Figure 6.S2. TGA thermograms showing degradation behavior under a nitrogen purge for: Na⁺MMT, PS*, PEI, and PNCs prepared from 10 and 15BL deposition of PEI (0.5wt% in DIW) and MMT (1 wt% in DIW) on PS* films, followed by melt pressing for 100 cycles at 200°C.

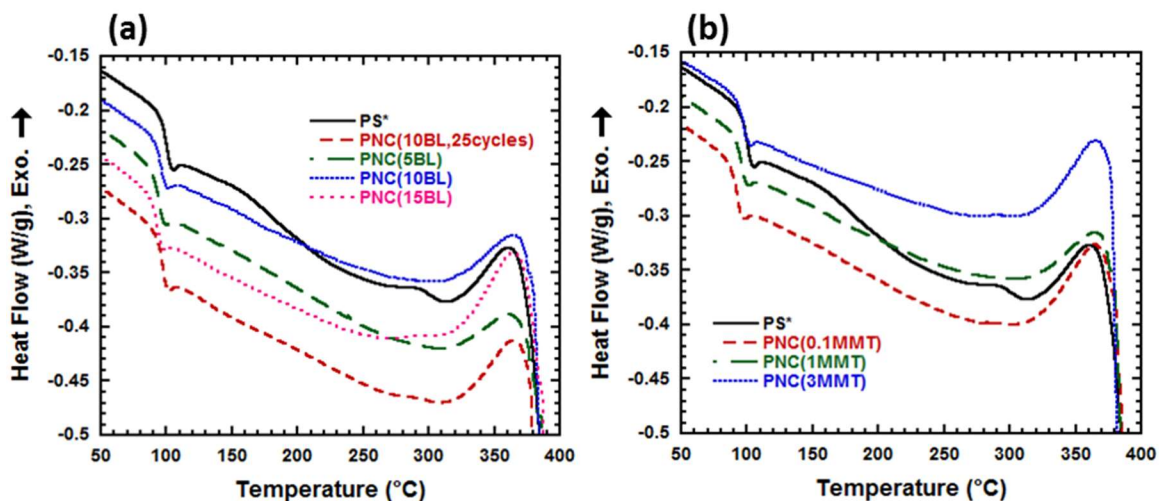


Figure 6.S3. DSC traces comparing glass transition and degradation temperatures of PS* and its PNC made from PS* coated with LBLs of PEI and MMT, followed by cyclic melt pressing at 200°C. (a) PNCs from top to down are prepared after: 25cycle pressing for PS* with 10BL coating; 100cycles pressing for PS* coated with 5, 10, and 15BL. (b) PNCs from top to down are prepared after 100 cycles pressing for PS* coated with 10BL coating from MMT suspensions of 0.1, 1, and 3wt% in DIW.

References

- [1] D.R. Paul, L.M. Robeson, Polymer nanotechnology: Nanocomposites, *Polymer* 49 (2008) 3187–3204.
- [2] S.S. Ray, Recent Trends and Future Outlooks in the Field of Clay-Containing Polymer Nanocomposites, *Macromol. Chem. Phys.* 215 (2014) 1162–1179.
- [3] G.W. Beall, C.E. Powell, *Fundamentals of Polymer-Clay Nanocomposites*, 1st ed., Cambridge University Press, Cambridge, UK, 2011.
- [4] M.A. Priolo, K.M. Holder, D. Gamboa, J.C. Grunlan, Influence of clay concentration on the gas barrier of clay–polymer nanobrick wall thin film assemblies, *Langmuir*. 27 (2011) 12106–12114.
- [5] P.F. Carcia, R.S. McLean, M.H. Reilly, Permeation measurements and modeling of highly defective Al₂O₃ thin films grown by atomic layer deposition on polymers, *Appl. Phys. Lett.* 97 (2010) 221901–221903.
- [6] S.S. Ray, *Clay-containing polymer nanocomposites: from fundamentals to real applications*, First, Elsevier, Amsterdam, 2013.
- [7] V. Mittal, *Optimization of Polymer Nanocomposite Properties*, 1st ed., Wiley-VCH, Weinheim, Germany, 2010.
- [8] M. Galimberti, Rubber Clay Nanocomposites, *Adv. Elastomers – Technol. Prop. Appl.* (2012).
- [9] R.K. Bharadwaj, Modeling the barrier properties of polymer-layered silicate nanocomposites, *Macromolecules*. 34 (2001) 9189–9192.
- [10] W. Huang, S. Zeng, J. Liu, L. Sun, Bi-axially oriented polystyrene/montmorillonite nanocomposite films, *RSC Adv.* 5 (2015) 58191–58198.
- [11] S. Nazarenko, P. Meneghetti, P. Julmon, B.G. Olson, S. Qutubuddin, Gas barrier of polystyrene montmorillonite clay nanocomposites: Effect of mineral layer aggregation, *J. Polym. Sci. Part B Polym. Phys.* 45 (2007) 1733–1753.
- [12] A. Panwar, V. Choudhary, D.K. Sharma, Review: A review: polystyrene/clay nanocomposites, *J. Reinf. Plast. Compos.* 30 (2011) 446–459.
- [13] A. Giannakas, A. Giannakas, A. Ladavos, Preparation and Characterization of Polystyrene/Organolaponite Nanocomposites, *Polym. Plast. Technol. Eng.* 51 (2012)

1411–1415.

- [14] N. Greesh, S.S. Ray, J. Bandyopadhyay, S. Sinha Ray, J. Bandyopadhyay, Role of nanoclay shape and surface characteristics on the morphology and thermal properties of polystyrene nanocomposites synthesized via emulsion polymerization, *Ind. Eng. Chem. Res.* 52 (2013) 16220–16231.
- [15] J. Golebiewski, A. Galeski, Thermal stability of nanoclay polypropylene composites by simultaneous DSC and TGA, *Compos. Sci. Technol.* 67 (2007) 3442–3447.
- [16] K.J. Lin, C.H. Lee, K.F. Lin, Extraordinary mechanical behavior of exfoliated montmorillonite/polymer nanocomposite films cast from soap-free emulsion polymerized latices, *J. Polym. Sci. Part B Polym. Phys.* 48 (2010) 1064–1069.
- [17] A. Bansal, H. Yang, C. Li, K. Cho, B.C. Benicewicz, S.K. Kumar, et al., Quantitative equivalence between polymer nanocomposites and thin polymer films., *Nat. Mater.* 4 (2005) 693–698.
- [18] T.D. Fornes, D.R. Paul, Modeling properties of nylon 6/clay nanocomposites using composite theories, *Polymer* 44 (2003) 4993–5013.
- [19] A.E. Özçam, Surface Modification and Characterization of Polymeric Materials for Targeted Functionality, Ph.D. Dissertation, North Carolina State University, 2011.
- [20] M. Ziadeh, B. Fischer, J. Schmid, V. Altstädt, J. Breu, On the importance of specific interface area in clay nanocomposites of PMMA filled with synthetic nano-mica, *Polymer* 55 (2014) 3770–3781.
- [21] A. Ammala, C. Bell, K. Dean, Poly (ethylene terephthalate) clay nanocomposites: improved dispersion based on an aqueous ionomer, *Compos. Sci. Technol.* 68 (2008) 1328–1337.
- [22] D.J. Frankowski, M.D. Capracotta, J.D. Martin, S. a. Khan, R.J. Spontak, Stability of organically modified montmorillonites and their polystyrene nanocomposites after prolonged thermal treatment, *Chem. Mater.* 19 (2007) 2757–2767.
- [23] M.N. Muralidharan, S.A. Kumar, S. Thomas, Morphology and transport characteristics of poly(ethylene-co-vinyl acetate)/clay nanocomposites, *J. Memb. Sci.* 315 (2008) 147–154.
- [24] I. Beaulieu, M. Geissler, J. Mauzeroll, Oxygen plasma treatment of polystyrene and zeonor: Substrates for adhesion of patterned cells, *Langmuir.* 25 (2009) 7169–7176.
- [25] C. Chaiwong, P. Rachtanapun, P. Wongchaiya, R. Auras, D. Boonyawan, Effect of plasma treatment on hydrophobicity and barrier property of polylactic acid, *Surf.*

Coatings Technol. 204 (2010) 2933–2939.

- [26] A. Ghanbari, M.-C.C. Heuzey, P.J. Carreau, M.-T.T. Ton-That, Morphology and properties of polymer/organoclay nanocomposites based on poly(ethylene terephthalate) and sulfopolyester blends, *Polym. Int.* 62 (2013) 439–448.
- [27] U. Yilmazer, G. Ozden, Polystyrene–organoclay nanocomposites prepared by melt intercalation, in situ, and masterbatch methods, *Polym. Compos.* 27 (2006) 249–255.
- [28] S.M. Miriyala, Y.S. Kim, L. Liu, J.C. Grunlan, Segregated Networks of Carbon Black in Poly (vinyl acetate) Latex : Influence of Clay on the Electrical and Mechanical Behavior, *Macromol. Chem. Phys.* 209 (2008) 2399–2409.
- [29] X. Hu, J. Tang, A. Blasig, Y. Shen, M. Radosz, CO₂ permeability, diffusivity and solubility in polyethylene glycol-grafted polyionic membranes and their CO₂ selectivity relative to methane and nitrogen, *J. Memb. Sci.* 281 (2006) 130–138.
- [30] N.P. Patel, A.C. Miller, R.J. Spontak, Highly CO₂-Permeable and Selective Polymer Nanocomposite Membranes, *Adv. Mater.* 15 (2003) 729–733.
- [31] S.N. Bhattacharya, M.R. Kamal, R.K. Gupta, *Polymeric nanocomposites: theory and practice*, Carl Hanser Publishers, Munich, 2008.
- [32] T.C.C. Drage, A. Arenillas, K.M.M. Smith, C.E.E. Snape, Thermal stability of polyethylenimine based carbon dioxide adsorbents and its influence on selection of regeneration strategies, *Microporous Mesoporous Mater.* 116 (2008) 504–512.
- [33] K.. P. Pramoda, T. Liu, Z. Liu, C. He, H.-J.J. Sue, Thermal degradation behavior of polyamide 6/clay nanocomposites, *Polym. Degrad. Stab.* 81 (2003) 47–56.
- [34] C.H. Davis, L.J. Mathias, J.W. Gilman, D. a. Schiraldi, J.R. Shields, P. Trulove, et al., Effects of melt-processing conditions on the quality of poly(ethylene terephthalate) montmorillonite clay nanocomposites, *J. Polym. Sci. Part B Polym. Phys.* 40 (2002) 2661–2666.
- [35] S.H. Kim, S.C. Kim, Synthesis and Properties of Poly (ethylene terephthalate)/ Clay Nanocomposites by In Situ Polymerization, 103 (2007) 1262–1271.
- [36] N. Greesh, R. Sanderson, P.C. Hartmann, Preparation of polystyrene colloid particles armored by clay platelets via dispersion polymerization, *Polymer* 53 (2012) 708–718.
- [37] X. Xu, C. Song, J.M. Andrésen, B.G. Miller, A.W. Scaroni, Preparation and characterization of novel CO₂ “molecular basket” adsorbents based on polymer-modified mesoporous molecular sieve MCM-41, *Microporous Mesoporous Mater.* 62 (2003) 29–45.

- [38] D. Wang, C. Wilkie, In-situ reactive blending to prepare polystyrene–clay and polypropylene–clay nanocomposites, *Polym. Degrad. Stab.* 80 (2003) 171–182.
- [39] A. Ranade, N.A. D’Souza, B. Gnade, Exfoliated and intercalated polyamide-imide nanocomposites with montmorillonite, *Polymer* 43 (2002) 3759–3766.
- [40] L. Qiu, W. Chen, B. Qu, Morphology and thermal stabilization mechanism of LLDPE/MMT and LLDPE/LDH nanocomposites, *Polymer* 47 (2006) 922–930.
- [41] F. Vilaplana, A. Ribes-Greus, S. Karlsson, Degradation of recycled high-impact polystyrene. Simulation by reprocessing and thermo-oxidation, *Polym. Degrad. Stab.* 91 (2006) 2163–2170.
- [42] P. Uthirakumar, Y.B. Hahn, K.S. Nahm, Y.S. Lee, Exfoliated high-impact polystyrene/MMT nanocomposites prepared using anchored cationic radical initiator-MMT hybrid, *Eur. Polym. J.* 41 (2005) 1582–1588.
- [43] M. Pluta, J.K. Jeszka, G. Boiteux, Polylactide/montmorillonite nanocomposites: Structure, dielectric, viscoelastic and thermal properties, *Eur. Polym. J.* 43 (2007) 2819–2835.
- [44] P. Hiemenz, *Polymer Chemistry*, CRC Press, Boca Raton, Florida, 2007.
- [45] F. Quadrini, D. Bellisario, C. Lucignano, L. Santo, The Role of Mixing Time in the Production of Nanocomposite Thermosetting Coatings, *Polym. Plast. Technol. Eng.* 52 (2013) 1200–1212.
- [46] W. Lertwimolnun, B. Vergnes, Influence of compatibilizer and processing conditions on the dispersion of nanoclay in a polypropylene matrix, *Polymer* 46 (2005) 3462–3471.
- [47] G. Decher, Layer-by-Layer Assembly, in: G. Decher, J.B. Schlenoff (Eds.), *Multilayer Thin Film.*, Willey-VCH, Weinheim, Germany, 2012: pp. 1–22.
- [48] D. Feldman, Polymer Nanocomposite Barriers, *J. Macromol. Sci. Part A.* 50 (2013) 441–448.
- [49] J. Brandrup, E.H. Immergut, E.A. Grulke, eds., *Polymer Handbook*, Fourth, Wiley-Interscience, New York, 2003.

CHAPTER 7

Morphology, Gas Transport, and Dynamic Mechanical Properties of Polymer Nanocomposites Derived From Layer-by-Layer Coated Polyvinylacetate Membranes

Abstract

In this study we performed our innovative method of preparing polymer nanocomposites (PNCx), through cyclic melt pressing of already layer-by-layer (LBL) coated polymeric substrates, for polyvinylacetate (PVAc), as a comparatively hydrophilic polymer, containing polar functional groups, relative to the previously examined polystyrene-based membranes. Thus, it was attempted to scrutinize possibility of reaching to highly dispersed and exfoliated PNCs with improved barrier and mechanical properties, as a result of increasing interaction intensity between polymeric matrix and clay ingredients. In addition, polyethyleneterephthalate ionomer (PETi), due to its previously demonstrated higher thermal stability, compared with polyethyleneimine, was used as the polyelectrolyte (PE) for making LBL assemblies, to diminish the risk of thermal degradation of samples through extended times of melt processing at elevated temperatures. Accordingly, optical microscopic images showed relatively higher contents of clay in these PNCs, relative to previous polystyrene-based ones, derived from equal numbers of bilayer (BL) coatings and initial PETi solutions and clay suspensions. Also, dynamic mechanical analysis and permeation experiments, respectively revealed noticeable increases in moduli values and significant improvement in gas barrier properties of the samples melt pressed for only 25 cycles. Besides, x-ray diffractometry traces postulated high levels of irregularities reached in clay platelets interdistance of the pressed

PNCs. Thus, it may be conjectured that relatively strong interaction between PVAc matrix, PETi, and clay particles occurred to promote PNCs' exfoliations and intercalations and increase their mentioned properties. However, their combinative morphological investigations conducted through polarized optical microscopy, transmission electron microscopy, and x-ray diffractometry, despite showing the aforementioned increases in clay contents and its platelets interdistance irregularities, pointed to qualitative similarities with the morphology of previous polystyrene-based PNCs. Since they mainly included distribution of a few hundred nanometer LBL assemblies portions, comprising swollen intercalated stacks of clay platelets and flocculated exfoliated tactoids of a few clay platelets, although occasionally peeled tactoids of a few platelets down to 2nm thick, out of those LBL assemblies, were observed as well. Thus, they pointed to the moderate state of global nanodispersion of clay in PNCs. Hence, it seems that despite the effectiveness of LBL deposition, in promoting initial intercalation and exfoliation, in otherwise aggregately clustered clay platelets, cyclic pressing at elevated temperatures was not capable of applying sufficiently intensive shear stresses on samples, needed to overcome the internal cohesion in LBL assemblies. Therefore, relatively significant improvements in the barrier properties of PNCs might be speculated as the result of the scavenging effect of high aspect ratio LBL portions, with their highly tortuous structure. In addition, decreasing moduli values and gas barrier properties with increasing the number of melt pressing cycles may point to the adverse effect of slight thermal degradation of samples. To sum up, it might be suggested that a more intensive melt pressing procedure, like twin-screw extrusion in high speeds, and under an inert atmosphere like nitrogen, to avoid thermal

oxidation, might be able to increase the nanodispersion of these novel PNCs, towards reaching to even more considerable amelioration in their properties.

7.1. Introduction

With the decrease in the size scale of inorganic fillers dispersed in polymeric composites down to micro and nanometers, their aspect ratio and interfacial area in contact with polymeric matrix increase. So, they induce significantly higher influences on properties of conventional polymer composites, when the dispersion loading is assumed to be equal [1–3]. Particularly, in the case of clays, such as montmorillonite (MMT), which are cheap, available, and environmentally safe, high aspect ratio of their impermeable platelets, if efficiently exfoliated, can increase the tortuosity of the composite significantly [1,4–6]. Thus, they can potentially decrease permeation of gases and vapors into and out of the composite significantly, to potentially improve its gas barrier properties [7–10] and thermal stabilities [1,11], in addition to more potent increasing effect they can put on stiffness and loss modulus of the polymeric materials [12,13]. In fact, packaging applications count for above 30% of about 1 billion dollars prospective market of PCN's market by 2016 [14]. Therefore, this comprehensive improvement approach of polymer nanocomposites, in addition to their processability through general polymer processing techniques for polymers, makes them superior compared with different coatings, which are vulnerable to defects and delamination issues induced by any external stress or impact [3,15].

Morphological studies, through microscopy [1,6,8,16,17] and x-ray diffractometry [1,8,12,18] have demonstrated that polymer nanocomposites are usually mixtures of different

microstructures, including phase-separated or clustered clay particles, polymer intercalated clay stacks, and exfoliated tactoids of a few platelets [6,17,19,20]. However, they are usually named after the most plentiful morphology they possess.

Different methods of solution mixing [10,13,17], in-situ polymerization of matrix monomer in a media containing clay platelets [12,8], melt mixing [7,16,21], and combinations of any of these approaches [22,23] are usually used to induce polymer nanocomposites, amongst which melt mixing, due to being direct, environmental friendly, and similar with conventional polymer processing techniques has been more attractive to scientists and technologists [1].

Organic modifications of clay platelets, with groups like alkyl ammonium, to replace alkali ions and intercalate between clay platelets, in favor of inducing better interactions with hydrophobic polymers, have been widely investigated; since they can potentially increase clay platelets interdistance and decrease their hydrophilicity, to promote dispersion of clay through shear stresses applied via processing [6,1]. However, due to their low thermal stabilities, the organic surfactants usually incur degradation, at high temperatures of melt processing of many polymers, to bring adverse effect on final properties of polymer nanocomposites [11,18,21].

Therefore, in these series of studies it was endeavored to exploit the potential compatibilizing effect of polyelectrolyte (PE) interlayers in already deposited LBL assemblies coating, for the purpose of promoting interactions between clay and the polymeric matrix. Accordingly in a two-step process, after depositing LBL assemblies of PE and MMT on polymeric substrates [1,24], cyclic melt pressing of coated membranes was practiced to embed and disperse clay platelets inside the polymeric matrix. Since, one of the possible reasons for

occurring low levels of dispersion in our PNCs with polystyrene-based matrices, was conjectured as low potential of such hydrophobic polymeric media to interact with hydrophilic clay effectively, in this article we decided to examine, an alternative polymeric matrix containing polar functional group, like polyvinyl acetate (PVAc), to scrutinize how increase in hydrophilic nature of our base polymer can possibly change the morphology, as well as gas barrier and dynamic mechanical thermal properties of resulted PNCs (Figure 7.1). In addition, excellent clarity of PVAc, as the matrix, is in favor of the easier investigation of morphologies for different clay microstructure in the resulted PNCs.

7.2. Experimental

7.2.1. Materials

Polyvinylacetate (PVAc) (density=1.18g/cm³ at 25°C, Mw=100kDa) was supplied by Sigma-Aldrich (St Louis, MO). Branched polyethyleneimine (PEI) (Mn=60kDa, Mw=750kDa, density=1.07 g/cm³ (at 20°C)) in DIW (50wt%), was purchased from Scientific Polymer Products (Ontario, NY). Compared with the polyethyleneimine grade (Mw=25kDa, Mn=10kDa), used by other researchers [24], this one demonstrated a higher thermal stability, according to the previous research conducted in this group [21]. Polyethylene terephthalate ionomer (AQ55S) (PETi) (density=0.82 g/cm³) was generously donated by Eastman Chemical Company (Kingsport, TN). The purified nanoclay, Cloisite Na⁺, was purchased from Southern Clay Products (SCP)(Gonzales, TX), with cation exchange capacity of 92mequiv/100g [25,26], and specific gravity of 2.86g/cm³ [26]. Irganox 1010 from Ciba was used as an antioxidant to avoid thermal oxidation of samples through cyclic melt pressing process.

Deionized water (DIW) used, mainly as a media for PEI and MMT, had a water resistivity of $18.2\text{M}\Omega$ at 25°C and was made by Direct-Q 3 UV water purification system of Millipore [24,27]. Ultra high purity (99.999% purity) O_2 was obtained from National Welders Supply Co. (Charlotte, NC) and Air Liquid America Specialty Gases LLC (Plumsteadville, PA). While high purity CO_2 (99.99% purity) was acquired from National Welders Supply Co. (Charlotte, NC).

7.2.2. Thin Film Preparation

Thin films of PVAc were prepared by solution casting from toluene at room temperature on crystallization plates, which were previously cleaned with acetone and methanol, before being rinsed by DIW, respectively. About 0.1wt% Irganox 1010 was added to the polymer as an antioxidant to prevent samples thermal oxidation, during cyclic melt pressing procedure. The resulted films were heated up to 50°C (around the glass transition temperature of PVAc), under vacuum, in order to assure complete removal of toluene.

7.2.3. Plasma Treatment

In order to promote hydrophilicity and surface adhesion properties of PVAc films for improving their adhesion to the subsequent LBL coatings, they were exposed to oxygen plasma in a laboratory and small-scale production plasma system FEMTO (low-pressure plasma), manufactured by Diener Electronics (Germany) at power of $10\text{W}/\text{cm}^2$, under gas flow rate of 20sccm (standard cubic centimeters per minute), or intensity of $0.5\text{W}/\text{sccm}$, for 60s, to induce polar groups such as carbonyl and carboxylic acid on their surface [28–30].

7.2.4. Layer-by-Layer (LBL) Coating of Thin Films

For coating the solution cast polymeric films with LBL assemblies, they were dipped in PETi solutions, which were previously made through stirring in DIW at 60°C, above PETi glass transition temperature. In fact, we used PETi, which is a PET with ionic functionalities and had been applied successfully for making PNCs [23,31], for making LBL assemblies. Then, the coated film was rinsed in DIW and dried under airflow. Suspensions of MMT in DIW were prepared through 20min ultrasonication, followed by stirring at about 600 rpm of MMT in DIW for 24 hours. The coating step is similar with that of PETi layer, and this bilayer coating procedure is repeated until reaching to the preferred number of bilayers (BLs). Due to the nature of the immersion process, bilayers are deposited on both sides of the polymeric substrate, but for simplicity, from now on we only count the number of bilayers (BLs) deposited on one side of the substrate in our remarks.

7.2.5. Cyclic Melt Pressing

PVAc films, already coated with LBL assemblies, were melt pressed with a Carver standard press between two aluminum plates covered by polyimide (PI) films, for up to 100 cycles. In fact, in each cycle the sample was folded 3 times, before being preheated for 3 minutes at 150°C and then being pressed at 3000 psi. Then the pressed sample was quenched between two big aluminum sheets.

7.2.6. Polarized Optical Microscopy (POM)

In order to picture the dispersion of clay particles in composites, membranes with thicknesses of about 50 μ m were observed with Nikon Optiphot2-Pol polarizing optical microscope, while the pictures were taken with a Canon camera.

7.2.7. Transmission Electron Microscopy (TEM)

Hot-pressed polymer nanocomposites were sectioned using freshly prepared glass knives with a Leica Ultracut 7 at ambient condition, to yield sections with an average thickness of about 80nm, which were floated onto DIW, and then were picked up on carbon coated 200 and 400 mesh copper TEM grids [7]. Then at an accelerating voltage of 200kV, using a JEOL 2000 FX (Parbody, MA) TEM and at calibrated magnifications a series of microscopic images were taken from microtomed thin sections.

7.2.8. X-Ray Diffractometry (XRD)

Prepared samples after being dried in vacuum oven at 30°C for 48 h (the same mechanism were examined through wide angle x-ray diffractometry at the ambient temperature on a Rigaku Rapid R-Axis Spider diffractometer (Rigaku, Texas) instrument, with CuK α radiation (wavelength $\lambda=0.15405$ nm) at 40kV and 36mA. XRD experiments were conducted in reflection mode using the Bragg-Brentano parafocusing geometry (powders and films), and diffraction intensity data were usually recorded in diffraction angle range of 3.0° to about 40.0° [18].

7.2.9. Dynamic Mechanical Analysis (DMA)

Samples, vacuum dried at 50°C for 48 h, with the dimensions of 15mmx6.5mm x0.5mm were probed by a Dynamic mechanical analysis (DMA) instrument Q800 from TA Instruments (New Castle DE), in tension mode. The experiments were conducted at constant-frequency mode (1.0Hz), with a strain of 0.3%, and at heating rate of 3°C/min from - 20 to 100°C, whereas the glass transition temperature (T_g) was measured as the peak of loss modulus plot (ASTM 1640-04) [12,32].

7.2.10. Gas Permeation

Gas permeation tests on samples, pre-dried for 48h at 50°C were conducted with a constant-volume/ variable-pressure technique, shown in the schematic Figure 4.1e. (Chapter 4) at 20°C and atmospheric pressure for both oxygen and carbon dioxide gases. Accordingly, after the evacuation of the whole system, the desired gas, with an upstream pressure of 1 atm was permeated through the membrane, while the pressure in the downstream chamber with known volume (V) was recorded, by a pressure transducer connected to a computer [33,34]. Consequently, the permeability values for the membranes were determined from the following equation.

$$P = \frac{VL}{ART\Delta P} \frac{dP}{dt} \quad ()$$

where L, A, R, ΔP , and $\frac{dP}{dt}$ are membrane thickness, membrane exposure area, universal gas constant, the difference between the constant upstream and initial downstream pressures, and steady rate of increase in gas pressure in downstream, respectively [33,34].

7.3. Results and Discussion

Due to holding functional acetate groups (carbonyl group, containing oxygen atoms) in its molecular chains, PVAc can potentially make a better interaction, than superhydrophobic polystyrene-based matrix, with both clay surface and polymeric interlayers (PETi contains polar oxygen groups as well to make hydrogen bonding with both clay and hydrogen of PVAc), possibly through hydrogen bonding. This good level of affinity, if aided by an intensive enough shear stress applied through melt mixing, peeling of clay platelets from their intercalated stacks might happen, towards reaching to a good level of nanodispersion [6].

In fact, despite observing a higher level of thermal stability for PNCs enclosing PETi interlayers, resulting in improved properties by increased time of mixing, in contrast with PEI-containing PNCs that due to incurring some slight degradation, sourced by PEI ingredient thermal degradation, did not show such improvement; PNCs containing PETi and polystyrene-based matrix did not show a good level of dispersion, which can be sought in insufficient interfacial interaction potential between the superhydrophobic matrix and LBL assemblies. Thus, a more hydrophilic and polar alternative, PVAc, was examined in this chapter (Chap.7) In addition, our PVAc is thermally stable up to 250°C, when its first degradation step, through deacetylation, occurs at above 300°C [35,36].

7.3.1. Polarized Optical Microscopy

Morphological investigations of our PNCs through microscopy were separated into two techniques. Due to taking images at low magnification scales, POM was used to determine general state of distribution and dispersion of clay particles throughout PNC [14,17,37],

whereas TEM micrographs dealt with probing delamination of clay platelets and swollen intercalation [38]. In the optical microscopy images under cross-polarized light condition (POM), amorphous polymeric matrix looks dark, while clay particle, due to scattering and depolarizing incident light, look bright.

For PNCs with PVAc matrix and containing PETi interlayers in their LBL assemblies it can be seen that, similar with previously studied polystyrene-based PNCs, with increase in number of pressing cycles from 25 to 100 (i.e. increase in time of melt mixing), dispersion (average sizes) and distribution of mashed portions of LBL assemblies in PS* matrix, presented significant improvement. This improvement can be related to low hydrophobicity of PVAc, and its potential for interaction with LBL assemblies through melt mixing [32,39] (Figure 7.2a,b).

Nevertheless, again like previous PNCs with polystyrene-based matrices, PNCs comprising PVAc and PETi showed decreased dispersion and distribution of LBL assemblies portion when clay content increases via the increased number of BL coatings [17] (Figure 7.2c,d). The low level of dispersion of clay in the polymeric matrix, particularly with the increase in clay contents, up to 5wt%, is a general negative feature of PNCs prepared through melt intercalation [1,22]. In our PNCs, it seems that due to existing significant cohesion in our LBL assemblies, the shear stress applied through cyclic pressing, despite possibly increased interaction between PVAc and LBL assemblies cannot provide a high level of global nanodispersion for clay platelets throughout the polymeric matrix. In addition, it should be considered that possibly due to higher interaction between hydrophilic PVAc and LBL ingredients these PNCs contain relatively higher contents of clay, compared with our

previously studied PNCs with polystyrene-based matrices. This increased clay content can be another reason for the decrease in the global dispersion of clay platelets in the matrix.

Estimating Clay Contents in PNCs. The volume fraction of LBL assemblies portions in PVAc matrix was determined by image analysis with Image J to estimate volume percentages of clay in PNCs [40,38,17] (Table 7.1). Comparing clay content estimated from image analysis of PNCs with PVAc matrices, containing PETi in their LBL assemblies with the former investigated PNCs with polystyrene-based matrices (Chapter 5), showed about three times higher clay content, in equal number of BL coating, which is possibly due to the higher hydrophilicity of PVAc matrix and its higher capability to attract clay platelets.

7.3.2. Transmission Electron Microscopy

TEM micrographs in different magnification scales from various regions of samples were taken in order to reveal the microstructure of our cyclically melt pressed PNCs. In this way, high clarity of PVAc provided a good visibility to observe the microstructure of clay particles, to investigate possible morphologies, complementing aforementioned POM observations [6,32]. In the bright-field TEM images, cross-sections of clay platelets are recognized as dark lines, relative to the bright polymeric matrix.

Looking at TEM micrographs of clay platelets in PNC samples it should be considered that TEM sections are not necessarily cut perpendicular to the clay's cross-section. Thus, their thicknesses may look thicker than their real size. On the other hand, due to the overlapping of clay platelets in each layer of LBL assemblies, we should be careful not to mistake the skewed

edge to edge flocculation of a few clay plates as one individual clay platelet [6,24] (Figures 7.3,7.4,7.5).

Qualitatively similar with the ones observed for PNCs based on styrenic matrices in our previous study (Chapter 5), in PVAc-based PNCs, while TEM images in low magnification scales, may mainly point to the existence of aggregated clusters [6,37] (which are portions of LBL assemblies, with size ranges of a few hundred nanometers up to a few micrometers); micrographs taken in higher magnification scales revealed the microstructure of clay particles, in form of swollen intercalations of face to face coagulated platelets [1,20,37], as well as, head to tail and head to face flocculated exfoliated platelets [1,6,17], down to the thickness of 2nm.

The reason behind significant flocculation, mainly edge to edge ones, may be due to the oriented structure of LBL assemblies, as a result of electrostatic attraction between layers. In fact, initial hydration of SiO groups into SiOH in deionized water, forms hydroxyl groups on clay platelets edges that promote their edge to edge attraction, to be deposited on PETi layers, and make edge-edge flocculations [1,8,41].

Yet again, almost similar with the PNCs with polystyrene-based matrix, it can be noticed that cyclic melt pressing of LBL-coated PVAc membranes, from one side crunches the LBL assemblies into smaller portions, and from the other side promotes the increase in the expansion of their already face-face intercalations, while improves the delamination of clay platelets, into exfoliated edge-edge and sometimes edge-face exfoliated tactoids of down to only a few clay platelets thick.

Nevertheless, despite the higher hydrophilicity of PVAc, and its possibly higher potential to interact with clay platelets, still the delamination observed is trivial, to almost rule out

formation of a global nanodispersion, the way that happens to traditional PNCs. Albeit those highly dispersed PNCs were mainly processed through more efficient approaches like solution or in-situ polymerization methods. This result can be partially related to high cohesion in LBL assemblies against their crushing into smaller portions, as an aftermath of their oriented layout, which by itself provides centers with high levels of flocculated exfoliations of clay platelets. Thus, it cannot necessarily be assumed as a negative issue with these innovative PNCs. While probably, low efficiency of cyclic pressing to apply shear force to LBL assemblies may be taken as an additional reason for the resulted morphology. In addition, as mentioned before increased clay content in hydrophilic PVAc matrix can be considered as another impediment to increasing the dispersion level.

Detailed Examples of Observed Morphologies in Different Samples. Once more, in qualitative consistency with polystyrene-based PNCs, each of different samples almost comprise all possible morphological features mentioned above. For instance, different TEM micrographs from different regions of PNC made from PVAc membranes with 10BL coatings showed various morphologies (Figure 7.3). In Figure 7.3a particularly in the higher magnified window, exfoliated layers of one to a few clay platelets, inside the expanded LBL are clearly observable. In Figure 7.3b, although in low magnification scales the LBL assembly looked completely unaffected, the image with higher magnification showed increased disorientations, where both face-face coagulated intercalations, plus edge-face and edge-edge flocculated exfoliated layers [1,20] of a few platelets (tactoids) with thicknesses of a few nanometers are observable. Another example can be signs of individual platelets delamination out of the left

side of intercalated LBL assemblies (Figures 7.3c and 7.3e). Another region (Figure 7.3d) showed so many head-tail flocculated (skewed) layers of one up to a few clay platelets, plus small areas of face-face coagulated intercalated stacks; while Figure 7.3f, particularly in higher magnification scale, showed a tiny aggregation of a few separated clay platelets, with some levels of edge-edge flocculation.

In addition, for samples melt pressed for only 25 cycles, exfoliation of layers of one up to a few clay platelets is observable (Figure 7.4a). Even in the case of observing an almost uncrushed LBL assemblies (Figure 7.4b), higher magnification images showed signs of expanded intercalations as well as split individual clay platelets out of LBL assemblies.

In a TEM micrograph taken from PNC made from PVAc substrate with 5BL coatings many dispersed exfoliated platelets with the thicknesses of about 2-4 nm and lengths of about 100nm, are vastly observed (Figure 7.5a). Finally, for the PNC of 15BL coatings, TEM image (Figure 7.5c) showed a large aggregation comprising swollen intercalations and face-edge as well as edge-edge flocculations of exfoliated clay tactoids and platelets. On the other hand, other regions of this PNC demonstrated crushing of LBL assemblies into small aggregations, with only a few clay platelets, which are mostly exfoliated (Figure 7.5b).

Thus, as mentioned before, despite observing some dispersion and distribution trend in POM images (and possibly XRD) taken from different PNCs, induced by variations in time of processing and number of BLs, TEM micrographs proved the occurrence of almost all possible theoretical morphologies in each sample.

7.3.3. X-Ray Diffractometry

In collaboration with microscopic imaging, XRD is considered as a technique to quantify the occurrence of any intercalation or exfoliations of clay species in PNCs, through detecting shift or possible disappearance of characteristic peaks related to basal planar spacing of clay platelets [1]. As previously studied (Chapter 3), XRD diffractograms detected a significant peak at 8.37° for neat MMT, related to the basal (001) distance of 1.056nm [24,27]. Then, as a result of intercalation of PETi interlayers between clay platelets in their LBL assemblies, clay interplanar spacing increased to show a shift in the corresponding intercalation peak to lower diffraction angles. Then, PNCs made with crushed LBL assemblies in polystyrene-based matrices showed both shifts in the intercalation peak to lower angles and decreases in its significance with the increase in time of mixing and decrease in clay content (Chapter 5), to point to possibly increased intercalations and exfoliations of clay in their PNCs [1,11,17].

In the case of cyclically melt pressed PNCs, prepared from LBL-coated PVAc films, studied in this article, all samples showed very broad and insignificant peaks around diffraction angle of 6° . The reason for this insignificance, in addition to a possible side effect of the big peak around 14° , as a feature of PVAc matrix, which is common for all PNCs, might be rising clay platelets interdistance irregularities, as a result of their increased intercalation and exfoliation induced through melt mixing process. This result implies the occurrence of significant interaction between hydrophilic PVAc and clay platelets, possibly more than what resulted for hydrophobic polystyrene-based matrices investigated in our previous study (Chapter 5), to overcome the van der Waals forces in galleries between clay layers, in order to improve their delamination and exfoliations. Also, it can be seen that with the increase in the

number of BL coatings, in other words, increasing clay content in PNCs, the corresponding peaks became a little more noticeable, pointing to relative decreases in their exfoliations [11,17,39]. It is similar to the trend observed for PNCs prepared with polystyrene-based matrices, studied in Chapter 5, but considering that PVAc PNCs have a higher clay content, as estimated from the POM images.

7.3.4. Dynamic Mechanical Investigations

Storage and Loss Moduli. In PNCs based on PVAc matrix and LBL assemblies of PETi and MMT, a noticeable increase in the elastic modulus, compared with pristine PVAc is observed, similar to what observed for PS* based PNCs, related to the reinforcing effect of clay platelets [1]. In addition, it can be seen that with the increase in the number of BL coating, and so increasing the clay content in PNCs, this increasing effect intensifies [6,12,40]. Similarly, clay particles increase the damping potential of the matrix with an increase in clay content, to observe a higher loss modulus for them. So, it can be conjectured that relatively less hydrophobic PVAc can develop a better interaction with PETi, than what PS* did, in favor of promoting dispersion of LBL assemblies, and so clay particles, through cyclic pressing. Thus, the experienced clay loading increase has more increasing effect on its interfacial area in PNC, rather than the decreasing role that may have, through the decrease in clay dispersion [22] (Figure 7.7).

POM image analysis showed higher clay content in PVAc PNCs, possibly due to higher hydrophilicity of PVAc, than that of PS* based PNCs. It may be a reason for observing more

significant increase in modulus values for PVAc-based PNCs, provided that the dispersion is kept at a comparative level to result in increased effective clay content.

On the other hand, it can be seen that with increased number of pressing cycles from 25 to 100, despite improved dispersion of clay particles observed by POM micrographs that raised the expectations for improvement in mechanical properties [22,42], both storage and loss moduli incur decrease, possibly due to slight thermomechanical degradation of PVAc [1]. Nevertheless, the PVAc (Aldrich, $M_w = 100\text{kDa}$) does not show any significant degradation below 300°C (Figure 7.8) [35,43].

Glassy Transition Temperature. In the case of glassy transition of matrix, from the POM and TEM micrographs it can be noticed that similar with PS* based PNCs, most crushed portions of LBL assemblies in the matrix are in scale of micrometer, despite reaching to flocculated exfoliation of clay platelets inside those LBL assemblies and tracking occasionally separated tactoids of one up to a few clay platelets. Thus, due to not observing a prominent nanodispersion throughout PVAc matrix, to provide interdistance of smaller than polymeric chains radii of gyration, the case of shift in glassy transition of the matrix by nano-effect, through nanoscale constraints for polymeric chains is ruled out [1,6,13,17,40,44].

Compared with pristine PVAc, despite close glassy transition temperatures of PVAc (49.2°C) and PETi (52°C), a slight rise in the PNC glassy transition is observed, again implying on the occurrence of significant interactions between PETi and PVAc [45]. Also, with the increase in the number of BL coatings, as a result of increased content of PETi, it poses stronger effect on PNC relaxation temperature (Fox Equation). Such increases in glassy transition are

similar to what had happened for PB phase in PS*. Conversely, with the surge in the time of cyclic hot pressing, despite possible improvement in the interactions between PETi and PVAc, T_g decreases, that like the aforementioned decrease in elastic and loss moduli, may be a clue to probably slight thermomechanical degradation of PVAc.

7.3.5. Permeation Properties

Looking at the oxygen and carbon dioxide permeation through PVAc and its PNCs, it can be noticed that with increasing number of BL coating on the polymeric substrate, in other words with an increase in the clay content, the barrier properties improve. This improvement, in confirmation of DMA results, may point to occurring significant interaction between PVAc matrix and clay that can keep dispersion and exfoliation of clay in the matrix at a suitable level, despite the increase in its content (Figure 7.9). On the other hand, from observing decreased gas barrier properties for our PNC, with increasing the number of pressing cycles from 25 to 100, despite observing clay's higher dispersion from corresponding POM images, and along with decreasing trend in moduli observed from DMA results, the occurrence of some degradation in PVAc matrix, through extended time of processing at 150°C, may be postulated. Nevertheless, the observed decrease in both gases permeations through our PNCs, particularly in the lower time of melt processing, is significant. It can be related to relatively high hydrophilicity of PVAc to interact with clay platelets, in favor of their delamination and exfoliation, as were previously discussed. It might also be due to high tortuosity of LBL assemblies portions, comprising of swollen intercalated and exfoliated clay platelets. Also, due to high length of these oriented assemblies, possibly as a result of initial hydration of clay in

water, electrostatic interaction between oppositely charged layers in LBL, and so promoting edge to edge flocculation of clay platelets in LBL assemblies, the resulting high aspect ratio, increases their barrier efficiency against permeating gases [9,22,46–48]. The additional reason for resulted barrier improvement might be increased orientation and delamination induced in clay layers, as a result of cyclic pressing of samples into thin films [7]. All in all, those oriented and high aspect ratio LBL assemblies' portions, with their significant internal tortuosity, may act very efficiently to improve barrier properties of the contained matrix against gases, despite moderate level of global dispersion of clay platelets throughout the polymeric matrix, as a negative feature of melt mixing approach that usually does not provide a very good level of dispersion [1,22] (Tables 7.2 and 7.3).

7.4. Conclusion

This article tried to examine PVAc as the matrix for polymer nanocomposites prepared through LBL deposition of PETi and MMT on polymeric membranes, followed by cyclic pressing of the coated substrate, similar to the baker's method used in our previous study with the polystyrene-based matrix. In fact, due to the potentially weak interaction of hydrophobic PS-based matrix with clay, which had been suggested as one of the main reasons for low dispersion of clay in the polymeric matrix, a more hydrophilic polymer was investigated in this study. In addition, as another postulated reason behind low level of dispersion in previous PNCs was slight degradation of PEI interlayers during extended times of cyclic pressing at elevated temperatures, this time only more thermally stable PETi was used.

Dynamic mechanical analyses showed relatively higher moduli and glassy transition temperature values for PNCs, compared with pristine polymers. Also, polarized optical microscopy images exhibited improve in dispersion and distribution of clay particles in PVAc matrix with increase in the time of melt processing and decrease in clay content, in accordance with our previously studied PNCs, using polystyrene-based matrices. In addition, TEM micrographs showed the occurrence of all possible morphologies, mainly including swollen intercalated stacks, flocculated exfoliated tactoids of skewed clay layers, and delaminated individual clay platelets.

Yet again, similar to what suggested for styrenic PNCs, relatively significant improvement in barrier properties of PNCs with PVAc matrix, postulated the scavenging effect of high aspect ratio LBL assemblies' crushed portions that include internal swollen intercalations and flocculated exfoliations, observed in microscopic images. Another reason for this improvement might be, promoted orientation and delamination of clay layers as a result of cyclic melt pressing of samples into thin films. Moreover, confirming DMA results that presented increase in moduli with increase in clay content, permeation results showed similar improvement in barrier properties of PNCs, pointing to occurring significant interaction between PVAc, PETi, and clay, to keep the exfoliation level of the PNCs significantly high (while their clay contents rise), to escalate overall effective interface between clay and matrix.

Also, POM images, showed higher contents of clay in these PNCs, compared with previous styrenic ones. Furthermore, for the samples, only melt pressed for 25 cycles, DMA experiment of our PVAc-based PNCs showed noticeable increases in moduli values, and permeation test exhibited significant improvement in their gas barrier properties. All these results postulated

occurrence of a significant interaction between PVAc matrix, PETi, and MMT, possibly more than what happened to PS-based PNCs, although downsizing in those improvements with the increase in the time of processing towards 100 melt pressing cycle, may conjecture occurrence of slight degradation in PVAc matrix.

Thus, it is concluded that although using a more hydrophilic polymer, as expected may improve the level of interaction occurred between organic and inorganic phases; due to existing significant internal cohesion within LBL assemblies, for reaching to a higher global dispersion of clay particles throughout polymeric matrix, a more intensive manner of mixing, like what is reached by a twin-screw extruder is suggested. While melt processing under the purge of an inert gas, like nitrogen, may decrease possible thermal degradation in PNCs, particularly in extended times of process.

Tables

Table 7.1. Estimation of the clay content in PNCs through image analysis.

PVAc, PETi, MMT, PNC	Particle vol%
5BL	1.85
10BL	3.05
15BL	4.95

Table 7. 2. Permeability results for O₂ through cyclically melt pressed PNCs, based on LBL-coated PVAc membranes at the standard atmospheric conditions.

Thin film assembly	O ₂ Permeability (cm ³ .m/m ² .day.atm)	BIF	MMT Content (vol %)	Temperature (°C)
PVAc	0.032206			293
10BL (0.5 PETi, 1M) (25cycle,150°C)	0.015167	2.12		293
10BL (0.5 PETi, 1M) (100cycle,150°C)	0.017991	1.79	3.05	293
5BL (0.5 PETi,1M) (100cycle,150°C)	0.022357	1.44	1.85	293
15BL (0.5 PETi,1M) (100cycle,150°C)	0.017597	1.83	4.95	293

Table 7.3. Permeability results for CO₂ through cyclically melt pressed PNCs, based on LBL-coated PVAc membranes at the standard atmospheric conditions.

Thin film assembly	CO ₂ Permeability (cm ³ .m/m ² .day.atm)	BIF	MMT Content (vol %)	Temperature (°C)
PVAc	0.11490			293
10BL (0.5 PETi, 1M) (25cycle,150°C)	0.053800	2.13		293
10BL (0.5 PETi, 1M) (100cycle,150°C)	0.068000	1.69	3.05	293
5BL (0.5 PETi,1M) (100cycle,150°C)	0.071200	1.61	1.85	293
15BL (0.5 PETi,1M) (100cycle,150°C)	0.066300	1.73	4.95	293

Figures

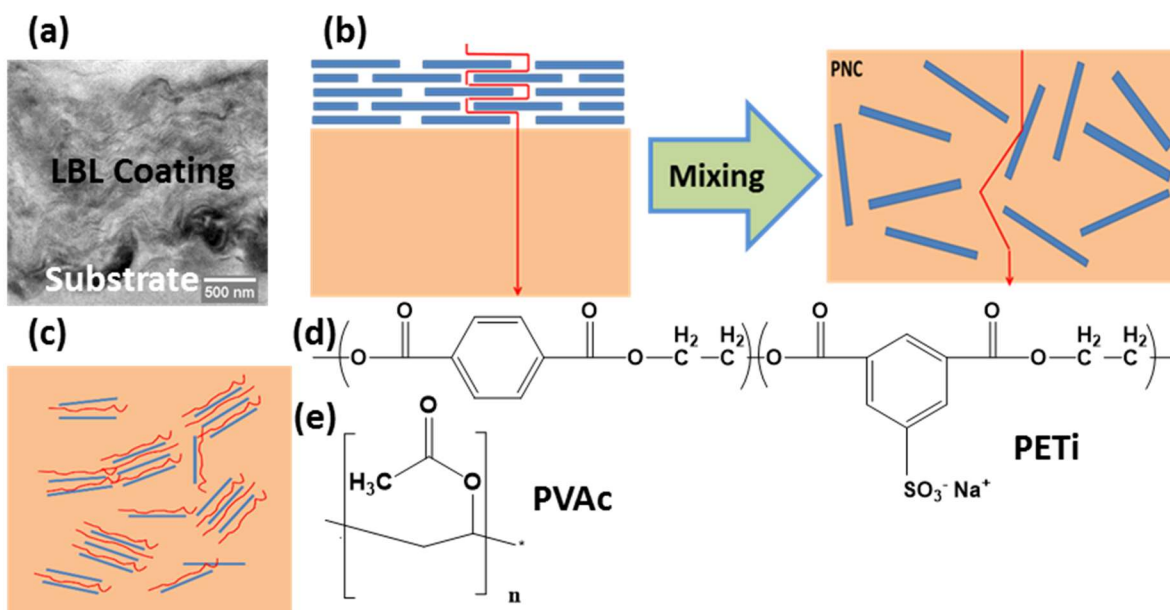


Figure 7.1. (a) Cross-section of a TEM image of a polymeric membrane coated with LBL assemblies. (b) Schematic of a polymer layer coated with LBL assemblies, the polymer nanocomposite (PNC) resulted after cyclic hot pressing, with gas permeation route in them. (c) A detailed schematic of LBL portions in PNC. (d) Chemical formulae of PETi as macromolecular glue. (e) The chemical formula of PVAc used as the polymeric matrix.

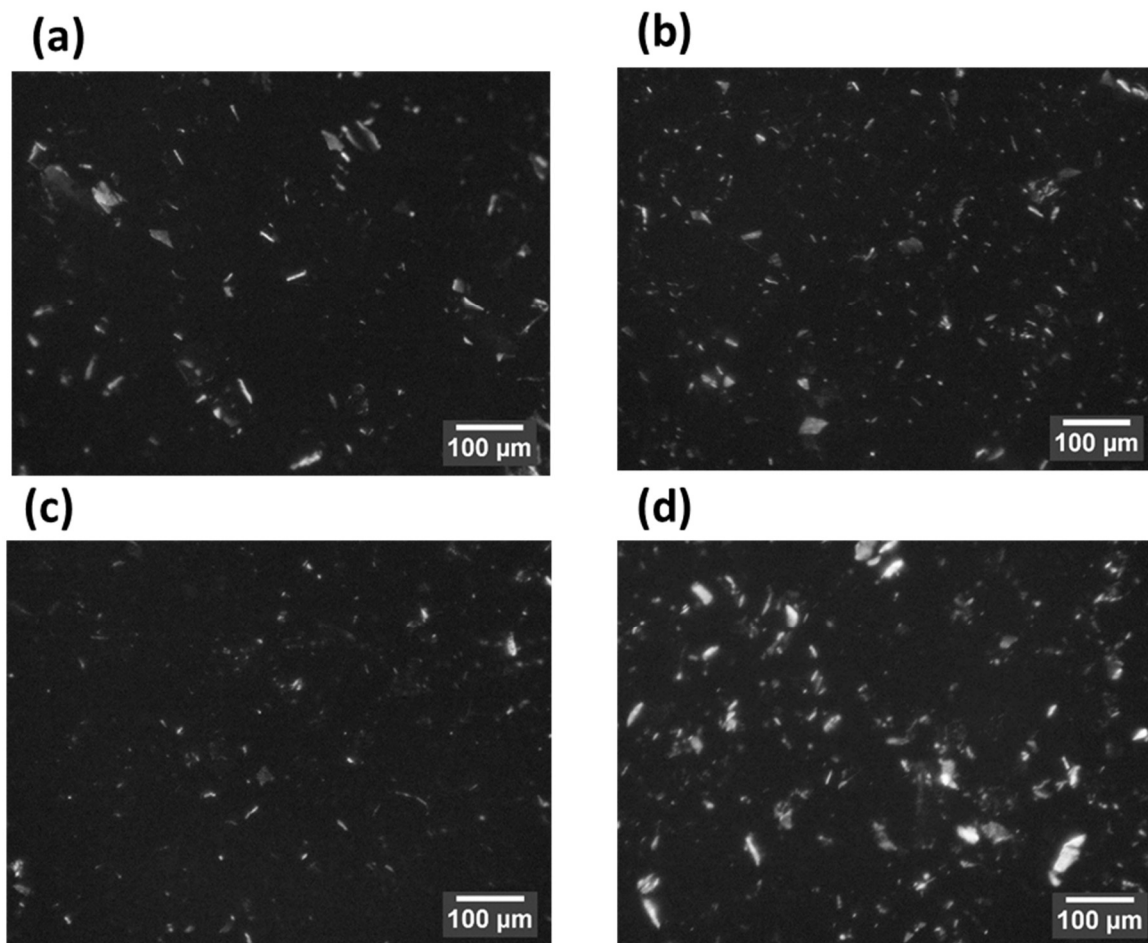


Figure 7.2. Optical microscope images of PNC of PVAc with PETi and MMT LBL assemblies, for (a) 10 times deposition of BL coating, after 25 cycles of melt pressing, and for 100 cycles pressing when the samples were coated with (b) 10, (c) 5, and (d) 15 times of BL depositions.

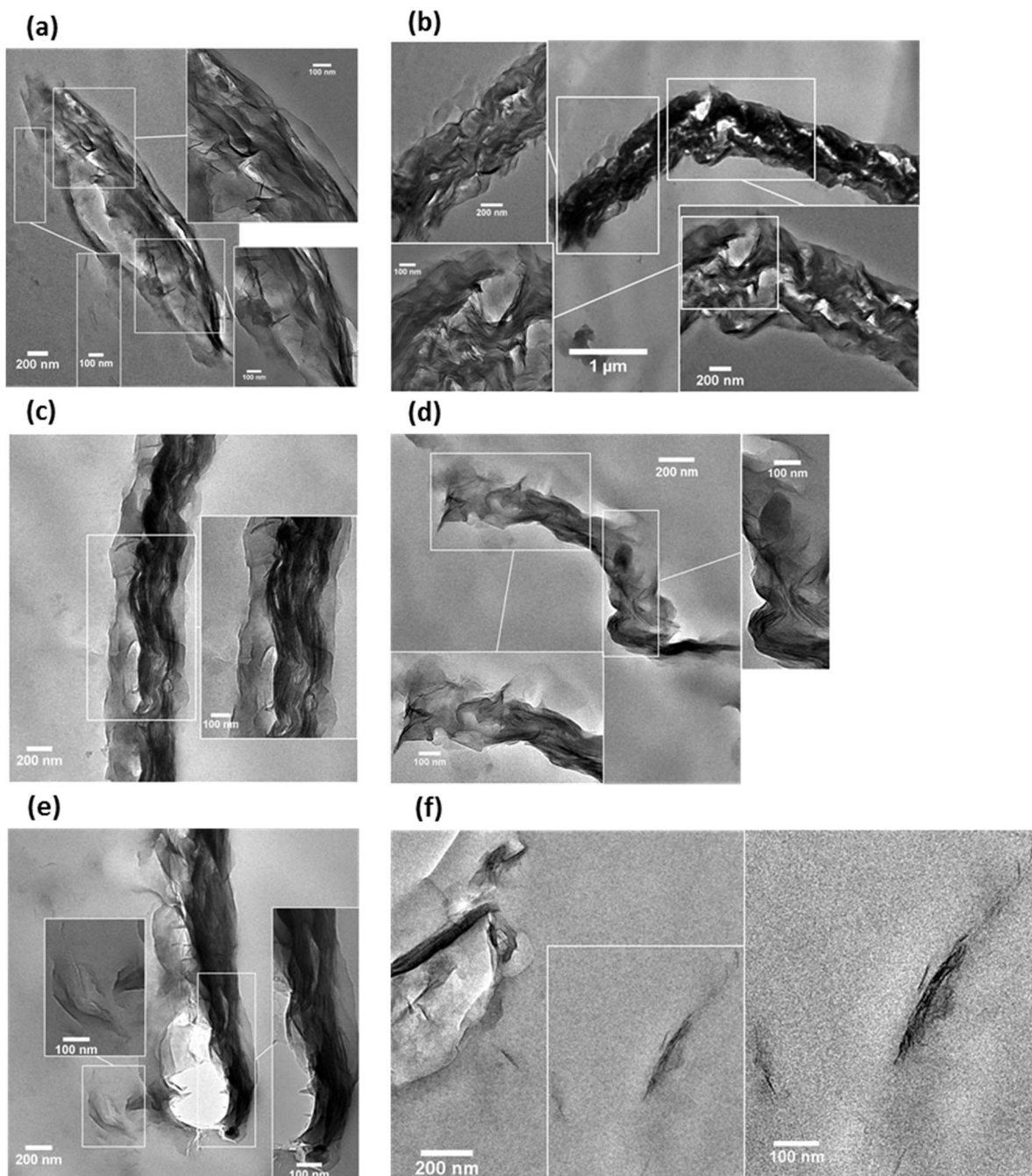


Figure 7.3. TEM micrographs of 100 cycles pressed PNCs containing PEI interlayers in their LBL assemblies' portions comprising 10-BL coatings.

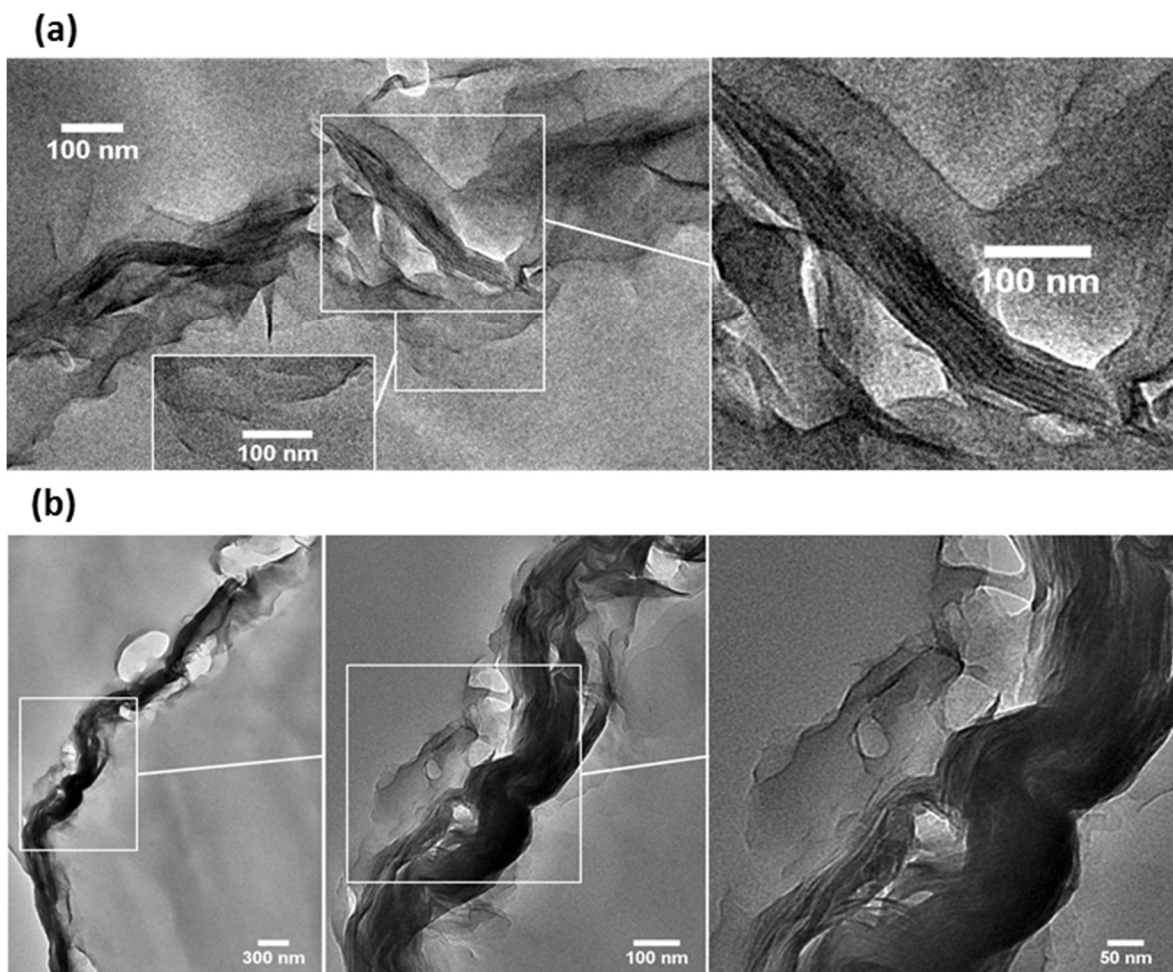


Figure 7.4. TEM micrographs of 25 cycles pressed PNCs containing PEI interlayers in their LBL assemblies' portions comprising 10-BL coatings.

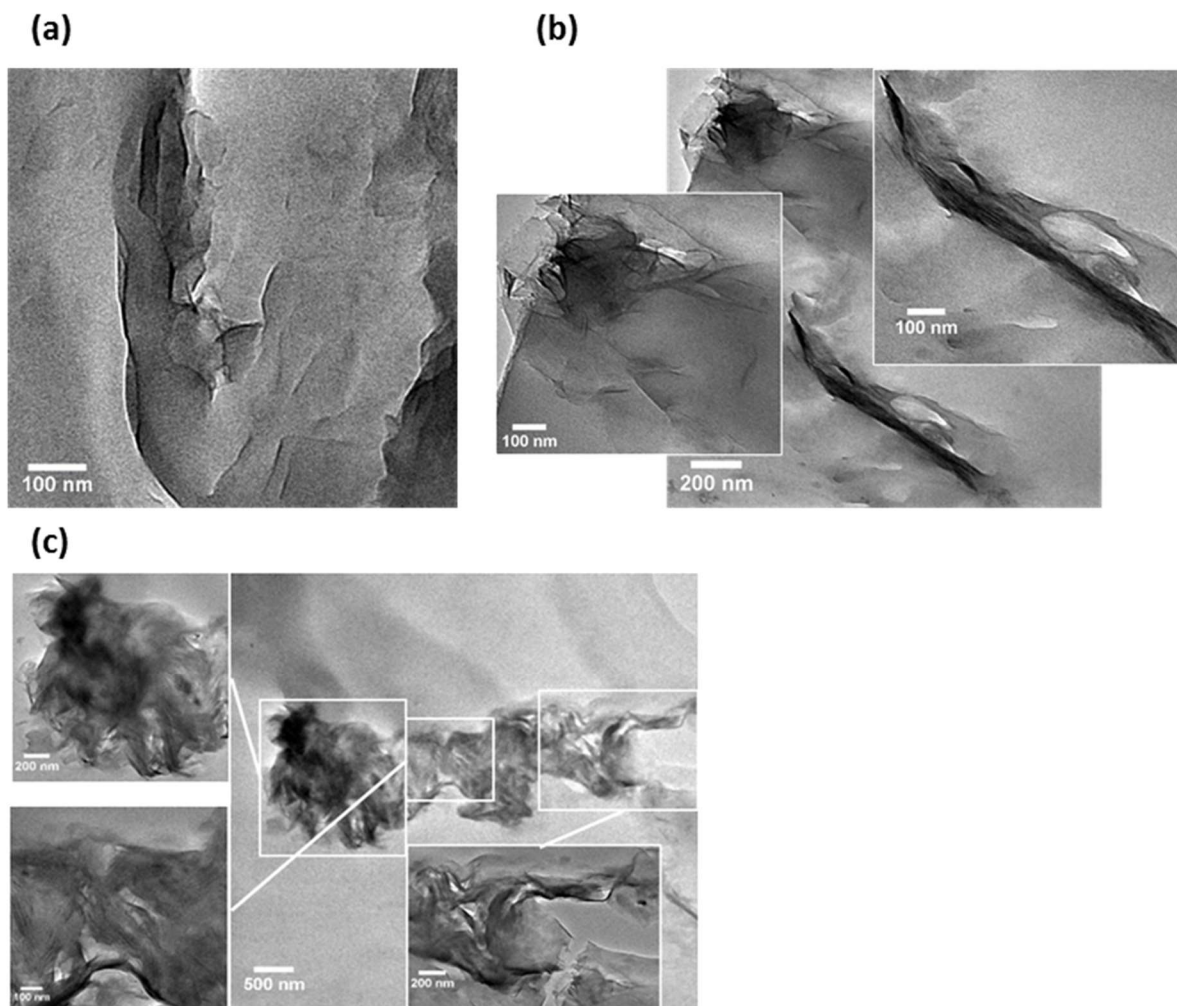


Figure 7.5. TEM micrographs of 100 cycles pressed PNCs containing PETi interlayers in their LBL assemblies' portions comprising (a) 5, (b) and (c) 15-BL coatings.

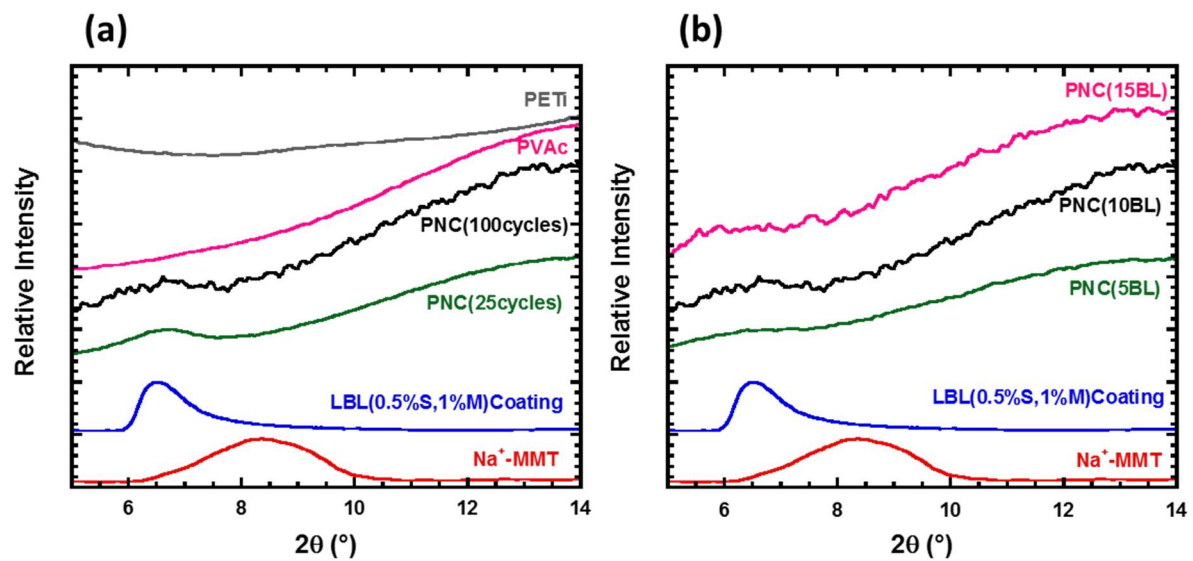


Figure 7.6. XRD patterns for neat MMT, its LBL assemblies coating with PETi, and melt processed PNC with (a) different numbers of pressing cycles of 25 and 100 and (b) different numbers of deposited BL coatings of 5, 10, and 15.

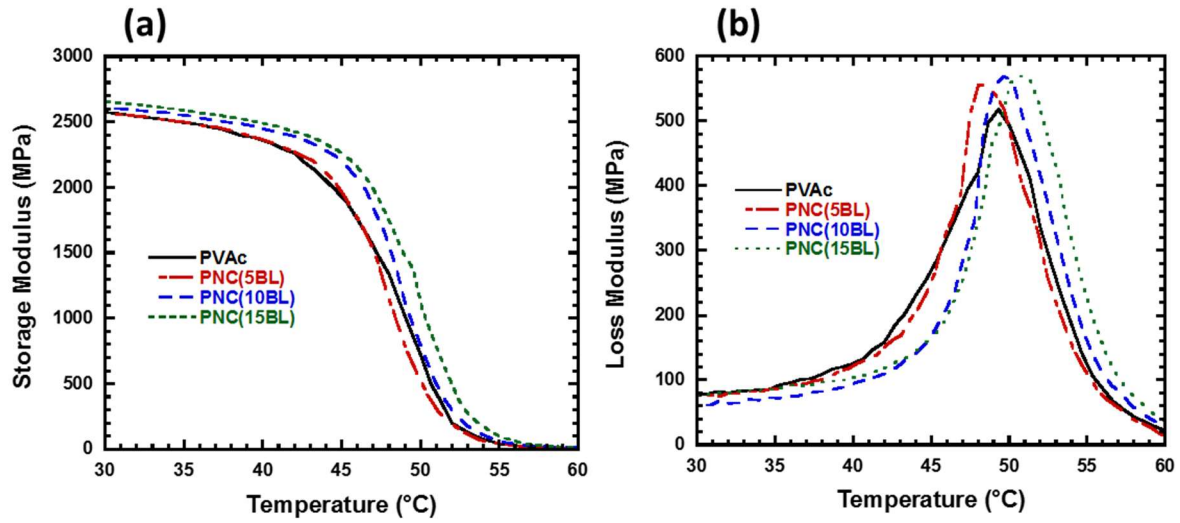


Figure 7.7. (a) Storage and (b) Loss Modulus as a function of temperature for PVAc and its PNCs made from 5, 10, 15BL deposition of PETi(0.5wt% in DIW) and MMT(1wt% in DIW), followed by 100 melt pressing cycles at 150°C.

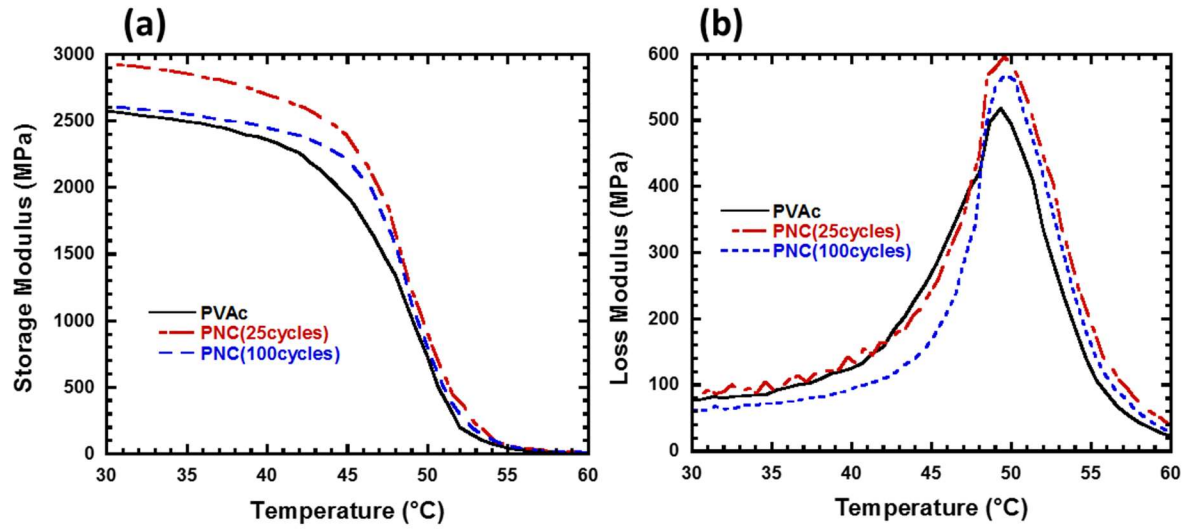


Figure 7.8. (a) Storage and (b) Loss Modulus as a function of temperature for PVAc and its PNCs made from the 10BL deposition of PETi(0.5wt% in DIW) and MMT(1wt% in DIW), followed by 25 and 100 melt pressing cycles at 150°C.

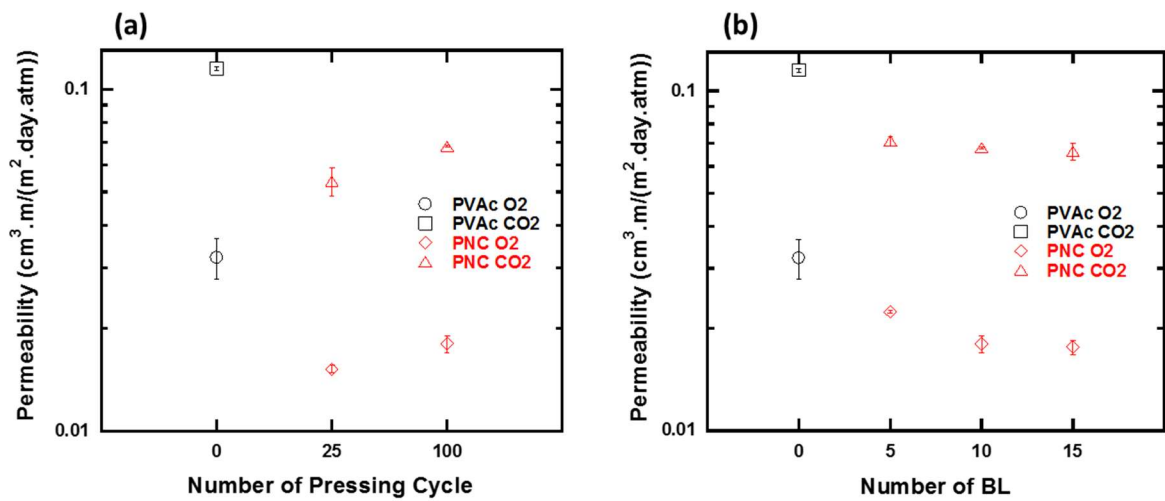


Figure 7.9. Permeation values of oxygen and carbon dioxide at 20°C, in PVAc and PNCs, as a function of (a) the number of melt pressing cycles, and (b) the number of BL coating applied initially on PVAc substrate.

References

- [1] S.S. Ray, Recent Trends and Future Outlooks in the Field of Clay-Containing Polymer Nanocomposites, *Macromol. Chem. Phys.* 215 (2014) 1162–1179.
- [2] E. Jacquelot, E. Espuche, J.F. Gérard, J. Duchet, P. Mazabraud, Morphology and gas barrier properties of polyethylene-based nanocomposites, *J. Polym. Sci. Part B Polym. Phys.* 44 (2006) 431–440.
- [3] G.W. Beall, C.E. Powell, *Fundamentals of Polymer-Clay Nanocomposites*, 1st ed., Cambridge University Press, Cambridge, UK, 2011.
- [4] L.E. Nielsen, Models for the permeability of filled polymer systems, *J. Macromol. Sci.* 1 (1967) 929–942.
- [5] R.K. Bharadwaj, Modeling the barrier properties of polymer-layered silicate nanocomposites, *Macromolecules*. 34 (2001) 9189–9192.
- [6] D.R. Paul, L.M. Robeson, Polymer nanotechnology: Nanocomposites, *Polymer* 49 (2008) 3187–3204.
- [7] W. Huang, S. Zeng, J. Liu, L. Sun, Bi-axially oriented polystyrene/montmorillonite nanocomposite films, *RSC Adv.* 5 (2015) 58191–58198.
- [8] S. Nazarenko, P. Meneghetti, P. Julmon, B.G. Olson, S. Qutubuddin, Gas barrier of polystyrene montmorillonite clay nanocomposites: Effect of mineral layer aggregation, *J. Polym. Sci. Part B Polym. Phys.* 45 (2007) 1733–1753.
- [9] A. Panwar, V. Choudhary, D.K. Sharma, Review: A review: polystyrene/clay nanocomposites, *J. Reinf. Plast. Compos.* 30 (2011) 446–459.
- [10] A. Giannakas, A. Giannakas, A. Ladavos, Preparation and Characterization of Polystyrene/Organolaponite Nanocomposites, *Polym. Plast. Technol. Eng.* 51 (2012) 1411–1415.
- [11] N. Greesh, S.S. Ray, J. Bandyopadhyay, S. Sinha Ray, J. Bandyopadhyay, Role of nanoclay shape and surface characteristics on the morphology and thermal properties of polystyrene nanocomposites synthesized via emulsion polymerization, *Ind. Eng. Chem. Res.* 52 (2013) 16220–16231.
- [12] K.J. Lin, C.H. Lee, K.F. Lin, Extraordinary mechanical behavior of exfoliated montmorillonite/polymer nanocomposite films cast from soap-free emulsion polymerized latices, *J. Polym. Sci. Part B Polym. Phys.* 48 (2010) 1064–1069.

- [13] A. Bansal, H. Yang, C. Li, K. Cho, B.C. Benicewicz, S.K. Kumar, et al., Quantitative equivalence between polymer nanocomposites and thin polymer films., *Nat. Mater.* 4 (2005) 693–698.
- [14] S.S. Ray, *Clay-containing polymer nanocomposites: from fundamentals to real applications*, First, Elsevier, Amsterdam, 2013.
- [15] M. Song, J. Jin, Rheological behavior of polymer nanocomposites, in: V. Mittal (Ed.), *Optim. Polym. Nanocomposite Prop.*, 1st ed., Wiley-VCH, Weinheim, Germany, 2010: pp. 93–122.
- [16] J. Golebiewski, A. Galeski, Thermal stability of nanoclay polypropylene composites by simultaneous DSC and TGA, *Compos. Sci. Technol.* 67 (2007) 3442–3447.
- [17] A. Ranade, N.A. D'Souza, B. Gnade, Exfoliated and intercalated polyamide-imide nanocomposites with montmorillonite, *Polymer* 43 (2002) 3759–3766.
- [18] D.J. Frankowski, M.D. Capracotta, J.D. Martin, S. a. Khan, R.J. Spontak, Stability of organically modified montmorillonites and their polystyrene nanocomposites after prolonged thermal treatment, *Chem. Mater.* 19 (2007) 2757–2767.
- [19] V. Mittal, *Optimization of Polymer Nanocomposite Properties*, 1st ed., Wiley-VCH, Weinheim, Germany, 2010.
- [20] M. Galimberti, *Rubber Clay Nanocomposites*, *Adv. Elastomers – Technol. Prop. Appl.* (2012).
- [21] A.E. Özçam, *Surface Modification and Characterization of Polymeric Materials for Targeted Functionality*, Ph.D. Dissertation, North Carolina State University, 2011.
- [22] M. Ziadeh, B. Fischer, J. Schmid, V. Altstädt, J. Breu, On the importance of specific interface area in clay nanocomposites of PMMA filled with synthetic nano-mica, *Polymer* 55 (2014) 3770–3781.
- [23] A. Ammala, C. Bell, K. Dean, Poly (ethylene terephthalate) clay nanocomposites: improved dispersion based on an aqueous ionomer, *Compos. Sci. Technol.* 68 (2008) 1328–1337.
- [24] M.A. Priolo, K.M. Holder, D. Gamboa, J.C. Grunlan, Influence of clay concentration on the gas barrier of clay–polymer nanobrick wall thin film assemblies, *Langmuir.* 27 (2011) 12106–12114.
- [25] M. Pluta, A. Galeski, M. Alexandre, M. a. Paul, P. Dubois, Polylactide/montmorillonite nanocomposites and microcomposites prepared by melt blending: Structure and some physical properties, *J. Appl. Polym. Sci.* 86 (2002) 1497–1506.

- [26] M.N. Muralidharan, S.A. Kumar, S. Thomas, Morphology and transport characteristics of poly(ethylene-co-vinyl acetate)/clay nanocomposites, *J. Memb. Sci.* 315 (2008) 147–154.
- [27] Y.-H. Yang, F.A. Malek, J.C. Grunlan, Influence of deposition time on layer-by-layer growth of clay-based thin films, *Ind. Eng. Chem. Res.* 49 (2010) 8501–8509.
- [28] I. Beaulieu, M. Geissler, J. Mauzeroll, Oxygen plasma treatment of polystyrene and zeonor: Substrates for adhesion of patterned cells, *Langmuir.* 25 (2009) 7169–7176.
- [29] C. Chaiwong, P. Rachtanapun, P. Wongchaiya, R. Auras, D. Boonyawan, Effect of plasma treatment on hydrophobicity and barrier property of polylactic acid, *Surf. Coatings Technol.* 204 (2010) 2933–2939.
- [30] S. Guruvenket, G.M. Rao, M. Komath, A.M. Raichur, Plasma surface modification of polystyrene and polyethylene, *Appl. Surf. Sci.* 236 (2004) 278–284.
- [31] A. Ghanbari, M.-C.C. Heuzey, P.J. Carreau, M.-T.T. Ton-That, Morphology and properties of polymer/organoclay nanocomposites based on poly(ethylene terephthalate) and sulfopolyester blends, *Polym. Int.* 62 (2013) 439–448.
- [32] S.M. Miriyala, Y.S. Kim, L. Liu, J.C. Grunlan, Segregated Networks of Carbon Black in Poly (vinyl acetate) Latex : Influence of Clay on the Electrical and Mechanical Behavior, *Macromol. Chem. Phys.* 209 (2008) 2399–2409.
- [33] X. Hu, J. Tang, A. Blasig, Y. Shen, M. Radosz, CO₂ permeability, diffusivity and solubility in polyethylene glycol-grafted polyionic membranes and their CO₂ selectivity relative to methane and nitrogen, *J. Memb. Sci.* 281 (2006) 130–138.
- [34] N.P. Patel, A.C. Miller, R.J. Spontak, Highly CO₂-Permeable and Selective Polymer Nanocomposite Membranes, *Adv. Mater.* 15 (2003) 729–733.
- [35] B. Rimez, H. Rahier, G. Van Assche, T. Artoos, M. Biesemans, B. Van Mele, The thermal degradation of poly(vinyl acetate) and poly(ethylene-co-vinyl acetate), Part I: Experimental study of the degradation mechanism, *Polym. Degrad. Stab.* 93 (2008) 800–810.
- [36] G. Wypych, *Handbook of Polymers*, 1st ed., ChemTec, Basel, Switzerland, 2012.
- [37] F. Bertini, M. Canetti, G. Audisio, G. Costa, L. Falqui, Characterization and thermal degradation of polypropylene-montmorillonite nanocomposites, *Polym. Degrad. Stab.* 91 (2006) 600–605.
- [38] S.H. Kim, S.C. Kim, Synthesis and Properties of Poly (ethylene terephthalate)/ Clay Nanocomposites by In Situ Polymerization, 103 (2007) 1262–1271.

- [39] W. Lertwimolnun, B. Vergnes, Influence of compatibilizer and processing conditions on the dispersion of nanoclay in a polypropylene matrix, *Polymer* 46 (2005) 3462–3471.
- [40] T.D. Fornes, D.R. Paul, Modeling properties of nylon 6/clay nanocomposites using composite theories, *Polymer* 44 (2003) 4993–5013.
- [41] G. Decher, Layer-by-Layer Assembly, in: G. Decher, J.B. Schlenoff (Eds.), *Multilayer Thin Film.*, Willey-VCH, Weinheim, Germany, 2012: pp. 1–22.
- [42] F. Quadrini, D. Bellisario, C. Lucignano, L. Santo, The Role of Mixing Time in the Production of Nanocomposite Thermosetting Coatings, *Polym. Plast. Technol. Eng.* 52 (2013) 1200–1212.
- [43] G. Sivalingam, R. Karthik, G. Madras, Blends of poly(ϵ -caprolactone) and poly(vinyl acetate): mechanical properties and thermal degradation, *Polym. Degrad. Stab.* 84 (2004) 345–351.
- [44] C. Ding, B. Guo, H. He, D. Jia, H. Hong, Preparation and structure of highly confined intercalated polystyrene/montmorillonite nanocomposite via a two-step method, *Eur. Polym. J.* 41 (2005) 1781–1786.
- [45] M. Pluta, J.K. Jeszka, G. Boiteux, Polylactide/montmorillonite nanocomposites: Structure, dielectric, viscoelastic and thermal properties, *Eur. Polym. J.* 43 (2007) 2819–2835.
- [46] J.P. DeRocher, B.T. Gettelfinger, J. Wang, E.E. Nuxoll, E.L. Cussler, Barrier membranes with different sizes of aligned flakes, *J. Memb. Sci.* 254 (2005) 21–30.
- [47] D. Feldman, Polymer Nanocomposite Barriers, *J. Macromol. Sci. Part A.* 50 (2013) 441–448.
- [48] G. Choudalakis, A. D. Gotsis, Permeability of polymer/clay nanocomposites: A review, *Eur. Polym. J.* 45 (2009) 967–984.

CHAPTER 8

Conclusions and Future Steps

8.1. Conclusions

Combinative morphological investigations of two types of LBL assemblies prepared from either PEI or PETi, as the polyelectrolyte, with MMT, through microscopic and XRD techniques, presented the formation of galleries between intercalated and exfoliated clay platelets layers, oriented parallel to the substrate surface, to form tortuous networks. It is postulated that, increasing the clay concentration in its suspensions, possibly through increasing the viscosity and decreasing the exfoliation level of their suspensions, might decrease the orientation and intercalation of LBL assemblies.

Then, gas permeation experiments demonstrated dramatic barrier improvement against oxygen and carbon dioxide, for the polystyrene-based films coated by these LBL assemblies, reaching to about 500 times decrease in oxygen permeability by only five times immersion in clay suspension. Such significant barrier improvement can be conjectured as a result of different reasons, like reaching to high level of clay exfoliation in its stirred suspension, capability of PE layers to interact with clay platelets to attract them oriented parallel to the substrate surface and then intercalate between them, forming tortuous network of galleries between deposited clay platelets, as resulted from morphological investigations. Additional possible reasons for this barrier improvement may perhaps be forming a firm interface between LBL assemblies and the plasma treated the polystyrene-based substrate. In addition, along with morphological studies that showed decreasing orientation of LBL assemblies with increased

concentration of clay in its suspensions, barrier improvement stabilized at about clay concentration of 3-5wt% in its suspensions. Also, the possible reason for relatively higher barrier improvement resulted for carbon dioxide might be due to its potential interaction with LBL assemblies and its larger van der Waals size relative to oxygen that increases the possibility to be trapped in the long path of tortuous galleries, rather than to traverse between adjacent clay platelets in a layer.

In the next study, repetitive melt pressing of already LBL-coated polystyrene-based samples was attempted to crush and embed the LBL assemblies into the polymeric matrix, to make innovative PNCs. Although microscopic images in low magnification scales showed LBL portions in the size of up to a few microns, implying the occurrence of basically microcomposites, high magnification TEM micrographs, revealed the existence of swollen intercalated clay layer stacks and flocculated exfoliated tactoids of a few clay platelets, as the main morphologies inside the crushed portions of LBL assemblies. The increased exfoliation and intercalation of clay platelets as a result of the cyclic melt pressing was tracked through XRD and TEM, and implied the occurrence of significant interaction between clay and the polymeric matrix, postulating the compatibilizing effect of PE interlayers. In addition, POM and XRD studies pointed to the rise in the dispersion, as well as exfoliation and intercalation of clay platelets, respectively, with increasing melt mixing time and the decrease in the initial number of BL coatings on the samples. However, moderate global dispersion of clay platelets throughout polymeric matrix may still conjecture the insufficient level of interaction occurred between the highly hydrophobic polystyrene-based matrix and hydrophilic clay, as well as the low potential of cyclic pressing to apply intensive enough shear stress on samples.

In the next step, DMA investigations on these innovative PNCs showed noticeably increased storage and loss moduli values, compared with those of the pristine styrenic polymer, confirming the aforementioned significance of interaction occurred between clay and the polymeric matrix, induced by PE interlayers. Particularly, PETi developed a considerable interaction with minor PB phase of the matrix, to raise its glass transition temperature towards higher temperatures, over extended times of melt processing. Besides, permeation experiments showed almost pronouncedly increased gas barrier properties for these PNCs. In fact, considering the slight content of clay in the PNC samples, and limited level of nanodispersion throughout the matrix, it might be hypothesized that highly tortuous (internal factor) LBL assemblies portions, with high aspect ratio (external factor), may work as almost efficient scavenging centers against transport of oxygen and carbon dioxide. In addition, promoting the orientation of these assemblies perpendicular to gas molecules permeation path, induced by melt pressing of samples into thin films, in each cycle, may be considered as another possible reason for improving barrier efficiency of LBL assemblies. Also, probably due to the higher thermal stability of PETi, its conforming PNCs exhibited remarkable improvement in both barrier properties and hardness, through increased time of melt processing, compared with those containing PEI, which could possibly incur slight thermal degradations.

Finally, using PVAc as the matrix for preparing PNC through our innovative two-step approach, was studied to investigate the effect of increased hydrophilicity of the polymeric matrix on morphology and dynamic mechanical properties of the processed PNCs, as well as gas transport through them. Also, more thermally stable PETi was chosen over PEI as the interlayer for LBL coating, to diminish the thermal degradation of processed PNCs. In fact,

both dynamic mechanical analysis and gas permeation experiments showed significantly raised moduli values and barrier properties for PNCs processed for only 25 melt pressing cycles. In addition, in identical conditions of LBL coating, the PNCs containing PVAc showed relatively higher contents of clay. Hence, it was postulated that as a result of using more hydrophilic PVAc, compared to the styrene-based polymer, stronger interactions were induced between polymeric matrix and clay. However, TEM micrographs showed the occurrence of mainly swollen intercalated stacks and flocculated exfoliated tactoids of a few clay platelets, pointing to qualitative similarities with previous PNCs based on styrenic polymers. Thus, it may again hypothesize the insufficiency of cyclic melt pressing to promote a global dispersion of clay throughout the matrix. In fact, one possible reason for low average dispersion of clay in our PNCs might be the significant cohesiveness of oriented LBL assemblies. Thus, they resist against being crushed into smaller particles by applied cyclic stress. Also, decreases in both hardness and gas barrier properties of our PNCs with increased time of melt processing may conjecture possible slight thermal degradation of PVAc matrices.

8.2. Future Steps

This innovative two-step approach for processing PNCs can be applied on a polymer like polyethylene terephthalate (PET), as one of the main polymeric choices in the packaging industry, due to its appropriate barrier and mechanical properties. In fact, functional esteric groups of PET can potentially make it more interactive with our LBLs, particularly, due to its chemical affinity with PETi interlayers, to result in the improved barrier and mechanical properties of its PNCs, specifically for packaging applications.

Therefore, preliminary steps were performed through LBL coating of PET films (thickness = 100 μ m), in PETi solution (0.5wt% in DIW) and MMT suspension (1wt% in DIW), for ten consecutive cycles. Then, it was followed by melt pressing of coated samples at 260°C for 25cycles (at the pressure of 3000 psi, following three minutes preheating at pressing temperature). Thus, morphological investigations through POM showed relatively improved levels of dispersion and distribution of clay particles, compared with previously investigated PNCs based on polystyrene and polyvinylacetate. Also, TEM micrographs in high magnification scales showed swollen intercalated stacks and flocculated exfoliated tactoids, where individual clay platelets with thicknesses of about one nanometer are observable (Figures 8.1, 8.2).

From all these studies it might be concluded that despite the positive effect of increased hydrophilicity of polymeric matrix on promoting its interaction with clay particles, considering the aforementioned internal cohesion in LBL assemblies, still a more intensive processing technique, like using a twin-screw extruder at high speeds may be able to induce stronger shear stress on LBL assemblies and to increase their dispersion level in the processed PNCs.

In addition, since the slight thermal degradation of samples during extended times of cyclic melt pressing at high temperatures were conjectured as one impediment to further improvement in gas barrier properties and hardness of our novel PNCs, processing the samples through high-speed extrusion may perhaps decrease this side effect. To eliminate this thermal degradation even further, melt processing under an inert atmosphere, like twin-screw extrusion purged with nitrogen gas, is recommended.

Also, since these nanocomposite approaches for improving the barrier properties of polymers, mainly rely on increasing the tortuosity of polymeric matrix, as a mean to increase the diffusing path of permeant species; increased aspect ratio of the impermeable inorganic embedded particles, might promote the tortuosity of the matrix, to improve its barrier properties, provided that a proper level of dispersion is developed through applying intensive enough shear stresses. Thus, using alternatives with higher aspect ratios, like vermiculite (with aspect ratio of about 1000) or fluoromica (e.g. Somasif ME100, with typical aspect ratio of around 500), might have a better potential for barrier improvement, particularly through melt intercalation, which despite its lower potential for improving dispersion, relative to other traditional methods of processing PNCs, like solution and polymerization, has a high capability in promoting platelets orientation along melt flow, in favor of improving barrier properties, particularly in thin films. Furthermore, as another alternative for MMT platelets, single atomic layer graphene can be mentioned that has recently attracted a significant amount of interest from scientists and researchers.

Despite the popularity of melt processing for processing PNCs, due to its compatibility with industrial instruments and its eco-friendly nature, generally it shows a moderated potential for increasing dispersion of inorganic particles throughout the polymeric matrix. In addition, as observed in our studies, one major drawback with melt mixing is the possibility of thermal degradation of materials during processing. So, the ability of PE for promoting intercalation and exfoliation of clay platelets might be examined through a solution-based method. Therefore, as an example proposal, PE and clay can be stirred with each other in the deionized water, at high stirring speeds, to possibly prepare exfoliated mixture of them. Then the resulted

mixture after being dried can be mixed at high stirring speeds with the desired polymer, in an appropriate solvent (For instance toluene might be an appropriate choice for polymers like PS or PVAc.), aiming at exfoliated PNCs.

Moreover, since one of the main applications for PNCs with high barrier properties is in food packaging, using polymeric compatibilizers that are safer for contact with food products, provided that they could provide comparable processability and final properties in processed PNCs, they can be considered as good alternatives choices for PEI and PETi. By the way of example, biodegradable chitosan, which has successfully been tried for building LBL assemblies with MMT can be proposed as an appropriate choice.

Figures

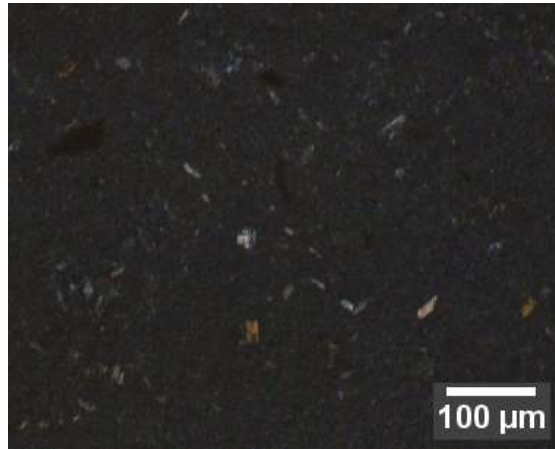
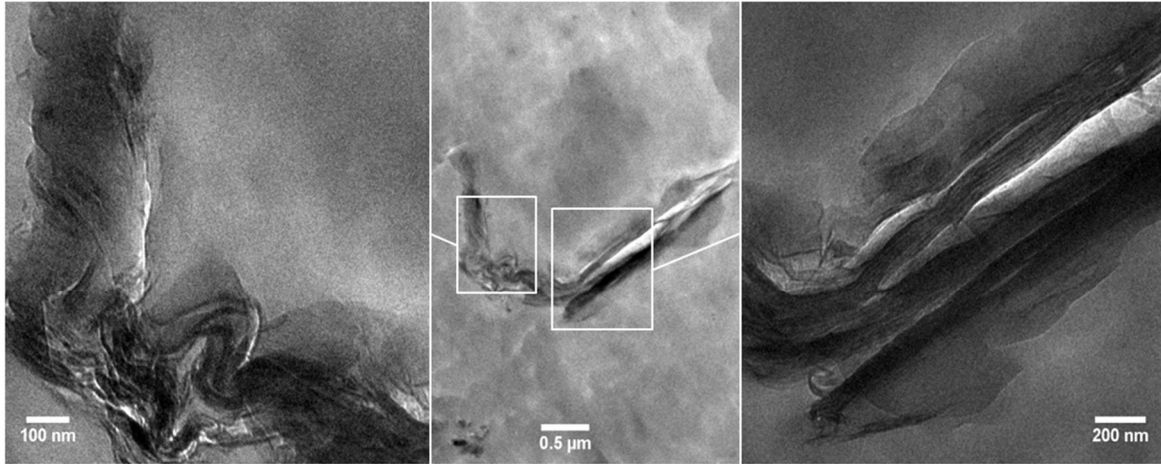


Figure 8.1. POM images of our innovative PNCs prepared after 25 melt pressing cycle at 260°C on PET films (thickness=100μm), already coated with 10BL deposition in PETi solution (0.5wt%) and MMT suspension (1wt%) in DIW.

(a)



(b)

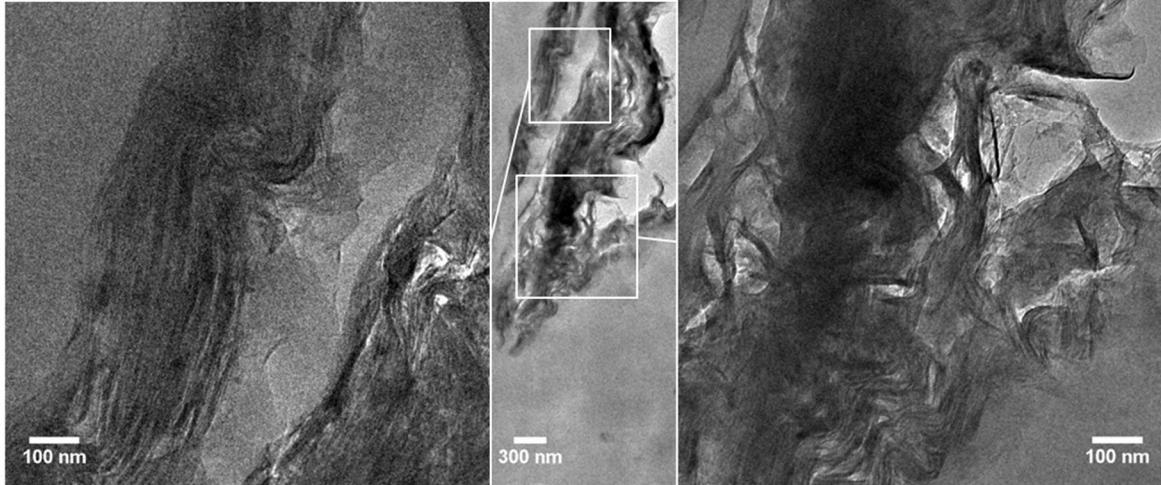


Figure 8.2. TEM images of our novel PNCs prepared after 25 melt pressing cycle at 260°C on PET films (thickness=100μm), already coated with 10BL deposition in PETi solution (0.5wt%) and MMT suspension (1 wt%) in DIW.